ASCE Manuals and Reports on Engineering Practice No. 140

Climate-Resilient Infrastructure

ADAPTIVE DESIGN AND RISK MANAGEMENT

Committee on Adaptation to a Changing Climate

Edited by

Bilal M. Ayyub, Ph.D., P.E.

ASCE

ASCE Manuals and Reports on Engineering Practice No. 140

Climate-Resilient Infrastructure

Adaptive Design and Risk Management

Edited by Bilal M. Ayyub,
Ph.D., P.E., Dist.M.ASCE

ASCE Committee on Adaptation to a
Changing Climate

ASCE AMERICAN SOCIETY OF CIVIL ENGINEERS

Published by the American Society of Civil Engineers

Library of Congress Cataloging-in-Publication Data

Names: American Society of Civil Engineers. Committee on Adaptation to a Changing Climate. | Ayyub, Bilal M., editor.
Title: Climate-resilient infrastructure : adaptive design and risk management / prepared by the Committee on Adaptation to a Changing Climate; edited by Bilal M. Ayyub, Ph.D., P.E.
Description: Reston, Virginia: American Society of Civil Engineers, [2018] |
Series: ASCE manuals and reports on engineering practice; no. 140 |
Includes bibliographical references and index.
Identifiers: LCCN 2018037421 | ISBN 9780784415191 (hardcover: alk. paper) |
ISBN 9780784481905 (pdf) | ISBN 9780784481922 (epub)
Subjects: LCSH: City planning—Climatic factors. | Building, Stormproof. |
Infrastructure (Economics) | Sustainable urban development. | Environmental protection. |
Environmental impact analysis.
Classification: LCC TD168.5 .A44 2018 | DDC 628—dc23
LC record available at https://lccn.loc.gov/2018037421

Published by American Society of Civil Engineers
1801 Alexander Bell Drive
Reston, Virginia 20191-4382
www.asce.org/bookstore | ascelibrary.org

Errata: **Errata, if any, can be found at https://doi.org/10.1061/9780784415191.**

ISBN 978-0-7844-1519-1 (print)
ISBN 978-0-7844-8190-5 (PDF)
ISBN 978-0-7844-8192-2 (ePub)
Manufactured in the United States of America.

25 24 23 22 21 20 19 18 1 2 3 4 5

MANUALS AND REPORTS ON ENGINEERING PRACTICE

(As developed by the ASCE Technical Procedures Committee, July 1930, and revised March 1935, February 1962, and April 1982)

A manual or report in this series consists of an orderly presentation of facts on a particular subject, supplemented by an analysis of limitations and applications of these facts. It contains information useful to the average engineer in his or her everyday work, rather than findings that may be useful only occasionally or rarely. It is not in any sense a "standard," however; nor is it so elementary or so conclusive as to provide a "rule of thumb" for nonengineers.

Furthermore, material in this series, in distinction from a paper (which expresses only one person's observations or opinions), is the work of a committee or group selected to assemble and express information on a specific topic. As often as practicable the committee is under the direction of one or more of the Technical Divisions and Councils, and the product evolved has been subjected to review by the Executive Committee of the Division or Council. As a step in the process of this review, proposed manuscripts are often brought before the members of the Technical Divisions and Councils for comment, which may serve as the basis for improvement. When published, each work shows the names of the committees by which it was compiled and indicates clearly the several processes through which it has passed in review, so that its merit may be definitely understood.

In February 1962 (and revised in April 1982), the Board of Direction voted to establish a series titled "Manuals and Reports on Engineering Practice," to include the Manuals published and authorized to date, future Manuals of Professional Practice, and Reports on Engineering Practice. All such Manual or Report material of the Society would have been refereed in a manner approved by the Board Committee on Publications and would be bound, with applicable discussion, in books similar to past Manuals. Numbering would be consecutive and would be a continuation of present Manual numbers. In some cases of joint committee reports, bypassing of Journal publications may be authorized.

A list of available Manuals of Practice can be found at http://www.asce.org/bookstore.

This page intentionally left blank

CONTENTS

This page intentionally left blank

PREFACE

This manual of practice, *Climate-Resilient Infrastructure: Adaptive Design and Risk Management* (MOP 140), was prepared by a development team that includes members of the ASCE Committee on Adaptation to a Changing Climate between 2016 and 2018.

Some of the content has been outdated by recent events. For instance, the book contains references to ASCE Standard 7-10, which has been superseded by ASCE Standard 7-16. The differences between the two versions are not central for the purposes of this manual. Therefore, the Development Team decided to keep the references to ASCE 7-10.

In addition, President Donald Trump has canceled Executive Order 13690 and the federal flood risk management standard. The review undertaken by standards experts and the ASCE Blue-Ribbon Panel considered these changes, and the Development Team has responded to applicable comments.

This page intentionally left blank

ACKNOWLEDGMENTS

The ASCE Committee on Adaptation to a Changing Climate acknowledges the contributions of the Blue-Ribbon Panel reviewers and in particular the suggestions provided by Dr. Sanj Malushte in the development of the concepts of fragility and reliability curves as they relate to adaptive design and related curves prepared by Huiling Hu. The committee is grateful for the contributions of Ana Caceres of Carnegie Mellon University. The committee also acknowledges the encouragement and the support provided by John E. Durrant, P.E., F.ASCE, ASCE's senior managing director for Engineering and Lifelong Learning and the Committee on Technical Advancement.

Development Team

Editor
Bilal M. Ayyub, Ph.D., P.E., Dist.M.ASCE

Lead Authors
Bilal M. Ayyub, Ph.D., P.E., Dist.M.ASCE
Miguel Medina, Ph.D., P.H., F.ASCE
Ted Vinson, Ph.D., P.E., M.ASCE
Dan Walker, Ph.D., A.M.ASCE
Richard N. Wright, Ph.D., NAE, Dist.M.ASCE

Contributing Authors
Amir AghaKouchak, Ph.D., P.E., M.ASCE
Ana Paula Barros, Ph.D., P.E., F.ASCE
A. Christopher Cerino, P.E., M.ASCE
Ryan P. Conry, P.E., S.E. M.ASCE
Robert E. Fields, P.E., M.ASCE
Oceana P. Francis, Ph.D., P.E., M.ASCE
J. Rolf Olsen, Ph.D., A.M.ASCE
Constantine Samaras, Ph.D., A.M.ASCE
Farshid Vahedifard, Ph.D., P.E., M.ASCE

Blue-Ribbon Panel

Bruce Ellingwood, Ph.D., P.E., Dist.M.ASCE, NAE (Colorado State University, Fort Collins, CO), *Chair*
James R. Harris, P.E., F.ASCE, NAE (ASCE/SEI 7, J.R. Harris & Company, Denver, CO), *Vice Chair*
Hugo Loaiciga, Ph.D., P.E., D.WRE, F.ASCE (University of California, Santa Barbara)
Christopher P. Jones, M.ASCE (ASCE 24, Durham, NC)
Sanj Malushte, Ph.D., P.E., F.ASCE (Bechtel, Reston, VA)

Additional Reviews by Organizations

Water Resources Committee, American Meteorological Society (AMS)
Water Utility Climate Alliance (WUCA)

Steering and Administrative Committees

Initiated by 2017 ASCE-CACC Executive Committee

Bilal M. Ayyub, Ph.D., P.E., Dist.M.ASCE, *Chair* (2017)
Ana Paula Barros, Ph.D., P.E., F.ASCE, *Vice Chair*
J. Rolf Olsen, Ph.D., A.M.ASCE, *Member*
Ted Vinson, Ph.D., P.E., M.ASCE, *Founding and Past Chair* (2012–2015)
Dan Walker, Ph.D., A.M.ASCE, *Member*
Richard N. Wright, Ph.D., NAE, Dist.M.ASCE, *Past Chair* (2016)

Approval of Initiative by ASCE Committee on Technical Advancement (CTA)

CTA represented by
Jonathan Esslinger, M.ASCE, *ASCE Staff*
Scott Murrell, P.E., M.ASCE, *CTA Liaison*
Jay Snyder, Aff.M.ASCE, *ASCE Staff Contact*

ACRONYMS

ADCIRC	Advanced Circulation Model
AEP	Annual exceedance probability
AMS	Annual Maxima Series
AR4	IPCC 4th Assessment Report
AR5	IPCC 5th Assessment Report
ARI	Average Return Interval
ARM	Adaptive Risk Management
ARRM	Asynchronous Regional Regression Model (cida.usgs.gov)
ASCE/SEI 24	*Flood Resistant Design and Construction*
ASCE/SEI 7	*Minimum Design Loads for Buildings and Other Structures*
ASD	Allowable Stress Design
BFE	Base Flood Elevation
CACC	Committee on Adaptation to a Changing Climate
CDF	Cumulative Density Function
CEM	US Army Corps of Engineer's Coastal Engineering Manual
CEQ	Council on Environmental Quality
CFS	Cubic feet per second
CI	Composite Index (Risk Rating)
CISA	Climate-Informed Science Approach
CMIP5	Coupled Model Intercomparison Project Phase 5
CMS	Cubic meters per second
COV	Coefficient of variation
CPT	Cone Penetration Test
csv	Comma separated values (file format)
CTA	ASCE Committee on Technical Advancement
DFE	Design Flood Elevation
DOE	Department of Energy
DOT	Department of Transportation

dpy	days per year
EMA	Expected Moments Algorithm
ENSO	El Niño Southern Oscillation
EO	Executive Order
EV1	Extreme-Value Type 1 (EV1) Gumbel (maximum) distribution
FBFE	Future Base Flood Elevation
FEA	Finite Element Analysis
FEMA	Federal Emergency Management Agency
FFRMS	Federal Flood Risk Management Standard
FHWA	Federal Highway Administration
FIRMs	Flood Insurance Rate Maps
FIS	Flood Insurance Study
FVA	Freeboard Value Approach
GCM	Global Climate Models
GEV	Generalized Extreme Value
GHG	Greenhouse gases
GMSL	Global mean sea level
GPM	Gallons per minute (gal./min)
HEC	USACE Hydraulic Engineering Center
HVAC	Heating, Ventilating, and Air Conditioning
IAM	Integrated Assessment Models
IBC	International Building Code
IDF	Intensity-Duration-Frequency
IPCC	Intergovernmental Panel on Climate Change (www.ipcc.ch)
ISO	International Organization for Standardization
LCCA	Life-Cycle Cost Analysis
LEED	Leadership in Energy and Environmental Design
LID	Low Impact Development
LiMWA	Limit of Moderate Wave Action
LPIII	Log-Pearson Type III Distribution
MACA	Multivariate Adaptive Constructed Analogs (maca.northwestknowledge.net)
MATLAB	MATrix LABoratory
MEOW	Maximum Envelopes of Water
MIT	Minimum Interevent Time
MIKE 21	Tool for coastal modeling by DHI (https://www.mikepoweredbydhi.com/products/mike-21, accessed 2/8/2018)
MLLW	Mean Low Low Water
MOM	Maximum of the MEOWs
MRI	Mean Recurrence Interval (same as ARI)

NA-CORDEX	North American Coordinated Regional Climate Downscaling Experiment (na-cordex.org)
NARCCAP	North American Regional Climate Change Assessment Program (narccap.ucar.edu)
NASA	National Aeronautics and Space Administration
NAVD88	North American Vertical Datum of 1988
NCA	National Climate Assessment (http://www.globalchange.gov/)
NCEI	National Centers for Environmental Information
NEPA	National Environmental Policy Act
NESDIS	National Environmental Satellite and Data Information Service
netCDF	Network Common Data Form
NEVA	Non-Stationary Extreme-Value Analysis
NFIP	National Flood Insurance Program
NGVD29	National Geodetic Vertical Datum of 1929
NIST	National Institute of Standards and Technology
NOAA	National Oceanic and Atmospheric Administration (www.noaa.gov)
NPCC	New York City Panel on Climate Change
NPV	Net Present Value
NS	Non-Stationary
NSIDC	National Snow and Ice Data Center
NWS	National Weather Service
NYCBC	New York City Building Code
NYCT	New York City Transit Authority
OM	Observational Method
PDF	Probability Density Function
PoR	Period of Record Practice on Adaptive Design and Risk Management
PWMs	Probability-Weighted Moments
RCP	Representative Concentration Pathway
RCP	Representative Concentration Pathway
RDM	Robust Decision Making
RDU	Raleigh-Durham International Airport
RegCM3	USGS Regional Climate Model Version 3 (regclim.coas.oregonstate.edu)
RISA-3D	Structural Engineering Software for Analysis and Design (http://risa.com/p_risa3d.html, accessed 2/8/2018)
RF	Radiative forcing
RL	Return Level
RP	Return Period
RSL	Regional Sea Level Rise
SAFB	Self-Activating Flood Barrier

SDOF	Single Degree of Freedom
SEI	Structural Engineering Institute
SFHA	Special Flood Hazard Area
SLOSH	Sea, Lake, and Overland Surge from Hurricanes (model)
SLR	Sea Level Rise
SOC	Soil Organic Carbon
SRES	Special Report on Emissions Scenarios
SREX	IPCC Special Report on Extremes
ST	Stationary
SWAN	Simulating Waves Nearshore
SWD	Still Water Depth
SWEL	Still Water Elevation Level
TAMP	Transportation Asset Management Plan
TL	Total Loss (Risk Quantification)
USACE	US Army Corps of Engineers
USBR	US Bureau of Reclamation
USGCRP	US Global Change Research Program http://www.globalchange.gov/
USGS	US Geological Survey
WBAN	Weather Bureau Army Navy station
WHAFIS	Wave Height Analysis for Flood Insurance Studies
WL	water level

CHAPTER 1
INTRODUCTION

1.1 PROBLEM DEFINITION, NEEDS, AND SIGNIFICANCE OF IMPACT

The climate science community informs us that extremes of climate and weather are changing from historical values and that the changes are driven substantially by emissions of greenhouse gases caused by human activities. The terminology of the climate science community is described in Appendix A, Terminology. Civil infrastructure systems traditionally have been designed, constructed, operated, and maintained for appropriate probabilities of functionality, durability, and safety while exposed to climate and weather extremes during their full service lives. Because of uncertainties in future greenhouse gas emissions and in the models for future climate and weather extremes, neither the climate science community nor the engineering community presently can define the statistics of future climate and weather extremes.

The Intergovernmental Panel on Climate Change (IPCC) concluded that warming of the climate system is unequivocal, and since the 1950s, many of the observed changes are unprecedented over decades to millennia (IPCC 2014). The IPCC also concluded that it is extremely likely that human influence has been the dominant cause of the observed warming since the mid-twentieth century. Increases in atmospheric and ocean temperatures, droughts and wildfires, extreme precipitation and intensity in many areas, and global sea-level rise have already been observed. These trends are projected to continue into the future. While there is considerable evidence that the climate is changing, understanding the significance of climate change at temporal and spatial scales relevant to engineering practice is more difficult.

1.2 OBJECTIVE AND SCOPE

The purpose of this manual of practice (MOP) is to provide guidance for and contribute toward the development and enhancement of standards for infrastructure analysis and design, as well as the numerous regulation and building codes that refer to them, in a world in which risk profiles are changing (non-stationarity) and climate change is a reality but cannot be projected with a high degree of certainty. It also offers guidance to inform engineering decisions and introduces adaptive risk management before standards have been updated to account for more severe climate or weather extremes.

In 2015, ASCE issued a report titled *Adapting Infrastructure and Civil Engineering Practice to a Changing Climate* (ASCE 2015) that is free to the public for download (http://dx.doi.org/10.1061/9780784479193). Infrastructure includes buildings of all types and facilities for communications, energy generation and distribution, industry, transportation of all modes, waste management, water resources, and urban potable, storm, and wastewater.

This MOP builds on the 2015 report to

- Foster understanding and transparency of analytical methods necessary to update and describe climate, including possible changes in the frequency and intensity of weather and extreme events, for planning and engineering design of the built and natural environments
- Promote exploration of the value of adaptive design methods such as the observational method (OM) and adaptive risk management as a central tenet of a new paradigm for engineering practice, including standards that acknowledge the implications of climate change as well as the uncertainties inherent in projections of future weather and climate extremes

Engineers build durable infrastructure. The rights of way and footprints of the infrastructure have even longer-term influences. The planning and design of new infrastructure should, therefore, account for the climate of the future. Considering the impacts of climate change in engineering practice is analogous to including forecasts of long-term demands for infrastructure use as a factor in design. Although the scientific community agrees that climate is changing, there is significant uncertainty about the spatial and temporal distributions of the changes over the lifetimes of infrastructure designs and plans. The requirement that engineering infrastructure meets future needs with the uncertainty of future climate is a challenge to engineers.

Engineering practice recognizes and accounts for uncertainties in future conditions. These methods include designing for a flood or wind velocity of a particular magnitude, the use of safety factors or freeboard, and probabilistic and statistical methods. Engineers use statistical methods to quan-

tify uncertainty for empirical probability distributions used in engineering design. The assumption of stationarity implies that the statistical properties of extremes in future time periods will be similar to those of past time periods. Recent papers have noted that climate change undermines this assumption (Milly et al. 2008).

Infrastructure designs and plans, as well as institutions, regulations, and codes and standards to which they must adhere, will need to be adapted and even be adaptable to accommodate a range of future climate conditions. Secondary effects from a changing climate such as changes in land cover or use, resource availability, and demographics in population are similarly uncertain and require flexibility in infrastructure location and design. The standards, codes, regulations, zoning laws, and so on that govern infrastructure are often finely negotiated or delicately balanced legally, which often makes them slower to adapt. In addition, different stakeholders may exploit the uncertainties associated with climate change to argue for positions they prefer. This manual provides a review of most relevant engineering practices and discusses how engineers can consider climate change in their practice given the uncertainty of the future. Incorporating climate change into engineering practice will require engineering judgment to balance costs and potential consequences of failure.

Even without anthropogenic climate change, climate varies naturally on decadal and longer time scales, and the observed record is a relatively short time period compared to the potential range of climate variability. There are also multiple other sources of change and uncertainty—changes in demand for infrastructure and services, changes in land use, urbanization, population increase, and economic development in vulnerable areas such as floodplains, deserts, shorelines, and earthquake zones. Population and development may stress natural resources, such as increased groundwater depletion, surface water withdrawals, and deforestation. In addition, society and engineers are increasingly concerned about the natural environment. Potential responses by ecosystems, including changes in biodiversity or the abundance of component species, are particularly difficult to project with a high degree of certainty.

In recognition that historical observations cannot be relied on to adequately describe extreme conditions in the future as well as uncertainty associated with model projections at the project scale, *Adapting Infrastructure and Civil Engineering Practice to a Changing Climate* (ASCE 2015) recommended that

- Engineers should communicate and collaborate with climate scientists to observe and model climate, weather, and extreme events. The purpose of the involvement is to improve the relevance of the modeling and observations for use in the planning, design, operation, maintenance, and renewal of the built and natural environment. It is only

when engineers work closely with climate scientists that the needs of the engineering community will be fully understood, limitations of the climate science community will be more transparent to engineers, and the uncertainties of the projections of future climate for engineering design purposes will be fully recognized.

- Practicing engineers, project stakeholders, and policy and decision makers should be informed about the uncertainty of the projections of future climate and the reasons for the uncertainty as elucidated by the climate science community. Because the uncertainty associated with future climate is not completely quantifiable, if projections of future climate are to be used in engineering practice, they require considerable engineering judgment to balance the costs of mitigating risk through adaptation against the potential consequences of failure.
- Engineers should develop a new paradigm for engineering practice in a world in which climate change may occur but cannot be projected with a high degree of certainty. When it is not possible to fully define and estimate the risks and potential costs and reduce the uncertainty in the time frame in which action should be taken, it may be feasible to use low-regret adaptive strategies to make a project more resilient to future climate and weather extremes.
- Critical infrastructure that is most threatened by changing climate in a given region of the country should be identified, and the public and decision makers should be made aware of this assessment. An engineering–economic evaluation of the costs and benefits of strategies for resilience of infrastructure should be undertaken.

1.3 WHY STANDARDS MATTER

Although Hurricane Katrina of 2005 affected major cities, flood resiliency for infrastructure and urban environments really came to the forefront with the damage caused by Hurricane Harvey in 2017 in the Houston metropolitan region (*New York Times* 2017). Land use and building practices contributed greatly to damages in the Houston area, but so did the 52 inches of rain that fell over four days, which was a rare event, perhaps influenced by modern-era climatic change. Since then, agencies and building owners have been trying to interpret the available codes and decide how to protect their assets against future storms. The results of this exercise are widely varied.

In general, transportation agencies are finding the current codes inadequate both in coverage and applicability for their assets, and thus they are navigating their way through writing their own standards or guides. Private building owners, with smaller-concentrated assets, are simply applying ASCE/SEI 7 (2010) and 24 (2014) in their pre–Hurricane Sandy based

on code-minimum levels. Whereas short-term actions are necessary, a comprehensive long-term campaign must be started to understand and reshape the available published guidance as it relates to dense urban environments.

Many engineers and scientists have been implementing Hurricane Sandy recovery and resiliency projects since 2012 and have a great deal of applied knowledge, including shortfalls, regarding the current codes. This MOP is intended to identify some of the current practices and knowledge gaps, offer guidance, suggest areas of further study and clarification, and be the springboard as a technical basis document for work on the next code development and revision cycles so that building owners are equipped with current guidance and agencies can become more unified by the research of experts in the field.

This book introduces the use of adaptive risk management including the observational method for achieving climate resilience of infrastructure. It has the added motivation that adaptive risk management would be considered for inclusion in currently used standards by the standards development community.

1.4 STRUCTURE OF MANUAL OF PRACTICE

This MOP has a varied style that includes a step-by-step guide in areas where technologies or methodologies are well established, suggested approaches in cases where several competing approaches are available, and leads based on research results for areas that are emerging. The manual is intended to eventually charter the way to changes to codes and standards.

The manual consists of the following chapters:

Chapter 1: Introduction
The first chapter sets the context, articulates the needs, provides objective and scope statements for the manual, lists topics warranting additional analysis, and defines users and uses of the manual.

Chapter 2: A Changing Climate: Problem Definition
This chapter summaries key drivers of climate variability and change and their effects on weather and climate extremes, as well as their relevance to existing ASCE standards.

Chapter 3: Observational Method
The third chapter describes the observational method and provides illustrative examples and a case study.

Chapter 4: Characterization of Extremes and Monitoring
This chapter focuses on methods for estimating extreme events, particularly related to precipitation, and suggests design methods and considerations

to address a changing climate. The chapter also offers guidance on monitoring methods and measures to enhance climate resilience.

Chapter 5: Flood Design Criteria

This chapter summarizes flood design criteria in relation to a changing climate. The chapter also provides guidance for developing project design flood elevations.

Chapter 6: Flood Loads

The sixth chapter covers computational methods of determining flood loads including hydrostatic loads and wave loads, among others.

Chapter 7: Adaptive Design and Risk Management

This chapter introduces adaptive design and adaptive risk management in the context of life-cycle engineering and economics.

Chapter 8: Data and Information Sources

This chapter provides leads to data and information sources related to climate change.

It should be noted that Chapter 3 provides a practical approach to adaptive risk management requiring no research beyond the use of existing standards and codes, whereas Chapters 4 and 5 guide the reader in approaches to research for estimating future climate or weather extremes. Chapter 3 is useful for practicing engineers who need to account for non-stationarity in a current project and for incorporation of the observational method in standards. Chapters 4 and 7 offer guidance to research the development of standards for more formal treatment of non-stationarity and adaptive risk management.

This manual also includes four appendixes on Terminology (Appendix A), ASCE Standards and Climate Change (Appendix B), Methodology for L-Moment and Other Statistical Computations (Appendix C), and Adaptation Technologies (Appendix D).

1.5 TOPICS WARRANTING ADDITIONAL ANALYSIS

Three areas are identified: (1) direct effects of increasing temperatures, (2) wildfires, and (3) adaptive design implementation. Other areas also could be added to this list.

1.5.1 Direct Effects of Increasing Temperatures

The impacts of increasing temperatures caused by climate change on society are well established (IPCC 2014, USGCRP 2014). Direct effects are ubiquitous and include impacts to agriculture, ecosystems, human health (e.g., to vulnerable populations and workers), economics of energy, facilities, and infrastructure. Additional work to analyze methods for minimizing

impacts from increasing heat, including the reduction of urban heat island effects, are warranted.

1.5.2 Wildfires

Although a clear trend of increased wildfires has not yet been established (Short et al. 2015), the average extent of area burned by wildfires each year appears to have been increasing since the 1980s (MTBS 2016), with severe wildfires in 2017. Recent research suggests that human-caused climate change contributed to an additional 4.2 million hectares of forest fire area from 1984 to 2015, nearly doubling the forest fire area expected in its absence (Abatzoglou and Williams 2016). Many environmental impacts associated with climate change can affect wildfire severity, extent, and frequency, including changes in precipitation, temperature, and drought. Additional analysis and development are needed for methods to reduce the financial, environmental, and health costs associated with wildfires.

1.5.3 Adaptive Design Implementation

Although adaptive design (including the observation method) offers an opportunity to increase the resilience of infrastructure while minimizing long-term regret, there are presently implementation challenges related to systematic frameworks within the agencies leading the largest infrastructure projects. Additional understanding of relevant financial, operational, budgetary, bureaucratic, and construction-related factors involved in implementing a cost-effective adaptive design is warranted.

1.5.4 Scale Disconnect

It should be noted that scale disconnect is a considerable concern that is addressed herein and elsewhere in the manual. Chapter 2 provides climate change information mostly from Global Climate Models (GCMs). The chapters that follow provide examples of specific tools for how to evaluate future extremes at the local level. Going from global to local scale creates this disconnect. For example, in Chapter 4, the Intensity-Duration-Frequency (IDF) technique is described assuming that GCMs are appropriate for this sort of analysis in the future. Although it does acknowledge that GCMs are currently "highly uncertain and models exhibit large intermodel variability," it should be noted that they are improving rapidly with a steady increase in reliability on rainfall statistics. There is improvement, but it is unrealistic to assume GCMs alone are the only appropriate approach for this sort of analysis. Raw GCM precipitation data are generated at large spatial scales that do not capture local processes and should

not be used directly, especially to evaluate place-specific extremes needed at the scale of much of our infrastructure.

1.5.5 Other Areas

IPCC forecasts that droughts in already dry regions will become more severe, as provided in Table 2-1 of Chapter 2. Droughts will create challenges for maintaining adequate water supplies for agriculture, cooling of power plants, transportation, and human consumption. Also, the desiccation of vegetation will increase the risk of wildfires that will be hazardous to infrastructure. Standards and recommended practices will be needed for landscaping to reduce exposures of infrastructure to wildfire effects and for increasing the fire resistance of roofing and cladding for infrastructure.

1.6 USES AND USERS

This book is intended to guide practitioners and developers of ASCE standards in the incorporation of adaptive risk management to deal with the uncertainties of future climate and weather extremes. The incorporation of adaptive risk management in standards will take some time. For instance, research with the climate or weather science community is needed to estimate the most likely and most severe future climate and weather extremes for 50 to 100 years and beyond for service lives of infrastructure projects and systems. Engineers responsible now for the design, construction, operation, and maintenance of infrastructure also can use this manual to implement adaptive risk management for decisions needed before standards are updated to incorporate adaptive risk management.

1.7 REFERENCES

Abatzoglou, J. T., and A. Park Williams. 2016. "Impact of anthropogenic climate change on wildfire across western US forests." *Proc., National Academy of Sciences* 113(42),11770–11775. Accessed November 22, 2017. http://www.pnas.org/content/113/42/11770.

ASCE. 2010. ASCE/SEI 7-16 *Minimum design loads for buildings and other structures*. Accessed February 13, 2016. http://www.asce.org/structural-engineering/asce-7-and-sei-standards/. Reston, VA: ASCE.

ASCE. 2014. ASCE/SEI 24 *Flood resistant design and construction*. Accessed February 13, 2016. http://ascelibrary.org/doi/book/10.1061/9780784408186. Reston, VA: ASCE.

ASCE. 2015. *Adapting Infrastructure and Civil Engineering Practice to a Changing Climate*. Accessed February 13, 2016. http://ascelibrary.org/doi/book/10.1061/9780784479193 103. Reston, VA: ACSE.

IPCC (Intergovernmental Panel on Climate Change). 2014. *Climate Change 2014: Impacts, Adaptation, and Vulnerability. Part A: Global and Sectoral Aspects. Contribution of Working Group II to the Fifth Assessment Report of the Intergovernmental Panel on Climate Change*. Cambridge, UK: Cambridge Univ. Press. Accessed February 13, 2016. https://www.ipcc.ch/report/ar5/wg2

Milly, P. C. D., J. Betancourt, M. Falkenmark, R. M. Hirsch, Z. W. Kundzwicz, D. P. Lettenmaier, et al. 2008. "Stationarity is dead: Whither water management?" *Sci*. 319(5863), 573–574.

MTBS (Monitoring Trends in Burn Severity). 2016. *MTBS Data Summaries*. Accessed September 12, 2018. https://www.mtbs.gov.

New York Times. 2017. "Mapping the devastation of Harvey in Houston." Accessed November 23, 2017. https://www.nytimes.com/interactive/2017/08/28/us/houston-maps-hurricane-harvey.html.

Short, K. C. 2015. "Sources and implications of bias and uncertainty in a century of U.S. wildfire activity data." *Int. J. Wildland Fire* 24(7), 883–891.

USGCRP (US Global Change Research Program). 2014. "Climate change impacts in the United States: The third national climate assessment." J. M. Melillo, T. C. Richmond, and G. W. Yohe (eds.), *US Global Change Research Program*. DOI:10.7930/J0Z31WJ2.

This page intentionally left blank

CHAPTER 2
A CHANGING CLIMATE: PROBLEM DEFINITION

2.1 SIGNIFICANCE OF CHANGES IN WEATHER AND CLIMATE

Weather, climate, and their extremes are factors in civil engineering design and practice. Weather is defined as "the state of the atmosphere with respect to wind, temperature, cloudiness, moisture, pressure, etc." (NOAA 2013a). Weather generally refers to short-term variations on the order of minutes to about 15 days (NSIDC 2012). Climate, conversely, "is usually defined as the average weather, or more rigorously, the statistical description in terms of the mean and variability of relevant quantities over a period ranging from months to thousands or millions of years" (IPCC 2014a). Changes in the statistical description of those relevant quantities that take place over periods fewer than 30 years are generally referred to as *climate variability*. Changes that persist for 30 years or more are generally referred to as *climate change* and can be the effect of a variety of drivers, including human activity. For the purposes of engineering practice, the nature of the drivers of climate variability is most relevant as an indicator of the persistence of trends and their projection.

Engineering design is primarily concerned about extremes. The IPCC defines an *extreme weather event* as "an event that is rare at a particular place and time of year" (IPCC 2012). Extreme weather varies from region to region. An *extreme climate event* would be a pattern of extreme weather that persists for some time, such as a season. Drought or heavy precipitation in a season are examples of such events (IPCC 2012). Climate scientists and civil engineers have differing views on what statistically constitutes an extreme event. The IPCC states that an extreme weather event would "normally be as rare as or rarer than the 10th or 90th percentile of the observed probability

density function." However, in civil engineering, *rare* is often defined in terms of an acceptable frequency of failure. Large dams may be designed for events with a mean recurrence interval (MRI) of about 10,000 years that denotes an annual probability of exceedance of 0.0001. Statistical nonstationarity in climate and weather extremes indicates that the AEP will be more meaningful than MRI and is used herein. Flood risk management is typically concerned with events with MRIs of 100 to 500 years (AEPs of 0.01 to 0.002). Transportation and stormwater design is concerned with events that occur more frequently, coming closer to the IPCC definition.

2.2 CONSENSUS ON OBSERVED CHANGES IN HISTORICAL CLIMATE

Since 2012, a series of reports of significance regarding the nature and magnitude of climate change on a global and national scale have been released. These reports form the technical basis of discussions in this manual about our current understanding of past and future climate change.

In 2012, the IPCC released *Special Report on Managing the Risks of Extreme Events and Disasters to Advance Climate Change Adaptation* (SREX) (IPCC 2012). Table 2-1 presents a summary of observed and projected changes to physical impacts that could affect infrastructure on a global scale. The findings of SREX were updated and largely confirmed by the IPCC in 2013 when it released *Climate Change 2013: The Physical Science Basis* (IPCC 2013a). They were updated again in 2014 when IPCC released *Climate Change 2014: Impacts, Adaptation, and Vulnerability. Part A: Global and Sectoral Aspects* (IPCC 2014a) and *Climate Change 2014: Synthesis Report* (IPCC 2014b). Climate change in the United States was thoroughly reviewed in a separate effort, led by the US Global Change Research Program (USGCRP), which released *Climate Change Impacts in the United States: The Third National Climate Assessment* (USGCRP 2014) and *Climate Science Special Report: Fourth National Climate Assessment*, Volume I (USGCRP 2017). These US-specific assessments provide more up-to-date information about the state of knowledge of changing conditions at regional levels of the United States, but the broader trends are generally consistent across this body of work.

These works document and assess the results of thousands of individual published journal articles published prior to 2012 that report findings and conclusions of thousands of independent examinations of scientific data regarding multiple aspects of the Earth's climate. On the basis of that assessment, the IPCC in 2013 concluded that the Earth's climate is changing in several observable ways (IPCC 2013a, provided in Figure 2-1). Note that subsequent analyses published separately or as part of a more recent assessment may suggest nuanced changes to Table 2-1. However, it is beyond the scope of this book to attempt to unilaterally update Table 2-1, and given that

Table 2-1. Summary of Observed and Projected Changes That May Affect Engineering on a Global Scale.

Physical impact	Observed changes	Projected changes
Temperature	*Very likely* decrease in number of unusually cold days and nights at the global scale. *Very likely* increase in number of unusually warm days and nights at the global scale. *Medium confidence* in increase in length or number of warm spells or heat waves in many (but not all) regions. *Low or medium confidence* in trends in temperature extremes in some subregions due either to lack of observations or varying signal within subregions.	*Virtually certain* decrease in frequency and magnitude of unusually cold days and nights at the global scale. *Virtually certain* increase in frequency and magnitude of unusually warm days and nights at the global scale. *Very likely* increase in length, frequency, and/or intensity of warm spells or heat waves over most land areas.
Precipitation	*Likely* statistically significant increases in the number of heavy precipitation events (e.g., 95th percentile) in more regions than those with statistically significant decreases, but strong regional and subregional variations in the trends.	*Likely* increase in frequency of heavy precipitation events or increase in proportion of total rainfall from heavy falls over many areas of the globe, in particular in the high latitudes and tropical regions, and in winter in the northern mid-latitudes.
Winds	*Low confidence* in trends due to insufficient evidence.	*Low confidence* in projections of extreme winds (with the exception of wind extremes associated with tropical cyclones).

Table 2-1. (Continued)

Physical impact	Observed changes	Projected changes
Tropical cyclones	*Low confidence* that any observed long-term (i.e., 40 years or more) increases in tropical cyclone activity are robust, after accounting for past changes in observing capabilities.	*Likely* decrease or no change in frequency of tropical cyclones. *Likely* increase in mean maximum wind speed, but possibly not in all basins. *Likely* increase in heavy rainfall associated with tropical cyclones.
Extra-tropical cyclones	*Likely* pole-ward shift in extratropical cyclones. *Low confidence* in regional changes in intensity.	*Likely* impacts on regional cyclone activity but low confidence in detailed regional projections due to only partial representation of relevant processes in current models. Medium confidence in a reduction in the numbers of mid-latitude storms.
Droughts	*Medium confidence* that some regions of the world have experienced more intense and longer droughts, in particular in southern Europe and West Africa, but opposite trends also exist.	*Medium confidence* in projected increase in duration and intensity of droughts in some regions of the world, including southern Europe and the Mediterranean region, central Europe, central North America, Central America and Mexico, northeast Brazil, and southern Africa. Overall *low confidence* elsewhere because of insufficient agreement of projections.

Floods	*Limited to medium evidence* available to assess climate-driven observed changes in the magnitude and frequency of floods at regional scale. Furthermore, there is *low agreement* in this evidence, and thus overall low confidence at the global scale regarding even the sign of these changes. *High confidence* in trend toward earlier occurrence of spring peak river flows in snowmelt- and glacier-fed rivers.	*Low confidence* in global projections of changes in flood magnitude and frequency because of insufficient evidence. *Medium confidence* (based on physical reasoning) that projected increases in heavy precipitation would contribute to rain-generated local flooding in some catchments or regions.*Very likely* earlier spring peak flows in snowmelt- and glacier-fed rivers.
Extreme sea-level and coastal impacts	*Likely increase* in extreme coastal high water worldwide related to increases in mean sea level in the late twentieth century.	*Very likely* that mean sea-level rise will contribute to upward trends in extreme coastal high water levels. *High confidence* that locations currently experiencing coastal erosion and inundation will continue to do so due to increasing sea level, in the absence of changes in other contributing factors.
Other impacts (landslides and cold regions)	*Low confidence* in global trends in large landslides in some regions. *Likely* increased thawing of permafrost with likely resultant physical impacts.	*High confidence* that changes in heavy precipitation will affect landslides in some regions. *High confidence* that changes in heat waves, glacial retreat, and/or permafrost degradation will affect high-mountain phenomena such as slope instabilities, mass movements, and glacial lake outburst floods.

Source: IPCC, Table 3.1 (2012) http://www.ipcc-wg2.gov/SREX).

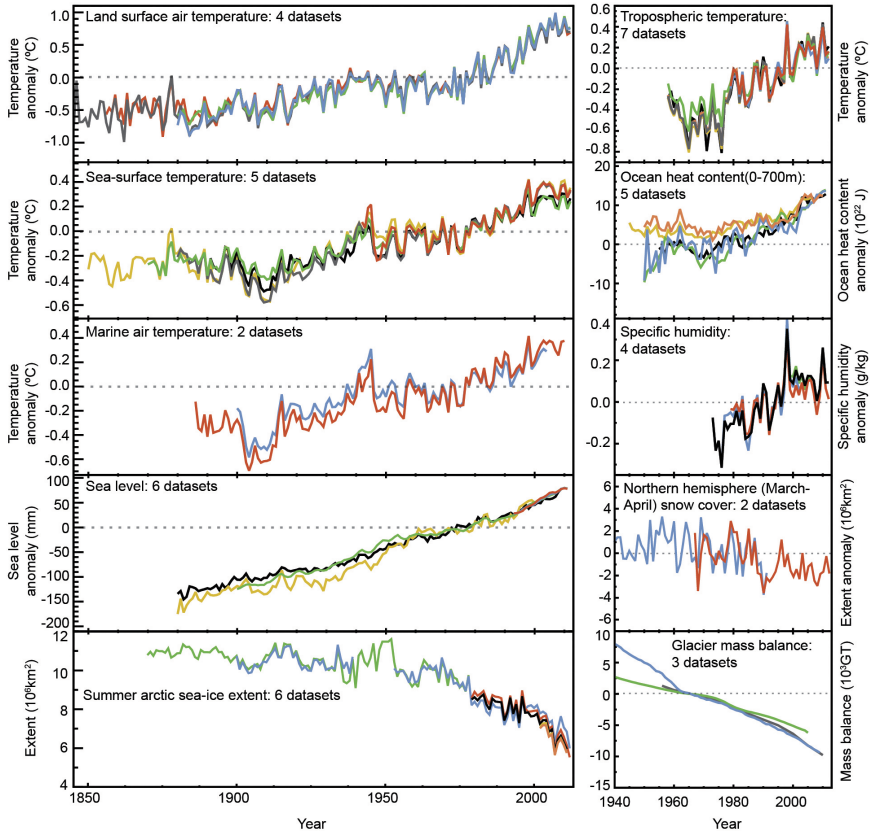

Figure 2-1. Multiple independent indicators of a changing global climate. Each line represents an independently derived estimate of change in the climate element. In each panel, all data sets have been normalized to a common period of record. Source: IPCC (2013a).

the table is provided to simply help inform the reader as to the wide variety of changes observed and expected, such an effort is not required. Engineers interested in the most up-to-date information about changes in any one parameter may wish to monitor the assessment literature accordingly.

2.2.1 Temperature, Precipitation, and Sea Level

Although the scientific literature covers many aspects of the response of climate systems to changes in the drivers of climate change, temperature, precipitation, and sea-level changes can be considered the most fundamental to engineering practice.

IPCC (2013a) concluded that "It is certain that global mean surface temperature has increased since the late 19th century. Each of the past three decades has been successively warmer at the Earth's surface than all the previous decades in the instrumental record, and the first decade of the 21st century has been the warmest."

The implications of the global average temperature increase for changes in precipitation are less clear at both observational and theoretical levels. For example, IPCC (2013a) concluded that "Confidence in precipitation change averaged over global land areas since 1901 is low for years prior to 1951 and medium afterward. Averaged over the mid-latitude land areas of the Northern Hemisphere, precipitation has likely increased since 1901 (medium confidence before and high confidence after 1951). For other latitudinal zones area-averaged long-term positive or negative trends have low confidence due to data quality, data completeness or disagreement amongst available estimates." In other words, understanding recent changes in precipitation and related hydrologic response at the project scale requires more site-specific analysis (see Chapter 4).

Conversely, the increase in the global mean surface temperature does correlate with an observed increase in ocean temperature and heat content and a related observed rise in sea level. IPCC (2013a) found that "It is virtually certain that the upper ocean (above 700 m) has warmed from 1971 to 2010, and likely that it has warmed from the 1870s to 1971" and "It is virtually certain that upper ocean (0 to 700 m) heat content increased during the relatively well-sampled 40-year period from 1971 to 2010." This increase in the observed global ocean temperature record, as well as observed changes in sea-ice extent, led IPCC (2013a) to conclude that "Ocean warming dominates the global energy change inventory. Warming of the ocean accounts for about 93% of the increase in the Earth's energy inventory between 1971 and 2010 (high confidence), with warming of the upper (0 to 700 m) ocean accounting for about 64% of the total." Observed increases in land surface and ocean temperature and ocean heat content correlate with the observed increase in sea level. Loss of continental ice mass and expansion of ocean waters related to these temperature changes are consistent with observed changes in sea level reported by IPCC (2013a), which stated that "Global mean sea level (GMSL) has risen by 0.19 [0.17 to 0.21] m over the period 1901–2010, calculated using the mean rate over these 110 years, based on tide gauge records and since 1993 additionally on satellite data. It is very likely that the mean rate was 1.7 [1.5 to 1.9] mm yr^{-1} between 1901 and 2010 and increased to 3.2 [2.8 to 3.6] mm yr^{-1} between 1993 and 2010."

2.2.2 Long-term Average Versus Extreme Events

The IPCC in its most recent global assessment reports (IPCC 2014a) state that "Warming of the climate system is unequivocal, and since the 1950s,

many of the observed changes are unprecedented over decades to millennia. The atmosphere and ocean have warmed, the amounts of snow and ice have diminished, sea level has risen, and the concentrations of greenhouse gases have increased." NCA reached a similar conclusion (USGCRP 2014).

As can be discerned from Table 2-1, the vast majority of research into climate change focuses on understanding the role of various climate drivers (e.g., changes in greenhouse gases, aerosols, solar irradiance) in terms of changes in global and regional conditions. Although the resulting insights are important for policy making and scientific understanding, they are not always well aligned with the needs of practicing engineers.

Although large-scale trends in the observed record may suggest that conditions at the project site may change over the design life of an engineered system or structure, there remain considerable challenges in quantifying changes in extreme events at the project scale (ASCE 2015). Changes in the mean values of various observations of weather and climate systems may belie more complex changes in the statistical description of those observations, including changes in variability or skewness (see Figure 2-2).

As discussed in the following sections, well-mixed GHGs can be assumed to exert a more or less uniform forcing globally. However, there are regional differences in other external forcings [e.g., solar radiation depends on latitude, sources of aerosols are not uniformly distributed (IPCC 2013b)]. As a consequence, global trends may simply be an indicator of local or regional change, which may need to be analyzed as part of an engineering study.

2.3 UNDERSTANDING DRIVERS OF CLIMATE CHANGE

The significant global investment in understanding the Earth's climate and the causes of observed and potential changes in it is driven by a desire to determine an appropriate mix of actions and policies that would allow society to avoid the most harmful impacts of those changes. The current state of understanding of the drivers of climate change are important for engineering practice because they also inform an understanding of sources of uncertainty in projections of future climate. One of the most common measures of the impact of changes in the various drivers of climate change is *radiative forcing*. IPCC (2015) described RF as the net change in the energy balance of the Earth system owing to some imposed perturbation. RF is usually measured in watts per square meter (w m^{-2}) averaged over a particular time interval, and it quantifies the energy imbalance that occurs when the perturbation takes place. RF is a measure of the net change in the energy balance of the Earth system in response to some external perturbation, with positive RF leading to warming and negative RF to cooling. The RF concept is valuable for comparing the influence of most individual agents affecting

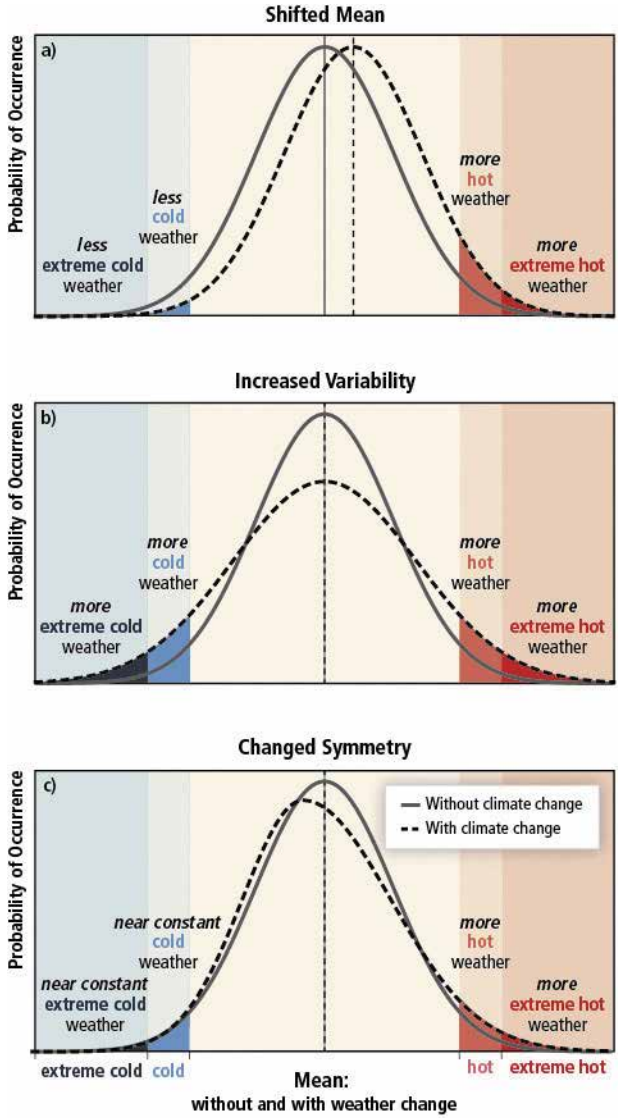

Figure 2-2. The effect of changes in temperature distribution on extremes. Different changes in temperature distributions between present and future climate and their effects on extreme values of the distributions: (a) effects of a simple shift of the entire distribution toward a warmer climate; (b) effects of increased temperature variability, with no shift of the mean; and (c) effects of the shape of the distribution, which in this example is an increased asymmetry toward the hotter part of the distribution.
Source: IPCC (2012), Table 3-1 (reproduced with permission).

the Earth's radiation balance. Effective RF (ERF) is used to quantify the impact of some forcing agents that involve rapid adjustments of components of the atmosphere and surface that are assumed constant in the RF concept. As shown in Figure 2-3, several physical phenomena contribute to RF associated with changes in global mean surface temperature. Of these phenomena, the two overwhelming contributors to climate change are changes in the concentrations of well-mixed GHGs and atmospheric aerosols. These contributors tend to affect the Earth's energy balance on different time scales and in opposite ways.

2.3.1 Well-mixed GHGs

IPCC (2013a) defines as *well mixed* those GHGs that are sufficiently mixed throughout the troposphere such that concentration measurements from a few remote surface sites can characterize the climate-relevant atmospheric burden, although these gases may still have local variation near sources and sinks and even small hemispheric gradients (e.g., GHG concentrations are slightly higher in the northern hemisphere relative to the southern hemisphere). Global forcing per unit emission and emission metrics for these gases thus do not depend on the geographic location of the emission, and forcing calculations can assume even horizontal distributions. These gases, or a subset of them, have sometimes been referred to as *long-lived greenhouse gases*, as they are well mixed, because their atmospheric lifetimes are much greater than the timescale of a few years for atmospheric mixing, but the physical property that causes the aforementioned common characteristics is more directly associated with their mixing within the atmosphere.

2.3.2 Aerosols

As a class, *atmospheric aerosols* tend to offset or negate the influence of greenhouse gases, because they either scatter or absorb both short-wave and long-wave solar radiation (IPCC 2013a). However, aerosols are typically made up of larger particles of dust or various organic compounds, which remain suspended in the atmosphere for relatively short periods (decades as opposed to centuries or millennia for GHGs). Thus, unless these aerosols are introduced constantly, their concentration in the atmosphere changes through time, as does their RF.

2.4 PROJECTED CHANGES IN FUTURE CLIMATE

In 2013, the IPCC found that "Global surface temperature change for the end of the 21st century is likely to exceed 1.5°C relative to 1850 to 1900 for

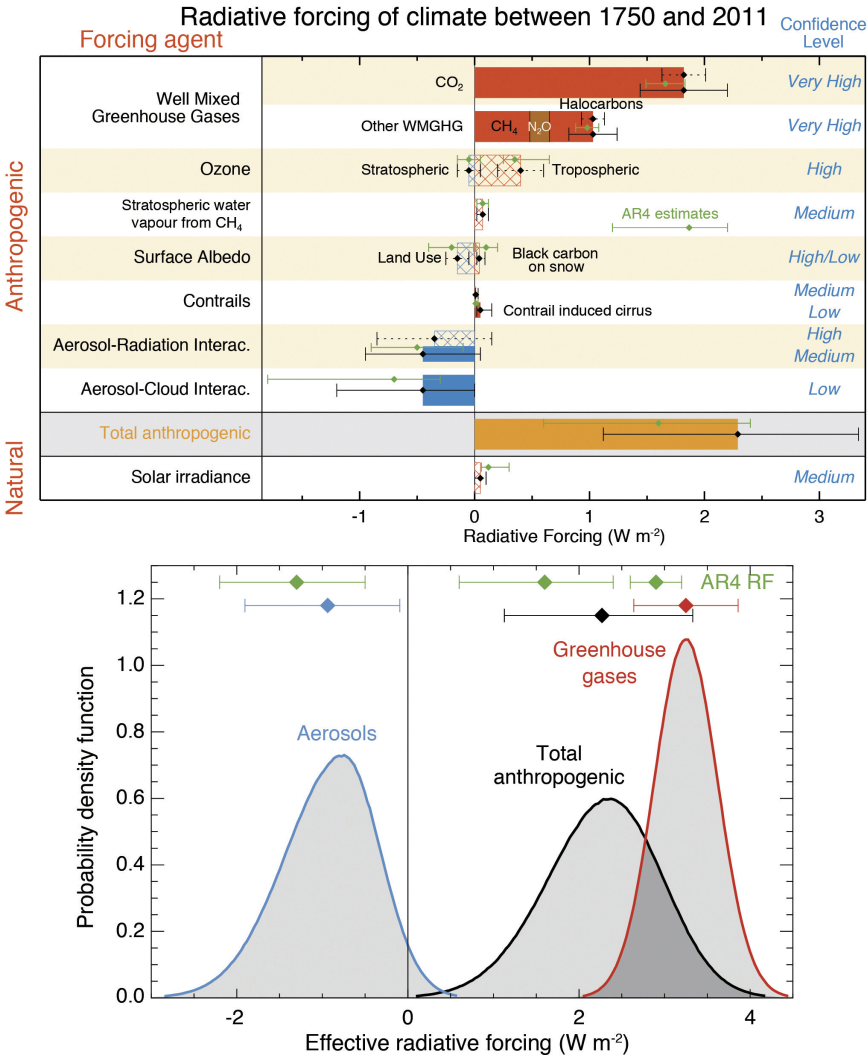

Figure 2-3. RF and ERF of climate change during the industrial era. Top: Forcing by concentration change between 1750 and 2011, with associated uncertainty range (solid bars are ERF, hatched bars are RF, green diamonds and associated uncertainties are for RF assessed in AR4). Bottom: PDFs for ERF, aerosols, GHGs, and total.
Source: IPCC Technical Summary, Figure 6 (IPCC 2013d).

all RCP scenarios except RCP2.6. It is likely to exceed 2°C for RCP6.0 and RCP8.5, and more likely than not to exceed 2°C for RCP4.5. Warming will continue beyond 2100 under all RCP scenarios except RCP2.6. Warming will continue to exhibit interannual-to-decadal variability and will not be regionally uniform" (IPCC 2013a, as provided in Figure 2-4).

Similar increases in the rate of SLR are also expected. Under all RCP scenarios, the rate of SLR is very likely to exceed that observed from 1971 to 2010 (see Figures 2-1 and 2-5).

USGCRP (2017) concluded that "The frequency and intensity of heavy precipitation events are projected to continue to increase over the 21st century (high confidence). Mesoscale convective systems in the central United States are expected to continue to increase in number and intensity in the future (medium confidence). There are, however, important regional and seasonal differences in projected changes in total precipitation: the northern United States, including Alaska, is projected to receive more precipitation in the winter and spring, and parts of the southwestern United States are projected to receive less precipitation in the winter and spring (medium confidence)."

Practicing engineers, as well as planners, land managers, and others, face a growing demand to understand and incorporate changes in weather and

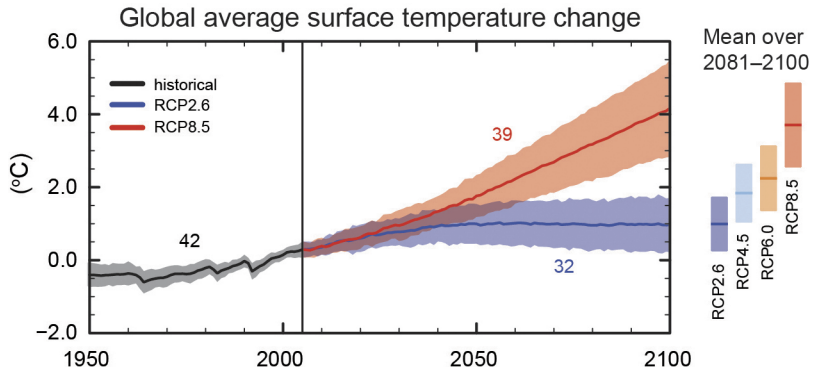

Figure 2-4. CMIP5 multimodel simulated time series from 1950 to 2100 for changes in global annual mean surface temperature relative to 1986 to 2005. Time series of projections and a measure of uncertainty (shading) are shown for scenarios RCP2.6 (purple shading) and RCP8.5 (orange shading). Black (gray shading) is the modeled historical evolution using historical reconstructed forcings. The mean and associated uncertainties averaged over 2081 to 2100 are given for all RCP scenarios as colored vertical bars. The numbers of CMIP5 models used to calculate the multimodel mean are indicated.
Source: Modified from IPCC (2013d).

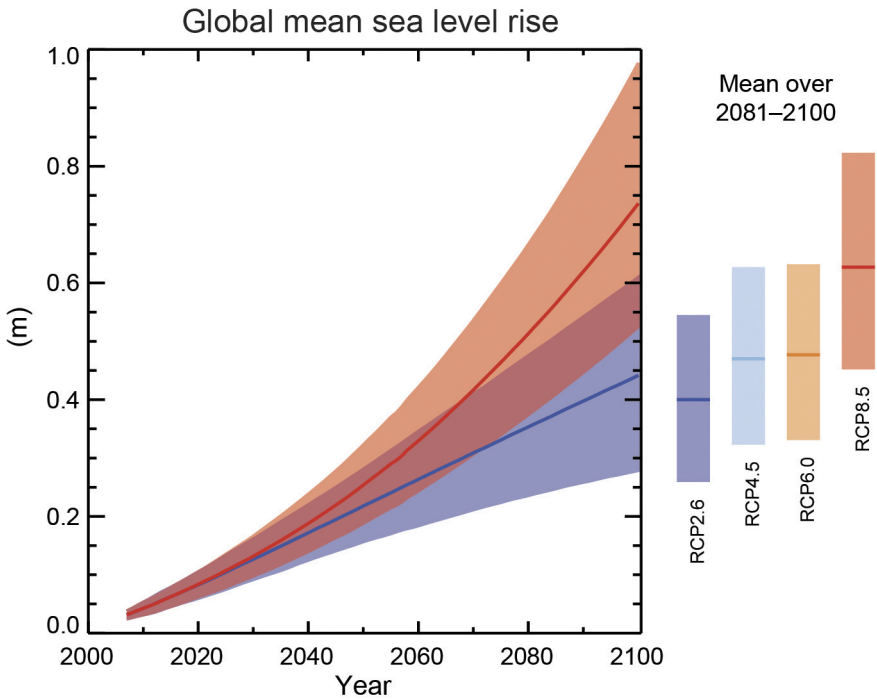

Figure 2-5. Projections of global mean SLR over the 21st century relative to 1986 to 2005 from the combination of the CMIP5 ensemble with process-based models for RCP2.6 and RCP8.5. The assessed likely range is shown as a shaded band. The assessed likely ranges for the mean over the period 2081 to 2100 for all RCP scenarios are given as colored vertical bars, with the corresponding median value given as a horizontal line.
Source: IPCC (2014a).

climate in project design and implementation. This need to anticipate future trends drives attempts to quantifiably simulate climatic processes through numerical modeling. Climate models combine scientific knowledge from a number of disciplines, including atmospheric sciences, oceanography, cryospheric sciences, hydrology, ecosystem modeling, and others to simulate past, present, and future climates. They are the best tools that climate science possesses to make quantitative projections of global, continental-scale climatic conditions under anthropogenic forcing. Their value at the project level, however, is the subject of much discussion and debate.

IPCC (2012) lists three main sources of uncertainty in the projections: (1) the natural variability of climate, (2) uncertainties in climate model response or sensitivity to anthropogenic and natural forcing, and (3) projections

of future emissions and other natural and anthropogenic climate drivers. The uncertainty in the response of the climate system to these drivers is manifest in the structure and parameter choices in climate models. Uncertainty in climate model parameters include the uncertainty in the representation of physical processes, such as cloud formation and land-cover effects, which largely occur at spatial scales smaller than the large spatial scales used in climate models. Some examples of complex and nonlinear feedbacks include biogeographical processes, such as changes in the distribution and composition of vegetation, land-use changes caused by humans, and deep-ocean circulation effects on ocean temperature and salinity. Barsugli et al. (2009) state: "(1) Climate model simulations have generally improved since the early 1990s in their ability to simulate the observed mean climate and seasonal cycle; (2) Despite the increase in model performance over the last two decades, the range of climate projections across all models has not appreciably narrowed; (3) The actual uncertainty of global and regional climate change (as scientists understand it) is larger than the range simulated by the current generation of models."

Assumptions about future greenhouse gas emissions are used as input to GCMs. The emissions are converted into atmospheric concentrations of greenhouse gases using IAMs that have extremely simplified representations of atmospheric and oceanic fluid dynamics. The GHG concentrations are then input into the GCMs, which simulate the effect of those concentrations on climate. Future GHG emissions depend on future social and economic development, land-use changes, population changes, and technological innovation. However, these factors are difficult to predict and highly uncertain. The IPCC developed scenarios to represent a wide range of the main economic, demographic, and technological driving forces that will determine future GHG emissions, but it did not assign probabilities to these scenarios (IPCC 2000). Over the last few years, actual emissions have equaled or exceeded the most *extreme* emission scenarios used for previous IPCC reports (Peters et al. 2013).

The most current generation of climate scenarios did not start with socioeconomic scenarios; instead, they were based on GHG concentration pathways (time-dependent values in the future) that spanned the possibilities generated by a number of IAMs. The names of the pathways were determined by their RF at the end of the 21st century—RF being the change in the balance between incoming and outgoing radiation caused by changes in GHG concentrations and other atmospheric constituents, whereas other aspects of the atmosphere were held constant. An RCP was associated with each of the RF trajectories (Moss et al. 2010). In total, a set of four pathways (Figure 2-6) were produced that would lead to RF levels of 8.5, 6.0, 4.5, and 2.6 w m^{-2} by the end of the century.

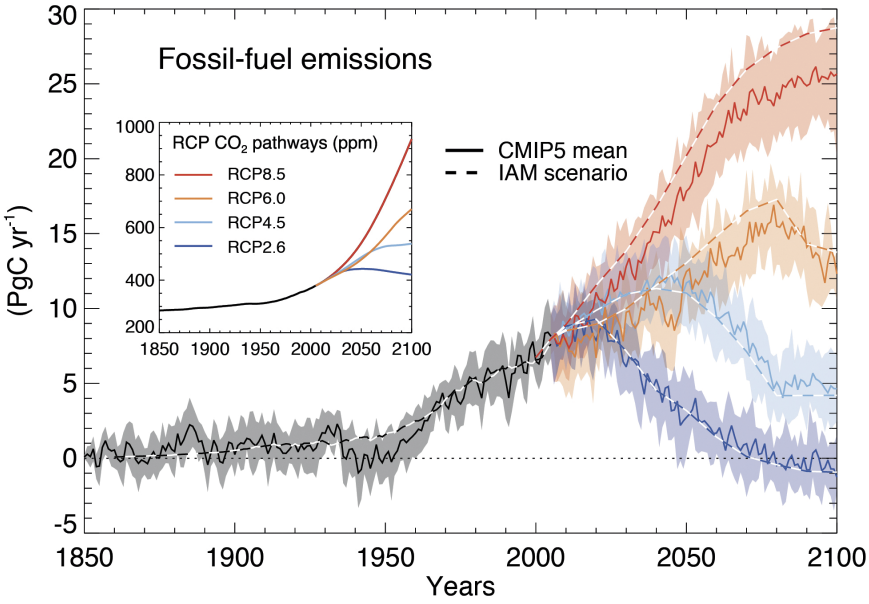

Figure 2-6. Projections of fossil fuel emissions in picograms of carbon per year (PgC yr–[1]) through time as reflected in the RCPs used to drive model and project climate response. The significant difference in emissions each pathway represents underscores the fact that energy policy and technology develop represent significant sources of uncertainty in future climate projections.
Source: Modified from IPCC (2013), Figure TS-9.

2.5 IMPLICATIONS FOR INFRASTRUCTURE AND SYSTEM PERFORMANCE

Changes in environmental conditions typically associated with weather and climate can affect structures and engineered systems in a variety of ways. As discussed previously, engineering practice calls for an understanding of the tails of the distribution of extreme events as a function of probability of exceedance or return frequency. Many ASCE standards appear to be sensitive to changes in weather and climate extremes and especially by changes in the probability of exceedance for known points of failure (see Appendix B). Of particular significance is the potential for changes in weather and climate extremes that can lead to unanticipated changes in environmental loads covered under ASCE/SEI 7 and ASCE 24.

2.5.1 Changes in Rain, Snow, Ice, Wind, Flood, and Impact Loads

ASCE/SEI 7 *Minimum Design Loads for Buildings and Other Structures*, published in 2010 and more recently in 2016, provides requirements for general structural design and includes means for determining dead, live, soil, flood, snow, rain, atmospheric ice, earthquake, and wind loads, as well as their combinations, which are suitable for inclusion in building codes and other documents. One of the most widely used ASCE standards, ASCE/SEI 7 is also referenced in many other ASCE standards when those standards discuss aspects of design or construction that may be affected by loads it covers. For example, Section 2.1 of ASCE/ANSI 3 *Standard for the Structural Design of Composite Slabs* specifies that "Loads not covered by the building code shall be in accordance with ASCE/SEI 7." Furthermore, the International Building Code adopts ASCE/SEI 7 by reference for virtually all its design load provisions, which amplifies the impact of ASCE 7 on the built environment in the United States and elsewhere.

Rain loads are primarily of concern to the integrity of roofs in engineered structures. Although understanding how changes in rainfall intensity, duration, and frequency may intuitively raise concerns about the potential for rain load to increase the probability of exceedance for key parameters, understanding those changes may be less significant than expected. The key element in determining the load the roof may experience at any time is the potential for ponding. Ponding is limited by roof drainage systems. Thus, even if rainfall intensity, frequency, or duration were to exceed the values used in the design specification, proper inclusion of secondary drainage systems may limit the potential for failure. In regions where increases in precipitation may be a concern for existing structures, retrofitting or adding of roof drainage may be appropriate. Studies of failure for such structures could determine if the roof would be stable under conditions where the drainage systems fail or are overwhelmed. In the event such studies show the potential for failure, modifications to the roof could be designed in a manner similar to that for new structures.

Snow and ice loads represent a more complex challenge, because ground snow loads or icing conditions may change through time with changing temperature and precipitation patterns, changes that may become more significant. In some areas, increases in wintertime temperatures may decrease the potential for snowfall accumulation, but concomitant changes in precipitation patterns may lead to an overall increase in accumulation from specific storm events. Furthermore, areas that currently are too cold and dry to experience freezing rain may begin experiencing icing events as temperature conditions change. For example, a comparison of Figures 2-7(a) and 2-7(b) suggests that some potential exists for a northward shift in the ice loading in the upper Midwest.

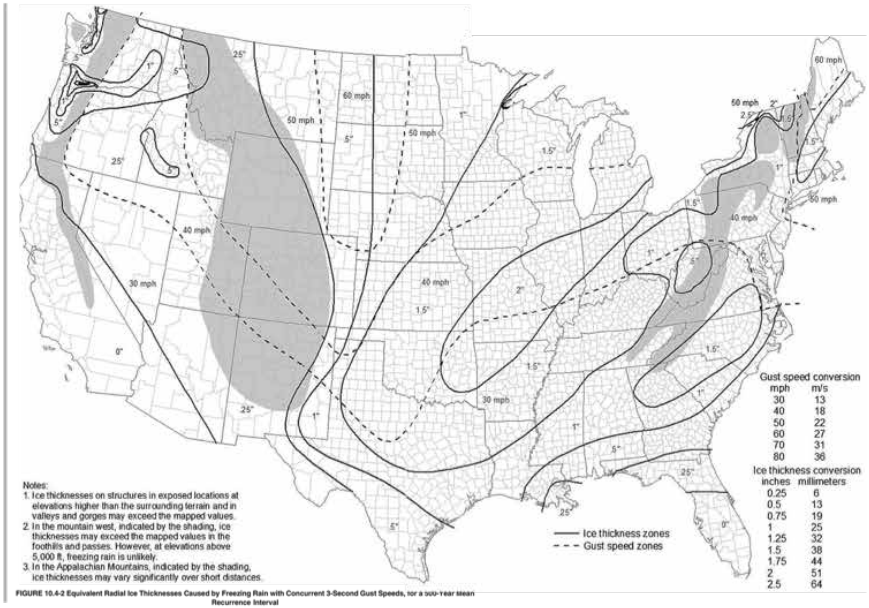

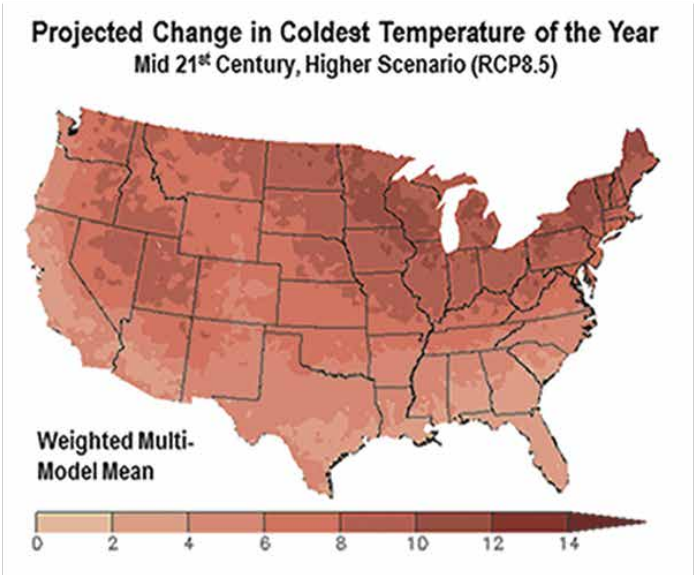

Figure 2-7. (a) Ground snow loads, Pg for the United States, lb/ft². Source: ASCE/SEI 7-10 (2010), *and (b) Projected increase in annual average temperatures by mid-century (2041–2070) as compared to 1971 to 2000. Source: USGCRP (2017).*

Wind loads represent similar challenges because peak wind velocities will be associated with individual storms. Although the current literature does not show a definitive trend in peak wind velocity and there are theoretical arguments for the maximum wind velocity associated with individual storms, storm frequency and track may change in a complex manner as climate changes. Areas not prone to tornado or hurricanes may experience those events more often. In addition, it is common practice for tall structures to have a site-specific wind tunnel study that supplements or replaces the code-defined general loads. These studies not only take into account the structural response of the building being designed but also the dynamic effects of the surrounding structures as the wind is channeled or buffeted.

Conversely, flood load definition is lagging. Although the effects of flood load on coastal structures and the use of coastal modeling in these regions is commonplace, there is missing refinement for baseline concepts of storm surge loading in dense urban areas. The state-of-the-practice for many engineers is simply to apply the formulas of ASCE/SEI 7, which produces the potential for both conservative and nonconservative results. Some specific areas where future research and development are needed include the following:

- Flood hazard identification is inadequate. NFIP maps are currently the major source of information on flood hazards. They do not take velocity into account explicitly, which is the major source of structural damage and scour to buildings and bridge foundations. NFIP maps were developed for the purpose of insurance underwriting, not for engineering analysis, and they are out of date in many locations.
- The average velocity of water (ASCE/SEI 7-10, Equation 5.4-1). There is very little data available on this subject without access to a detailed hydraulic model–typically unavailable to urban building engineers. Even if a hydraulic model is available, it is likely to be on a scale that will miss micro-phenomena. Like wind, floodwaters experience higher velocities and local vortices as they channel through a dense city center. Granular hydraulic modeling must be performed to understand this velocity, which is then squared, potentially leading to significantly nonconservative forces on a local building element.
- Wave loads (ASCE/SEI 7-10, Section 5.4.4). As with water velocity, an urban building engineer likely does not have access to a detailed coastal model and will rely on ASCE/SEI 7 to define wave loads. In this case, the loading is very conservative, because it represents the maximum load that could be seen should idealized wave conditions exist. Rarely is this idealized condition actually possible in an urban environment, leading to much higher calculated loads. When designing a new structure, it is easier to incorporate robust structural systems, but this approach can lead to impossible design conditions for

a building retrofit, because the wave load generally dwarfs the hydrostatic, hydrodynamic, and debris loads. In addition, in ASCE/SEI 7-10, Section 2.3.3 provides magnifications of the flood load depending on the coastal location. Guidance needs to be provided on the use of these load combinations when site-specific studies or flood elevations beyond the base flood elevation are considered to ensure loads are not excessively magnified or double-counted.

- Impact loads (ASCE/SEI 7-10, Section 5.4.5). The code defers simply to the use of a rational approach that is described further in Appendix C. Research cited applies common practices for suburban-type debris in riverine or coastal applications. Debris in urban areas will be significantly different in terms of weight and cross-sectional area of impact, whether it will be channeled around cities at right-angled streets (such that a modified orientation coefficient is required for each building face), and whether it will hit a variety of resisting elements. These factors require a much clearer definition of the maximum response ratio and fundamental period. Depending on how the engineer interprets and applies each of these factors, there is a potential either to significantly overestimate or underestimate an urban debris impact load.

A further discussion on these factors and ideas for urban environments is presented in Chapter 6.

2.5.2 Changes in Surface and Groundwater Hydrology

ASCE/SEI 24, *Flood Resistant Design and Construction*, published in 2014, provides minimum requirements for the design and construction of structures located in flood hazard areas and subject to building code requirements. Identification of flood-prone structures is based on flood hazard maps, studies, and other public information. This standard applies to new structures, including subsequent work, and to work classified as substantial improvement of existing structures that are not historic. Standard ASCE/SEI 24-14 introduces a new concept, Flood Design Class, that bases requirements for a structure on the risk associated with unacceptable performance.

The complex interaction between snowfall, runoff, infiltration, and land cover makes understanding how potential changes in rainfall may change flood probability or groundwater elevation difficult to quantify. Changes in land development and utilization patterns affect the surficial characteristics of ground cover and may amplify the impact of changes in precipitation extremes. Some regions of the United States are expected to experience an increase in both the wettest five-day total and the number of consecutive dry days (Polade et al. 2014). This suggests that although the total amount

of precipitation received per year may not change significantly, that rainfall is coming in fewer but larger events, separated by periods of little or no rain (see Figure 2-7). Continued changes of this nature will make the need for periodic updates to products such as NOAA *Atlas 14: Precipitation-Frequency Atlas of the United States* essential (NOAA 2006, 2008, 2011a, 2011b, 2011c, 2012b, 2013b, 2013c, 2014, 2015).

2.5.3 Changes in Soil Properties and Associated Mechanics

The focus of much climate change discussion has been the identification of primary factors contributing to global temperature rise and mitigation of their effects. However, it is equally important to understand the effects of climate change on geotechnical infrastructure and natural soils. Because earthen materials and structures support and protect other built systems, changes in the loading and performance of geotechnical structures can have serious, widespread effects on all other types of civil infrastructure. Climate change impacts on soil–atmospheric interactions, soil properties, and loading conditions, thus directly affecting the performance of earthen structures and natural slopes. Figure 2-8 provides a summary of key interactions between geotechnical infrastructure and the atmosphere. Climate change will influence these interactions through increased temperatures, higher sea levels, and increased frequency and intensity of precipitation events, such as drought, rainfall, and flood (Vardon 2015).

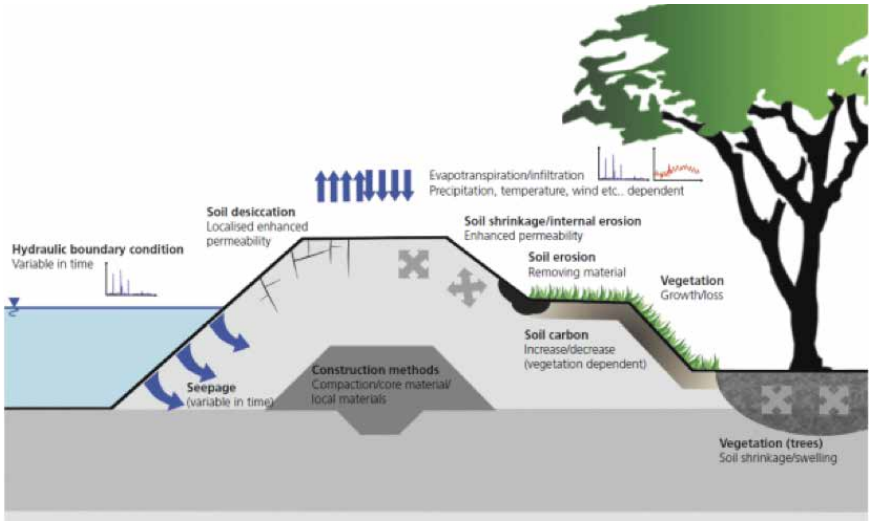

Figure 2-8. Potential climatic interactions and earthen structures and slopes. Source: Vardon (2015), with permission from ICE Publishing.

Based on current climate change trends, exposure to the projected atmospheric conditions is unfavorable and may cause earthen structures to weaken through strength reduction, drying, soil desiccation cracking, shrinkage, microbial oxidation of soil organic matter, fluctuation in the groundwater table, significant land and surface erosion, and highly dynamic pore pressure changes (e.g., Dunbar et al. 2007, Vicuña et al. 2006, Dyer et al. 2009, Port and Hoover 2011, Brooks et al. 2012, Bates and Lund 2013, ASCE 2015). These processes affect the soil's strength properties and the structural mechanics within the body of the structure (slope, levee, etc.). The effect on soil strength properties is primarily related to changes in soil moisture and suction within the unsaturated zone. A summary of major climate change features and their effects on existing infrastructure and natural slopes can be found in Table 2-2. A more detailed discussion is provided in the following paragraphs.

Possible changes in precipitation include variation in total rainfall amounts, as well as an increased occurrence of extreme events, such as intense rainfall, flood, or drought. An increase in the total precipitation will increase the level of saturation within the unsaturated zone and may decrease the depth to the water table. Resulting increases in pore pressure may decrease suction, lowering the shear strength of soil, possibly resulting in failure (Clarke et al. 2006, Dehn et al. 2000, Lee and Jones 2004). Conversely, a decrease in total precipitation will lower the level of saturation, increasing the soil's effective strength through higher suction. However, extended drought conditions may result in a loss of these improvements because of excessive soil drying, resulting in a decreased contribution from suction, desiccation cracks, heavy shrinking, and loss of organic matter (Robinson and Vahedifard 2016).

High precipitation intensity can have a significant negative effect on natural slopes and geotechnical structures. Sudden increases in saturation will reduce the effect of suction, thus lowering the effective strength of the soil (Lu and Likos 2004). In addition, intense rainfall often causes erosion of surface materials, and it has also been associated with soil piping within slopes (Jones 2010). These processes may cause or enhance the failure of natural and built slopes (Hungr et al. 2005, Iverson et al. 2011). Furthermore, the effects of intense rainfall can be enhanced if preceded by an extended period of drought (Vahedifard et al. 2016). In addition, models have illustrated that under partially saturated conditions, even non-extreme above-average rainfall can result in slope failures such as shallow landslides (Leshchinsky et al. 2015). Because of this, expected changes in precipitation occurrence (e.g., storm duration, storm intensity, mix of storm types) are significant, because most geotechnical infrastructure in the United States is designed using IDF curves established under the stationary assumption (i.e., statistics of extreme events will not vary significantly over a long period). Because climate change is anticipated to influence precipitation

Table 2-2. Potential Impacts of Climate Change on Earthen Structures and Slopes.

Climate change feature	Fundamental impact	Practical impact
Increased temperature	Higher evaporation rate/soil drying	Increased suction, desiccation cracking, shrinkage
	SOC oxidation	Land subsidence
	Changes in vegetation amount;	Varied effect depending on type of vegetation
	Snow, ice, and permafrost melting	Reduced strength of arctic soils, release of entrapped carbon, increased risk of mass wasting at higher elevations
Decreased mean precipitation	Soil drying and water table lowering	Possible desiccation cracking and shrinkage, increase in suction
	Vegetation reduction	Loss of cover and increased risk of erosion
Increased Mean Precipitation	Soil wetting and water table rise	Decreasing suction leading to reduced shear strength
Drought	Extreme soil drying and water table lowering	Significant desiccation cracking and shrinkage, increased susceptibility to intense precipitation owing to increased permeability from cracking and shrinkage
Intense precipitation	Rapid soil wetting	Sudden changes in suction possible leading to heightened failure risk
	Overland flow	Possible erosion and mass wasting
Flood/ SLR	Large pore pressure increases; Soil wetting	Lowered suction within flood protection infrastructure owing to wetting, increased risk of multiple failure mechanisms, such as piping and overtopping, erosion

patterns, the resulting changes in the statistics of extreme events may render the use of stationary IDF curves and previous designs ineffective for the mitigation of risk (Vardon 2015).

Rainfall-triggered instabilities in artificially created and natural geotechnical structures are analyzed primarily using extreme precipitation estimates derived using the so-called stationary assumption (i.e., statistics of extreme events will not vary significantly over a long period). However, extreme precipitation patterns have been shown to vary substantially because of climate change, leading to unprecedented changes in the statistics of extremes, a notion known as *non-stationarity*. It has been shown that the use of stationary rainfall data can lead to underestimations in the hydromechanical behavior of natural and man-made earthen structures (Robinson et al. 2017, Vahedifard et al. 2017). The findings highlight the importance of site-specific assessments to quantify the potential impacts of climate change on the performance of current and future earthen structures. Rainfall-triggered landslides are widespread natural hazards that annually cause several millions of dollars in damage to property and infrastructure and occasionally cause loss of human life. Climatic trends have been shown to increase landslide activity by influencing extreme precipitation patterns (e.g., Coe and Godt 2012, Gariano and Guzzetti 2016). There are two major issues that obstruct our advancement in fully understanding how landslide processes are affected by a changing climate: (1) the high uncertainty in forecasting landslide activation owing to heavy precipitation, and (2) limitations in predicting precipitation and storm patterns at appropriate scales (e.g., Coe and Godt 2012). Moreover, landslide studies typically project the mean precipitation, because it is very difficult to estimate the variations in the frequency and magnitude of extreme rainfall events (e.g., Coe and Godt 2012). Although some more recent publications have used projected values of extreme precipitation, their use in project design is still being explored.

Extended precipitation events, both extreme and moderate, can cause flood conditions. Floods pose risks similar to those of extreme precipitation, with increased levels of erosion, soil wetting, and high pore pressures. Significantly, high water levels may cause overtopping of levees and dams, causing significant external erosion of the earthen structure. The possible changes in precipitation event occurrence may change the rate of flood occurrence, rendering existing flood protection infrastructure and planning insufficient (Vardon 2015). In addition, the increased pore pressures may cause piping and other forms of failure to occur. Similar risks are posed by SLR to coastal infrastructure. Although the effects of SLR will occur gradually, the sea will not recede like floodwaters, which steadily increases the risk for coastal communities.

Although the expected changes in precipitation and weather patterns are projected on the basis of changes in global temperatures, these increasing temperatures pose their own influence on geotechnical infrastructure

(IPCC 2014). Higher temperatures will likely speed evaporation and SOC oxidation (Davidson and Janssens 2006, Conant et al. 2011), although care is needed when projecting hydrologic response (Milly and Dunne 2011). Increased evaporation rates, combined with precipitation changes, will increase the frequency of pore pressure cycling, which has been known to cause strain softening and changes in permeability (Kovacevic et al. 2001, Potts et al. 1997, Nyambayo et al. 2004). In addition, increased evaporation rates owing to high temperatures may exacerbate the development of negative effects owing to drought conditions. Oxidation of SOC may cause land subsidence in highly organic peat soils and may cause an increased rate of SLR in some regions. SOC oxidation accounts for approximately 75% of the elevation loss in the California delta because of peat subsidence, whereas the other 25% is attributed to secondary consolidation and compaction of organic soils (Mount and Twiss 2005). In addition to these effects, temperature increases cause the melting of permafrost in arctic regions, greatly reducing soil strength, as well as melting ice and snow at high elevations, increasing the risk of mass wasting (NRC 2016, Gariano and Guzzetti 2016).

The possible effects of changes in atmospheric conditions presented in the previous paragraphs affect the potential failure modes of existing geotechnical infrastructure. The relationships among these effects and potential failure modes are summarized in Table 2-3.

2.5.4 Changes in Sea Level

Sea level is a complex and dynamic manifestation of a series of local, regional, and global geophysical processes (geologic, meteorologic, hydrologic, and climatic) that has profound implications for engineering practice at or near the shoreline. Simply defining a datum against which to measure sea surface elevation (or *sea level*) is a daunting challenge, and terms such as *shoreline*, *high tide*, *low tide*, and *coastal zone* vary in meaning from state to state. This manual, however, focuses on understanding how non-stationarity in weather and climate extremes may affect engineering practice, so this discussion will focus more narrowly on understanding the behavior of sea level under climate change, and it will discuss the most widely adopted methods for describing sea level at the project scale.

Global SLR, often referred to as eustatic SLR, reflects the balance of processes that affect the volume of water in the Earth's ocean basins. Because the Earth's hydrologic cycle is essentially closed, the volume is controlled by the amount of water that is sequestered in continental ice sheets and glaciers and the temperature of ocean water. Increases in the atmospheric concentration of GHGs and the resulting increase in global temperature drive an increase in sea level by melting continental ice sheets and glaciers, releasing more water to the ocean basins, as well as by warming sea water, resulting in thermal expansion, referred to as *steric effects* (NRC 2012).

Table 2-3. Relationships Between Atmospheric Events and Geotechnical Failure Modes.

Climate change feature	Impact on earthen structures/slopes	Potential failure modes affected
Increased temperature	Drying	Uplift
	Ice and snow melt at higher elevations	Slope stability failure
Decreased mean precipitation	Possible desiccation cracking	Piping, internal erosion, slope stability
	Shrinkage	Piping
	Loss of vegetation cover	Piping slope stability
Increased mean precipitation	Soil wetting and water table rise	Erosion, slope stability, piping
Drought	Elevated risk of impacts given for decrease in mean precipitation	See decreased mean precipitation
Intense precipitation	Rapid soil wetting	Piping, slope stability
	Overland flow	Slope stability, erosion
Flood/SLR	Large pore pressure increases, soil wetting	Piping, internal erosion, slope stability, erosion

Source: Modified from Vardon (2015).

Local SLR, often referred to as relative SLR, is a locally observable phenomenon that reflects changes in the eustatic sea level, the subsidence or uplift of the sea floor, and the accumulation, erosion, or compaction of sediment along the coast. Sediment accumulation and erosion are greatly affected by subsidence and uplift, so these processes are often mutually reinforcing. The tectonic setting of continental margins plays a primary role in determining whether a section of coastline will experience uplift or subsidence. As large landmasses break up because of plate tectonics, the newly formed continental landmass will typically have both an active and passive plate margin. The active plate margin represents the leading edge of the continent, where *lighter* continental crust overrides denser oceanic crust. The subduction of oceanic crust beneath the continental crust causes uplift of the latter to varying degrees (MacDonald 1991). Conversely, the trailing or passive margin, originally formed along a series of volcanic rifts in the

parent continent, will experience subsidence as the thinner passive margin cools (Steckler and Watts 1982). Consequently, most major coastal rivers or embayments are located above crustal features (often inherited from the initial continental breakup) that allowed greater subsidence early in the evolution of the continental margin. Sediment loading is then concentrated in the resulting low-lying area, leading to even greater rates of subsidence. Conversely, glacial loading during periods of widespread continental glaciation depressed continental landmasses locally. As continental glaciers retreated, isostatic adjustment occurred and margins rebounded, creating uplift at rates slower than that of the glacial retreat itself. Such areas thus experienced less relative SLR than other portions of the continental margin. In addition to long-term changes that take place on geologic time scales, RSL can also be influenced by fluid withdrawal, diversion or elimination of sediment sources, and other human activities.

As can be discerned from the previous discussion, SLR will vary through time and space. Warming of ocean waters is not uniform due both to differences in water depth (shallow basins such as the Mediterranean or Caribbean will warm more quickly than deep basins like the Pacific) and the regional nature of convective heat flow (manifest as ocean currents). The contribution of freshwater inflow from continental glaciers is also variable, as competition between increased snowfall in the interior of a continental glacier, owing to increased water vapor in a warming atmosphere, and greater loss of ice mass, driven by the same warming atmosphere, varies through time. The greatest source of uncertainty in predicting both eustatic and local SLR is the rate at which continental-scale glaciers (where significant fresh water is sequestered) will melt because of mechanical failure along their margins. These regions experience significant mass loss owing to the mechanical formation of icebergs, which greatly accelerates ocean world flow of glacial ice and accelerate melting. All these factors must be accounted for when various projections of SLR are developed (NRC 2012).

The availability of high-resolution local sea-level projections is important for the development of durable engineering works. To support the needs of engineers, there is a need for a more robust open climate model framework based on a range of models with enhanced process parameterizations and calibration by observations to produce more granular relative sea-level projections (including subsidence). Currently, probabilistic SLR projections are useful tools to support coastal hazard mitigation design criteria and communicate projected changes to stakeholders. However, engineering works must also consider the significant unknowns in future SLR, including those resulting from a range of possible future GHG emissions scenarios and based on the resulting behavior of ice sheets, which remains an area of great uncertainty. Because there is presently considerable disagreement within the scientific community on the shape of the tails of the SLR probability distributions for the second half of this century and beyond, the development of improved

sea-level projections with time frames extending beyond 2100 are in great demand.

A variety of SLR projections are currently available. Perhaps the most complete and transparent set of projections (at least for the United States) is available from NOAA. Released in January 2017, *Global and Regional Sea Level Rise Scenarios for The United States* (NOAA 2012b) covers these topics in some detail, providing global SLR projections under a variety of climate change scenarios and a set of gridded regional sea-level responses (Figure 2-9). The report incorporates a framework developed using the CMIP5 archive (Kopp et al. 2014), with recent scientific literature and includes modeling of Antarctic ice-sheet instability. The report indicates an end-of-century global SLR outcomes higher than the ranges previously published by NOAA (2012b) and plausibly in the range of 0.3 to 2.5 m. From this range, local SLR rates are projected on a 1° grid covering the US mainland coastline,

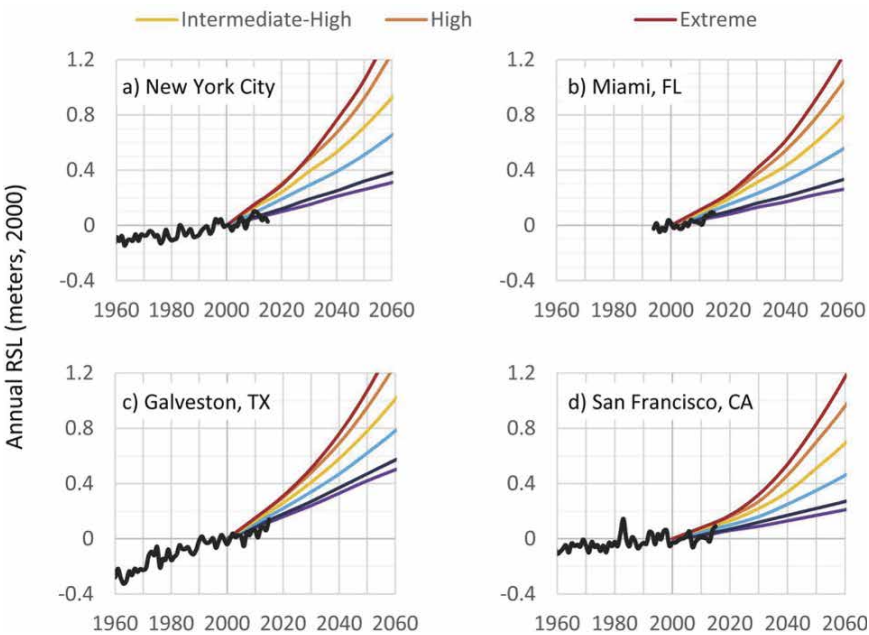

Figure 2-9. Observed and projected relative sea-level changes for New York City (The Battery); Miami (Virginia Key), FL; Galveston, TX; and San Francisco, CA, with their respective (median value) RSL under the six scenarios. The NOAA RSL observations (tidesandcurrents.noaa.gov/sltrends) are shown relative to the midpoint (year 2000) of the 1991–2009 epoch (1994–2009 at Virginia Key), which is the reference level for the scenarios.
Source: NOAA (2017b).

Alaska, Hawaii, the Caribbean, and the Pacific Island territories for six representative scenarios: low, intermediate-low, intermediate, intermediate-high, high, and extreme.

Local SLR will expose infrastructure or engineered facilities to different wave regimes and increased salinity of coastal groundwater (salinization), and it will inundate low-lying areas near the coast. In addition, the combination of SLR with extreme natural events, such as storm surges and waves, will become increasingly problematic for the dense populations, growing economies, and ecosystems that exist on many coasts. Major human and economic losses have occurred in recent years owing to storm surge (e.g., more than 100,000 deaths during Cyclone Nargis in 2008 and at least 233 deaths and approximately $75 billion in losses during Superstorm Sandy in 2012). The development of important engineering works in coastal regions must consider various factors with respect to SLR and storm surge to address vulnerabilities, such as the asset planning horizon based on useful life and overall risk tolerance based on the criticality of the asset. A further discussion of coastal flooding and design criteria for engineering works is presented in Chapter 5.

2.5.5 Increased Frequency of Coastal Flooding Events

SLR exacerbates short-term flooding over a range of elevation thresholds. At very high thresholds, such as those resulting from a 1% annual chance storm event, SLR will nonlinearly compress recurrence probabilities in the future, because less intense (higher probability) storm surges will result in higher peak flood elevations. In addition to affecting peak flooding during surge events, SLR will positively shift the distribution of periodic (e.g., tidal) and seasonal variation in sea level toward higher means.

Nuisance flood events, or the occurrence of flood events in developed coastal areas concurrent with high tides and little or no storm effects, are increasing in frequency and affecting larger areas of coastal communities proportional to the extent of relative SLR. In addition, nuisance flood events normally affecting areas during a particular tidal event will result in higher levels of inundation and longer durations. Two measures to quantify nuisance flooding are cumulative hours above the nuisance flood-level elevation threshold during a year and the number of days affected by nuisance-level flooding during a year (e.g., one day could represent one hour or an entire 24-hour period above the nuisance flood level) (NOAA 2014). The rate of nuisance flooding event occurrence accelerates as the gap closes between the local flood threshold elevation and high tide. As shown in Figure 2-10, acceleration (quadratic) constants characterizing how nuisance flood days change over time versus the nuisance flood levels reveals a strong negative correlation ($p < 0.01$) for East Coast gauges, reflecting a statically demonstrable increase in flooding rate for the region.

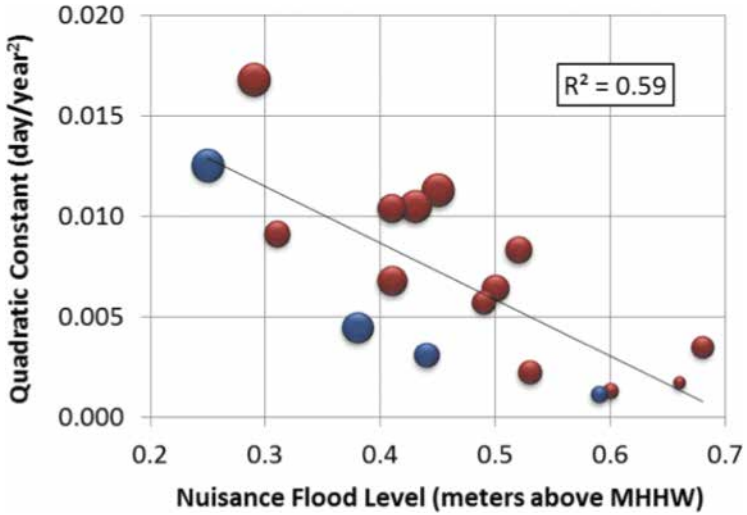

Figure 2-10. Bubble plot of nuisance flood level (x-axis) versus quadratic constant (y-axis) from fit of annual number of nuisance flood days East Coast gauges (Northeast region in red and Southeast region in blue).
Source: NOAA (2014).

The effects of such events include overwhelming of storm systems, road closures, saturation of ground surfaces, and deterioration of infrastructure (e.g., roads and rail). The nonlinear trajectory in nuisance flooding should be considered for coastal planning and engineering works. Probabilistic analyses can be performed using historic tidal data, local elevations (e.g., LiDAR), and SLR projections to develop risk-based mitigation strategies based on the time horizon for when critical elevation thresholds for particular assets will become increasingly affected by tidal flooding.

2.5.6 Changes in Severe Storm Frequency, Intensity, and Location

Work in paleotempestology has identified large, centennial- to millennial-scale variations in regional tropical cyclone incidence, the causes of which are at present not understood (Donnelly et al. 2015). The potential intensity of tropical storms is measured by the degree of disequilibrium between the ocean surface and the atmosphere (i.e., an increased differential resulting from a warmer ocean or a cooler atmosphere, accounting for temperature, humidity, and stratification from the surface to the lower stratosphere, increases potential intensity). Although GHG-driven warming increases this potential by disproportionately warming the ocean, climate model simulations suggest that until the mid-1970s, aerosol cooling largely canceled the

effect. Thus, it is projected that in the absence of strong reductions in GHG emissions, future GHG forcing is likely to further dominate over aerosol forcing, leading to larger increases in tropical cyclone intensities than what has been observed (Sobel et al. 2016).

The Geophysical Fluid Dynamics Laboratory of NOAA (GFDL 2018) has examined global warming and hurricanes and changes in hurricane activity for the late 21st century, given the pronounced global warming scenarios from IPCC models. GFDL's primary conclusions are

- "Sea level rise–which very likely has a substantial human contribution to the global mean observed rise according to IPCC AR5–should be causing higher storm surge levels for tropical cyclones that do occur, all else assumed equal.
- Tropical cyclone rainfall rates will likely increase in the future owing to anthropogenic warming and accompanying increase in atmospheric moisture content. Models project an increase on the order of 10% to 15% for rainfall rates averaged within about 100 km of the storm for a 2°C global warming scenario.
- Tropical cyclone intensities globally will likely increase on average (by 1% to 10% according to model projections for a 2°C global warming). This change would imply an even larger percentage increase in the destructive potential per storm, assuming no reduction in storm size.
- There are better than even odds that anthropogenic warming over the next century will lead to an increase in the occurrence of very intense tropical cyclones globally–an increase that would be substantially larger in percentage terms than the 1% to 10% increase in the average storm intensity. This increase in intense storm occurrence is projected despite a likely decrease (or little change) in the global numbers of all tropical cyclones. However, there is at present only low confidence that such an increase in very intense storms will occur in the Atlantic basin.
- In terms of detection and attribution, much less is known about hurricane/tropical cyclone activity changes, compared to global temperature. In the northwest Pacific basin, there is emerging evidence for a detectable poleward shift in the latitude of maximum intensity of tropical cyclones, with a tentative link to anthropogenic warming. In the Atlantic, it is premature to conclude that human activities–and particularly greenhouse gas emissions that cause global warming–have already had a detectable impact on hurricane activity. Reduced aerosol forcing since the 1970s probably contributed to the increased Atlantic hurricane activity since then, but the amount of contribution, relative to natural variability, remains uncertain. Human activities may have already caused other changes in tropical cyclone activity that are not

yet detectable due to the small magnitude of these changes compared to estimated natural variability, or due to observational limitations."

Figure 2-11 shows tracks and intensities of all storms reaching Category 4 or 5 intensity (>59 m/s) in the GFDL hurricane model downscaling experiments. Results are shown for the control climate (upper left); CMIP3/A1B 18-model ensemble late 21st century (lower left); and CMIP5/RCP4.5 18-model ensemble early (upper right) or late (lower right) 21st century. All results shown are based on model version GFDL. Track colors indicate the intensity category during the storm's lifetime. Figure 2-12 shows results globally. Figure 2-13 shows late-21st-century projections of tropical storms.

Changes in the frequency, intensity, and location of severe storms under a changing climate are complex. According to the IPCC (2013a),

- There is low confidence in long-term (centennial) changes in tropical cyclone activity, after accounting for past changes in observing capabilities. However, over the satellite era, increases in the frequency and intensity of the strongest storms in the North Atlantic are robust (very high confidence). However, the cause of this increase is debated, and there is low confidence in attribution of changes in tropical cyclone activity to human influence owing to insufficient observational evidence, lack of physical understanding of the links between anthropogenic drivers of climate and tropical cyclone activity, and the low level of agreement between studies as to the relative importance of internal variability, and anthropogenic and natural forcings.

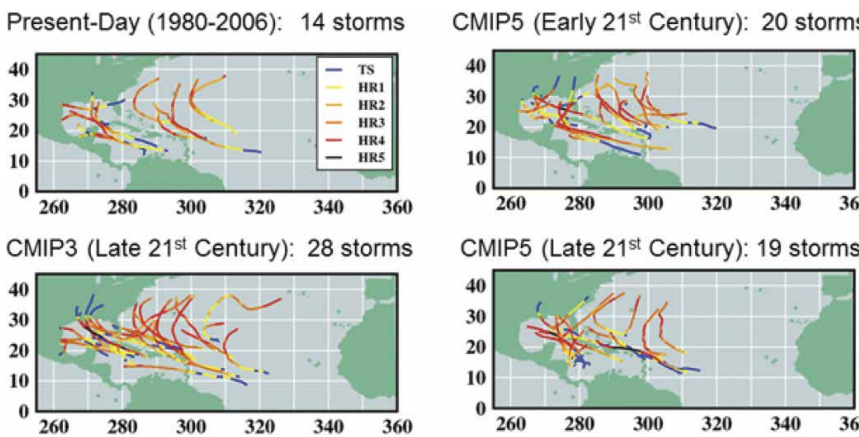

Figure 2-11. GFDL-NOAA Hurricane model: Categories 4 and 5 hurricane tracks for the mid-Atlantic (27 simulation years).
Source: GFDL (2018).

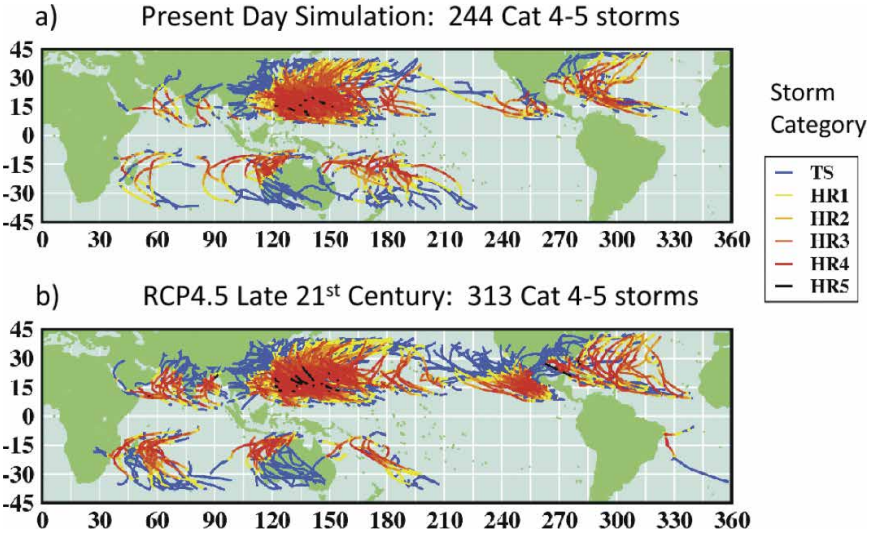

Figure 2-12. GFDL-NOAA hurricane model: Categories 4 and 5 hurricane tracks. Source: GFDL (2018).

- Some high-resolution atmospheric models have realistically simulated tracks and counts of tropical cyclones, and models are able to capture the general characteristics of storm tracks and extratropical cyclones with evidence of improvement since the AR4. Storm track biases in the North Atlantic have improved slightly, but models still produce a storm track that is too zonal and underestimate cyclone intensity. While projections indicate that it is likely the global frequency of tropical cyclones will either decrease or remain essentially unchanged, concurrent with a likely increase in both global mean tropical cyclone maximum wind speed and rainfall rates, there is lower confidence in region-specific projections of frequency and intensity. However, because of improvements in model resolution and downscaling techniques, it is more likely than not that the frequency of the most intense storms will increase substantially in some basins under projected 21st-century warming. Research subsequent to the AR4 and SREX continues to support a likely poleward shift of storm tracks since the 1950s. However, over the last century, there is low confidence of a clear trend in storminess due to inconsistencies between studies or lack of long-term data in some parts of the world, [particularly in the Southern Hemisphere (SH)].
- Despite systematic biases in simulating storm tracks, most models and studies are in agreement that the global number of extratropical cyclones is unlikely to decrease by more than a few percentage points.

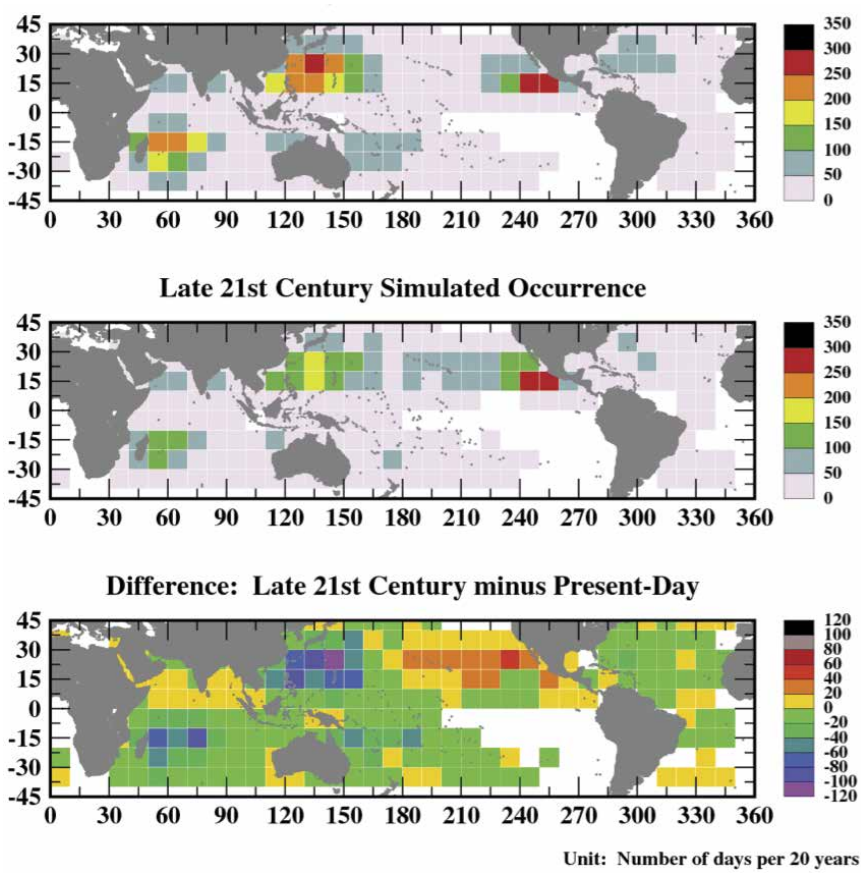

Figure 2-13. Late-21st-century projections of tropical storms. Source: GFDL (2018).

A small poleward shift is likely in the SH storm track. It is more likely than not (medium confidence) for a projected poleward shift in the North Pacific storm track, but it is unlikely that the response of the North Atlantic storm track is a simple poleward shift. There is low confidence in the magnitude of regional storm track changes, and the impact of such changes on regional surface climate. Against the background of global climate change and sea-level rise, it will be important to have quantitative assessments on the potential increase in risk of tropical and extratropical cyclone induced storm surge to developed coastal regions in the coming decades and century.

2.6 REFERENCES

ASCE. 2010. *Minimum design loads for buildings and other structures*. ASCE/SEI 7-10. Reston, VA: ASCE.

ASCE. 2014. *Flood resistant design and construction*. ASCE/SEI 24-14. Accessed February 13, 2016. http://ascelibrary.org/doi/book/10.1061/9780784413791. Reston, VA: ASCE.

ASCE. 2015. *Adapting infrastructure and civil engineering practice to a changing climate*. Accessed February 13, 2016. http://ascelibrary.org/doi/book/10.1061/9780784479193. Reston, VA: ASCE.

Barsugli, J. S., C. A. Anderson, J. B. Smith, and J. M. Vogel. 2009. "Options for improving climate modeling to assist water utility planning for climate change." White Paper Prepared for Water Utility Climate Alliance, San Francisco.

Bates, M. E., and J. R. Lund. 2013. "Delta subsidence reversal, levee failure, and aquatic habitat—a cautionary tale." *San Francisco Estuary and Watershed Science* 11(1), 1–20. Accessed August 14, 2018. https://escholarship.org/uc/jmie_sfews/11/1.

Brooks, B. A., G. Bawden, D. Manjunath, C. Werner, N. Knowles, J. Foster, et al. 2012. "Contemporaneous subsidence and levee overtopping potential, Sacramento–San Joaquin Delta, California." *San Francisco Estuary and Watershed Science* 10(1). Accessed August 15, 2018. http://escholarship.org/uc/item/15g1b9tm.

Clarke, G. R. T., D. A. B. Hughes, S. L. Barbour, and V. Sivakumar. 2006. "The implications of predicted climate changes on the stability of highway geotechnical infrastructure: A case study of field monitoring of pore water response." *Proc., 2006 IEEE EIC Climate Change Conf*. Piscataway, NJ: IEEE.

Coe, J. A., and J. W. Godt. 2012. "Review of approaches for assessing the impact of climate change on landslide hazards." In Vol. I of *Proc., 11th Int. and 2nd North American Symp. on Landslides and Engineered Slopes*, E. Eberhardt et al. (eds.). London: Taylor & Francis, 371–377.

Conant, R., M. Ryan, G. Agren, H. Birge, E. Davidson, P. Eliasson, et al. 2011. "Temperature and soil organic matter decomposition rates—Synthesis of current knowledge and a way forward." *Global Change Biol*. 17, 3392–3404.

Davidson, E. A., and I. A. Janssens. 2006. "Temperature sensitivity of soil carbon decomposition and feedbacks to climate change." *Nature* 440, 165–173.

Dehn, M., G., Bürger, J. Buma, and P. Gasparetto. 2000. "Impact of climate change on slope stability using expanded downscaling." *Eng. Geol*. 55(3), 193–204.

Donnelly, J. P., A. D. Hawkes, P. Lane, D. MacDonald, B. N. Shuman, M. R. Toomey, et al. 2015. "Climate forcing of unprecedented intense-hurricane activity in the last 2,000 years." *Earth's Future* (3)2, 49–65. DOI:10.1002/ 2014EF000274.

Dunbar, J., J. Llopis, G. Sills, E. Smith, R. Miller, J. Ivanov, et al. 2007. "Condition assessment of levees, US section of the international boundary and water commission." *Tech. Rep. No. TR-03-4*, Vicksburg, MS: US Army Engineer Geotechnical and Structures Laboratory.

Dyer, M. R., S. Utili, and M. Zielinski. 2009. "Field survey of desiccation fissuring of flood embankments." *Proc., Inst. of Civil Engineers-Water Management* 162(3), 221–232. London: Thomas Telford.

Gariano, S. L., and F. Guzzetti. 2016. "Landslides in a changing climate." *Earth-Sci. Rev*. 162, 227–252.

GFDL (Geophysical Fluid Dynamics Laboratory). 2018. "Global warming and hurricanes." *Geophysical Fluid Dynamics Laboratory of NOAA*. Accessed June 17, 2018. https://www.gfdl.noaa.gov/global-warming-and-hurricanes.

Hungr, O., S. McDougall, and M. Bovis. 2005. "Entrainment of material by debris flows." In *Debris-flow hazards and related phenomena*, O. Hungr and M. Jakob (eds.). Berlin: Springer, 135–158.

IPCC (Intergovernmental Panel on Climate Change). 2000. *Special report on emissions scenarios: special report of the intergovernmental panel on climate change*. Cambridge, UK: Cambridge Univ. Press. http://www.grida.no/climate/ipcc/emission/index.htm.

IPCC. 2012. *Managing the risks of extreme events and disasters to advance climate change adaptation: Special report of the intergovernmental panel on climate change*, C. B. Field et al. (eds.). Cambridge, UK: Cambridge Univ. Press.

IPCC. 2013a. "Summary for policymakers." In *Climate change 2013: The physical science basis*, T. F. Stocker et al. (eds.). Cambridge, UK: Cambridge Univ. Press.

IPCC. 2013b. "Anthropogenic and natural radiative forcing." In *Climate change 2013: The physical science basis*, T. F. Stocker et al. (eds.). Cambridge, UK: Cambridge Univ. Press.

IPCC. 2013c. "Observations: atmosphere and surface." In *Climate change 2013: The physical science basis*, T. F. Stocker et al. (eds.). Cambridge, UK: Cambridge Univ. Press.

IPCC. 2013d. "Technical summary." In *Climate change 2013: The physical science basis*, T. F. Stocker et al. (eds.). Cambridge, UK: Cambridge Univ. Press.

IPCC. 2013e. "Climate phenomena and their relevance for future regional climate change." In *Climate change 2013: The physical science basis*, T. F. Stocker et al. (eds.). Cambridge, UK: Cambridge Univ. Press.

IPCC. 2014a. *Climate change 2014: Impacts, adaptation, and vulnerability. Part A: Global and sectoral aspects*, C. B. Field et al. (eds.). Cambridge, UK: Cambridge Univ. Press.

IPCC. 2014b. *Climate Change 2014: Synthesis report*, P. K. Pachauri and L. M. Meyer (eds.). Geneva, Switzerland: IPCC.

Iverson, R. M., M. E. Reid, M. Logan, R. G. LaHusen, J. W. Godt, and J. P. Griswold. 2011. "Positive feedback and momentum growth during debris-flow entrainment of wet bed sediment." *Nat. Geosci*. 4(2), 116–121. Accessed September 12, 2018. http://dx.doi.org/10.1038/NGEO1040.

Jones, J. A. A. 2010. "Soil piping and catchment response." *Hydrol. Process*. 24(12), 1548–1566. Accessed September 12, 2018. http://dx.doi.org/10.1002/hyp.7634.

Kopp, R. E., R. M. Horton, C. M. Little, J. X. Mitrovica, M. Oppenheimer, D. J. Rasmussen, et al. 2014. "Probabilistic 21st and 22nd century sea-level projections at a global network of tide-gauge sites." *Earth's Future* 2(8), 383–406.

Kovacevic, K., D. M. Potts, and P. R. Vaughan. 2001. "Progressive failure in clay embankments due to seasonal climate changes." *5th Int. Conf. Soil Mechanics and Geotechnical Engineering*. Rotterdam, Netherlands: AA Balkema, 2127–2130.

Lee, E. M., and D. K. C. Jones. 2004. *Landslide risk assessment*. London: Thomas Telford.

Leshchinsky, B., B. Vahedifard, H. B. Koo, and S. H. Kim. 2015. "Yumokjeong landslide: An investigation of progressive failure of a hillslope using the finite element method." *Landslides* 12(5), 997–1005. DOI:10.1007/s10346-015-0610-5.

Lu, N., and W. J. Likos. 2004. *Unsaturated soil mechanics*. Hoboken, NJ: Wiley.

MacDonald, D. 1991. "Sedimentation, tectonics, and eustasy: Sea-level changes at active margins." *Special Publication Number 12 of the Int. Assoc. of Sedimentologists*. Oxford, UK: Blackwell Scientific.

Milly, P. C. D., and K. A. Dunne. 2011. "On the hydrologic adjustment of climate-model projections: The potential pitfall of potential evapotranspiration." *Earth Inter*. 15(1), 1–14. Accessed September 12, 2018. https://doi.org/10.1175/2010EI363.1.

Moss, R. H., J. E. Edmonds, K. A. Hibbard, M. R. Manning, S. K. Rose, D. P. van Vuuren, et al. 2010. "The next generation of scenarios for climate change research and assessment." *Nature* 463, 747–756. DOI:10.1038/nature08823.

Mount, J., and R. Twiss. 2005. "Subsidence, sea level rise, seismicity in the Sacramento–San Joaquin delta." *San Francisco Estuary and Watershed Science* 3(1). Accessed September 12, 2018. http://repositories.cdlib.org/jmie/sfews/vol3/iss1/art5.

NOAA (National Oceanic and Atmospheric Administration). 2006. "Precipitation-frequency atlas of the United States." *NOAA Atlas 14, Vol. 2*. Accessed August 16, 2017. http://www.nws.noaa.gov/oh/hdsc/PF_documents/Atlas14_Volume2.pdf.

NOAA. 2008. "Precipitation-frequency atlas of the United States." *NOAA Atlas 14, Vol. 3*. Accessed August 16, 2017. http://www.nws.noaa.gov/oh/hdsc/PF_documents/Atlas14_Volume3.pdf.

NOAA. 2011a. "Precipitation-frequency atlas of the United States." *NOAA Atlas 14, Vol. 1*. Accessed August 16, 2017. http://www.nws.noaa.gov/oh/hdsc/PF_documents/Atlas14_Volume1.pdf.
NOAA. 2011b. "Precipitation-frequency atlas of the United States." *NOAA Atlas 14, Vol. 4*. Accessed August 16, 2017. http://www.nws.noaa.gov/oh/hdsc/PF_documents/Atlas14_Volume4.pdf.
NOAA. 2011c. "Precipitation-frequency atlas of the United States." *NOAA Atlas 14, Vol. 5*. Accessed August 16, 2017. http://www.nws.noaa.gov/oh/hdsc/PF_documents/Atlas14_Volume5.pdf.
NOAA. 2012a. "Global sea level rise scenarios for the US National Climate Assessment." *Tech. Memo OAR CPO-1*. Silver Spring, MD: NOAA.
NOAA. 2012b. "Precipitation-frequency atlas of the United States." *NOAA Atlas 14, Vol. 7*. Accessed August 16, 2017. http://www.nws.noaa.gov/oh/hdsc/PF_documents/Atlas14_Volume7.pdf.
NOAA. 2013a. National Weather Service glossary. Accessed March 14, 2013. http://w1.weather.gov/glossary.
NOAA. 2013b. "Precipitation-frequency atlas of the United States." *NOAA Atlas 14, Vol. 8*. Accessed August 16, 2017. http://www.nws.noaa.gov/oh/hdsc/PF_documents/Atlas14_Volume8.pdf.
NOAA. 2013c. "Precipitation-frequency atlas of the United States." *NOAA Atlas 14, Vol. 9*. Accessed August 16, 2017. http://www.nws.noaa.gov/oh/hdsc/PF_documents/Atlas14_Volume9.pdf.
NOAA. 2014. "Precipitation-frequency atlas of the United States." *NOAA Atlas 14, Vol. 6*. Accessed August 16, 2017. http://www.nws.noaa.gov/oh/hdsc/PF_documents/Atlas14_Volume6.pdf.
NOAA. 2015. "Precipitation-frequency atlas of the United States." *NOAA Atlas 14, Vol. 10*. Accessed August 16, 2017. http://www.nws.noaa.gov/oh/hdsc/PF_documents/Atlas14_Volume10.pdf.
NOAA. 2017a. "Precipitation-frequency data server." Silver Spring, MD: National Weather Service. Accessed March 28, 2017. http://hdsc.nws.noaa.gov/hdsc/pfds/.
NOAA. 2017b. "Global and regional sea level rise scenarios for the United States." W. V. Sveet et al. (eds). *NOAA Tech. Rep. NOS CO-OPS 083*. Silver Spring, MD: NOAA.
NRC (National Research Council). 2012. "Sea-level rise for the coasts of California, Oregon, and Washington: Past, present, and future." Washington, DC: National Academies Press. DOI: 10.17226/13389.
NRC. 2016. "Transportation resilience: adaptation to climate change." Washington, DC: National Academies Press.
NSIDC (National Snow and Ice Data Center). 2012. "Arctic climatology and meteorology glossary." Accessed October 9, 2012. http://nsidc.org/arcticmet/glossary/weather.html.
Nyambayo, V. P., D. M. Potts, and T. I. Addenbrooke. 2004. "The influence of permeability on the stability of embankments experiencing seasonal

cyclic pore water pressure changes." *Advances in Geotechnical Engineering: Skempton Conf*. London: Thomas Telford, 898–910.

Peters, G. P., M. S. Robbie, T. Boden, J. G. Canadell, P. Ciais, C. L. Quéré, et al. 2013. "The challenge to keep global warming below 2 [deg] C." *Nat. Clim. Change* 3(1), 4–6. Accessed August 15, 2018. https://www.earth-syst-sci-data.net/8/605/2016/essd-8-605-2016.html.

Polade, S. J., D. W. Pierce, D. R. Cayan, A. Gershunov, and M. D. Dettinger. 2014. "The key role of dry days in changing regional climate and precipitation regimes." *Sci. Rep*. 4, 4364. DOI:10.1038/srep04364.

Port, P. S., and S. A. Hoover. 2011. "Anticipating California levee failure: The state of the delta levees and government preparation and response strategies for protecting natural resources from freshwater oil spills." *Proc., Int. Oil Spill Conf*. 2011(1), abs112.

Potts, D. M., K. Kovacevic, and P. R. Vaughan. 1997. "Delayed collapse of cut slopes in stiff clay." *Géotechnique* 47(5), 953–982.

Robinson, J. D., and F. Vahedifard. 2016. "Weakening mechanisms imposed on California's levees under multiyear extreme drought." *Clim. Change* 137(1–2), 1–14.

Robinson, J. D., F. Vahedifard, and A. AghaKouchak. 2017. "Rainfall-triggered slope instabilities under a changing climate: comparative study using historical and projected precipitation extremes." *Can. Geotech. J.* 54(1), 117–127. DOI: 10.1139/cgj-2015-0602.

Sobel, A. H., S. J. Camargo, T. M. Hall, C. Y. Lee, M. K. Tippett, and A. A. Wing. 2016. "Human influence on tropical cyclone intensity." *Science* 353(6296), 242–246.

Steckler, M. S., and A. B. Watts. 1982. "Subsidence history and tectonic evolution of Atlantic-type continental margins." In *Dynamics of passive margins*, Series Vol. 6, R. A. Scratton (ed.). Washington, DC: American Geophysical Union Geodynamics, 184–196.

USGCRP (US Global Change Research Program). 2014. *Climate change impacts in the United States: The third national climate assessment*. J. M. Melillo, T. C. Richmond, and G. W. Yohe (eds.). Washington, DC: US Global Change Research Program. DOI:10.7930/J0Z31WJ2.

USGCRP. 2017. "Climate Science Special Report: Fourth National Climate Assessment, Volume I." D. J. Wuebbles et al. (eds.). Washington, DC: U.S. Global Change Research Program. DOI: 10.7930/J0J964J6.

Vahedifard, F., J. D. Robinson, and A. AghaKouchak. 2016. "Can protracted drought undermine the structural integrity of California's earthen levees?" *J. Geotech. Geoenviron. Eng*.142(6). Accessed August 15, 2018. https://doi.org/10.1061/(ASCE)GT.1943-5606.0001465.

Vahedifard, F., F. S. Tehrani, V. Galavi, E. Ragno, and A. AghaKouchak. 2017. "Resilience of MSE walls with marginal backfill under a changing climate: Quantitative assessment for extreme precipitation events."

J. Geotech. Geoenviron. Eng. 143(9). Accessed August 15, 2018. https://doi.org/10.1061/(ASCE)GT.1943-5606.0001743.

Vardon, P. J. 2015. "Climatic influence on geotechnical infrastructure: A review." *Environ. Geotech*. 2(3), 166–174.

Vicuña, S., M. Hanemann, and L. Dale. 2006. "Economic impacts of delta levee failure due to climate change: a scenario analysis." *PIER Project Report*, CEC-500-2006-004, UC Berkeley, Berkeley, CA.

This page intentionally left blank

CHAPTER 3
OBSERVATIONAL METHOD

3.1 BACKGROUND

3.1.1 The Paradigm

As discussed in Chapter 2, resolving climate-related uncertainties to a significant level during the planning and design stage of infrastructure systems is unfeasible. As a result, a paradigm for planning and design is necessary that would either a) identify potential system changes during planning and design that could be implemented as needed throughout the life of the infrastructure systems or b) adequately ensure that the structure or engineered system can withstand the most-credible unfavorable future extremes. Both approaches have drawbacks, because the cost of implementation may be significant. Changes made after construction and the monitoring needed to support them may in some cases be costlier than simply designing for the most-credible unfavorable future extreme. Conversely, designing for the most-credible future extreme may add unnecessary costs to the initial construction that may later prove to have been unnecessary. As a first step in the exploration of this paradigm, Chapter 3 explores a class of design methods derived from the *observational method* favored by geotechnical engineers that produce systems with adaptive characteristics. Chapter 4 explores approaches that may be used for various classes of engineering projects that, for whatever reason, do not lend themselves to post-construction adaptation.

3.1.2 The Observational Method

Civil engineers have dealt with uncertainty in geotechnical engineering practice by employing the observational method (OM), originally proposed by Karl Terzaghi and described in Terzaghi and Peck (1948) and Peck (1969). A succinct definition of the OM is provided in UK CIRIA Report 185D (Nicholson et al. 1999):

> The Observational Method [in ground engineering] is a continuous, managed, integrated, process of design, construction control, monitoring and review that enables previously defined modifications to be incorporated during or after construction as appropriate. All these aspects have to be demonstrably robust. The objective is to achieve greater overall economy without compromising safety.

By using the OM in geotechnical engineering, initial construction costs are reduced by designing infrastructure based on the most-probable conditions rather than the most-unfavorable conditions. Uncertainty in the available information is augmented during the life of the infrastructure by observations of the performance of the infrastructure. As time passes, more and more uncertainties are documented and quantified, and data the collected become the foundation for changes and updates to standards. It is through such changes that the OM manifests itself as a global benefit to the practice of engineering and ultimately to the public. Decades of geotechnical observations have taken the work by Terzaghi and others to shape our practice, such as in soil capacity tables, settlement guidance, liquefaction potential guidance, and many other parameters used in standards today. With this end goal in mind, it may be possible to employ a modified version of the OM to accommodate the inherent uncertainty in future climate.

The OM has been extensively studied and discussed by the European engineering community (Eurocode 7 2004, Nicholson et al. 1999, 2006). Patel et al. (2007) provided a comprehensive review of the OM as applied in the European engineering community and summarized how the OM should be applied across Europe within the design and contractual framework of an engineering project. They stated, "The OM is most effective where there is a wide range of uncertainty." Korff et al. (2013) suggested that projects particularly amenable to OM entail low risk but unacceptable a priori probabilities of exceedance with significant consequences or projects with multiple stages or incremental construction processes. The OM is appropriate for gradual changes such as sea-level rise or melting permafrost owing to warming temperatures. The OM may be less appropriate if there are safety concerns about the impacts of sudden extreme climate events that can occur and inflict damages before changing conditions are observed.

3.2 MODIFYING THE OBSERVATIONAL METHOD TO MEET DESIGN NEEDS FOR A CHANGING CLIMATE

The specific steps in a climate change OM are as follows (modified after Terzaghi and Peck 1948):

1. Project design is based on the most-probable weather or climate condition(s) rather than the most unfavorable. The most-credible unfavorable deviations from the most-probable conditions are identified.
2. A course of action or design modification is devised (in advance) for every foreseeable unfavorable weather or climate deviation from the most-probable condition(s).
3. The performance of the project is observed over time (using preselected quantities) and the response of the project to observed changes is assessed.
4. Design and construction modifications (previously identified) can be implemented in response to observed changes.

Step I. Distinguishing Most Probable from Most Unfavorable.

The successful application of OM under future climate conditions requires some thoughtful consideration of various aspects of the underlying processes. Weather, climate, and their extremes are factors in civil engineering design and practice. Weather is defined as "the state of the atmosphere with respect to wind, temperature, cloudiness, moisture, pressure, etc." (NWS 2013). Weather generally refers to short-term variations on the order of minutes to about 15 days (NSIDC 2012). Climate, however, "is usually defined as the average weather, or more rigorously, as the statistical description in terms of the mean and variability of relevant quantities over a period of time ranging from months to thousands or millions of years" (IPCC 2014). As discussed in Chapter 2, changes in the statistical mean that persist for 30 years or more are indicative of climate change. Changes that cannot be accounted for by natural variability on that timescale are likely components of anthropogenically forced climate change and can be expected to persist for centuries or even millennia.

Engineering design is primarily concerned about extremes. The IPCC (2012) defines an *extreme weather or climate event* as "The occurrence of a value of a weather or climate variable above (or below) a threshold value near the upper (or lower) ends of the range of observed values of the variable. For simplicity, both extreme weather events and extreme climate events are referred to collectively as 'climate extremes.'" Drought or heavy precipitation in a season are examples of such events. Climate scientists and civil engineers may not agree on how uncommon an event should be to be

called extreme. According to the IPCC, an *extreme weather event* would "normally be as rare as or rarer than the 10th or 90th percentile of the observed probability density function." However, in civil engineering, *rare* is often defined in terms of an acceptable frequency of failure. Large dams may be designed for events with a Mean Recurrence Interval (MRI) of about 10,000 years. Flood risk management is concerned with events with MRIs of 100 to 500 years. Transportation and stormwater design is concerned with events that occur more frequently, coming closer to the IPCC definition (Bonnin et al. 2011).

Defining the *most-probable weather or climate condition(s)* is problematic with weather or climate change. As previously discussed, climate model projections cannot determine accurate probability distributions for future climate. In this step, engineers must use engineering judgment to determine reasonable conditions for design. In addition, there may be reasonable disagreement among stakeholders on what those conditions should be.

Timely guidance on magnitudes of extremes for design, such as *probable maximum* or *design basis* values for initial design with *bounds* or *maximum credible* levels for adaptations during service life, is needed and should be given precedence. As a starting point, *probable maximum* values would be set as currently cited in standards or based on current knowledge of extremes consistent with the desired MRI; and *maximum credible* values would be consistent with those physically possible and recently observed on a regional or world basis using a similar or greater MRI. The NRC (2016) examined the attribution of extreme weather events in the context of climate change and provided guidance on forecasting the frequencies and intensities of climate or weather extremes.

However, non-stationarity indicates that the MRI, such as the 100-year event, is no longer meaningful, but the corresponding Annual Exceedance Probability (AEP) (of 0.01 for an MRI of 100 years) would remain meaningful. Climate/weather scientists must provide their estimates of such intensities for 10, 50, and 100 years in the future.

Step II. Identifying a Course of Action.

The most serious error in applying the OM is failing to select an appropriate course of action for all foreseeable deviations (disclosed by observation) of initial design assumptions. The OM should not be used unless the engineer has preselected a course of action for every unfavorable situation that might be disclosed by the observations. The engineer must devise in advance a course of action or design modification (in advance) for every foreseeable unfavorable climate deviation from the most-probable condition(s). Under the original philosophy of the OM, if the engineer cannot solve these hypothetical problems (even if the probability of their occurrence is very low), then it becomes necessary to base the design on the least-favorable

conditions. An advantage of the OM is that it often permits a more economic design while assuring safety, provided that changing conditions can be observed and the design can be modified over time.

Step III. Monitoring for Changes in Climate/Weather and Their Extremes.

The observations must be reliable, must reveal the significant phenomena, and must be reported so as to encourage prompt action. In practice, an OM applied to climate change requires a continuous (and funded) monitoring program that observes relevant metrics. The concept of applying the OM to the monitored infrastructure must be passed to the owners of the infrastructure who succeed the owners or engineers who originally applied the OM. Site-specific monitoring may not be possible or even necessary in some situations. If project-specific threshold values can be identified, it is possible that ongoing weather and climate observations conducted by various government entities (especially those responsible for collecting observation used to define the most-probable conditions used during design) may be more than adequate to trigger planned modifications.

Step IV. Implementing a Plan of Action.

For the OM to be effective with changing weather or climate, infrastructure owners must have funds, authority, and a willingness to make design modifications if conditions have changed and a new course of action is required. Although the concept of reserving funds to carry out these modifications may seem impractical in many instances, such forward funding may not be necessary. In many instances, recognition that changes in unfavorable extremes threaten failure, the owner (whether a public or private entity) can choose to either invest the resources necessary to implement planned modification, invest in the cost of total replacement, or suffer the loss because of failure. The advantage of the OM is that its use allows the owner to delay the choice until the unfavorable extremes are observed. Conversely, designing for the most-probable extreme (based on historical observations and assuming stationarity) restricts the owner or operator to partial or total replacement of the infrastructure.

3.3 OBSERVATIONAL METHOD IN PRACTICE

3.3.1 Example 1. Adaptive Design for Sea Level Rise (SLR)

Designing infrastructure under a changing climate based on available projections and data entails significant and time-variant uncertainty. Adaptive design methods with risk control offer a way to deal with associated

uncertainties, as illustrated in the following hypothetical example of the design and construction of a rail system in a coastal region experiencing SLR owing to a changing climate with the potential for surges and waves. As discussed previously, application of the OM involves four steps, each of which will be explored.

Step I. Distinguishing Most-probable from Most-unfavorable Conditions.

The design and construction of infrastructure in coastal areas requires an understanding of the potential for SLR as discussed in Chapter 2. In this hypothetical example, the proposed system is being considered to provide high-speed rail transportation between Miami and Homestead, Florida. The planning horizon is to the year 2100. As can be seen in Figure 3-1, the region is expected to experience significant relative SLR through the

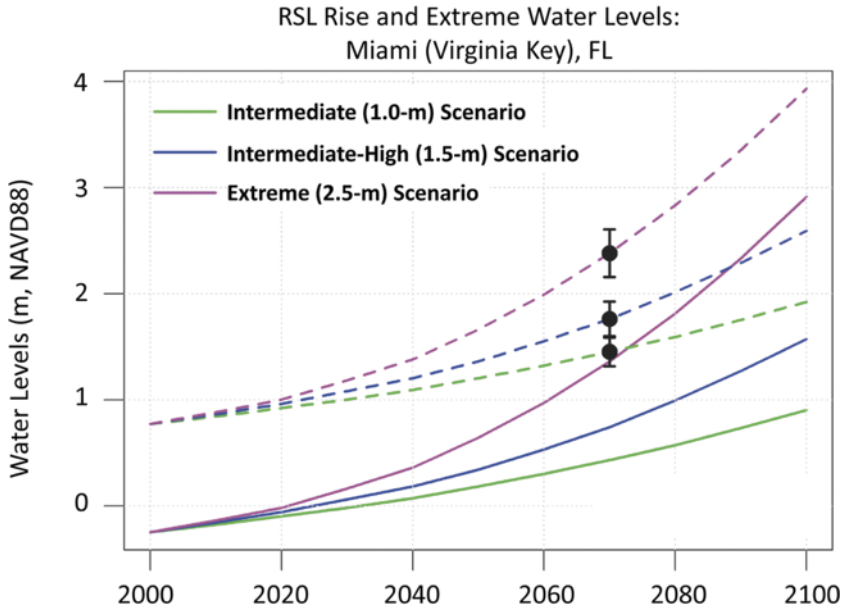

Figure 3-1. Rise of sea level under the intermediate (1-m), intermediate-high (1.5-m), and extreme (2.5-m) GMSL rise scenarios (solid curves) for the Florida Keys region, showing how the water-level height with a 1% annual exceedance probability (AEP of 0.01; dashed lines) and 95% confidence intervals (black error bars) estimated for year 2070 from hourly water levels at the NOAA Key West tide gauge changes in magnitude under each scenario. All curves are expressed in terms of the geodetic datum NAVD88 using the tidal datums at Key West.
Source: Modified from NOAA (2017).

remainder of the century. Using an AEP of 0.01 (dashed lines), three scenarios are available, each assuming varying rates of continental glacier melting. Beyond 2060, the difference between the intermediate-high scenario (1.5 m SLR) and the extreme scenario (2.5 m SLR) is 1 m. Analysis of associated construction costs indicates that building the rail system to reduce potential for failure owing to coastal flooding under the most-credible unfavorable condition (2.5 m of SLR) will add significantly to the project cost, making the project unfeasible. Additional analysis suggests that if the project can defer some costs projected under the extreme scenario until the future, funding for necessary modifications could be borne should they be necessary Thus, the OM seems to be a potential path forward for this project.

For the purposes of this project, the intermediate-high (1.5 m) scenario was chosen as the most-probable extreme, and the extreme (2.5 m) scenario was chosen as the most-credible unfavorable extreme.

Step II. Identifying a Course of Action.

Design and construction analyses must be performed to determine critical decision points during the life of the rail system at which modifications may be required. Figure 3-2 depicts the relationship between projected SLR and its associated uncertainty. The vertical axis shows the predicted sea level for the year 2100 as a function of time starting with a prediction made in the 2015. The uncertainty is assumed to decrease as the prediction year approaches the year 2100. The height of the rail bed can be based on the most-probable level, with appropriate consideration for potential needs to increase the height. Accommodating such a potential increase might require the installment of an oversized foundation system and other details to facilitate the height increase without needing to demolish the rail system itself. The sea level is tracked in future years and the height is kept the same or increased as needed. Several decision points are shown on the figure for the purpose of illustration. Such an adaptive management approach would help to counter the indecisiveness associated with great uncertainty levels. This approach can be combined with risk methods to create adaptive risk control strategies for economic and trade-off analysis as provided by Ayyub (2014).

Step III. Monitoring for Changes in Climate/Weather and Their Extremes.

In this example, no specific monitoring of the rail system is needed because local, state, and federal agencies are monitoring SLR in the region for a variety of applications. Operators of the rail system simply leverage these ongoing efforts as well as reports of nuisance or *sunny day* flooding in the area to determine whether the projected sea level is exceeding the

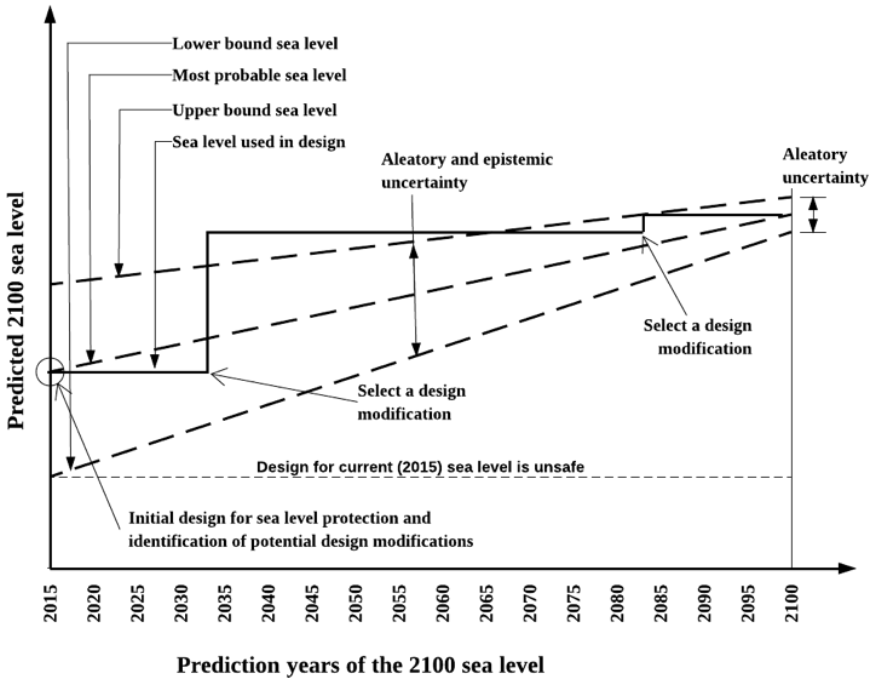

Figure 3-2(a). Adaptation with increasing sea level and decreasing uncertainty. Source: Ayyub and Wright (2016).

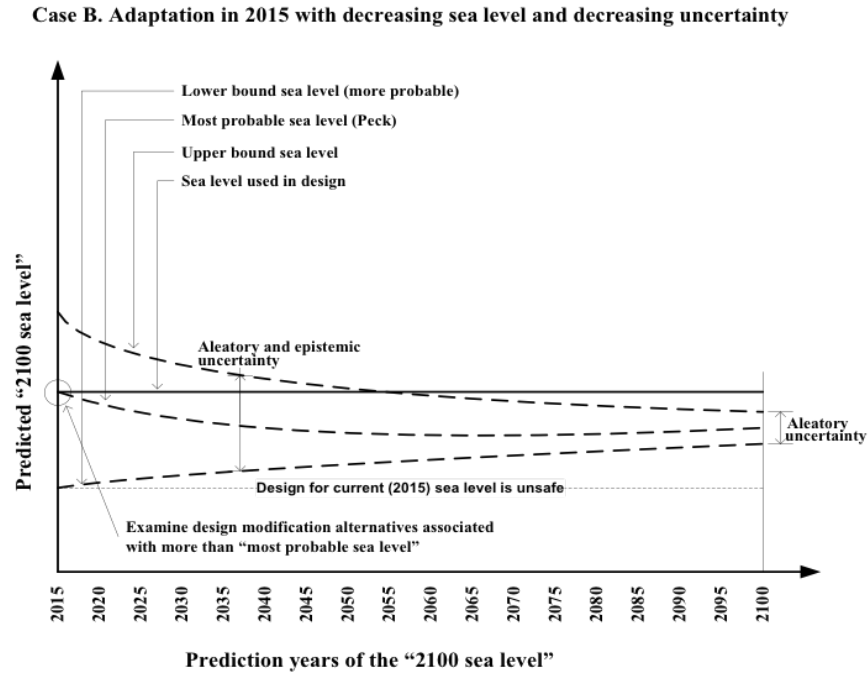

Figure 3-2(b). Adaptation unneeded with decreasing sea level and decreasing uncertainty.

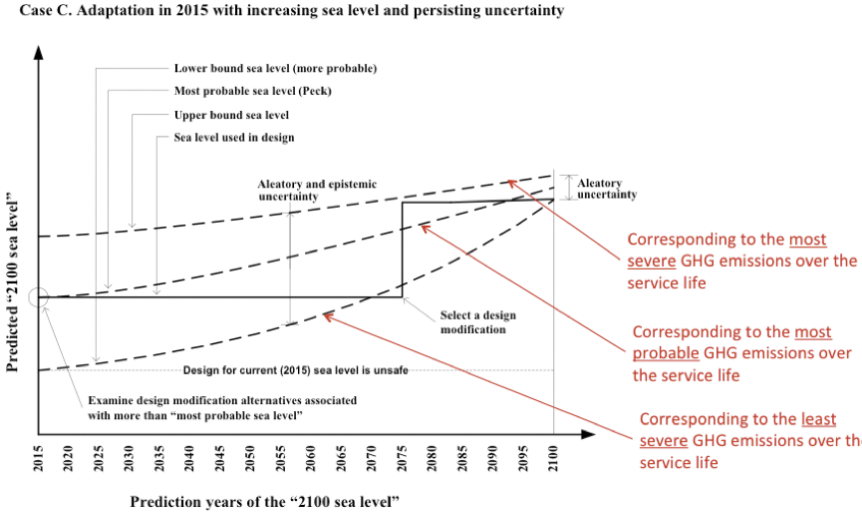

Figure 3-2(c). Adaptation in 2075 with increasing sea level and decreasing uncertainty.

most-probable projections used in the original design (intermediate-high scenario shown in Figure 3-1).

Step IV. Implementing a Plan of Action.

In this hypothetical example, planned modifications include the raising of tracks through the insertion of taller piers. The rail system is designed and constructed with a foundation capable of supporting the weight of additional precast piers should they be needed. A similar approach was used for the design of the Los Angeles to San Diego (LOSSAN) Rail Corridor (Dial et al. 2014), presented in Figures 3-3(a) and (b).

3.3.2 Example 2. Adaptive Design for Warming Permafrost Foundation

The OM has been applied numerous times over the past decade by cold-region engineers working in Alaska. This is a direct result of warmer air and warmer permafrost temperatures at many locations in North America compared to 40 years ago (Yarmack 2017).

Step I. Distinguishing Most-probable from Most-unfavorable Condition.

In Bethel, Alaska, a new hospital and the expansion of an existing clinic are under construction (2017). The driven pile foundations for the expansion are embedded in the warm permafrost that underlies the site.

Figure 3-3(a). Los Angeles to San Diego (LOSSAN) Rail Corridor that follows the sea coast and crosses low-lying areas on trestles.
Source: Dial et al. (2014).

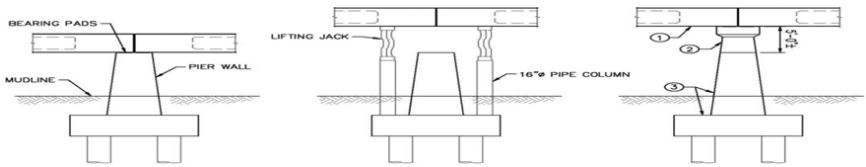

Figure 3-3(b). LOSSAN Rail Corridor uses a Moffatt and Nichol concept of precast piers and caps to allow insertion of additional pier segments if needed to adapt to flooding hazard.
Source: Dial et al. (2014).

Thermosyphons are installed adjacent to the piles to provide passive cooling of the surrounding permafrost.

The existing clinic was built 40 years ago in the late 1970s (Figure 3-4). In addition to an increase in the thawing index (and reduction of the freezing index) in Bethel over the past four decades, drainage and snow removal on the clinic grounds has not been maintained with respect to preserving permafrost in the area. Temperatures have risen to the extent that there is a *talik* (i.e., an area of unfrozen ground surrounded by frozen ground) in some areas between the seasonal frost and the permafrost, and the pile capacities are substantially less than the former design capacities.

Temperature monitoring was neglected until 2015. Although data is lacking to accurately quantify a future most-unfavorable thawing and freezing index, it is prudent to assume that both will change in a manner that is averse to the performance of the proposed driven pile foundations.

Figure 3-4. Existing clinic built in the 1970s in Bethel, AK. Source: Photo courtesy of E. Yarmack (used with permission).

Step II. Identifying a Course of Action.

The existing hospital was built on driven piles (Figure 3-5). On each individual pile or on at least one pile in a pile group, there are 2 × 2 in. square tubes attached to the piles that go close to full depth of the pile. These tubes will provide access for temperature-monitoring sensors. Furthermore, they may be used for passive or active cooling to decrease the temperature of the permafrost and increase pile capacity.

Construction for the new structure began in 2017. The piling and pile caps for the new building and the vertical thermosyphons used for passive cooling of the permafrost are shown in Figure 3-6. A surficial insulation layer was installed to mitigate surface thawing and enhance the cold sink effect created by the thermosyphons. The piles are driven to an approximate depth of 50 ft, and the vertical thermosyphons extend to a depth of approximately 40 ft.

In anticipation of warming temperatures and an increase in the thawing index, a flat-loop evaporator system was designed. The below-grade portion of the flat-loop evaporator thermosyphon system was assembled during construction when the foundation area was open (Figure 3-7). This part of the system was very inexpensive to install before the building was constructed.

Figure 3-5. Driven pile foundation supporting the existing clinic. Square tubes attached to the piles may be used for temperature monitoring and passive or active cooling of the surrounding permafrost.
Source: Photo courtesy of E. Yarmack (used with permission).

Figure 3-6. Driven pile foundation with thermosyphons for new hospital and clinic expansion.
Source: Photo courtesy of E. Yarmack (used with permission).

Figure 3-7. Flat-loop evaporator system installed during construction (white PVC pipes). The system will be used if permafrost temperatures rise to levels greater than anticipated under the most-probable condition.
Source: Photo courtesy of E. Yarmack (used with permission).

Step III. Monitoring for Changes in Climate/Weather and Their Extremes.

There are temperature-monitoring wells to the 50 ft depth that are currently manually monitored, but they can be attached to a data logger once the building is constructed. The black pipe coming out of the ground adjacent to the pile is the temperature-monitoring tube (Figure 3-8).

As previously noted, there are 2 × 2 in. square tubes attached to the driven piles under the existing building that will provide access for temperature-monitoring sensors. Furthermore, they may be used for passive or active cooling to decrease the temperature in the permafrost and increase pile capacity.

Step IV. Implementing a Plan of Action.

The evaporator pipes were pressure tested, sealed, and the ends capped. Should that system ever have to be activated, the evaporators can be located, condensers can be attached, and the system placed in operation. As previously noted, the 2 × 2 in. square tubes attached to the driven piles under the existing building may be used for passive or active cooling to decrease the temperature of the permafrost and increase pile capacity.

Figure 3-8. Temperature-monitoring well (black plastic pipe) adjacent to driven pile and thermosyphon.
Source: Photo courtesy of E. Yarmack (used with permission).

3.4 LOOKING BEYOND THE OBSERVATIONAL METHOD

As can be deduced from the previous discussion, the OM can offer a way to manage uncertainty in future weather and climate extremes owing to climate change for structures and projects that can accommodate post-construction modification. Unfortunately, much of the cost of projects in urban areas is driven by temporary measures such as force account, staging, access, and general construction difficulties that dramatically increase the cost of subsequent modification. In other systems, such as stormwater management, modification itself (e.g., installing larger culverts) would require nearly complete replacement. In these situations, other methods for managing risk owing to uncertainty about future weather and climate extremes are needed. Chapters 5, 6, and 7 cover these methods.

3.5 REFERENCES

Ayyub, B. M. 2014. *Risk analysis in engineering and economics*, 2nd Ed. Boca Raton, FL: Chapman & Hall/CRC.

Ayyub, B. M., and R. N. Wright. 2016. "Adaptive climate risk control of sustainability and resilience for infrastructure systems." *J. Geogr. Nat. Disast*. 6(2). Accessed August 15, 2018. http://dx.doi.org/10.4172/2167-0587.1000e118.

Bonnin, G. M., K. Maitaria, and M. Yekta. 2011. "Trends in rainfall exceedances in the observed record in selected areas of the United States." *J. Am. Water Resour. Assoc*. 47(6), 1173–1182.

Dial, R., B. Smith, and G. Rosca Jr. 2014. "Evaluating sustainability and resilience in infrastructure: Envision™, SANDAG, and the LOSSAN Rail Corridor," *Proc., 2014 Int. Conf. Sustain. Infra*. Reston, VA: ASCE, 164–174.

Eurocode 7. 2004. "Geotechnical design—Part 1: General rules." *BS EN 1997-1:2004*. London: Springer.

IPCC (Intergovernmental Panel on Climate Change). 2012. "Summary for policymakers." In *Managing the risks of extreme events and disasters to advance climate change adaptation: Special report of the intergovernmental panel on climate change*, C. B. Field et al. (eds.). Cambridge, UK: Cambridge Univ. Press.

IPCC. 2014. *Climate change 2014: Impacts, adaptation, and vulnerability. Part A: Global and sectoral aspects*, C. B. Field et al. (eds.). Cambridge, UK: Cambridge Univ. Press. Accessed February 13, 2016. https://www.ipcc.ch/report/ar5/wg2/.

Korff, M., E. de Jong, and T. J. Bles. 2013. "SWOT analysis Observational Method applications." *Proc., 18th Int. Conf. on Soil Mechanics and Geotechnical Engineering*. London: International Society for Soil Mechanics and Geotechnical Engineering.

Nicholson, D. P., C. E. Dew, and W. J. Grose. 2006. "A systematic 'Best Way Out' approach using back analysis and the principles of the Observational Method." Hawthorne, NJ: Deep Foundations Institute.

Nicholson, D., C. Tse, C. Penny, S. O'Hana, and R. Dimmock. 1999. "The Observational Method in ground engineering—principles and applications," Vol. 185. London: Construction Industry Research and Information Association.

NOAA (National Oceanic and Atmospheric Administration). 2017. "Global and regional sea level rise scenarios for the United States." W. V. Sveet et al. (eds.). *NOAA Tech. Rep. NOS CO-OPS 083*. Silver Spring, MD: NOAA.

NRC (National Research Council). 2016. *Attribution of extreme weather events in the context of climate change*. Washington, DC: National Academies Press. DOI: 10.17226/21852.

NSIDC (National Snow and Ice Data Center). 2012. "Arctic climatology and meteorology glossary." Accessed October 9, 2012. http://nsidc.org/arcticmet/glossary/weather.html.

NWS (National Weather Service). 2013. "National Weather Service glossary." Accessed March 14, 2013. http://w1.weather.gov/glossary/.

Patel, D., D. Nicholson, N. Huybrechts, and J. Maertens. 2007. "The observational method in geotechnics." In *14th European Conf. on Soil Mechanics and Geotechnical Engineering*. Amsterdam: IOS Press, 24–27.

Peck, R. B. 1969. "Advantages and limitations of the Observational Method in applied soil mechanics." *Geotechnique* 19(2), 171–187.

Terzaghi, K. and R. B. Peck. 1948. *Soil mechanics in engineering practice*. Hoboken, NJ: Wiley.

Yarmack, E. 2017. Personal communication, July 29, 2017.

CHAPTER 4
CHARACTERIZATION OF EXTREMES AND MONITORING

4.1 INTRODUCTION

This chapter reviews the characterization of extreme precipitation (both stationary and non-stationary approaches), the statistical properties of both record storm events and the flooding events generated by such events, flooding, multihazard scenarios, and hazard monitoring versus risk monitoring. Section 4.2 defines and describes methodologies in terms of stationary time series and non-stationary approaches. For example, the use of IDF curves under the assumption of stationarity is presented. Design and failure risk assessment procedures for infrastructure cases (e.g., dams, roads, sewer and stormwater drainage systems) rely on rainfall IDF curves. Section 4.3 follows with the use of the multimodel non-stationary approach. A non-stationary approach to define IDF curves is necessary upon detection of a statistically significant trend in the time series for a better characterization of the statistics of future rainfall events. GCMs provide multimodel simulations of the future climate under different scenarios. Currently, model simulations are highly uncertain, and models exhibit large intermodel variability. Although work on GCMs to make them more convection-resolving and provide more reliable rainfall statistics is progressing, it is unrealistic to expect they can be used alone to resolve the scale issues. Raw GCM precipitation data are generated at large spatial scales (hundreds of kilometers) that do not capture local processes (tens of kilometers) and should not be used directly, especially to evaluate place-specific extremes (at the scale of much of our infrastructure).

Section 4.3 (Precipitation and Flooding) describes methodologies to compute the recurrence intervals of precipitation events (both mean and extreme), as well as the statistical properties of flooding events generated

by those extreme storm events. The differences in the statistical properties are attributed to complex surface and subsurface processes independent of climatic inputs. Computation of the statistical moments for flooding events follows primarily the method of L-moments (Hosking 1990). The *NOAA Atlas 14* computations of extreme precipitation depths also use L-moment regionalization (NOAA 2017). Note that Section 4.3 reviews the statistical correlation between rainfall events and streamflow produced by those events, whereas Section 4.4 describes modeling trends in flood peak distributions, estimating the parameters of the non-stationary model and frequency analysis.

4.2 EXTREME PRECIPITATION

Extreme precipitation events are commonly represented using precipitation IDF curves. Extreme climatic events are growing more severe and frequent, calling into question how prepared our infrastructure is to deal with these changes. Infrastructure design relies on precipitation IDF curves with the so-called stationary assumption, meaning extremes do not vary significantly over time. However, climate change is expected to alter climatic extremes, a concept termed non-stationarity. This section provides a framework for generating non-stationary IDF curves based on multimodel simulations.

4.2.1 Introduction

During the last century, we have been observing a warming climate with more intense precipitation extremes, likely because of increases in the atmosphere's water-holding capacity. Reports indicate that many regions, including the United States, central Africa, parts of southwest Asia (i.e., Thailand, Taiwan), Central America, Australia, and parts of Eastern Europe, have experienced an increase in extreme events (DeGaetano 2009, Fischer and Knutti 2016, USGCRP 2014, Wasko et al. 2016, Zheng, et al. 2015).

The observed trends and projected changes in future extreme events have fueled the debate in the scientific community on the inclusion of the observed trend in hydrologic data analysis. (Cohn and Lins 2005, Katz 2010, Katz et al. 2002, Klemeš 1974, Koutsoyiannis 2005, Lins and Cohn 2011, Milly et al. 2008, Montanari and Koutsoyiannis 2014, Serinaldi 2015). Moreover, several studies have addressed the same issue for extreme-value analysis (Mondal and Mujumdar 2015, Sarhadi and Soulis 2017). Following Ragno et al. (2017), a framework for deriving IDF curves that can account for the expected changes in rainfall extremes is presented that combines concepts from the analysis of time-dependent data and information brought by multimodel simulations. Hereafter, *return level* (RL) refers to the intensity of a

rainfall event, whereas *return period* (RP) defines the average expected time (in years) between two consecutive extreme events of the same intensity. Given a rainfall intensity (i.e., RL) with a probability p of occurrence, the RP is derived as RP = $1/(1–p)$.

4.2.2 IDF Curves with Stationarity

IDF curves represent the probable intensity of a rainfall event given a particular duration (or time of concentration, e.g., a day) and an average RP (recurrence interval). Design and failure risk assessment procedures for infrastructures (e.g., dams, roads, sewer and storm water drainage systems) rely on rainfall IDF curves. *The use of projections for IDF curves is an ongoing research pursuit. Currently, accepted practices for projecting IDF curves are unavailable. The MOP does not imply that practicing engineers should develop projected IDF curves for their stormwater management design needs where such curves are unavailable for cases without stationarity.*

Generally, the process for estimating IDF curves involves the following steps:

1. Fitting a representative distribution function to rainfall records (usually annual maxima) for a given storm duration [Figures 4-1(a), 4-1(b), 4-1(c)];
2. Delineating rainfall intensities as a function of the MRIs (RL–RP curves) for a given storm duration [Figure 4-1(d)]; and
3. Plotting rainfall intensities with the same RP as a function of storm duration (IDF curves, Figure 4-2).

These steps describe the general procedure, even though the detailed guidelines differ region-wise. The current procedure follows the idea that rainfall events that happened in the past are representative of what might happen in the future (known as the stationary assumption), and so the distribution function selected for describing the rainfall data is time-invariant. However, an expected impact of global warming is the higher capability of the atmosphere to hold water vapor, causing an intensification of rainfall events and increasing the flood risk in infrastructure systems. Consequently, for a time series with a statistically significant trend over time, the assumption of a time-invariant distribution function may not be reasonable.

4.2.3 IDF Curves without Stationarity

The approach proposed here aims to define IDF curves to include potential time-dependent changes in the precipitation observations (or simulations of the future precipitation). *Again, as noted in Section 4.2.2, the use of projections for IDF curves is a recent research effort, particularly to account for nonstationarity. Currently, accepted practices for projecting IDF curves without*

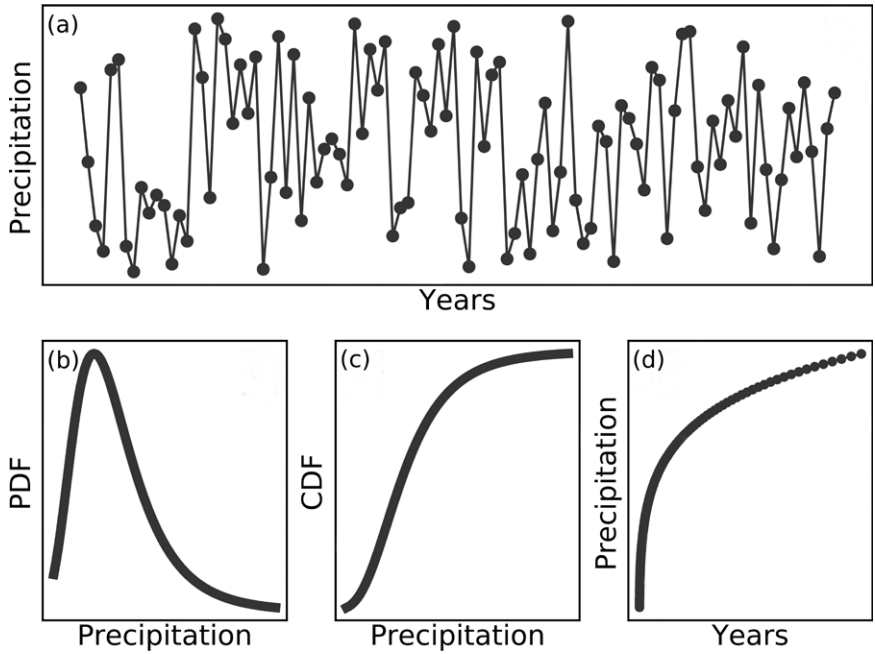

Figure 4-1. Annual maxima time series and the representative distribution functions: (a) annual maxima time series; (b) fitted PDFs; (c) fitted cumulative density function; and (d) corresponding RL–RP curve.

stationarity are unavailable. The MOP does not imply that practicing engineers should develop projected IDF curves for their stormwater management design needs where such curves do not exit for cases without stationarity.

Non-Stationary Extreme Rainfall Analysis. A non-stationary approach to define IDF curves is necessary upon detection of a statistically significant trend in the time series under study (Figure 4-2) for a better characterization of the statistics of future rainfall events. A trend can be detected using commonly used trend tests and hypothesis testing methods (e.g., Mann–Kendall trend test). In case a trend is statistically significant, the assumption of a distribution function with time-invariant parameters may not be reasonable. The procedure proposed here to handle non-stationary data assumes the parameters of the distribution to be a function of time.

A GEV distribution (Equation 4-1, CDF) is selected to be representative of the rainfall extremes, being widely used for block maxima.

$$\Psi(x) = \exp\left\{-\left(1+\xi\cdot\left(\frac{x-\mu}{\sigma}\right)^{-\frac{1}{\xi}}\right)\right\} \tag{4-1}$$

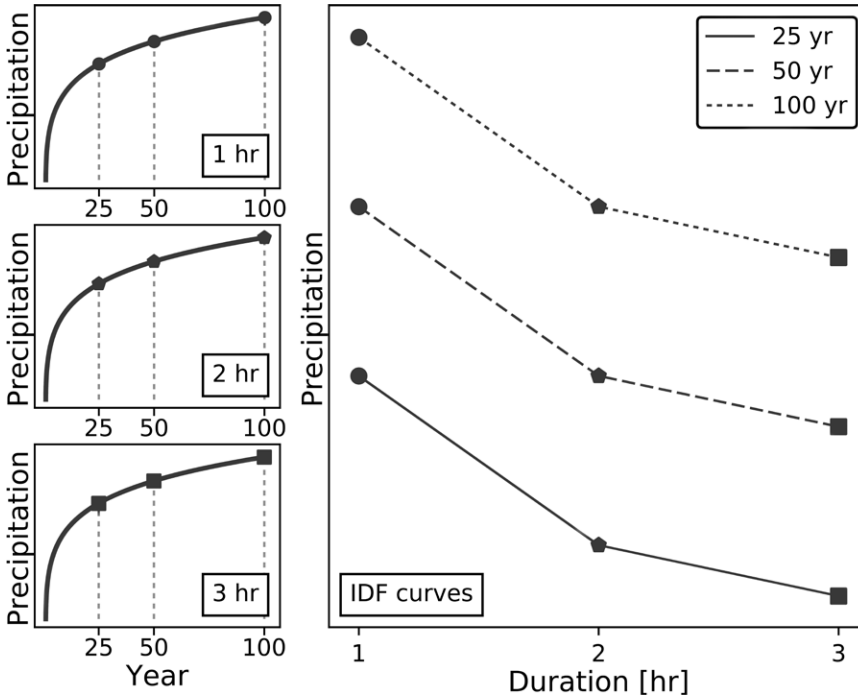

Figure 4-2. IDF curves definition combining rainfall intensities of different durations.

Equation 4-1 is defined for $1+\xi\cdot\left(\frac{x-\mu}{\sigma}\right)>0$ and $\sigma>0$.

The GEV distribution is a function of three parameters: μ (location parameter) represents the center of the distribution; σ (scale parameter) describes the distribution of the data around μ; and ξ (shape parameter) defines the tail behavior of the distribution. The detected trend indicates changes in the mean of the time series over time, so the location parameter μ is modeled as a function of time [$\mu(t) = \mu_1 t + \mu_0$], whereas the other two parameters are kept time-invariant. However, the scale parameter can be modeled as a function of time [$\sigma(t) = \sigma_1 t + \sigma_0$] if changes in the distribution of the data around the location parameters are detected. The shape parameter, though, is hardly defined with precision, so it is advisable to keep it constant (Coles 2001). The outcome of the parameters estimation procedure is a distribution function that changes over time [Figure 4-3(b)].

To proceed with the IDF curves definition, a distribution function should be selected. When observed data and/or historical simulation are used, the

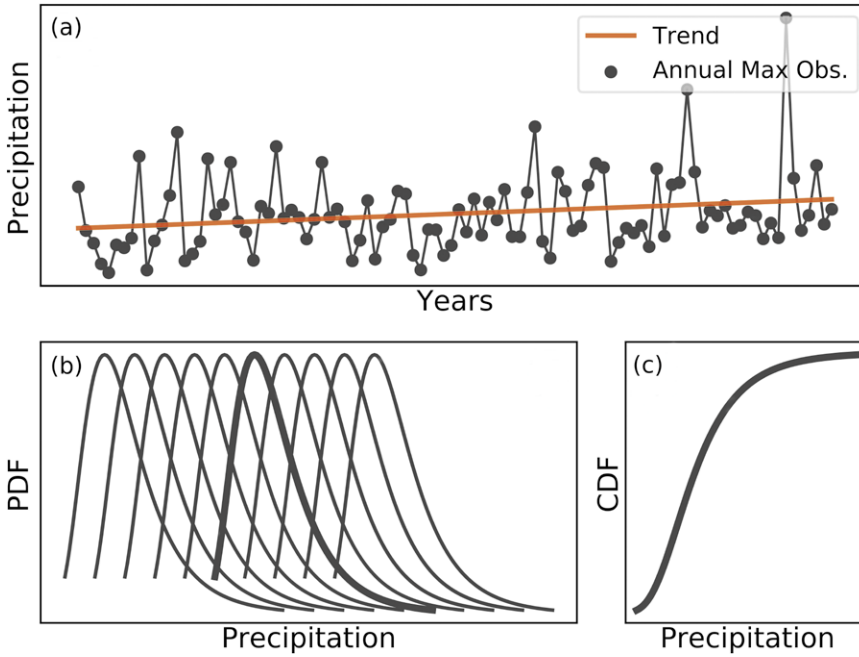

Figure 4-3. Annual maxima time series with trends: (a) annual maxima time series; (b) PDFs as a function of time (the thicker line is the selected one); and (c) cumulative density function selected for IDF curves definition.

distribution function can be fixed within the observed period [e.g., μ is equal to the median of $\mu(t)$, Figures 4-3(b) and 4-3(c)] or forward in time to project IDF curves in the future. The latter assumption can be seen as more conservative. Once the distribution function is fixed, the precipitation intensity (or RL) associated to the non-exceedance probability p [or RP, $T = 1/(1 - p)$] can be evaluated using the following equation:

$$RL(p) = \left(\left(-\frac{1}{\ln(p)} \right)^{\xi} - 1 \right) \frac{\sigma}{\xi} + \mu \tag{4-2}$$

for $\xi \neq 0$. Finally, IDF curves can be plotted combining rainfall intensities with the same RP as a function of storm duration (similar to the stationary case shown in Figure 4-2).

Incorporating Multimodel Climate Model Simulations of the Future. GCMs provide multimodel simulations of the future climate under different scenarios. Currently, model simulations are highly uncertain and

models exhibit large intermodel variability. However, GCMs have been improving rapidly, and they are expected to provide more reliable rainfall statistics as they evolve. Assuming that the current multimodel future precipitation simulations are reliable, we propose a framework for incorporating them in estimating future IDF curves. The procedure involves

- Estimating historical IDF curves using model simulations;
- Estimating projected IDF curves using each model in a multimodel ensemble of the future precipitation (non-stationary GEV will be used if a statistically significant trend in the data is detected; otherwise a time-independent distribution function will be considered); and
- Evaluating the change in the future relative to the past.

The climate projections highly depend on the future scenario selected and the characteristics of the models used to generate them. For this reason, each simulation should be processed independently (Figure 4-4). In addition, in the case of statistically significant trends in the future climate projections, it is advisable to select a time to fix the distribution function

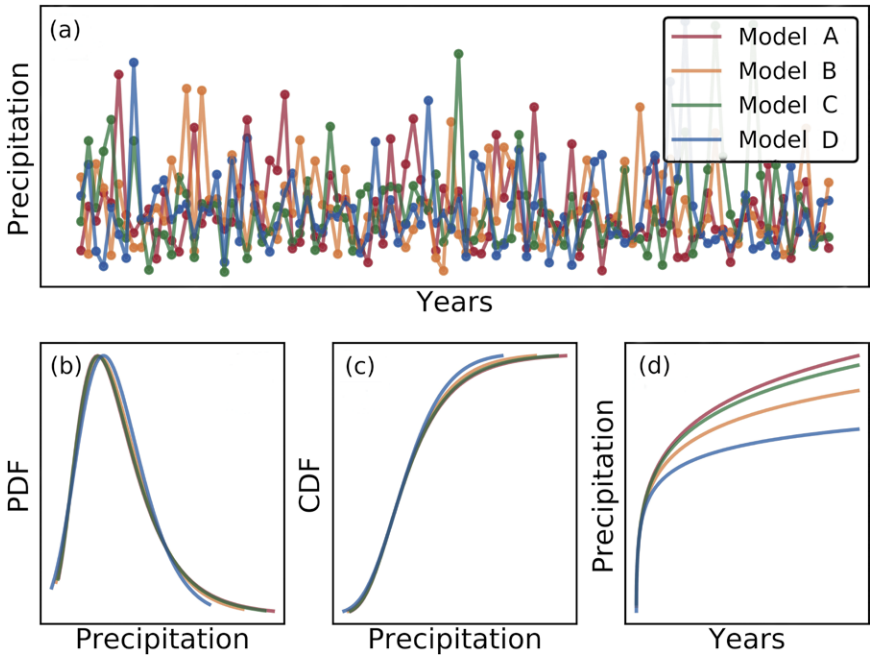

Figure 4-4. Annual maxima time series from GCM simulations: (a) Time series from four different models; (b) PDFs of each model output; (c) cumulative density functions of each model output; and (d) RP–RL curves for each model output.

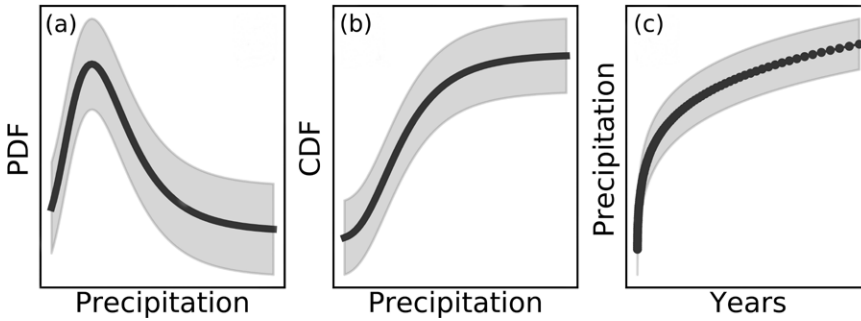

Figure 4-5. Probabilistic approach: (a) PDFs; (b) cumulative density functions; and (c) RL–RP. Solid lines: expected value—ensemble median; shaded areas: uncertainty bounds –90% confidence interval.

within the time period of the simulation to avoid accounting for the trend multiple times.

For both historical and projected simulations, once the distribution functions are selected and fixed over time, two ensembles of historical and projected IDF curves are obtained. Each ensemble provides the variability of the IDF curves across climatic models.

Finally, a bias correction is applied to the historical IDF curves so that the median of the simulated ensemble overlays current IDF curves provided by the *NOAA Atlas 14* series (NOAA 2006, 2008, 2011a, 2011b, 2011c, 2012a, 2012b, 2013a, 2013b, 2014, 2015). The historical IDF curves are retrieved under the stationary assumption in accordance with the approach adopted by NOAA, making the comparison valid. The same bias correction used for historical IDF curves is applied to IDF curves derived using future climate data to define future IDF curves.

Probabilistic Approach. Extreme-value analysis usually deals with small data sets. Consequently, a probabilistic approach for parameter estimation is recommended to quantify the uncertainty in the fitted parameters. The outcome of the probabilistic approach is an ensemble of solutions (e.g., multiple sets of parameters as a possible solution). The ensemble captures the variability of the solution owing to the estimation procedure selected (Figure 4-5), and it can be used to quantify the uncertainty around the parameters estimated.

The methodology here described adopts a probabilistic approach (Bayesian inference approach) for both the stationary and non-stationary procedures, as well as for observed data and climate model simulations. Therefore, the procedures described so far (stationary or non-stationary cases) should be applied to each time series independently. Afterward, the

ensembles of solutions are combined together. Thus, the uncertainty within the models and across the models in the parameter estimation is accounted for in the IDF curve definition. As a result, the ensemble of IDF curves can be summarized as follows:

- Expected IDF curve: ensemble median; and
- Uncertainty bounds:
  - Lower bound: 5th percentile; and
  - Upper bound: 95th percentile.

When model simulations are considered, each model is processed independently, and afterward it is combined with the other models. Consequently, the final outcome of the expected IDF curve and the uncertainty bounds account for the variability within each model and across models.

Expected Change in RP. The probabilistic approach allows quantifying the changes in the frequency of past events when historical and projected IDF curves are available. To assess the expected future RP of a historical event, the following steps should be taken:

1. Select the event with rainfall intensity I and return period T_I (e.g. 25-, 50-, 100-year) based on historical records, (Figure 4-6, left panel).
2. Extract all the return periods ($T_{I,1}, \ldots, T_{I,i}, \ldots, T_{I,n}$) with rainfall intensities equal to I from which the ensemble of RL–RP curves associated with future climate scenario are extracted (Figure 4-6, right panel).
3. The median of the return periods $T_{I,i}$ extracted as described in step 2 is the expected future RP of the historical event with rainfall intensity I. To be conservative, if the expected future RP is higher than the historical one, the latter is taken as the future RP.
4. The 95th and the 5th quantiles of the return periods $T_{I,i}$ extracted are respectively the upper and the lower bounds of the estimate.

Step-by-Step Guide. The methodology proposed here is general and can be applied to any geographical location. The following are the steps to evaluate future IDF curves based on multimodel simulations:

Data. This model can be used with historical data only and with multimodel climate simulations. Extract historical and/or future precipitation from the latest set of available climate model simulations (currently, CMIP5), for example, daily, 2-day, 3-day, and 7-day annual maxima from each model separately. In the case of GCM simulations, users can use downscaled/bias-corrected simulations or implement a reliable downscaling/bias-correction approach to refine the spatial and/or time resolution and improve the simulations. Users can use different types of indicators to sub-sample from available observations based on the application in hand. For example, when

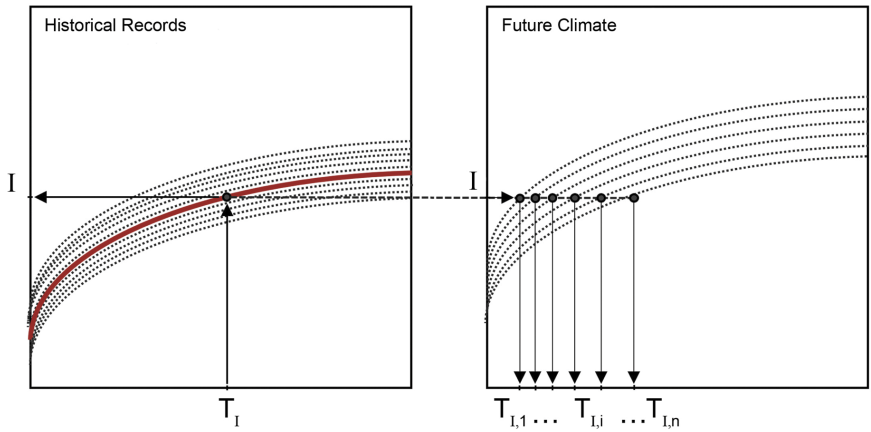

Figure 4-6. Conceptual explanation of the methodology adopted to quantify changes in the occurrences of historical events under future climate.

using precipitation extremes, the users can use only climate model simulations that reasonably reproduce historical extremes. For methods for evaluating climate model simulations, the interested reviewer is referred to Mehran et al. (2014) and references therein.

Distributional Parameter Estimation. A GEV distribution should then be fitted to each time series of annual maxima. To select the most suitable approach (stationary vs. non-stationary), a Mann–Kendall trend test can be used at a certain significance level (e.g., 0.05). If there is no trend, then the commonly used stationary approach would be sufficient. Otherwise, the non-stationary GEV should be used. The entire procedure, including trend analysis and stationary/non-stationary GEV fitting, are built into the NEVA software package (Cheng et al. 2014). The software is available to the public for free on MATLAB File Exchange (https://www.mathworks.com/matlabcentral/fileexchange/48238-nonstationary-extreme-value-analysis--neva--toolbox). NEVA_GEV should be used for block maxima analysis. In the NEVA_GEV folder, the ReadData folder is stored, which contains the following files:

- *GEV_sta_nonsta.txt*: includes model parameters;
- *names.txt*: includes figure titles and axes labels (they appear in the output figures);
- *prior.txt*: include prior parameters (ranges of model parameters used for sampling); and
- *si1.txt*: includes input data.

These files should be updated based on the data under study. The *Nonsta* parameter in *GEV_sta_nonsta.txt* defines the type of approach performed. When *Nonsta* is set equal to 1, NEVA first performs a Mann–Kendall test, and then automatically, based on the test results, performs the stationary or non-stationary analysis. The non-stationary analysis will be carried out while considering the parameter μ as time-dependent.

If a non-stationary analysis is performed, NEVA provides as output three different RL–RP curves considering the parameter μ equal to the following:

- Median of $\mu(t)$ over time period of observations;
- Median of $\mu(t)$ over 100 years beyond the period of observations; and
- 95th percentile of $\mu(t)$ over the 100 years beyond the period of observations.

IDF Curves. After the RP–RL curves are evaluated, rainfall intensities with the same RP are plotted as a function of storm duration to get an ensemble of IDF curves. The ensemble of IDF curves will account for the variability within the model (owing to the probabilistic approach) and the variability across models (owing to multiple climatic models). The median of the ensemble will be used as the expected IDF curve and the 5th and 95th quantiles will be used as the lower and upper bounds, respectively, to define the 90% confidence interval.

A quantile-based bias correction should then be applied to historical IDF curves so that the expected historical IDF curve overlays the IDF curve provided by the *NOAA Atlas 14* series (NOAA, 2006, 2008, 2011a, 2011b, 2011c, 2012a, 2012b, 2013a, 2013b, 2014, 2015). The same bias correction is applied to the ensemble of IDF curves calculated using projected simulations.

Figure 4-7 shows a sample of historical and projected IDF curves derived using the procedure just described. Figure 4-7(a) compares the future IDF curve (red line) with the historical IDF curve (blue line). Based on the method presented in Figure 4-6, the change in RP of extreme precipitation can be estimated using multimodel simulations [Figure 4-7(b)].

4.3 PRECIPITATION AND FLOODING

An understanding of these factors guides the methodology for describing extreme precipitation events. An understanding of some of these factors, and the desirability to examine past records of extreme storm events and corresponding stream stages, was recognized a century ago by engineering staff of the Miami Conservancy District (1917), Dayton, Ohio.

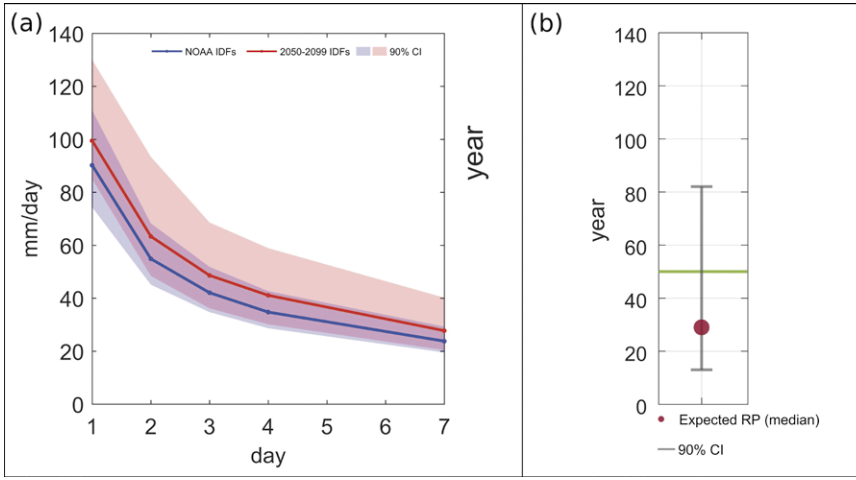

Figure 4-7. Sample outputs from NEVA: (a) IDF curves using multimodel simulations; and (b) expected change in RPs.

4.3.1 Storm Event and Flood Frequency Methodology

A common basis for comparison among these events is the MRI in years. In order to determine rainfall record historical extreme events, a number of options are available. Event MRIs, which are also called RPs as previously discussed, may be computed from Cunnane (1978) as follows:

$$T = \frac{n + 1 - 2\alpha}{m - \alpha} \tag{4-3}$$

where
T = MRI (e.g., in years),
n = number of peak values (e.g., number of years),
m = relative ranking of values (largest = 1), and
α = a constant ($0 < \alpha \leq 1$).

Note that Equation 4-3 describes how an RP or MRI value is obtained from rank-order data rather than from an annual extreme distribution as discussed in the previous section. Cunnane (1978) recommends $0.375 < \alpha \leq 0.44$ for the Log-Pearson distribution. Thus, a commonly used value of 0.4 yields

$$T = \frac{n + 0.2}{m - 0.4} \tag{4-4}$$

The AEP may be defined as

$$p_n = 1 - (1 - p)^n \tag{4-5}$$

where p is the AEP for each year. USGS software such as the PeakFQ computer program (Flynn et al. 2006) expresses the AEP as percent in plots of annual peak discharge (ordinate) versus the AEP in percent (abscissa). Version 7.1 of PeakFQ incorporates some of the recommendations documented in Bulletin 17C (England et al. 2016), such as the EMA (Cohn et al. 1997). The EMA has been thoroughly evaluated by Paretti et al. (2014).

A number of alternative methods are available to compute *flood frequency* (Kite 1977, Cunnane 1988, Pandey and Nguyen 1999, England 2011, Dawdy et al. 2012). There are significant differences between long-term averaged storm events and historical extreme events, and these analyses serve different purposes. Nonetheless, both approaches are complementary to each other.

The mathematical basis for the more complex statistical distributions used to calculate the recurrence intervals is presented in Appendix C.

The GEV probability distribution is the one of the most relevant distributions used for climate change scenarios, whether applied to floods or droughts, combining the Gumbel, Fréchet, and Weibull distributions. L-moment techniques use linear combinations of order statistics (Hosking 1990), and these techniques have been applied to both floods and point rainfall (Vivekanandan 2014, NOAA 2013b). The primary advantage of L-moments is that they are much less influenced by the effects of sampling variability or outliers, and they are virtually unbiased for small samples. Computation of the precipitation depth d for a given point nonexceedance probability F is as follows (Asquith 1998):

$$X_d(F) = \xi + \frac{\alpha}{\kappa}\left\{1 - [-\ln(F)\ ]^{\kappa}\right\} \tag{4-6}$$

If a storm depth for a given duration is known, the storm's *point* annual nonexceedance probability can be estimated by

$$F = \exp - \left\{1 - \frac{\kappa}{\alpha}[X_d(F) - \xi]\right\}^{1/\kappa} \tag{4-7}$$

Implementation of the L-moment method for the GEV distribution follows Hosking (1990) and is presented in Appendix C.

The US Water Resources Council (1967) adopted the Log-Pearson Type III distribution as the standard flood frequency distribution (peak flood discharges) to be used by all federal agencies, such that the PDF is defined as

$$f_X(x) = \frac{1}{\alpha\, x\, \Gamma(\beta)}\left(\frac{\ln x - \gamma}{\alpha}\right)^{\beta-1} \exp\left[-\left(\frac{\ln x - \gamma}{\alpha}\right)\right] \tag{4-8}$$

which states that if the logarithms ($ln\ x$) of variable x are distributed as a Pearson Type III variate, then the variable x is also distributed as a

Log-Pearson Type III variate. Note: with *zero skew*, the Log-Pearson Type III distribution reduces to a log-normal distribution. Kite (1977) reviewed in detail alternative methods for computing the moments of the distribution when a particular technique does not converge to a solution for a particular peak flow data set.

Implementation of the L-moment method for the Log-Pearson Type III distribution follows Hosking (1990) and is presented in Appendix C.

EV1 is defined by

$$f(x) = \frac{1}{\beta}\exp\left(-\frac{x-\mu}{\beta}\right)\exp\left[-\exp\left(-\frac{x-\mu}{\beta}\right)\right]$$

where

μ = location parameter β = scale parameter

x = extreme (large) value (4-9)

The L-moment implementation of EV1 is also presented in Appendix C.

4.3.2 Long-term Average Storm Event Analysis

It has been recognized for over three decades that the large number of factors that affect surface runoff quantity (rainfall duration, intensity, time between events, volume, infiltration, antecedent soil moisture, etc.) and surface runoff quality (pollutant loads and buildup between storms, surface washoff, transport, kinetic interactions, etc.) limits the exclusive use of any single event for a general understanding of historical storm event characteristics. Regardless of whether water quantity or quality is the primary objective, long-term historical rainfall data are required. An hourly or shorter-interval precipitation time series at least 30 to 40 years long is desirable. The purpose in quantitative analysis of the rainfall time series is to summarize the variables of interest (depth, duration, intensity, and time between storm events) and to statistically characterize the rainfall record to assess the probability of the occurrence of storm events of various magnitudes. To properly analyze the rainfall time series, storm events must first be defined in terms of their statistical independence (see Figure 4-8). A common approach is to derive an MIT such that the intervals between storm event midpoints are nearly *exponentially distributed* (Restrepo-Posada and Eagleson 1982). Trial values of the MIT are chosen until a COV near 1.0 is finally obtained for the time interval between event midpoints.

A reliable source of precipitation data is the NOAA NCEI: access to a large number of rainfall stations and their data is available online. The historical record of hourly precipitation from 1948 to 2011 at RDU, located only 12 miles from Durham, North Carolina, was analyzed to obtain storm event statistics, which are summarized in Table 4-1. This represents over

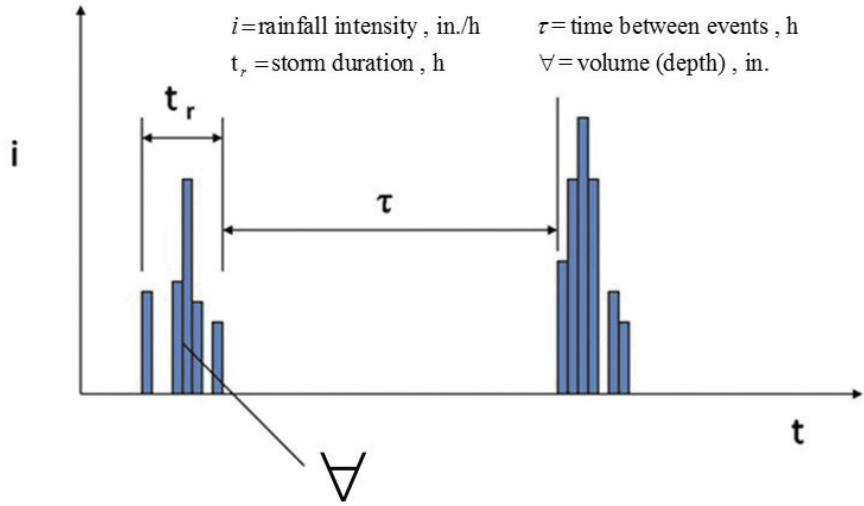

Figure 4-8. Storm event variables.

Table 4-1. NOAA Hourly Rainfall Station Description and Statistics of Storm Events, Raleigh-Durham, Wake County, NC (Station No. 317069, Lat: N 35:52:00, Long: W 78:47:00, Elevation: 416 ft, 1948 to 2011).

Storm event variable	Maximum	Mean	COV
No. of storms[a] per year[b]		99.523	0.105
Depth, in.	7.45	0.421	1.394
Intensity, in./h	1.21	0.070	1.352
Duration, h	67	6.869	1.097
Time between events, h	1032	87.403	**1.002**
Total no. of storms[a]		6359	

[a]Number of storms is based on an MIT of 6 h, which yielded a COV very near 1.0 for time between events for the rainfall time series.

6,300 storms using an MIT of 6 hours of dry weather to separate independent storm events. The average storm duration was 6.9 hours. The annual variability in the rainfall record is presented in Figure 4-9, with a mean annual rainfall of 41.5 in. Figure 4-10 shows that the mean *monthly* rainfall is distributed rather uniformly throughout the year, with hurricane-related extremes occurring from June to October, peaking in September. Figure 4-11 illustrates that storms are more frequent in July and least frequent in October.

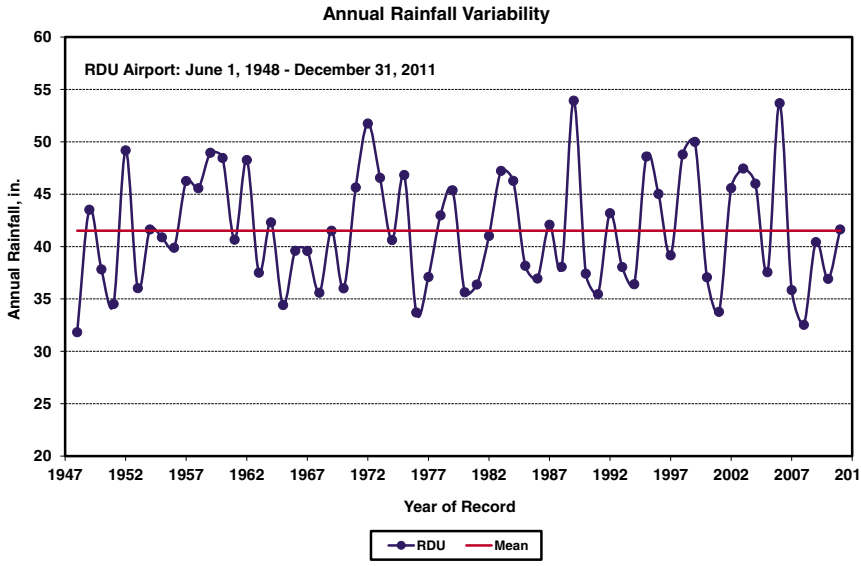

Figure 4-9. Annual rainfall variability at RDU.

4.3.3 Extreme Historical Storm Events and Floods

This section illustrates analyzing extreme historical storm events and floods. The *storm event* MRIs for the top 25 events in terms of volume (depth) for RDU were computed and are presented in Table 4-2. The storm event of September 4, 1999, constituted a record for total volume (depth, 7.45 in.), illustrated in Figure 4-12. It generated a flow of 1,390 cfs at the Eno River near the Durham USGS station the next day. It was influenced by Hurricane Dennis, which made landfall 188 miles southeast of RDU at Cape Lookout. However, the *maximum hourly intensity* (2.64 in.) was observed at RDU for the event of July 24, 1997: a short-duration, high-intensity summer thunderstorm that generated much larger local urban flooding. Through application of *NOAA Atlas 14*, Vol. 2 (NOAA 2006), point precipitation-frequency estimates are presented in Table 4-3. The storm event of September 4, 1999, would rank near a 50-year event (7.34 in.) for a 48-hour duration. An estimate applying the GEV fitted using L-moments (Hosking 1990) yielded 6.91 in. for a 50-year RP.

Rain gauges and streamflow stations nearby are shown in Figure 4-13. There are two located northeast of RDU in the Durham, North Carolina, area (Eno River near Durham and Sandy Creek, downstream from Duke University's West Campus), one located slightly southwest (Haw River at Bynum), and two located southeast of RDU (Crabtree Creek, at US 1 in

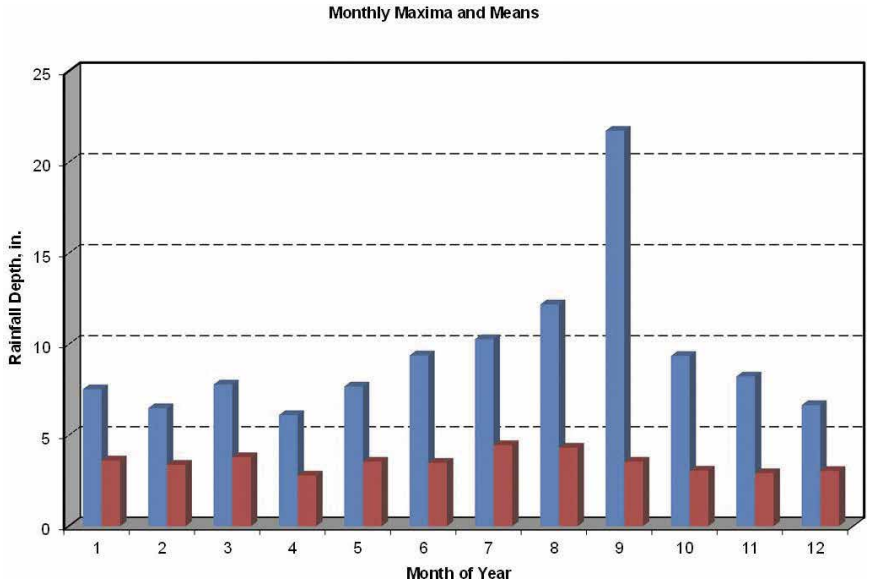

Figure 4-10. Monthly maxima and means at RDU.

Figure 4-11. Time between storm events at RDU.

Table 4-2. MRIs for RDU.

Recurrence interval (years)	Rank	Depth (in.)	Date	Time of day	Event hours
70.44	1	7.45	09/04/1999	14:00	44.00
36.26	2	6.44	09/14/1999	23:00	35.00
22.18	3	5.79	10/10/2002	19:00	27.00
19.63	4	5.64	06/14/2006	3:00	13.00
17.91	5	5.53	06/06/2013	12:00	29.00
16.03	6	5.4	08/16/1955	18:00	34.00
13.32	7	5.19	09/05/2008	15:00	21.00
10.28	8	4.91	11/05/1963	17:00	37.00
9.80	9	4.86	04/25/1978	6:00	54.00
9.70	10	4.85	10/04/1995	8:00	27.00
6.50	11	4.45	11/10/2009	10:00	67.00
6.23	12	4.41	03/17/1998	16:00	43.00
6.17	13	4.4	05/11/1957	11:00	18.00
5.60	14	4.31	08/06/2011	4:00	7.00
5.25	15	4.25	07/23/1997	23:00	13.00
4.87	16	4.18	08/20/1986	6:00	11.00
4.46	17	4.1	10/14/1954	24:00	16.00
4.27	18	4.06	09/04/2006	20:00	7.00
3.99	19	4	11/20/1985	13:00	55.00
3.64	20	3.92	10/13/1994	13:00	32.00
3.40	21	3.86	03/17/1983	2:00	39.00
3.25	22	3.82	11/09/1962	6:00	21.00
2.93	23	3.73	11/12/1975	19:00	10.00
2.93	24	3.73	08/12/1992	16:00	10.00
2.80	25	3.69	08/26/2008	14:00	36.00

Raleigh, and at Eno River near Clayton). The stations' geographic coordinates are listed in Table 4-4. The rain gauge on Duke University's West Campus was installed in 2010. The Sandy Creek at Cornwallis Road station (tributary of the Haw River) and the Haw River at Bynum USGS station are the only ones not located within the Neuse River Basin; the Haw River is a tributary of the Cape Fear River. The rain gauge on the campus of NC State University records precipitation in 15-minute intervals.

Streamflow generated from the September 4, 1999, storm is shown in Figure 4-14 for Crabtree Creek at US 1 (USGS Station 02087324, Raleigh, NC). The daily maximum was 3,500 cfs. A Log-Pearson Type III frequency analysis using the maximum likelihood method ranks a 2-year flood as having a flow of 3,140 cfs and a 50-year flood as having a flow of 11,755 cfs. A peak flow of 12,700 cfs was reported after Hurricane Fran in Crabtree Creek

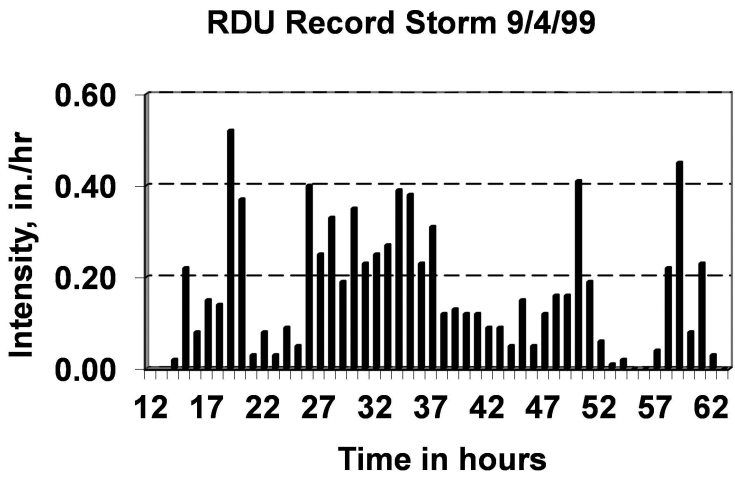

Figure 4-12. Storm of September 4, 1999, at RDU.

on September 6, 1996 (see Figure 4-15). It is important to point out that the *concentration and contribution of areal precipitation* from Hurricane Fran (see Figure 4-16) was such that peak flows were reported at the Eno River near the Durham gauging station (14,700 cfs, USGS 02085070), at the Crabtree Creek station at US 1 (12,700 cfs, USGS 02087324, Raleigh, NC), and the Haw River at Bynum station (76,700 cfs, USGS 02096960) on September 6, 1996. A peak flow of 19,700 cfs was measured at the Eno River near Clayton station (USGS 02087500) the next day, September 7, 1996. The path of the hurricane was centered through the Raleigh-Durham area.

It is also noteworthy to emphasize the areal variability of specific rainfall events. In Figure 4-17, the observed rainfall for May 27, 2011, is illustrated for the Duke West Campus first-order continuous recording rain gauge (at Lat. 36° 00′ 20″ N, Long. 78° 56′ 48″ W) and the Raleigh State University rain gauge (at Lat. 35° 47′ 00″ N, Long. 78° 41′ 00″ W); distance and bearing are 21 miles and 136° 14′ 50″, respectively. This particular storm is significant because it matched (at least on the Duke University campus) the previous highest recorded rainfall intensity of 2.64 in. at RDU, albeit for 15 minutes. Yet, the hourly rainfall totals at the NC State University gauge were significantly lower.

The local urban flooding in Durham near West Campus was severe, and a pronounced daily streamflow jump from 19 cfs the previous day to 642 cfs on May 27, 2011, recorded at the Eno River near Durham (USGS Station 02085070, Figure 4-18). The mean daily discharge (September 1963 to January 2017) at this location is 123 cfs. The MRIs for storm events and the floods they produced are summarized in Table 4-5. A Log-Pearson Type III frequency analysis using L-moments ranks a 50-year flood as having a flow of

Table 4-3. Point Precipitation-Frequency Estimates for RDU.

	MRI (years)									
Duration	1	2	5	10	25	50	100	200	500	1000
5-min:	0.394	0.461	0.53	0.587	0.647	0.689	0.727	0.758	0.792	0.819
10-min:	0.63	0.738	0.848	0.939	1.03	1.1	1.16	1.2	1.25	1.29
15-min:	0.787	0.927	1.07	1.19	1.31	1.39	1.46	1.52	1.58	1.62
30-min:	1.08	1.28	1.53	1.72	1.94	2.09	2.24	2.36	2.51	2.62
60-min:	1.35	1.61	1.96	2.24	2.58	2.84	3.08	3.31	3.6	3.83
2-h:	1.56	1.86	2.29	2.65	3.08	3.43	3.76	4.09	4.51	4.84
3-h:	1.65	1.98	2.44	2.84	3.33	3.75	4.15	4.56	5.11	5.55
6-h:	2	2.39	2.95	3.44	4.06	4.57	5.09	5.62	6.33	6.92
12-h:	2.37	2.84	3.52	4.11	4.89	5.56	6.22	6.93	7.88	8.69
24-h:	2.83	3.42	4.27	4.94	5.84	6.55	7.27	8.01	9.01	9.79
2-day:	3.26	3.92	4.86	5.58	6.55	7.31	8.07	8.85	9.9	10.7
3-day:	3.45	4.14	5.1	5.86	6.87	7.67	8.47	9.29	10.4	11.2
4-day:	3.63	4.35	5.35	6.13	7.19	8.03	8.88	9.73	10.9	11.8
7-day:	4.21	5.02	6.1	6.95	8.1	9.01	9.94	10.9	12.2	13.2
10-day:	4.79	5.69	6.83	7.72	8.92	9.86	10.8	11.8	13.1	14.1
20-day:	6.39	7.54	8.9	9.98	11.5	12.6	13.8	15	16.6	17.8
30-day:	7.93	9.33	10.8	12	13.5	14.7	15.9	17.1	18.6	19.8
45-day:	10.1	11.8	13.6	14.9	16.6	17.9	19.2	20.5	22.1	23.4
60-day:	12.2	14.2	16	17.4	19.2	20.5	21.8	23.1	24.7	25.9

Source: NOAA (2017).

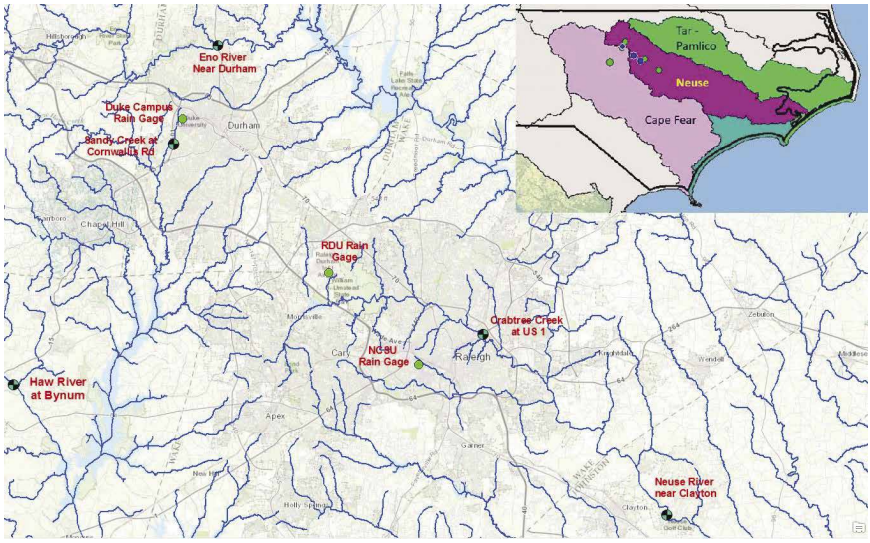

Figure 4-13. Rain gauges and streamflow stations in the Raleigh-Durham area.

Table 4-4. Latitude, Longitude, and Elevation of Raleigh-Durham Area Stations.

Gauging Station	Lat.	Long. (W)	Elev. (ft)	Record Length
Rainfall:				
RDU Airport	35° 52′ 00″	78° 47′ 00″	416	1948–2014
NCSU Raleigh	35° 47′ 40″	78° 41′ 56″	400	1984–2014
Duke West Campus	36° 00′ 20″	78° 56′ 48″	378	2010–2017
Streamflow:				
Sandy Creek	35° 59′ 00″	78° 57′ 25″	266	2008–2017
Eno River, Durham	36° 04′ 20″	78° 54′ 28″	270	1985–2017
Haw River, Bynum	35° 45′ 55″	79° 08′ 09″	283	2007–2017
Crabtree Creek	35° 48′ 40″	78° 36′ 39″	182	1990–2017
Neuse River, Clayton	35° 38′ 50″	78° 24′ 19″	128	1985–2017

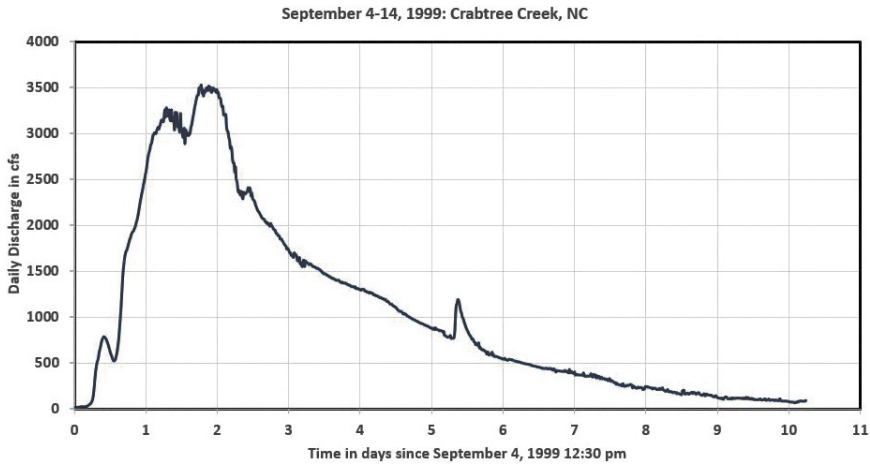

Figure 4-14. Crabtree Creek hydrograph for September 4–14, 1999.

14,200 cfs at the Eno River (observed peak of 14,700 cfs). An EV1 frequency analysis using L-moments ranks a 50-year flood as having a flow of 20,232 cfs at the Neuse River near Clayton station and a Log-Pearson Type III 50-year flood value of 19,588 cfs (observed peak of 19,700 cfs).

The coordinates for rain gauges and a streamflow station for the Lower Pecos River, near Shumla and Pandale, Texas, are presented in Table 4-6 and illustrated in Figure 4-19.

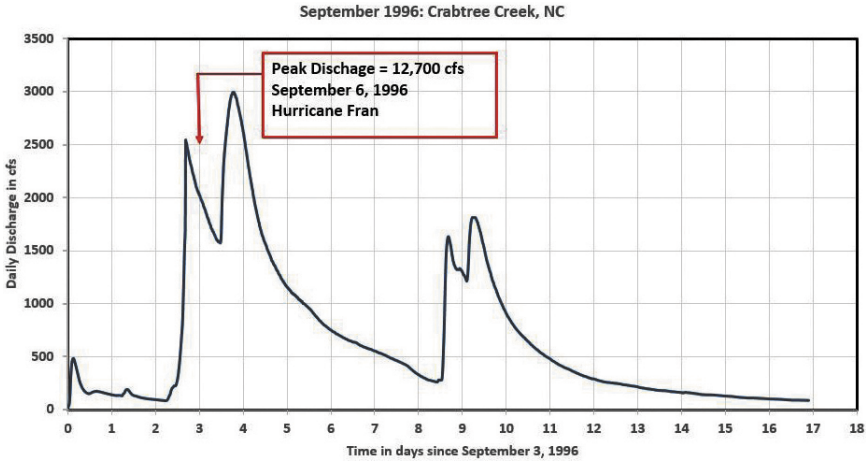

Figure 4-15. Crabtree Creek daily flow for September 3–20, 1996.

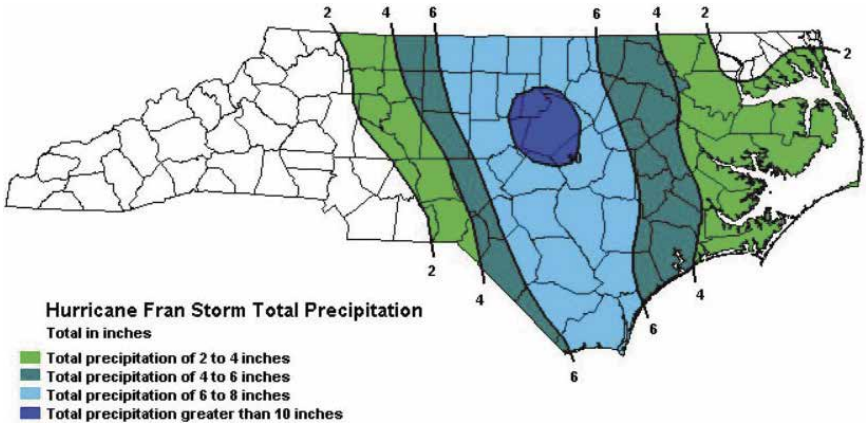

Figure 4-16. Area-wide precipitation totals from Hurricane Fran.

The path of Hurricane Alice from June 25 to June 26, 1954, is illustrated in Figure 4-20. It resulted in significant areal precipitation just upstream of the Pecos River near the Shumla gauging station (USGS 08447400), dropping a point maximum amount of 15.5–16.02 in. in 24 hours at Pandale, Texas (27.1 in. in 48 hours, Weather Bureau, 1954), and 29.2 in. in 24 hours at SW-3-22. The computation of the point precipitation depth at the Pandale 2 NE station is presented in Table 4-7 and that for SW-3-22 is presented in Table 4-8. Asquith (1998) and Asquith and Roussel (2004) determined that the GEV distribution was the best fit for *storm durations from 1 to 7 days*

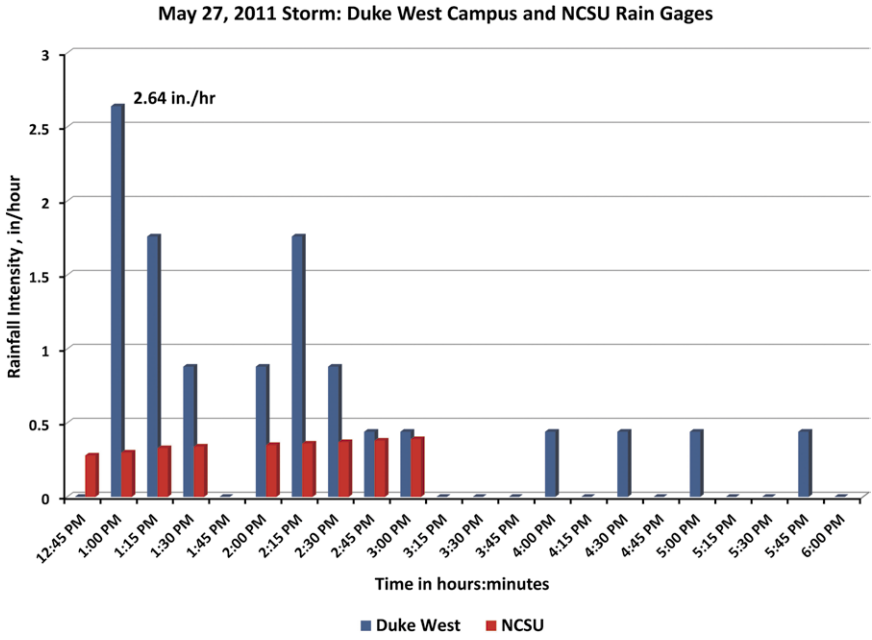

Figure 4-17. Storm of May 27, 2011, at RDU and Duke West Campus rain gauges.

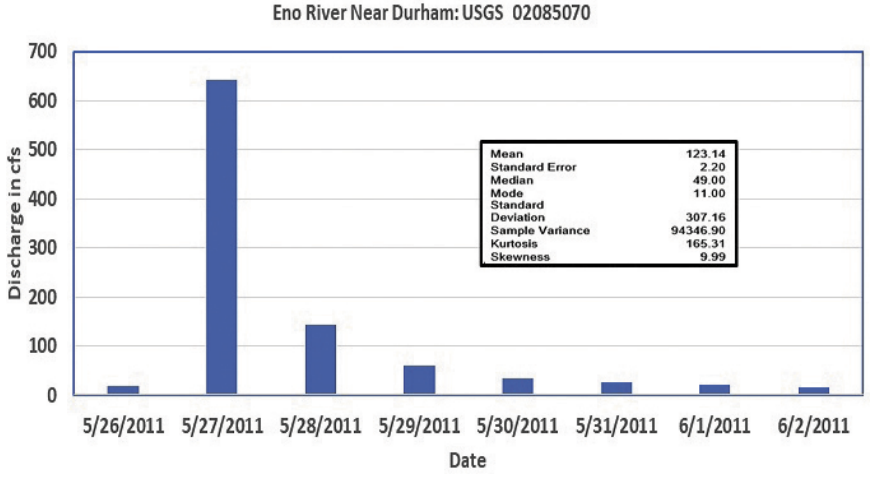

Figure 4-18. Daily flow for May 2011 at Eno River near Durham, NC.

Table 4-5. MRIs for Storms and Floods Generated Subsequently.[a]

Rainfall/ stream station	Storm event-duration	MRI, years [in.]	Flood	Distribution, MRI (years) [cfs]
RDU	9/4/1999 – 48 h	**50 [7.45]**		
Eno River (Durham)			9/5/1999	**LPIII, <2 [1390]**
Crabtree Creek			9/4/1999	**LPIII, 2 [3500]**
RDU	9/6/1996 – 24 h	**10 [4.96]**		
Eno River (Durham)			9/6/1996	**LPIII, 50 [14700]**
Eno River (Durham)			9/6/1996	**EV1, 100 [14700]**
Eno River (Durham)			9/6/1996	**PeakFQ, 100 [14700]**
Haw River (Bynum)			9/6/1996	**LPIII, 100 [76700]**
Haw River (Bynum)			9/6/1996	**EV1, 150 [76700]**
Haw River (Bynum)			9/6/1996	**PeakFQ, 100 [76700]**
NCSU Rain Gauge		**10 [5.03]**		
Crabtree Creek			9/6/1996	**LPIII, 50 [12700]**
Neuse River (Clayton)			9/7/1996	**EV1, 50 [19700]**
Neuse River (Clayton)			9/7/1996	**LPIII, 50 [19700]**
Duke West Campus	5/27/2011 – 6 h	**< 5 [2.97]**		
Eno River (Durham)			5/27/2011	**LPIII, <<2 [642]**

[a]Large flooding after Hurricane Fran (1996) caused by concentration of extensive areal precipitation upstream of streamflow gauge locations.

Table 4-6. Rain Gauges and a Streamflow Station for the Lower Pecos River, Near Shumla, TX.

Gauging Station	Lat.	Long. (W)	Elev. (ft)	Record Length
Rainfall:				
SW-3-22*	30° 22′ 00″	101° 23′ 00″	2244	6/23–28/1954
Pandale 2 NE**	30° 12′ 00″	101° 33′ 00″	1646	1909–1994
Del Río WSO Airport***	29° 22′ 27″	100° 55′ 38″	1168	1951–2013
Streamflow:				
USGS 08447400	29° 50′ 00″	101° 23′ 00″	1159	1900–1966

*Bucket survey, USACE SW Division; ** Daily precipitation; *** Hourly precipitation

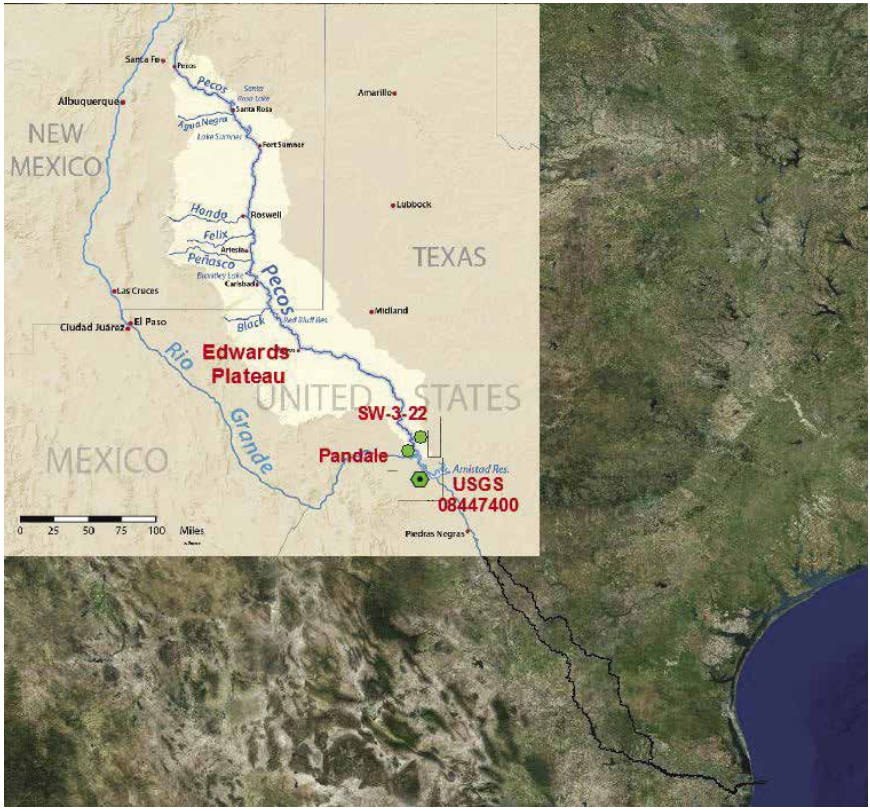

Figure 4-19. Rain gauges and streamflow station on the Lower Pecos River.

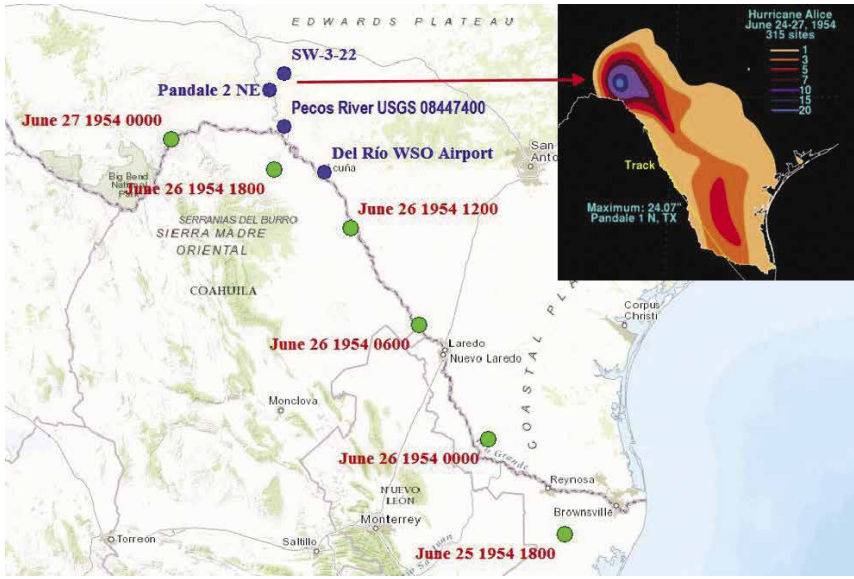

Figure 4-20. Hurricane path, rain gauges, and Pecos River streamflow station near Shumla, TX.

Table 4-7. Point 1-day Precipitation Depth for 24-hour Rainfall (15.5–16.02 in.) Using GEV and L-Moments (Station Pandale 2 NE, Lat. 30° 12′ 00″ and Long. –100° 55′ 00″, June 26, 1954).

Xi	Alpha	K	T (years)	F	X_d (in.)
2.5	1	-0.219	100	0.990	10.44
			200	0.995	12.50
			250	0.996	13.23
			300	0.997	13.85
			400	0.998	14.89
			500	0.998	15.74
			540	0.998	16.04

for Texas. The computation of the MRI for the Pecos River near Shumla yielded 800 years for the flood of June 26, 1954: a flow of 948,768 cfs was calculated (summarized in Table 4-9). The actual recorded flow was reported to be 948,000 cfs.

A plot of daily peak flow rates versus the EV1 reduced variate is shown in Figure 4-21 for the Eno River near Durham, North Carolina. The distributions indicate that a *distribution choice* can be a major issue for design risk-

Table 4-8. Point 1-day Precipitation Depth for 24-hour Rainfall (29.2 in.) Using GEV and L-Moments (Station SW-3-22, Lat. 30° 22′ 00″ and Long. –101° 23′ 00″, June 26, 1954).

Xi	Alpha	K	T (years)	F	X_d (in.)
2.5	1	–0.219	100	0.990	10.44
			200	0.995	12.50
			250	0.996	13.23
			300	0.997	13.85
			400	0.998	14.89
			500	0.998	15.74
			1000	0.999	18.66
			2000	1.000	22.06

level exceedance probabilities. A similar plot for the Haw River at Bynum is presented in Figure 4-22, with better results. A plot of the AEP predicted by PeakFQ using the EMA option is presented in Figure 4-23. The EMA method calculates moments using an iterative procedure that adjusts the initial moment estimators based on threshold information. The AEP value for Hurricane Fran for the Eno River site is approximately 0.01 ($T \approx 100$ years) for a flow of 15,120 cfs (14,700 cfs were measured). The code discarded 37 peaks out of 90 for the Neuse River station (owing to known urbanization and/or regulation issues), and the results were not representative; thus, they are not presented here. A plot of the AEP predicted by PeakFQ using the EMA option for the Haw River at Bynum is presented in Figure 4-24.

The huge uncertainty that can develop in risk assessment is presented in Figure 4-25, where the flood of June 26–28, 1954, at the Pecos River near the Shumla, Texas, streamflow station (948,000 cfs, 26,844 cms) was over eight times larger than the previous peak flow. The figure shows Log-Pearson Type III frequency curves with and without the 1954 flood.

It is clear from Table 4-9 that the MRI of the storm events and the subsequently generated floods downstream are not of the same magnitude. The floods generated by Hurricanes Fran (North Carolina) and Alice (Texas) were influenced by concentrated areal precipitation, particularly for Hurricane Fran. In the case of Hurricane Alice near Pandale, Texas (and Station SW-3-22 further northeast), the storm event point precipitations were extreme, but it appears there was much less concentration and contribution of areal precipitation upstream of the Pecos River USGS streamflow gauging station near Shumla, Texas.

Table 4-9. Summary of MRIs for Storms and Floods Generated Subsequently.

Rainfall/ stream (NC)	Storm event-duration	MRI, years [in.]	Flood	Distribution, MRI, years [cfs]
RDU Airport	9/4/1999 – 48 hrs.	**50 [7.45]**		
Eno River (Durham)			9/4/1999	**LPIII, <2 [1,390]**
Crabtree Creek			9/4/1999	**LPIII, 2 [3,500]**
RDU Airport	9/6/1996 – 24 hrs.	**10 [4.96]**		
Eno River (Durham)			9/6/1996	**EV1, 100 [14,700]**
Eno River (Durham)			9/6/1996	**PeakFQ, 100**
Eno River (Durham)			9/6/1996	**LPIII, 50**
Haw River (Bynum)			9/6/1996	**LPIII, 100 [76,700]**
Haw River (Bynum)			9/6/1996	**EV1, 150**
Haw River (Bynum)			9/6/1996	**PeakFQ, 100**
NCSU Rain Gauge	9/6/1996 – 24 hrs.	**10 [5.03]**		
Crabtree Creek			9/6/1996	**LPIII, 50 [12,700]**
Neuse River (Clayton)			9/7/1996	**LPIII, 50 [19,700]**
Neuse River (Clayton)			9/7/1996	**EV1, 50**
Duke West Campus	5/27/2011 – 6 hrs.	**< 5 [2.97]**		
Eno River (Durham)			5/27/2011	**LPIII, <<2 [642]**

Table 4-9. (Continued)

Rainfall/ stream (NC)	Storm event-duration	MRI, years [in.]	Flood	Distribution, MRI, years [cfs]
Rainfall/ Stream (Texas)	**Storm Event - Duration**	**MRI, yrs. [in.]**	**Flood**	**Distribution, MRI, yrs. [cfs]**
Pandale 2 NE	06/26/1954 24 hrs.	**540 [16.02]**		
SW-3-22	06/27/1954 24 hrs.	**3000 [29.2]**		
USGS 08447400			06/26-27/ 1954	**LPIII, 800 [948,000]**
			06/26-27/ 1954	**PeakFQ, 500**

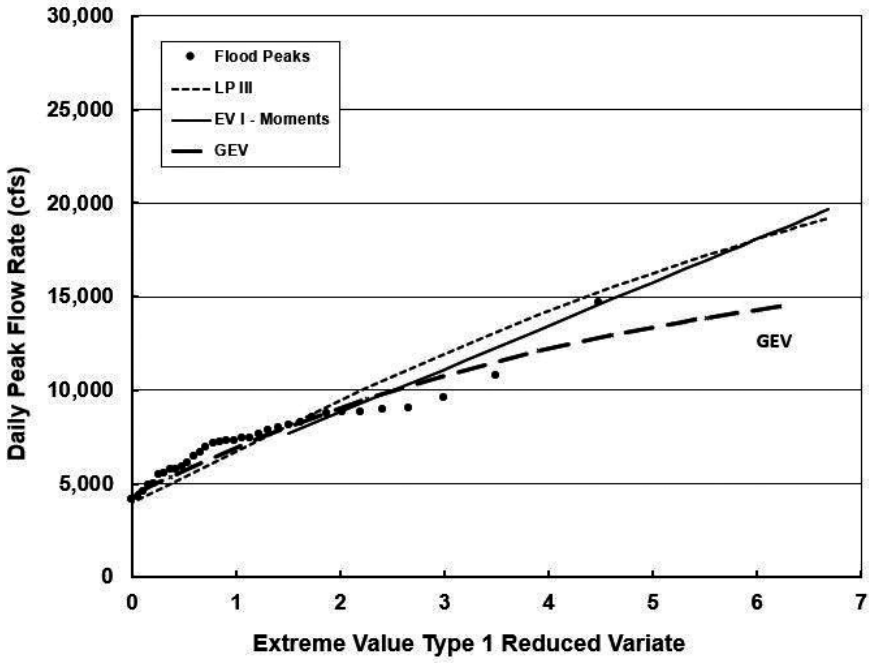

Figure 4-21. Flood frequency—annual maximum peak flow rates, Eno River near Durham, NC, USGS Station 02085070, 1964–2016.

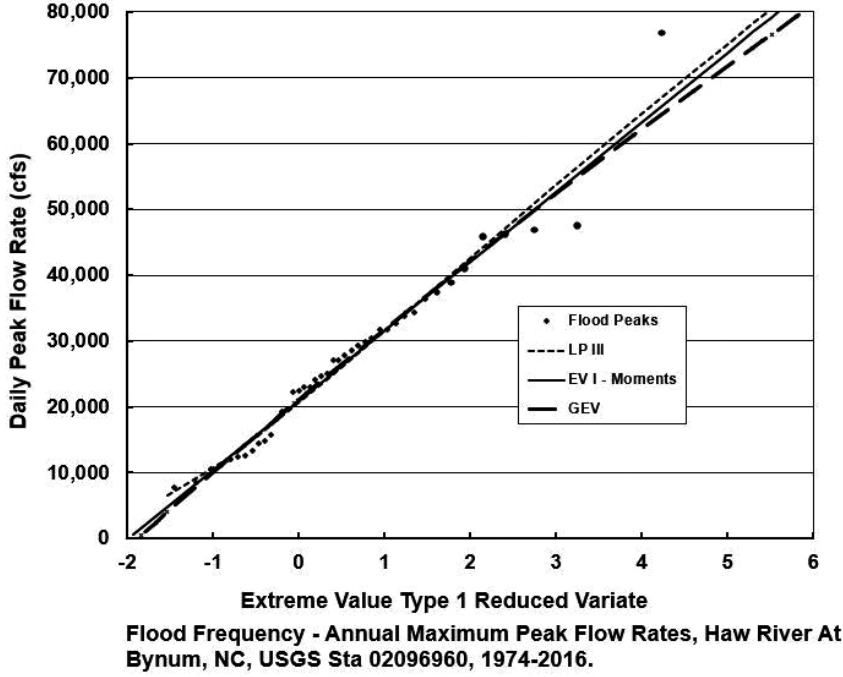

Figure 4-22. Flood frequency—annual maximum peak flow rates, Haw River at Bynum, NC, USGS Station 02096960, 1974–2016.

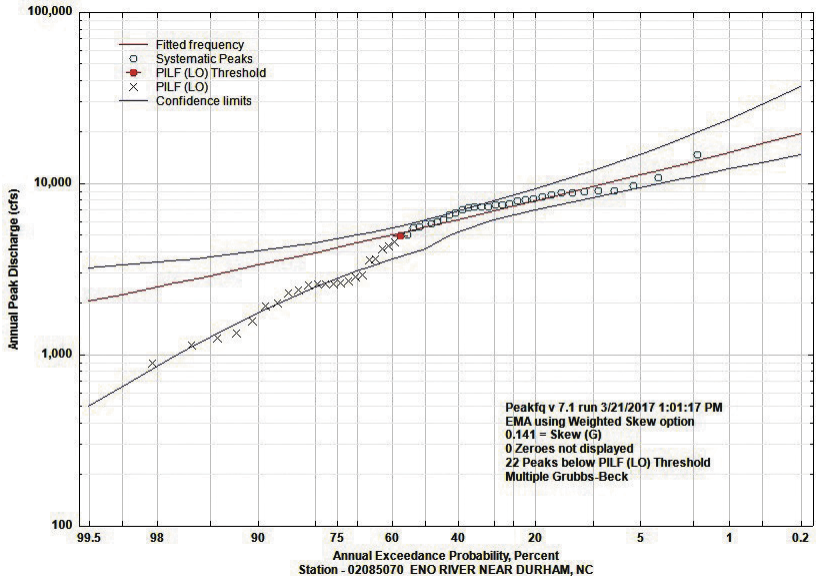

Figure 4-23. PeakFQ annual exceedance probabilities for the Eno River near Durham, NC.

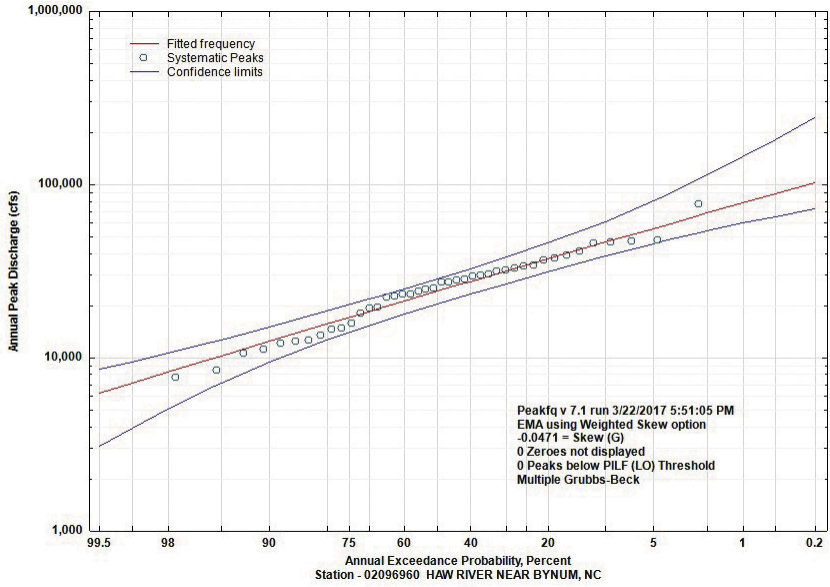

Figure 4-24. PeakFQ annual exceedance probabilities for the Haw River at Bynum, NC.

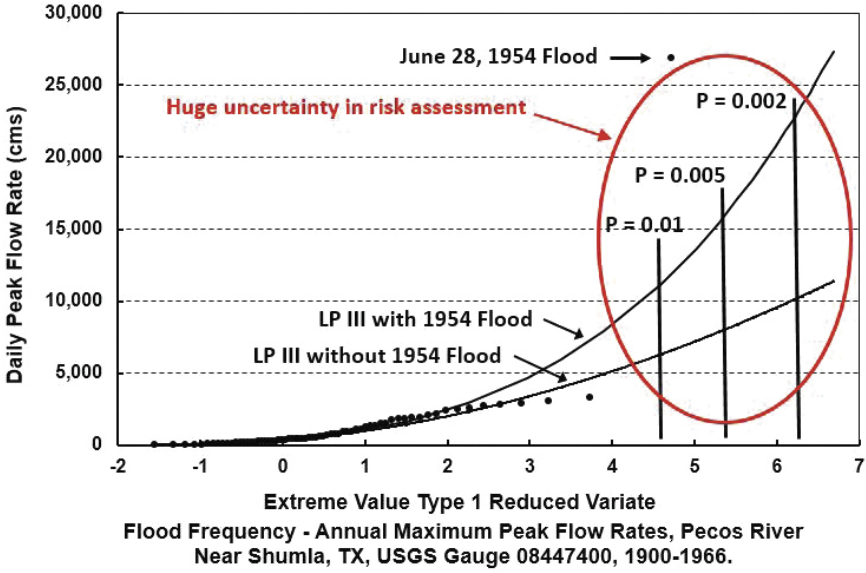

Figure 4-25. Uncertainty in risk assessment.
Source: Modified after Burges (2016).

4.3.4 Coastal Urban Areas

This section illustrates analyzing rainfall in coastal urban areas. Rainfall over coastal cities presents unique challenges. The extreme rainfall events tend to be larger, and runoff to the sea is compounded by SLR as a downstream boundary condition. Examples of rainfall analyses for two coastal cities are presented in Tables 4-10 (Miami International Airport) and 4-11 (Charleston International Airport). These locations are either coastal or very near coastal areas, as compared to RDU (130–150 miles from the coastline); however, their *average storm event depths* and *intensities* are comparable.

The storm event MRIs for the top 25 events in terms of volume (depth) for the Miami International Airport were computed and are presented in Table 4-12. The storm event of April 24–25, 1979, constituted a record storm in term of both volume (depth) and hourly rainfall intensity (6.14 in.), which is rather unusual, as illustrated in Figure 4-26. The ground surface was probably saturated by the time the peak intensity was reached. This particular storm was examined in detail by staff at the South Florida Water Management District (SFWMD 1979). Available data suggest that during the early morning hours of April 25, 1979, rainfall intensities exceeded the highest rates previously recorded (and since then through 2016) in portions of Dade, Broward, and southern Palm Beach counties. At the Miami International Airport, a new maximum 24-hour rainfall record of 16.39 in. was established. Through application of *NOAA Atlas 14*, Vol. 9 (NOAA 2013b), depth–duration–frequency curves were obtained, as illustrated in Figure 4-27, and the values are presented in Table 4-12. The storm event of April 24–25, 1979, ranks near a 200-year event for a duration of 24 hours and as a 100-year event for a 48-hour duration.

From Table 4-13, for a 1-hour duration, the Miami storm event of April 24–25, 1979 (with a peak intensity of 6.14 in.) would rank as at least a

Table 4.10. NOAA Hourly Rainfall Station Description and Statistics of Storm Events, Miami International Airport, FL (Station No. 085663, Lat: N 25.7905°, Long: W –80.3163°, Elevation: 28.87 ft, 1950–2011).

Storm event variable	Mean	COV
Depth, in.	0.592	1.867
Intensity, in./h	0.102	1.535
Duration, h	8.609	1.518
Time between events, h	83.451	1.071
Total no. of storms[a]	6426	

[a]Number of storms is based on an MIT of 8 hours, which yielded a COV very near 1.0 for the time between events for the rainfall time series.

Table 4-11. NOAA Hourly Rainfall Station Description and Statistics of Storm Events, Charleston International Airport, SC (Station No. 381544, Lat: N 32.8986°, Long: W –80.0402°, Elevation: 40 ft, 1954–2011).

Storm event variable	Mean	COV
Depth, inches	0.519	1.548
Intensity, in./h	0.091	1.477
Duration, h	6.882	1.185
Time between events, h	88.503	0.997
Total no. of storms[a]	5726	

[a]Number of storms is based on an MIT of 8 hours, which yielded a COV very near 1.0 for the time between events for the rainfall time series.

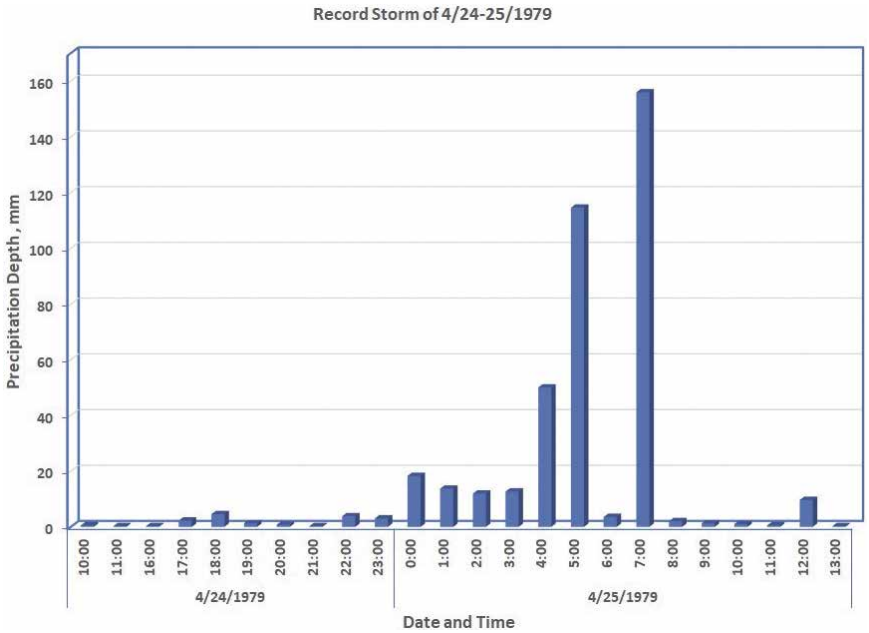

Figure 4-26. Record storm at Miami International Airport, FL.

200-year event, probably higher. Applying the GEV distribution, fitted using L-moments (Hosking 1990), the 24-hour duration depth yields a 100-year storm. The *Atlas 14* (NOAA 2013b) values include data from a regional analysis and should be considered more accurate. However, *Atlas 14* assumes stationarity of the historical data set based on research that indicated minimal trends in the data (Heineman 2012). Thus, new approaches are needed to extend the forecasting into the future assuming non-stationarity.

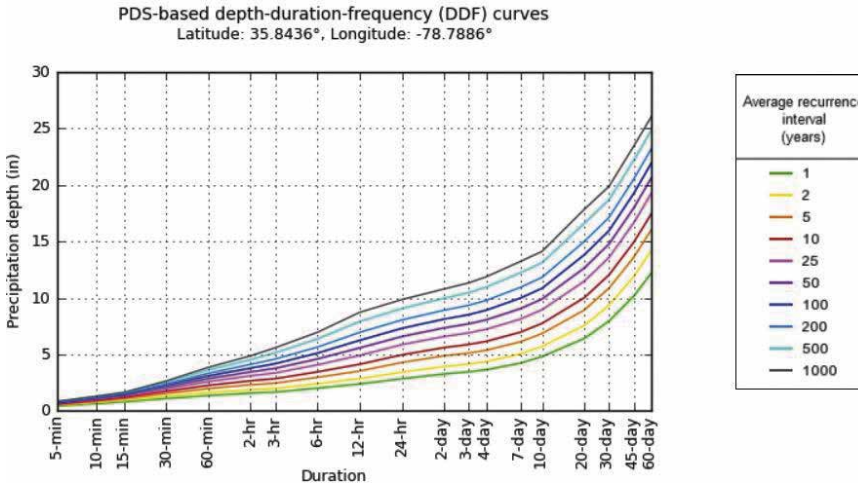

Figure 4-27. Depth–duration–frequency curves for Miami International Airport, FL.
Source: NOAA (2017).

The climatology of heavy precipitation in Florida is strongly influenced by the warm, humid, subtropical air that is generated by the Gulf of Mexico and the Atlantic Ocean (NOAA 2013b). The precipitation-frequency analysis approach used in the *Atlas 14* series (NOAA 2006, 2008, 2011a, 2011b, 2011c, 2012a, 2012b, 2013a, 2013b, 2014, 2015) is based on analysis of annual maxima series (AMS) across a range of durations. The AMS for each station were obtained by extracting the highest precipitation amount for a particular duration in each successive calendar year. Station screening was done in the following order: (a) examination of geospatial data, (b) screening for duplicate records at co-located daily, hourly, and/or 15-minute stations and extending records using data from colocated stations, (c) screening nearby stations for potentially merging records or removing shorter, less reliable records in station-dense areas, and (d) screening for sufficient number of years with usable data.

A similar approach was conducted to determine the historically most extreme storm event recorded at the Charleston International Airport, South Carolina. This was the October 1–5, 2015, event, illustrated in Figure 4-28, which was a five-day event that produced a total depth of 17.32 in. at that airport. The storm event of October 1–5, 2015, ranks near a 1,000-year event, as shown in Table 4-14 (NOAA 2017). Across the Cooper River from Charleston is Mount Pleasant, South Carolina (Figure 4-29), and at the Faison Airport (WBAN 00390, Lat: 32.9°N, Long. –79.8°W, Elev. 14 ft) the total

Table 4.12. MRIs for Miami International Airport, FL.

MRI (years)	Rank	Depth (in.)	Date and time	Event hours
83.50	1	16.24	4/24/1979 10:00	28
65.89	2	15.30	10/02/2000 9:00	42
32.00	3	12.76	10/07/1991 15:00	52
21.84	4	11.59	05/04/1977 8:00	23
17.75	5	11.00	10/13/1999 21:00	57
13.69	6	10.30	05/23/1958 4:00	36
11.30	7	9.81	05/22/2012 12:00	22
6.55	8	8.52	11/18/1959 13:00	36
6.29	9	8.43	09/09/1960 7:00	32
6.09	10	8.36	06/20/1995 5:00	42
6.06	11	8.35	10/26/1952 17:00	26
5.93	12	8.30	10/13/1965 9:00	42
5.74	13	8.23	06/01/1977 11:00	30
5.38	14	8.09	05/26/1984 22:00	71
5.35	15	8.08	04/23/1982 13:00	43
5.18	16	8.01	11/17/1992 16:00	23
4.97	17	7.92	09/27/2001 12:00	47
4.72	18	7.81	12/03/2015 17:00	55
4.48	19	7.70	06/08/1966 2:00	30
3.93	20	7.43	06/17/1959 22:00	24
3.28	21	7.06	03/20/1949 8:00	12
3.26	22	7.05	06/27/1966 19:00	89
3.16	23	6.99	05/01/1957 13:00	10
3.12	24	6.96	08/11/1994 11:00	41
3.09	25	6.94	08/26/1964 8:00	26

rainfall reported was 25.35 in. The distance and bearing from the two rainfall stations are 13.9 miles and 89° 40′ 03″, respectively.

The hyetograph for the October 1–5, 2015, event at the Faison regional airport is presented in Figure 4-30. The storm event would likely rank substantially greater than a 1,000-year event at the Mount Pleasant regional airport. Hyetographs are presented throughout because it is important to show why these storms produced such severe urban flooding; their highest intensities came well after the land surface was saturated.

Atlas 14 Vol. 2 (NOAA 2006) contains precipitation-frequency estimates for Delaware, the District of Columbia, Illinois, Indiana, Kentucky, Maryland, New Jersey, North Carolina, Ohio, Pennsylvania, South Carolina, Tennessee, Virginia, and West Virginia. The revised publication includes application of regional frequency analysis using L-moments for selecting

Table 4-13. Point Precipitation-Frequency Estimates for Miami International Airport, FL.

	MRI (years)									
Duration:	1	2	5	10	25	50	100	200	500	1000
5-min:	0.58	0.66	0.8	0.91	1.07	1.19	1.31	1.43	1.6	1.72
10-min:	0.85	0.97	1.17	1.34	1.57	1.74	1.92	2.1	2.34	2.52
15-min:	1.03	1.18	1.43	1.63	1.91	2.12	2.34	2.56	2.85	3.07
30-min:	1.58	1.81	2.2	2.53	2.97	3.31	3.65	4	4.46	4.8
60-min:	2.09	2.39	2.92	3.39	4.07	4.63	5.22	5.84	6.71	7.4
2-h:	2.6	2.97	3.64	4.25	5.17	5.95	6.78	7.68	8.97	10.01
3-h:	2.89	3.29	4.06	4.78	5.92	6.9	7.98	9.16	10.88	12.29
6-h:	3.4	3.91	4.9	5.86	7.38	8.72	10.21	11.85	14.26	16.25
12-h:	3.97	4.66	5.95	7.18	9.11	10.77	12.59	14.61	17.52	19.91
24-h:	4.64	5.5	7.09	8.57	10.84	12.79	14.89	17.2	20.52	23.22
2-day:	5.46	6.43	8.2	9.85	12.37	14.52	16.84	19.38	23.02	25.99
3-day:	6.06	7.07	8.91	10.6	13.18	15.37	17.74	20.32	24.01	27.01
4-day:	6.61	7.61	9.43	11.11	13.68	15.87	18.24	20.82	24.51	27.52
7-day:	8.07	8.97	10.64	12.22	14.69	16.82	19.15	21.72	25.44	28.48
10-day:	9.32	10.23	11.91	13.51	15.98	18.11	20.44	23	26.69	29.71
20-day:	12.63	14.02	16.37	18.4	21.31	23.66	26.08	28.63	32.12	34.87
30-day:	15.43	17.29	20.29	22.76	26.13	28.69	31.23	33.78	37.12	39.61
45-day:	19.11	21.49	25.24	28.21	32.08	34.91	37.59	40.16	43.34	45.57
60-day:	22.37	25.12	29.39	32.71	36.95	39.97	42.76	45.37	48.45	50.52

Source: NOAA (2017).

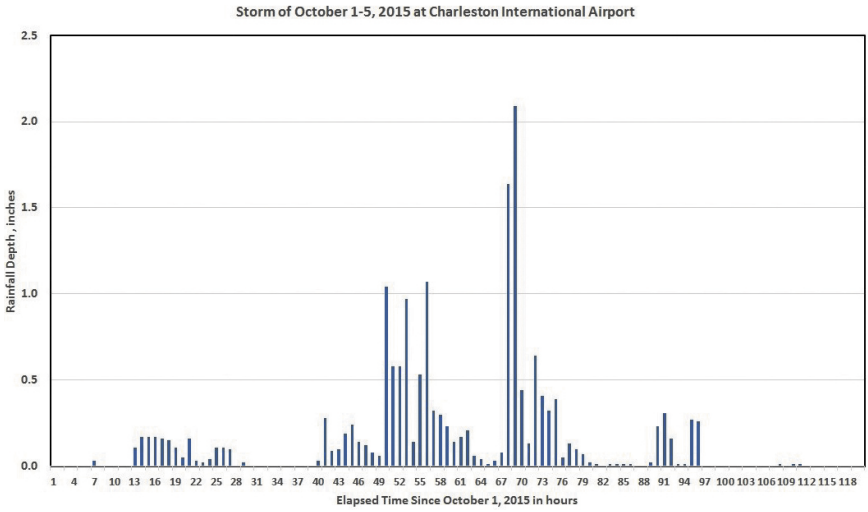

Figure 4-28. The October 1–5, 2015, storm event recorded at Charleston International Airport, SC.

and parameterizing probability distributions and new techniques for spatial interpolation and mapping.

Hurricane Joaquin did play an indirect role in South Carolina's October 1–5, 2015, deluge (Halverson 2015):

> as Hurricane Joaquin tracked North, well East of the coast, a separate, non-tropical low pressure system was developing over the Southeast. This system drew in a deep, tropical plume of water vapor off the tropical Atlantic Ocean. At the same time, this upper-level low pressure system tapped into the moist outflow of Hurricane Joaquin.

Runoff from storms in Miami is distributed through a large number of canals, with computer-controlled gates operated by the South Florida Water Management District. Gauges on the Cooper and Wando rivers record only gauge height, and these are tidally influenced. Both the Miami, Florida, and Charleston, South Carolina, urban areas are subject to SLR concerns. Unified SLR projections produced by the Southeast Florida Regional Climate Change Compact (SFRCCC) partners are illustrated in Figure 4-31. Included are scenarios from the USACE, NOAA, and IPCC AR5. A similar approach can be developed for Charleston: a linear mean sea-level trend of 0.13 in./year is predicted with a 95% confidence interval of +/–0.009 in./year based

Table 4-14. Point Precipitation-Frequency Estimates for Charleston International Airport, SC.

	MRI (years)									
Duration:	1	2	5	10	25	50	100	200	500	1000
5-min:	0.51	0.6	0.7	0.79	0.89	0.97	1.05	1.12	1.23	1.31
10-min:	0.82	0.96	1.12	1.26	1.42	1.54	1.67	1.78	1.94	2.07
15-min:	1.02	1.21	1.42	1.59	1.8	1.95	2.1	2.25	2.44	2.59
30-min:	1.4	1.67	2.02	2.3	2.66	2.94	3.22	3.5	3.89	4.2
60-min:	1.75	2.1	2.59	3	3.54	3.98	4.44	4.91	5.58	6.13
2-h:	2.06	2.5	3.16	3.71	4.43	5.01	5.59	6.18	6.97	7.6
3-h:	2.19	2.65	3.37	3.99	4.81	5.5	6.21	6.94	7.96	8.8
6-h:	2.58	3.13	3.98	4.72	5.72	6.56	7.42	8.34	9.6	10.66
12-h:	2.99	3.62	4.63	5.52	6.73	7.76	8.85	10	11.62	13
24-h:	3.48	4.23	5.47	6.47	7.89	9.04	10.25	11.54	13.34	14.79
2-day:	4.06	4.92	6.29	7.41	8.98	10.26	11.61	13.03	15.02	16.62
3-day:	4.33	5.24	6.67	7.81	9.42	10.72	12.08	13.51	15.51	17.11
4-day:	4.61	5.56	7.04	8.21	9.85	11.17	12.55	13.99	15.99	17.59
7-day:	5.37	6.47	8.09	9.36	11.11	12.51	13.96	15.46	17.54	19.18
10-day:	6.08	7.29	8.95	10.23	11.95	13.32	14.71	16.12	18.04	19.54
20-day:	8.07	9.63	11.63	13.2	15.31	16.95	18.6	20.29	22.58	24.37
30-day:	9.91	11.74	13.93	15.59	17.76	19.45	21.11	22.78	25	26.72
45-day:	12.35	14.61	17.08	18.93	21.34	23.16	24.95	26.72	29.05	30.84
60-day:	14.66	17.3	20.06	22.11	24.75	26.73	28.65	30.54	33.01	34.86

Source: NOAA (2017).

Figure 4-29. Charleston-Mount Pleasant, SC, and rain-gauge distance and bearing.

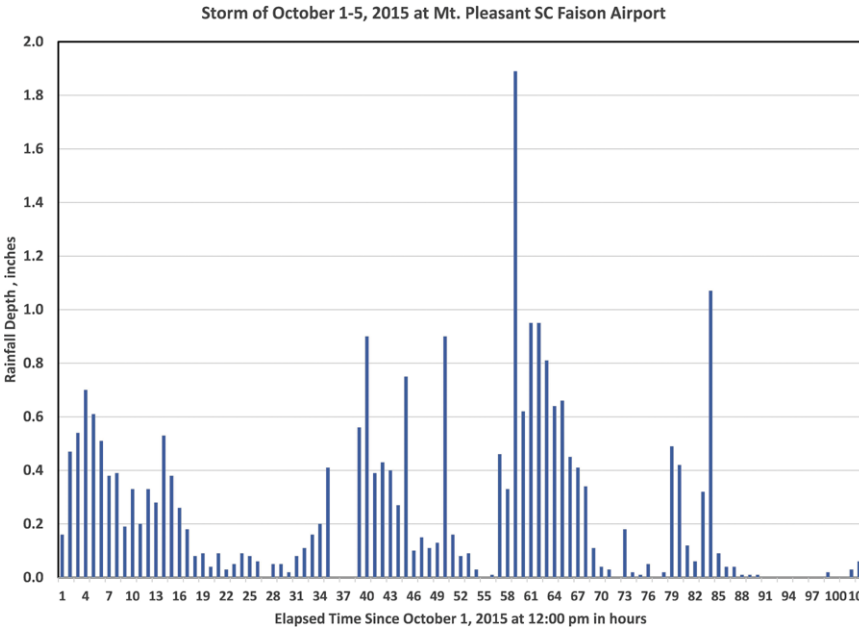

Figure 4-30. Storm of October 1–5, 2015, at Faison Airport, Mount Pleasant, SC.

on monthly mean sea-level data from 1921 to 2015 (NOAA 2017). This is equivalent to a change of 1.05 ft in 100 years. Downstream boundary conditions for stormwater simulation models and/or dynamic-wave open-channel models would have to incorporate these data for future planning scenarios.

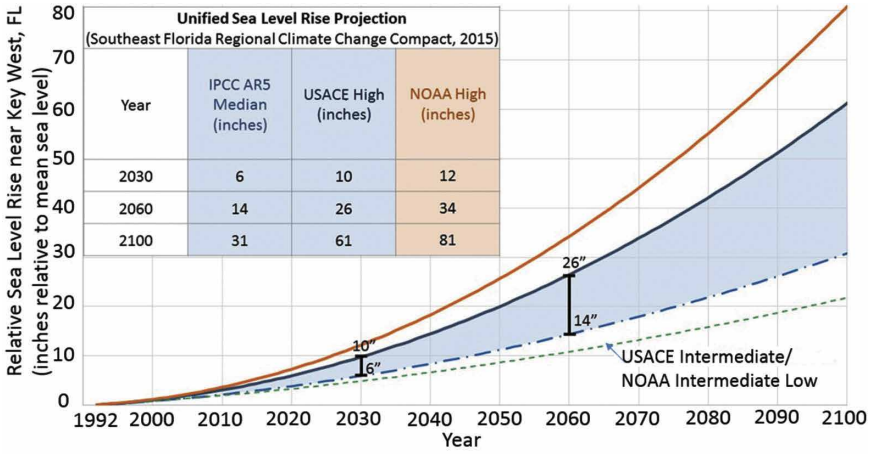

Figure 4-31. Unified SLR projections for Southeast Florida for regional planning purposes.
Source: SFRCCC (2015).

4.4 FLOODING

4.4.1 Introduction

Although a warming climate can directly affect the statistics of extreme precipitation events over time (Trenberth 2011), climatic change does not lead to distinct or obvious changes in streamflow statistics. As described in Section 4.3, the generation of runoff and eventual streamflow is a complex mechanism that is affected by many processes other than climatic conditions. There is low confidence that river discharges have increased globally throughout the twentieth century (IPCC 2013), and there is no consistent pattern of trends in annual maximum discharge records throughout the continental United States (Villarini et al. 2009). However, Vogel et al. (2011) found that significant trends in peak discharge records occur in heavily urbanized regions of the United States, such as the northeastern coastal corridor and the greater Los Angeles, Chicago, and Seattle areas. This finding highlights the need to address non-stationarity (or time-variant statistics) that can result from anthropogenic influences, such as land-use changes and urbanization. The remainder of this section presents a method for flood frequency analysis when a record of annual maximum discharges exhibits a trend likely caused by anthropogenic watershed changes. An example application is also included.

4.4.2 Modeling Trends in Flood Peak Distributions

The recommended model for addressing trends in an n-year annual maximum discharge record, $\mathbf{Q} = \{Q_1, \ldots, Q_n\}$, is an NS Log-Pearson Type III (LPIII) distribution.

$$X_t \sim \text{LPIII}(\mu_t, \sigma, \gamma) \tag{4-10}$$

where the random variable X_t is the logarithm of the annual maximum discharge, t denotes time, μ_t is the time-variant mean of the LPIII distribution, and (σ,γ) denote the standard deviation and skewness, respectively. The LPIII PDF was previously defined in Equation (4-8). The time-variant mean is given by

$$\mu_t = \mu_o + \alpha t \tag{4-11}$$

where μ_o signifies the intercept and α is the slope of the (t, α_t) relationship. The value of μ_o is equivalent to the LPIII mean of the first year of the discharge record.

The use of a log-linear time dependency in the LPIII mean seems simplistic, but it has several subtle implications. First, the linear trend model describes changes in the *logarithmic* mean of **Q**. The log-linear trend equates to an exponential trend in the mean of the original **Q** values. The exponential trend model may seem questionable, but it is supported by analysis of trends in flood peaks in the United States (Vogel et al. 2011) and the United Kingdom (Prosdocimi et al. 2014). Second, despite the use of the constant value for σ, the standard deviation of **Q** will increase with the logarithmic mean, α_t. This property is desirable because changes in land use and urbanization do not only alter the mean of flood peaks but also simultaneously affect their dispersion. The suggested model is analogous to the simplest NS model proposed by Stedinger and Griffis (2011), which was tested for predictive ability by Luke et al. (2017).

4.4.3 Estimating the Parameters of the NS Model

Following Luke et al. (2017), we recommend a Bayesian approach to estimate the NS LPIII model parameters. The primary advantage of the Bayesian approach for parameter estimation is that the procedure results in a distribution of parameter values rather than a point estimate. This allows the engineer to calculate probabilistic uncertainty bounds for any variable that is a function of the parameter estimates, such as RPs and design flood estimates. Bayesian parameter inference also allows the engineer to incorporate information other than the data record in the parameter estimation procedure via the so-called prior. This aspect of Bayesian inference is particularly useful for estimating tail parameters, such as γ, because

regional information is typically included when approximating the skewness of extreme value distributions. Thus, the Bayesian approach for parameter estimation is recommended so that (1) uncertainty in LPIII quantiles can be explicitly characterized and (2) an informative prior can be used to incorporate regional information on the estimate of γ. This recommended procedure for parameter estimation, uncertainty analysis, and NS analysis is available online on MATLAB File Exchange as a software package named Non-Stationary Flood Frequency Analysis (https://www.mathworks.com/matlabcentral/fileexchange/63858-non-stationary-flood-frequency-analysis). For further details on the theory of Bayesian parameter estimation in the context of flood frequency analysis, please see Luke et al. (2017) and Reis and Stedinger (2005).

4.4.4 Frequency Analysis

Following parameter estimation, we recommend using the parameter values of the NS model at the end of the n-year record to estimate the RPs of specified flood peaks. Specifically, we recommend estimating RPs using the traditional stationary (ST) paradigm.

$$T = \frac{1}{1 - F_n(x)} \tag{4-12}$$

where T is the MRI (in years) of the RL x and $F_n(x)$ is the cumulative distribution function of the NS LPIII model in year n or the probability that the random variable X_n is less than or equal to x according to the most recent parameterization of the NS LPIII distribution. Here, the mean of LPIII distribution is defined as the mean at the end of the discharge record, or μ_n. This is referred to by Luke et al. (2017) as an *updated* stationary distribution (uST). It is very important to note that we assume the distribution is stationary, or time-invariant, following the fitting period when calculating RPs in this manner. The validity of this assumption is primarily context-specific. If the distribution continues to change owing to future watershed alterations, T values will be inaccurate. However, Luke et al. (2017) showed that estimating changing probabilities by extrapolating the μ_t trend into the future leads to unreliable predictions. It is possible to calculate RPs under the assumption of changing probabilities (Cooley 2013); however, this would require extensive extrapolation of the μ_t trend. For example, estimating the T = 100-year RP assuming continued non-stationarity would require extrapolation of the μ_t trend 100 years into the future, which is almost certainly inaccurate and not recommended in light of the exponential trend model applied here. If future watershed changes are anticipated, we recommend either (1) using conservative values of the T-year estimates obtained from computed uncertainty intervals or (2) avoiding RP calcula-

tions altogether and applying the model to estimate the present AEPs of specified flood peaks. The following section provides an example of the recommended methodology using the Non-Stationary Flood Frequency Analysis software package.

4.4.5 White Oak Bayou Example

Figure 4-32 shows the annual maximum discharges of White Oak Bayou at Houston, Texas. There is a statistically significant trend in the peak discharge record at the 0.05 significance level according to the Mann–Kendall test for monotonic trends. Each annual peak in the data record was flagged with USGS code "C," which means all or part of the record is affected by urbanization, mining, agricultural changes, channelization, or other human related activity. Moreover, examination of historic aerial photos reveals that the White Oak Bayou watershed has experienced extensive urbanization because of its proximity to the Houston area. The statistically significant trend and supporting evidence that the observed trend was caused by urbanization justifies application of the recommended NS model for flood frequency analysis.

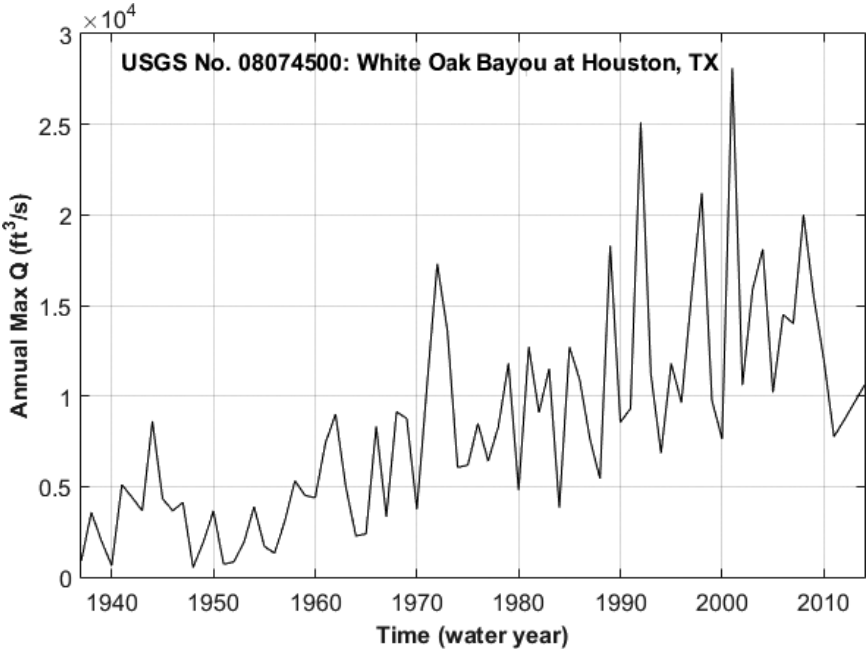

Figure 4-32. Annual maximum discharge record of White Oak Bayou in Houston, TX. Historic peaks were removed from the data record.

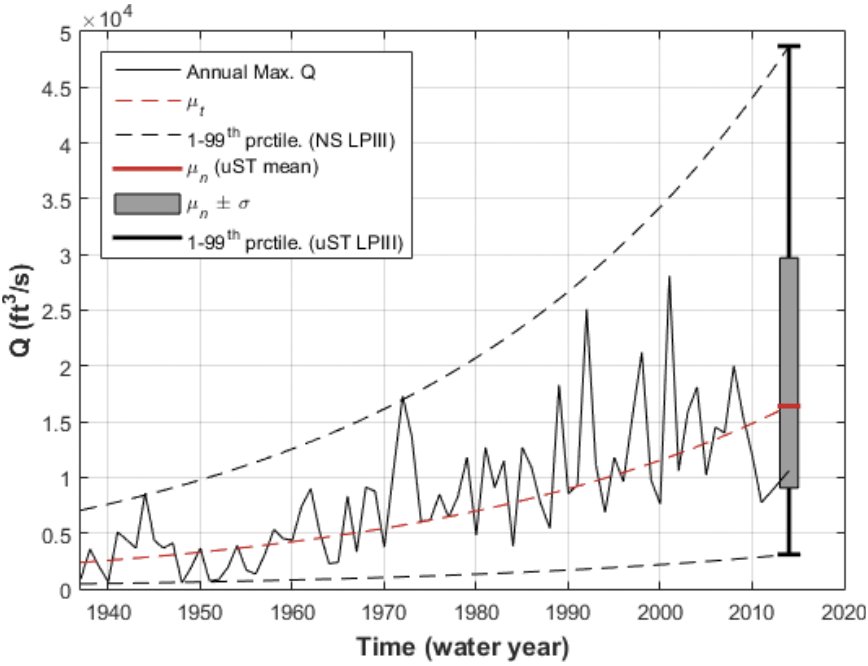

Figure 4-33. NS LPIII model fitted to the White Oak Bayou annual maximum discharge record.

Figure 4-33 shows the NS LPIII model fit to the annual maximum discharge record. The time-variant distribution shown in Figure 4-2 is defined by the most likely parameter estimates from the fitting procedure. In this example, we used an informative prior to weight the regional skewness with the station skew. The informative prior on γ was specified as a normal distribution with a mean of –0.3 and a standard deviation of 0.55. The mean of the informative prior was taken from the *Bulletin 17B* (USGS 1982) map of regional skews near Houston, Texas, and the standard deviation was set to 0.55 per *Bulletin 17B*.

The thin solid black line denotes the discharge values, the red dashed line is the time-variant mean, and the black dashed lines show the time-variant 1st–99th percentiles of the NS LPIII model. The uST distribution is shown at the end of the fitting period. The red solid line is the mean of the uST LPIII distribution, the gray box shows the mean ± one standard deviation, and the thick black solid lines show the 1st–99th percentiles of the uST LPIII distribution. We recommend using the uST distribution for flood frequency estimates and approximating current annual exceedance probabilities (USGS 1982). We note that the *Bulletin 17B* regional skew estimates will

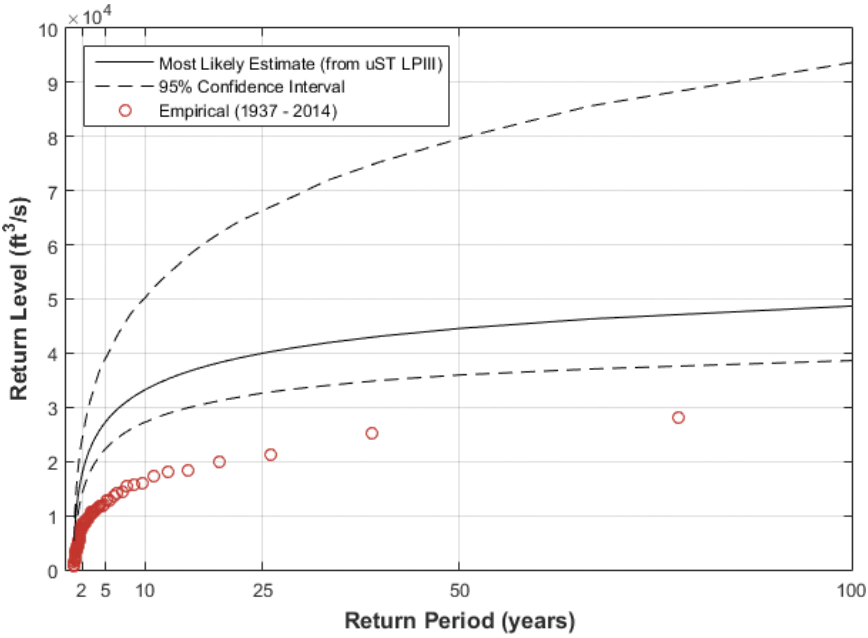

Figure 4-34. RLs versus RPs derived from the uST distribution. The estimates derived from the uST distribution have shifted away from the empirical frequency estimates, indicating that the distribution of flood peaks has changed throughout the historic record. Also, there is large uncertainty in the 100-year RP estimate, even when assuming the distribution remains stationary.
Source: After Luke et al. (2017).

be superseded by *Bulletin 17C* estimates (England et al. 2016), and the more recent regional skewness estimates should be used in practice when available. The uST distribution is also shown in Figure 4-33 as a box plot, which we recommend for estimating current AEPs and calculating RPs via Equation 4-13. Figure 4-33 shows the RPs derived from the uST distribution and associated uncertainty bounds, assuming the uST distribution remains stationary into the future. Note that the uncertainty bounds shown in Figure 4-34 result from limited sample size (or parameter uncertainty) and are not related to the uncertainty regarding the continuation of the trend in annual maximum discharges.

To evaluate if RPs calculated from the uST distribution are meaningful, the engineer must consider if the ST assumption is appropriate following the historic period. In this example, the engineer would consider if future urbanization is likely to continue altering the streamflow statistics. If so, RP estimates should be viewed cautiously. Depending on the context, it may

be more appropriate to avoid frequency analysis and only use the uST distribution to estimate present-day or current AEPs.

4.4.6 Conclusions

The methodology presented here can be used to model trends in peak discharge distributions and estimate the current exceedance probabilities of flood peaks. In this example, we applied the model to a flood record where non-stationarity was obviously caused by urbanization. The methodology presented here could be applied to flood records exhibiting trends not attributable to land-use changes; however, the engineer should always search for the cause of the trend to determine if the uST distribution is likely to persist. The validity of frequency estimates (RPs) derived from the uST distribution depends on site-specific considerations and the anticipated future conditions of the watershed. We refer the interested reader to Luke et al. (2017) for more details on Bayesian methods, evaluation of the model's predictive ability, and other issues related to NS modeling of flood peak distributions.

4.5 MULTIHAZARD SCENARIOS

Infrastructure systems are exposed to a variety of hazards. When assessing the performance of infrastructure under extreme events, it is prudent to consider a multihazard scenario, especially if hazards are dependent (e.g., fluvial flooding and storm surge). Ignoring the underlying relationships between multiple events can lead to underestimation/overestimation of the risk of extreme events and their impacts.

Recent structural design codes attempt to account for multihazard scenarios by considering load combinations and load factors intended to include uncertainties and the significance of different hazards. However, current design methods still cannot properly capture the complex and intertwined nature of multiple hazards at system and societal levels (e.g., Zaghi et al. 2016, Bruneau et al. 2017).

Civil infrastructure may be subjected to a variety of complex loading mechanisms related to environmental conditions. Some examples of environmental events that produce extreme loading include intense precipitation or flooding, extreme temperatures owing to fire, seismic loading during earthquakes, and so on. Under a changing climate, the occurrence of such extreme events is expected to increase. This poses a significant risk as the designs of much existing infrastructure do not account for changes in extreme event occurrence statistics (Seneviratne et al. 2012). Furthermore, these events may occur simultaneously or sequentially, leading to severe multihazard conditions. Multihazard conditions can affect a system and any

of its individual elements differently depending on associated times. For example, a storm event that produces extreme coastal surge and precipitation requires their consideration simultaneously. However, a single floodwall element is not impacted by a multihazard event if the resulting loads are not present at the same time. This section focuses on system-wide multihazard effects, whereas Section 6.3 investigates the effects on individual elements of a system. There have been several examples of both types of multihazard events in the United States in recent years, primarily related to precipitation events. Two recent examples include the 2016 Louisiana flood and the damage to the Oroville Dam in 2017.

The flooding that occurred in southern Louisiana during August 2016 caused extensive damage throughout the affected region. At peak flood conditions, the Amite River rose 1.5 m over the previous record flood that occurred in 1983 (Vahedifard et al. 2016). The flood occurred as a result of compounding local floods occurring in multiple locations draining downstream, surpassing the capacity of levees and floodwalls as rain continued to fall in the region (Vahedifard et al. 2016).

For an example of the possible effects of sequential extreme events, consider a series of events experienced at the Oroville Dam in 2017. After a record-setting 5-year drought, the region experienced tremendous amounts of precipitation. These series of events culminated on February 7, 2017, when the Oroville Dam suffered serious damage in the form of a large hole in the primary spillway and severe erosion of the emergency spillway (Vahedifard et al. 2017). The drought conditions may have weakened the underlying soil and increased the permeability through cracking, allowing for the significant erosion experienced by the dam (Robinson and Vahedifard 2016).

These examples illustrate the need for the repair and revaluation of existing infrastructure in light of increased risk of severe, compounding, and multihazard events. This is especially true given the currents state of US infrastructure as a majority of flood protection and transportation infrastructure is already in a marginal state (ASCE 2017). The effects of multiclimatic trends and hazards must be estimated in order to properly plan for and estimate the risk of extreme events. Possible extreme events can be estimated based on climate models and the change in risk owing to these events can be examined based on increased probability of failure. Such analysis for many systems requires an increased understanding of the fundamental behavior of civil structures under extreme loading. However, research has already begun in this area, as well as the analysis of compounding effects.

Here we discuss a methodological framework outlined by Moftakhari et al. (2017) designed for multihazard assessment of extreme events and capturing the compounding effects of SLR and terrestrial flooding in coastal communities. Current models typically account for flooding and SLR separately, but coastal cities are at risk from SLR and storm surge–driven flooding. Moftakhari et al. (2017) proposed a bivariate flooding assessment

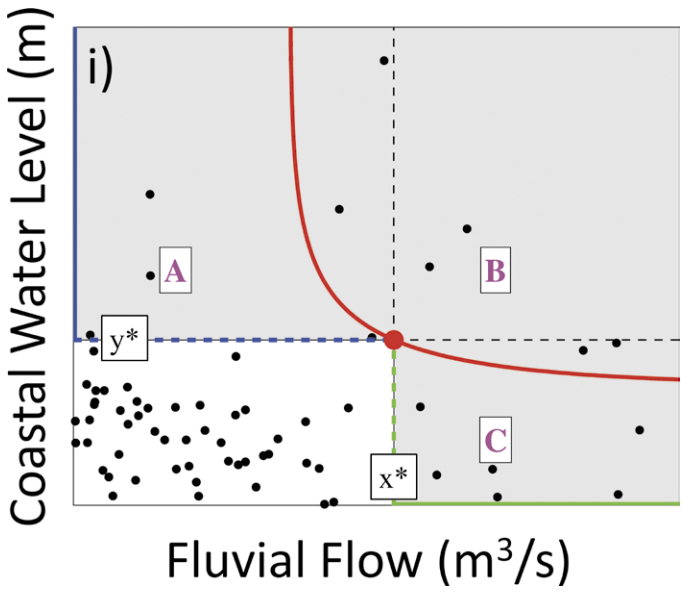

Figure 4-35. Illustration of the univariate and bivariate hazard scenarios. The black circles represent observed bivariate occurrences, the red circle is the reference occurrence $z^*=(x^*,y^*)$, the red line is the isoline of F_{XY} crossing z^*, with level $F_{XY}(x^*,y^*) \leq min\{F_X(x^*),F_Y(y^*)\}$, and the black line is the isoline of F_{XY} crossing z^*, under the simplifying assumption of independence between fluvial flow and coastal WL. Hazardous regions A, B, and C are indicated as dashed areas.
Source: Moftakhari et al. (2017).

approach that accounts for the compounding effects of fluvial flooding and coastal sea level considering future SLR. The approach integrates the notion of failure probability to achieve a practical tool for assessing future hazards.

The importance of the proposed multivariate frequency analysis approach is explained using conceptual diagram (Figure 4-35). This hypothetical example plots the annual peak fluvial flow to a given coastal system versus its associated coastal water level (black circles in Figure 4-35). For a given design RP, r, using common univariate frequency analysis approaches, one may find a specific threshold for fluvial flow (i.e., x^*, shown as a dashed green line) above which events are considered to be hazardous (i.e., have RPs greater than r, say, a 50-year event) and below which events are assumed to be safe. So, following the results of univariate frequency analysis, only the compound events lying in regions B and C with fluvial flows greater than x^* are thought to be hazardous and events with fluvial flows less than x^* (i.e. points in shaded region A) are assumed to be safe. Using the same

approach, one may analyze the observed coastal water level and end up with the threshold y^* (shown as a blue dashed line) above which events are considered as hazardous and below that (i.e., events lying in region *C*) are safe. Thus, following the univariate approach, we may not appropriately characterize the risk. The points located in regions *A* and *C* are hazardous from one point of view and safe from another point of view. In these situations, for appropriate characterization of hazard we need to use multivariate probability analysis-based approaches that take the correlation structure between variables into account and robustly characterize the risk of compound events. In the bivariate approach, given a critical pair (x^*,y^*), shown as a red circle in the hypothetical illustration, the corresponding bivariate hazard can be well characterized by the notion of *OR hazard scenario*, defined as the set of occurrences such that the fluvial flow is greater than x^* or the coastal water level is greater than y^* or both. The choice of a bivariate OR approach is consistent with the nature of coastal flooding because it is sufficient that either the fluvial discharge or the coastal water level or both be large enough to produce a potentially hazardous occurrence. Thus, all the occurrences in regions *A*, *B*, and *C* would be hazardous according to the (bivariate) OR criterion.

Moftakhari et al. (2017) used copula functions to describe the correlation structure between hazard drivers (e.g., fluvial flow and coastal water level). Copulas make it possible to account separately for the marginal and the joint behavior of the variables of interest, and marginal distributions can be of any type, which make them robustly applicable to any kind of multivariate hazard scenarios. Thus, the bivariate RP can be estimated as (T_{OR} = $1/(1 - F_{XY}(x^*,y^*))$, where F_{XY} is the joint distribution of the pair (X,y) and 1- F_{XY} is equal to the probability of $X > x^*$ OR $Y > y^*$, i.e., the probability that a bivariate occurrence lies in the shaded region A∪B∪C in Figure 4-35. We can show that potentially hazardous bivariate OR occurrences (x^*,y^*) are more frequent than the associated univariate x^* and y^* ones (both $T_{OR}<T_X$ and $T_{OR}<T_Y$). We present an example of compound flooding in Washington, DC, showing how taking different approaches (univariate versus bivariate frequency analysis) and making different assumptions (dependent versus independent variables) might affect the estimation of RP for a given compound flooding event, as shown in Figure 4-36.

In this case, the green dashed line shows a river flow threshold with the estimated RP of 20 years, and the blue dashed line is associated with a coastal water level threshold having a 20-year RP, both of which were calculated using the univariate frequency analysis approach (Figure 4-36). If we take the compounding impacts of flood rivers into account, the estimated RP for the bivariate OR occurrence (x^*,y^*), shown as a red circle, would be 16 years. This example shows how taking the univariate approach may inappropriately estimate (i.e., overestimate) the RP of a hazardous compound event. For the sake of comparison, we also plotted the estimated RP based

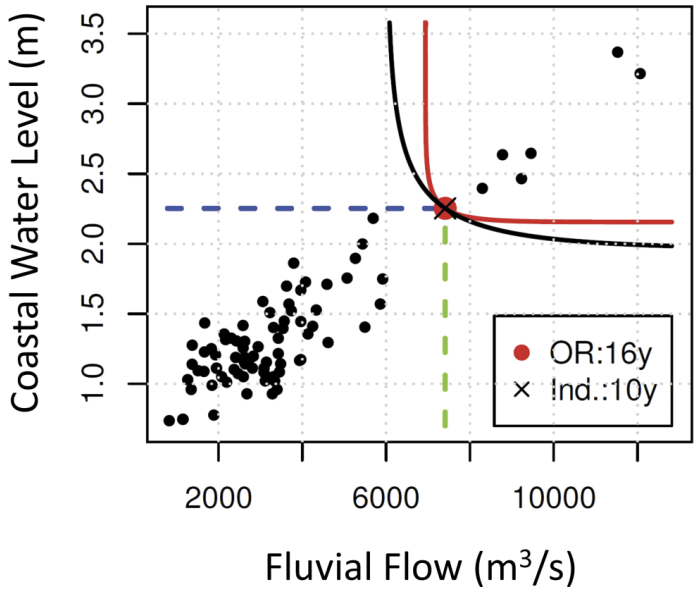

Figure 4-36. The estimates of the bivariate OR RPs against univariate frequency estimates. The RPs associated with occurrence z^* are indicated in the legends for Washington, DC.
Source: Moftakhari et al. (2017).

on an inappropriate assumption of independence between the variables, shown by the black curve. In this example, bivariate frequency analysis that does not address the dependence structure between variables underestimates the RP estimated using the bivariate OR scenario. Therefore, neglecting the compounding effects of hazard drivers may result in an underestimation of the hazard when the combined action of multiple drivers plays a significant role.

This multivariate OR hazard scenario analysis can be linked to the notion of failure probability. For a given design life time T (typically in years), considering $(S_1, \ldots, S_T)$ as a sequence of annual bivariate OR hazard scenarios, the probability that at least no hazardous event occurs in T years is called failure probability (p_T). In bivariate hazard analysis, this probability is equal to $p_T = 1 - [C_{XY}(F_X(x^*), F_Y(y^*))]^T$, where C_{XY} is the copula function describing the correlation structure between variables in a multihazard scenario (here, fluvial flooding and coastal water level). Theoretically, $p_{T,OR} \geq p_{T,X}$ and $p_{T,OR} \geq p_{T,y}$ for all design life times, implying that OR occurrences are generally more hazardous than univariate ones. Following the estimated RPs for Washington, DC (Figure 4-36), Figure 4-37 displays the estimated failure probability over the given design life time of 30 years based on the estimated

univariate and multivariate RPs. In Figure 4-37 the continuous black and red curves show the failure probability estimates based on univariate and bivariate OR frequency analysis results, respectively. As the results show, the estimated failure probability is ~10% greater under compound hazard assessment compared to the ones calculated using traditional univariate approaches.

This approach also allows considering future SLR. Figure 4-37 shows estimated failure probabilities using perturbed coastal water level by the SLR projections provided by Kopp et al. (2014). The resulting failure probability estimates are plotted in Figure 4-37 (see the solid purple line). The uncertainties associated with future projections are plotted using dotted purple lines (upper and lower bounds). As shown, this approach allows considering multihazard scenarios and compares the failure probability of the common univariate approach.

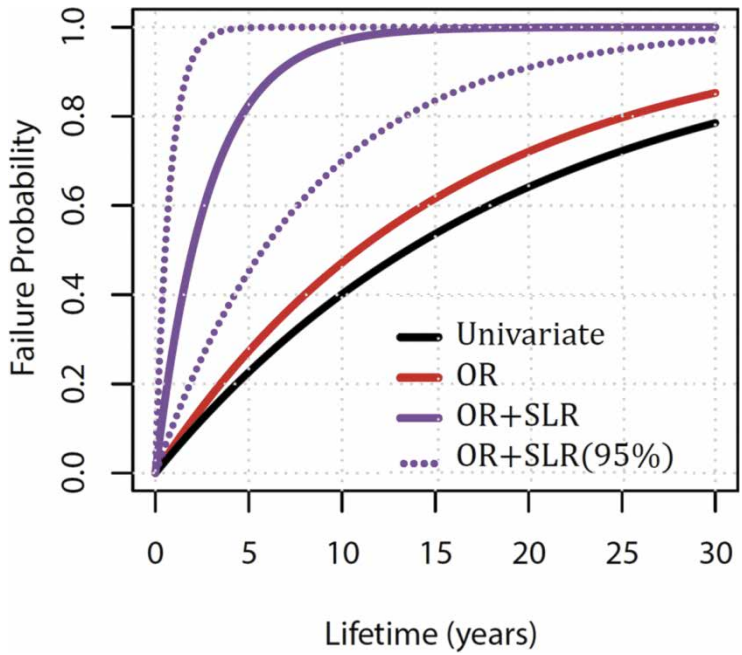

Figure 4-37. Estimated failure probability for a temporal horizon of 30 years. The solid black and red curves show the estimated failure probability computed based on the univariate and bivariate OR hazard scenarios, respectively, according to the presently observed climate conditions. The solid and dashed purple curves show the estimated probability of failure using a bivariate OR approach and an associated 95% confidence band considering the projected SLR for 2030 under RCP 4.5.

4.6 HAZARD MONITORING VERSUS RISK MONITORING

Timely guidance on magnitudes of extremes for design, such as *probable maximum* or *design basis* values for initial design with *bounds* or *maximum credible* levels for adaptations during service life, is needed and should be given precedence. As a starting point, *extreme* values for a specific exceedance probability would be set consistent with currently cited values in standards. It should be noted that the extreme values are random variables and could be probabilistically characterized in terms of their mean and variance values and a probability distribution. The mean value could be treated as equivalent to the *probable extreme value*, and the 90th percentile of an extreme value could be treated as the *credible extreme value*. The NRC (2016) examines the attribution of extreme weather events in the context of climate change and provides guidance on forecasting the frequencies and intensities of climate or weather extremes.

4.7 POSITIONING RISK IN THE CONTEXT OF HYDROCLIMATIC NON-STATIONARITY

In Sections 4.2 to 4.4, evidence of non-stationarity was linked to the presence of linear trends in the data. Specifically, it was pointed out in Section 4.4.2 that log-linear trends in flood frequency analysis of log-transformed data (e.g., log **Q**) corresponds to an exponential trend of the mean of **Q**. Here, we address non-stationarity in the context of multiyear, decadal, and multi-decadal internal climate variability, which may or may not be compounded by a trend, which is different from and in addition to and compounded with non-stationarity tied to land-use change, infrastructure, and urbanization (Barros et al. 2014) and often goes unrecognized and/or is simply implicitly wrapped into epistemic uncertainty under current risk modeling approaches. Although aleatory uncertainty may be dominant in the estimates of extreme events of very long return periods, T, such as the *probable maximum precipitation* and *probable maximum flood* (Douglas and Barros 2003), internal climate non-stationarity can strongly modulate the magnitude of low- and moderate-risk events, that is, the shape of the distribution (Read and Vogel 2015). In practical terms, this implies that the design criteria for the same level of risk varies depending on the underlying hydroclimate regime, with major consequences for economic, safety, and project performance. Here, we argue that positioning risk within the space–time continuum of relevant regional non-stationarity is a matter of due diligence in engineering design (Barros and Evans 1997, Jain and Lall 2001). Finally, positioning risk in engineering design requires situational awareness (knowledge of climate regime, natural and built physical support, and data) and sound engineering judgment.

Independently of climate change, hydroclimatic non-stationarity manifests itself in the form of persistence and long-range memory at multiple timescales associated with internal climate variability, which either cannot be detected or can only be partly detected (see Section 4.7.1) in the analysis of a streamflow time series because of insufficient length of the historical record (Barros et al. 2014, Matalas 1997). This speaks to the need for maintaining long-term high-fidelity observing systems to acquire the long-term records needed to elucidate the signature of climate in the historical record. Generally, streamflow records covering 50 to 60 years are needed to reduce the uncertainty in 100-year flood estimates to values below 50% (Barros et al. 2014). Because of the nonlinear interactions among physical processes in the Earth system, including climate change and land-use change, the characteristics of this non-stationary may change in the future in ways that require going beyond trend analysis to assess climate change impacts. That is, future non-stationarity may not resemble current and past non-stationarity, and how changes in atmospheric hydrological processes impact terrestrial hydrological processes can be complex because increases in precipitation do not necessarily translate into increased runoff owing to changes in seasonality (Simoes and Barros, 2007) and changes in land use (e.g., Bhatkoti et al. 2016) among other possible nonlinear interactions. This appeals directly to the importance of maintaining large-scale observing systems capable of monitoring multiscale changes that can also be used to benchmark and evaluate predictive models, including climate change assessment models.

4.7.1 Due Diligence–Detecting and Assessing Non-stationarity from Observations

Wavelet analysis of 100 years of discharge data averaged to a monthly timescale for a streamgauge near Parsons, West Virginia, is shown in Figure 4-38. First, note the signature of the annual cycle for most of the length of the record in Figure 4-38(b) (red band). Second, note two additional peaks in the wavelet power spectrum in the 1990s, one peak corresponding to 2- to 3-year timescales in the beginning of the decade, the second peak centered at 8 years from the mid-1990s through the early years of the 21st century. Because increased variability at these scales concurrent with a strong annual cycle is only present in the recent record, a possible interpretation is that this variability reoccurs at lags longer than 100 years or that it is an indication of a possible change in hydroclimatic variability at temporal scales of 2 to 4 years, as shown in Figure 4-39 (see also Li et al. 2013, Barros et al. 2017). Nevertheless, this has significant implications for flood risk.

Careful inspection of the flood frequency analysis at the same station (Figure 4-40) shows the importance of non-stationarity in flood estimates for all RPs, and especially becomes larger for the 100-year flood (~50%),

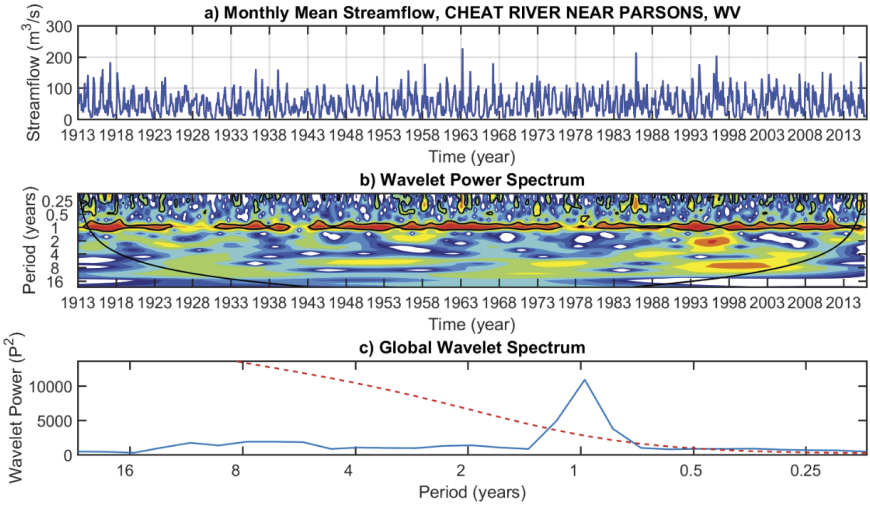

Figure 4-38. Analysis of streamflow record (100 years) from the Cheat River streamgauge in the Appalachian Mountains: (a) monthly streamflow discharge; and (b) wavelet power spectrum. The wavelet power spectrum shows the evolution of variability in the monthly streamflow at different timescales and as a function of time. Warm colors indicate higher power.

with values between 20% and 30% for 10- to 50-year events. The crossing of the red and green lines indicates a change in the nature of hydroclimatic variability at the short timescales as compared to the long timescales between 1973 and 1993. By contrast, adding ten years of data in the beginning of the century makes no difference to flood statistics (compare black and pink lines), which is consistent with the results from the wavelet analysis shown in Figure 4-38.

Overall, the longer the period of record, the larger the flood estimates generally because a 100-year-long record is long in the context of existing historical observations, but it is not long enough to capture the signature of long climate cycles that maybe present. However, this is not the case for the small events with $T < 10$ years in the last decade of the twentieth century (notice the difference between the green and pink lines in Figure 4-40).

The wavelet power spectra of monthly streamflow for the common PoR at three locations [Figure 4-41(a)] are shown in Figure 4-40(b). The temporal evolution of the non-stationarity in the annual cycle and at 2- to 4- and 4- to 8-year timescales between 1960 and today is different among the three streamgauges, including between the two West Virginia streamgauges in the Appalachian Mountains. These differences illustrate the role of regional climate and the different teleconnections of regional climate with large-scale

circulation, as well as the orographic precipitation enhancement and landform and hydrogeological impacts on streamflow (e.g., Sun and Barros 2010, Barros et al. 2017).

4.7.2 Engineering Judgment

In practice, generally, and independently of the type of non-stationarity (trend or internal variability), estimates of the magnitude of precipitation

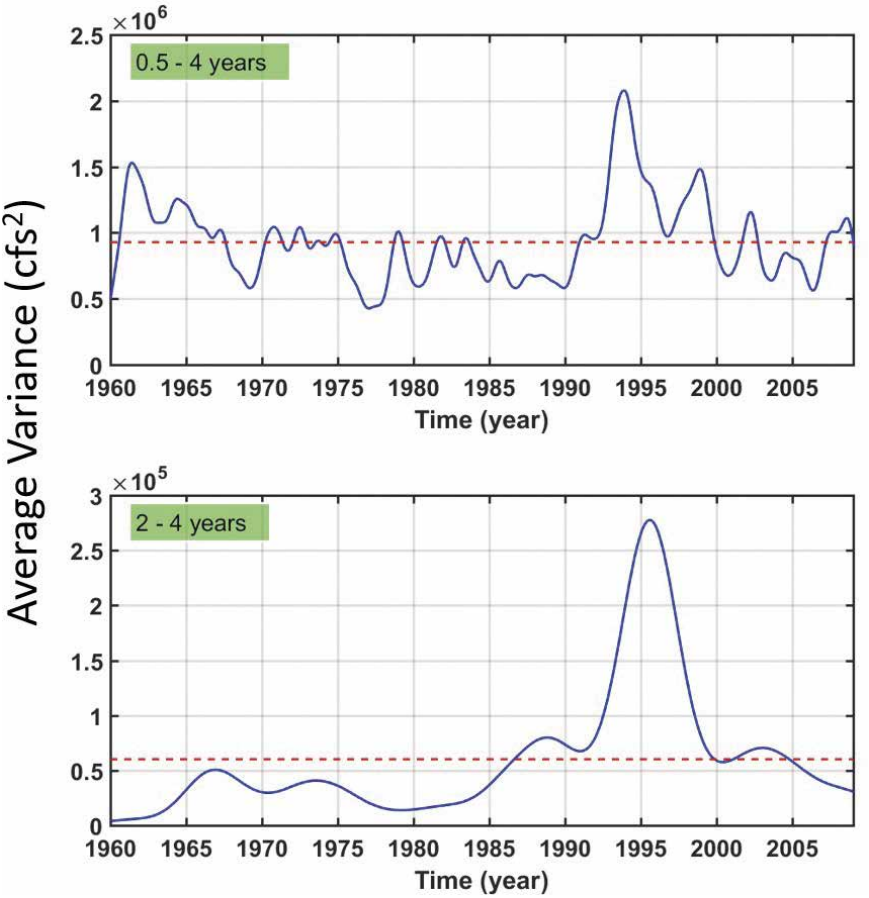

Figure 4-39. Temporal evolution of variance between 1960 and 2010 at the Cheat River streamgauge. Top panel—daily streamflow; bottom panel—streamflow time series after removing annual and shorter timescales. There is one order of magnitude difference in variance between the top and bottom panels. The red dashed line indicates mean values.

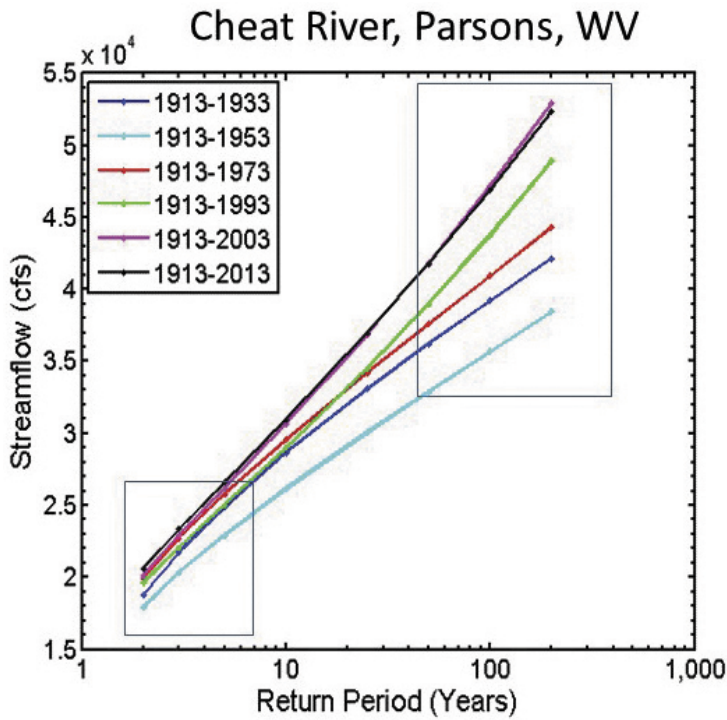

Figure 4-40. Flood frequency (Log-Pearson Type III) analysis using different periods of the record, as indicated by the legend. The two boxes highlight the uncertainty associated with non-stationarity on the estimates of the 2- to 5-year event (~20%) and the 100-year flood (~50%).
Source: Barros et al. (2014).

and floods for a desired risk level are plagued by uncertainty owing to data limitations (Barros et al. 2014). As pointed out earlier, 50- to 60-year-long records are needed to maintain the uncertainty in flood frequency estimates below 50%, and thus often the uncertainty owing to non-stationarity is significantly lower than the statistical uncertainty. However, an increase in the frequency of the design event, which is the equivalent of *under-design*, can have larger economic and social implications than the upfront cost of *over-design* to account for uncertainty in the design event estimation (Rosner et al. 2014). Arguably, *over-design* (i.e., hedging uncertainty) has long been the engineer's choice and is embedded in codes and standards to address questions of uncertainty, which explains the fact that higher levels of reliability have been achieved in the past for large infrastructure projects as compared to the theoretical value associated with a specific event over the project life (e.g., Matalas 1997, Read and Vogel 2015). Whether past

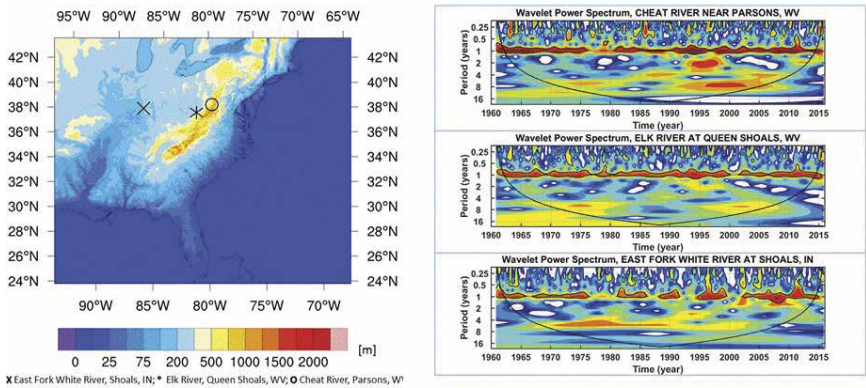

Figure 4-41. Left panel—topographic map of the CONUS east of 95°W. Colors correspond to terrain elevations in meters. The three streamgauges marked are located in the East Fork of the White River, Shoals, IN (X), at Queen Shoals, in the Elk River in WV (*), and in the Cheat River, at Parsons, WV (o). Right panel—wavelet spectra for the three streamgauges using the common PoR. Black lines are 95% cfl.

levels of *over-design* and implicitly accepted project reliability are adequate to capture uncertainty as our understanding and quantitative assessment of non-stationarity improves, including nonlinear impacts of climate change, is therefore the question at hand.

Bhatkoti et al. (2016) examined changes in bridge flood risk owing to climate change impacts on precipitation using results from four different regional climate model simulations in Maryland, and they found that although risk increased for all types of bridges, the highest increase in median failure risk probability (up to four times higher) for three of the models was for the bridges on local and rural roads, which have less stringent design requirements. They also found through sensitivity analysis that uncertainty in both flood and precipitation frequency is comparable to the uncertainty owing to climate change in the context of their specific modeling framework. Hiarabayashi et al. (2013), using a different methodology and different climate projections, found that, on average, the frequency of the twentieth century 100-year event along both the eastern and western seaboards of the United States would double in the 21st century. These studies suggest potentially significant decreases in project reliability because current *over-design* standards may prove insufficient. The purpose of positioning risk, which is companion to the OM proposed by Olsen et al. (2015), is to reduce epistemic uncertainty associated with non-stationarity, and thus the ambiguity (and economic regrets) in *over-design*.

Take the NS log-normal flood frequency model proposed by Read and Vogel (2015):

$$X(t) = \ln[Q(t)] = \mu + \beta \times t + \epsilon(t) \tag{4-13}$$

where α and β are model parameters and ε is a random variable with mean zero. The corresponding flood magnification factor M at timescale D is

$$M = \exp(\beta \times D) \tag{4-14}$$

For a given planned project life, reliability increases as the COV, Cx, decreases for the large RPs and increases as M decreases for the short RPs (Read and Vogel 2015). Consider that it is possible to estimate the contribution of internal climate variability (*) associated in the N years of the planned project life starting on year Y as follows:

$$\alpha^*(t) = \gamma_1 + \gamma_2 \times (t - Y) + \gamma_3 \times (t - Y)^2 \tag{4-15}$$

Then

$$X(t) = \mu + \alpha^*(t) + \beta^* \times (t - Y) + \epsilon^*(t), \quad with \quad Y \le t \le Y + N,\ \beta^* \le \beta,\ \epsilon^* < \epsilon \tag{4-16}$$

and

$$X^*(t) = X(t) - \alpha^*(t) = \mu + \beta^* \times (t - Y) + \epsilon^*(t) \quad \text{and} \quad M^* < M, \quad C_x{}^* < C_x \tag{4-17}$$

4.8 REFERENCES

ASCE. 2017. *Report Card for America's Infrastructures*. Accessed September 12, 2018. www.infrastructurereportcard.org/. Reston, VA: ASCE.

Asquith, W. H. 1998. "Depth-duration frequency of precipitation for Texas." *USGS Water-Resources Investigations Report 98-4044*. Reston, VA: USGS.

Asquith, W. H., and M. C. Roussel. 2004. "Atlas of depth-duration frequency of precipitation annual maxima for Texas." *USGS Report 2004–5041*, Reston, VA: USGS.

Barros, A. P., and J. L. Evans. 1997. "Designing for climate variability." *J. Prof. Issues Eng. Educ. Pract*. 123(2), 62–65.

Barros, A. P., Y. Duan, J. Brun, and M. A. Medina Jr. 2014. "Flood nonstationarity in the Southeast and Mid-Atlantic regions of the United States." *J. Hydrol. Eng*. 19(10), 05014014.

Barros, A. P., J. L. Hodes, and M. Arulraj. 2017. "Decadal climate variability and the spatial organization of deep hydrological drought." *Environ. Res. Lett*. 12(10), 104005. DOI: 10.1088/1748-9326/aa81de.

Bhatkoti, R., G. E. Moglen, P. M. Murray-Tuite, and K. P. Triantis. 2016. "Changes to bridge flood risk under climate change." *J. Hydrol. Eng*. 21(12), 04016045. DOI: 10.1061/(ASCE)HE.1943-5584.0001448.

Bruneau, M., M. Barbato, J. E. Padgett, A. E. Zaghi, J. Mitrani-Reiser, and Y. Li. 2017. "State-of-the-Art on multihazard design." *J. Struct. Eng*. 143(10), 03117002.

Burges, S. 2016. "The importance of studying past extreme floods to prepare for uncertain future extremes." *AGU Fall Meeting, Paper NH54A-02*. Washington, DC: American Geophysical Union.

Cheng, L., A. AghaKouchak, E. Gilleland, and R. W. Katz. 2014. "Non-stationary extreme value analysis in a changing climate." *Clim. Change* 127(2), 353–369. Accessed September 12, 2018. https://doi.org/10.1007/s10584-014-1254-5.

Cohn, T. A., and H. F. Lins. 2005. "Nature's style: Naturally trendy." *Geophys. Res. Lett*. 32(23), 1–5. Accessed September 12, 2018. https://doi.org/10.1029/2005GL024476.

Cohn, T. A., W. L. Lane, and W. G. Baier. 1997. "An algorithm for computing moments-based flood quantile estimates when historical flood information is available." *Water Resour. Res.* 33(9), 2089–2096.

Coles, S. G. 2001. *An introduction to statistical modeling of extreme values*, Vol. 208. London: Springer. Accessed September 12, 2018. https://doi.org/10.1007/978-1-4471-3675-0.

Cooley, D. 2013. "Return periods and return levels under climate change." In *Extremes in a Changing Climate—Detection, Analysis & Uncertainty*, S. Sorooshian et al. (eds.). Dordrecht, Netherlands: Springer-Verlag.

Cunnane, C. 1978. "Unbiased plotting positions—A review." *J. Hydrol.* 37(3–4), 205–222.

Cunnane, C. 1988. "Methods and merits of regional flood frequency analysis." *J. Hydrol*. 100(1–3), 269–290.

Dawdy, D. R., V. W. Griffis, and V. K. Gupta. 2012. "Regional flood-frequency analysis: How we got here and where we are going." *J. Hydrol. Eng*. 17(9), 953–959. DOI: 10.1061/(ASCE)HE.1943-5584.0000584.

DeGaetano, A. T. 2009. "Time-dependent changes in extreme-precipitation return-period amounts in the continental United States." *J. Appl. Meteorol. Climatol*. 48(10), 2086–2099. Accessed September 12, 2018. https://doi.org/10.1175/2009JAMC2179.1.

Douglas, E., and A. P. Barros. 2003. "Probable Maximum Precipitation Estimation Using Multifractals: Application in the Eastern United States." *J. Hydrometeorol*. 4(6), 1012–1024.

England, J. F. 2011. "Flood frequency and design flood estimation procedures in the United States: Progress and challenges." *Aust. J. Water Resour*. 15(1), 33–46.

England, J. F., T. A. Cohn, B. A. Faber, J. R. Stedinger, W. O. Thomas Jr., A. G. Veilleux, et al. 2016. "Guidelines for determining flood flow frequency." *Bulletin 17C*. Reston, VA: USGS.

Fischer, E. M., and R. Knutti. 2016. "Observed heavy precipitation increase confirms theory and early models." *Nat. Clim. Change* 6(11), 986–991. Accessed September 12, 2018. https://doi.org/10.1038/nclimate3110.

Flynn, K. M., W. H. Kirby, and P. R. Hummel. 2006. "User's manual for program PeakFQ, annual flood-frequency analysis using Bulletin 17B guidelines." *No. 4-B4.* Reston, VA: USGS.

Halverson, J. 2015. "The meteorology behind South Carolina's catastrophic, 1,000-year rainfall event." *Washington Post*, October 5, 2015. https://www.washingtonpost.com/news/capital-weather-gang/wp/2015/10/05/the-meteorology-behind-south-carolinas-catastrophic-1000-year-rainfall-event/?utm_term=.43ada2a50c77.

Heineman, M. 2012. "Trends in precipitation maxima at US Historical Climatology Network stations 1893-2010." *World Environmental and Water Resources Congr. 2012*. Reston, VA: ASCE.

Hirabayashi, Y., R. Mahendran, S. Koirala, L. Konoshima, D. Yamazaki, S. Watanabe, et al. 2013. "Global flood risk under climate change." *Nat. Clim. Change* 3(9), 816–821.

Hosking, J. R. M. 1990. "L-moments: Analysis and estimation of distributions using linear combinations of order statistics." *J. Royal Statist. Soc. Series B (Methodological)* 52(1), 105–124. www.jstor.org/stable/2345653.

IPCC (International Panel on Climate Change). 2013. "Observations: Atmosphere and surface" In *Climate Change 2013: The Physical Science Basis*. T. F. Stocker et al. (eds.). Cambridge, UK: Cambridge Univ. Press.

Jain, S., and Lall, U. 2001. "Floods in a changing climate: does the past represent the future?" *Water Resour. Res.* 37, 3193–3205.

Katz, R. W. 2010. "Statistics of extremes in climate change." *Clim. Change* 100(1), 71–76. Accessed September 12, 2018. https://doi.org/10.1007/s10584-010-9834-5.

Katz, R. W., M. B. Parlange, and P. Naveau. 2002. "Statistics of extremes in hydrology." *Adv. Water Resour*. 25(8–12), 1287–1304. Accessed September 12, 2018. https://doi.org/10.1016/S0309-1708(02)00056-8.

Kennard, M. J., S. J. Mackay, B. J. Pusey, J. D. Olden, and N. Marsh. 2010. "Quantifying uncertainty in estimation of hydrologic metrics for ecohydrological studies." *River Res. Appl*. 26(2), 137–156.

Kite, G. W. 1977. *Frequency and risk analysis in hydrology*. Fort Collins, CO: Water Resources Publications.

Klemeš, V. 1974. "The Hurst phenomenon: A puzzle?" *Water Resour. Res*. 10(4), 675–688. Accessed September 12, 2018. https://doi.org/10.1029/WR010i004p00675.

Kopp, R. E., R. M. Horton, C. M. Little, J. X. Mitrovica, M. Oppenheimer, D. J. Rasmussen, et al. 2014. "Probabilistic 21st and 22nd century sea-level projections at a global network of tide-gauge sites." *Earth's Future* 2(8), 383–406.

Koutsoyiannis, D. 2005. "Nonstationarity versus scaling in hydrology." *J. Hydrol.* 324(1–4), 239–254. Accessed September 12, 2018. https://doi.org/10.1016/j.jhydrol.2005.09.022.

Li, L., W. Li, and A. P. Barros. 2013. "Atmospheric moisture budget and its regulation of the summer precipitation variability over the Southeastern United States." *Clim. Dyn*. 41(3–4), 613–631. DOI:10.1007/s00382-013-1697-9.

Lins, H. F., and T. A. Cohn. 2011. "Stationarity: Wanted dead or alive?" *J. Amer Water Resour. Assoc*. 47(3), 475–480. Accessed September 12, 2018. https://doi.org/10.1111/j.1752-1688.2011.00542.x.

Luke, A., J. A. Vrugt, A. AghaKouchak, R. Matthew, and B. F. Sanders. 2017. "Predicting nonstationary flood frequencies: Evidence supports an updated stationarity thesis in the United States." *Water Resour. Res*. 53(7), 5469–5494. DOI:10.1002/2016WR019676.

Matalas, N. 1997. "Stochastic hydrology in the context of climatic change." *Clim. Change* 37(1), 89–101.

Mehran, A., A. AghaKouchak, and T. Phillips. 2014. "Evaluation of CMIP5 continental precipitation simulations relative to satellite observations." *J. Geophys. Res.* 119, 1695–1707.

Miami Conservancy District. 1917. "Storm rainfall of Eastern United States." Dayton, Ohio: Miami Conservancy District.

Milly, P. C. D., J. Betancourt, M. Falkenmark, R. M. Hirsch, Z. Kundzewicz, D. P. Lettenmaier, et al. 2008. "Stationarity is dead: Whither water management?" *Science* 319(5863), 573–574. https://doi.org/10.1126/science.1151915.

Moftakhari, H. R., G. Salvadori, A. AghaKouchak, B. F. Sanders, and R. A. Matthew. 2017. "Compounding effects of sea level rise and fluvial flooding." *Proc., National Academy of Sciences* 114(37), 9785–9790.

Mondal, A., and P. P. Mujumdar. 2015. "Modeling non-stationarity in intensity, duration and frequency of extreme rainfall over India." *J. Hydrol.* 521, 217–231. Accessed September 12, 2018. https://doi.org/10.1016/j.jhydrol.2014.11.071.

Montanari, A., and D. Koutsoyiannis. 2014. "Modeling and mitigating natural hazards: Stationarity is immortal!" *Water Resour. Res*. 50(12), 9748–9756. Accessed September 12, 2018. https://doi.org/10.1002/2014WR016092.

NOAA (National Oceanic and Atmospheric Administration). 2006. "Precipitation-frequency atlas of the United States, Ohio River Basin and

Surrounding States." *NOAA Atlas 14, Vol. 2*. Accessed August 16, 2017. http://www.nws.noaa.gov/oh/hdsc/PF_documents/Atlas14_Volume2.pdf.

NOAA. 2008. "Precipitation-frequency atlas of the United States, Puerto Rico and the US Virgin Islands." *NOAA Atlas 14, Vol. 3*. Accessed August 16, 2017. http://www.nws.noaa.gov/oh/hdsc/PF_documents/Atlas14_Volume3.pdf.

NOAA. 2011a. "Precipitation-frequency atlas of the United States, Semiarid Southwest." *NOAA Atlas 14, Vol. 1*. Accessed August 16, 2017. http://www.nws.noaa.gov/oh/hdsc/PF_documents/Atlas14_Volume1.pdf.

NOAA. 2011b. "Precipitation-frequency atlas of the United States, Hawaiian Islands." *NOAA Atlas 14, Vol. 4*. Accessed August 16, 2017. http://www.nws.noaa.gov/oh/hdsc/PF_documents/Atlas14_Volume4.pdf.

NOAA. 2011c. "Precipitation-Frequency Atlas of the United States, Selected Pacific Islands." *NOAA Atlas 14, Vol. 5*. Accessed August 16, 2017. http://www.nws.noaa.gov/oh/hdsc/PF_documents/Atlas14_Volume5.pdf.

NOAA. 2012a. "Precipitation-frequency atlas of the United States, Alaska." *NOAA Atlas 14, Vol. 7*. Accessed August 16, 2017. http://www.nws.noaa.gov/oh/hdsc/PF_documents/Atlas14_Volume7.pdf.

NOAA. 2012b. "Global and regional sea level rise scenarios for the United States" *NOAA Technical Report NOS CO-OPS 083*. Silver Spring, MD: NOAA.

NOAA. 2013a. "Precipitation-frequency atlas of the United States, Midwestern States." *NOAA Atlas 14, Vol. 8*. Accessed August 16, 2017. http://www.nws.noaa.gov/oh/hdsc/PF_documents/Atlas14_Volume8.pdf.

NOAA. 2013b. "Precipitation-frequency atlas of the United States, Southeastern States." *NOAA Atlas 14, Vol. 9*. Accessed August 16, 2017. http://www.nws.noaa.gov/oh/hdsc/PF_documents/Atlas14_Volume9.pdf.

NOAA. 2014. Precipitation-frequency atlas of the United States, California." *NOAA Atlas 14, Vol. 6*. Accessed August 16, 2017. http://www.nws.noaa.gov/oh/hdsc/PF_documents/Atlas14_Volume6.pdf.

NOAA. 2015. "Precipitation-frequency atlas of the United States, Northeastern States." *NOAA Atlas 14, Vol. 10*. Accessed August 16, 2017. http://www.nws.noaa.gov/oh/hdsc/PF_documents/Atlas14_Volume10.pdf.

NOAA. 2017. "Precipitation-frequency data server." Accessed March 28, 2017. http://hdsc.nws.noaa.gov/hdsc/pfds/.

NRC (National Research Council). 2012. *Sea-level rise for the coasts of California, Oregon, and Washington: Past, present, and future*. Washington, DC: National Academies Press. DOI: 10.17226/13389.

NRC. 2016. *Attribution of extreme weather events in the context of climate change*. Washington, DC: National Academies Press. DOI: 10.17226/21852.

Olsen, J. R., B. M. Ayyub, A. Barros, W. Lei, M. Medina, C. Samaras, et al. 2015. "Adapting infrastructure and civil engineering practice to a changing climate." http://dx.doi.org/10.1061/9780784479193. Reston, VA: ASCE.

Pandey, G. R., and V.-T.-V. Nguyen. 1999. "A comparative study of regression-based methods in regional flood frequency analysis." *J. Hydrol.* 225(1–2), 92–101.

Paretti, N. V., J. R. Kennedy, and T. A. Cohn. 2014. "Evaluation of the expected moments algorithm and a multiple low-outlier test for flood frequency analysis at streamgauging stations in Arizona." *Scientific Investigations Report 2014–5026*. Reston, VA: USGS.

Prosdocimi, I., Kjeldsen, T. R., and C. Svensson. 2014. "Non-stationarity in annual and season series of peak flow and precipitation in the UK." *Nat. Hazards Earth Syst. Sci.* 14(5), 1125–1144. DOI:10.5194/nhess-14-1125-2014.

Ragno, E., A. AghaKouchak, C. A. Love, L. Cheng, F. Vahedifard, and C. H. R. Lima. 2017. "Quantifying changes in future intensity-duration-frequency curves using multi-model ensemble simulations." *Water Resour. Res.* 54(3), 1751–1764.

Read, L. K., and R. M. Vogel. 2015. "Reliability, return periods, and risk under nonstationarity." *Water Resour. Res.* 51(8), 6381–6398. DOI:10.1002/2015WR017089.

Reis Jr., D. S., and J. R. Stedinger. 2005. "Bayesian MCMC flood frequency analysis with historical information." *J. Hydrol.* 313(1–2), 97–116. DOI:10.1016/j.jhydrol.2005.02.028.

Restrepo-Posada, P., and P. S. Eagleson. 1982. "Identification of independent rainstorms." *J. Hydrol.* 55, 303–319.

Robinson, J. D., and F. Vahedifard. 2016. "Weakening mechanisms imposed on California's levees under multiyear extreme drought." *Clim. Change* 137(1–2), 1–14.

Rosner, A., R. M. Vogel, and P. H. Kirshen. 2014. "A risk-based approach to flood management decisions in a nonstationary world." *Water Resour. Res.* 50(3), 1928–1942. DOI:10.1002/2013WR014561.

Sarhadi, A., and E. D. Soulis. 2017. "Time-varying extreme rainfall intensity-duration-frequency curves in a changing climate." *Geophys. Res. Lett.* 44(5), 2454–2463. Accessed September 12, 2018. https://doi.org/10.1002/2016GL072201.

Seneviratne, S. I., N. Nicholls, D. Easterling, C. Goodess, S. Kanae, J. Kossin, et al. 2012. "Managing the risks of extreme events and disasters to advance climate change adaptation: Special report of the Intergovernmental Panel on Climate Change (IPCC)." Cambridge, UK: Cambridge Univ. Press.

Serinaldi, F. 2015. "Dismissing return periods!" *Stoch. Environ. Res. Risk Assess.* 29(4), 1179–1189. https://doi.org/10.1007/s00477-014-0916-1.

SFRCCC (Southeast Florida Regional Climate Change Compact). 2015. "A unified sea level rise projection for Southeast Florida." Accessed February 10, 2018. http://www.southeastfloridaclimatecompact.org/wp-content/uploads/2015/10/2015-Compact-Unified-Sea-Level-Rise-Projection.pdf.

SFWMD (South Florida Water Management District). 1979. "Preliminary report on the severe storm of April 24-25, 1979." West Palm Beach, FL: SFWMD.

Simoes, S. J., and A. P. Barros. 2007. "Regional hydroclimatic variability and Brazil's 2001 energy crisis." *Manage. Environ. Quality: An Int. J.* 18(3), 263–273.

Stedinger, J. R., and V. W. Griffis. 2011. "Getting from here to where? Flood frequency analysis and climate." *J. Am. Water Resour. Assoc*. 47(3), 506–513.

Sun X., and A. P. Barros. 2010. "An evaluation of the statistics of rainfall extremes in rain gauge observations, and satellite-based and reanalysis products using universal multifractals." *J. Hydrometeorol*. 11(2), 388–404. DOI:10.1175/2009JHM1142.1

Trenberth, K. E. 2011. "Changes in precipitation with climate change." *Clim. Res*. 47, 123–138. DOI:10.3354/cr00953.

USGCRP (US Global Change Research Program). 2014. *Climate change impacts in the United States: The third national climate assessment*. J. M. Melillo et al. (eds.). Washington, DC: US Global Change Research Program. DOI:10.7930/J0Z31WJ2.

USGS (US Geological Survey). 1982. "Guidelines for determining flood flow frequency" *Bulletin 17B*. Reston, VA: USGS. Accessed August 16, 2017. https://water.usgs.gov/osw/bulletin17b/dl_flow.pdf.

US Water Resources Council. 1967. "A technique for determining flood flow frequencies." *Bulletin No. 15*. Washington, DC: Water Resources Council. Accessed August 17, 2017. https://water.usgs.gov/osw/bulletin17b/Bulletin_15_1967.pdf.

Vahedifard, F., A. AghaKouchak, N. H. Jafari. 2016. "Compound hazards yield Louisiana flood." *Science* 353(6306), 1374–1374.

Vahedifard, F., A. AghaKouchak, E. Ragno, S. Shahrokhabadi, and I. Mallakpour. 2017. "Lessons from the Oroville Dam." *Science* 355(6330), 1139–1140.

Villarini, G., F. Serinaldi, J. A. Smith, and W. F. Krajewski. 2009. "On the stationarity of annual flood peaks in the continental United States during the 20th century." *Water Resour. Res*. 45(8). DOI:10.1029/2008WR007645.

Vivekanandan, N. 2014. "Rainfall frequency analysis using L-moments of probability distributions." *Int. J. Comp. Appl. Eng. Technol*. 3(3), 248–256.

Vogel, R. M., C. Yaindl, and M. Walter. 2011. "Nonstationarity: Flood magnification and recurrence reduction factors in the United States." *J. Am. Water Resour. Assoc*. 47(3), 464–474.

Wasko, C., A. Sharma, and S. Westra. 2016. "Reduced spatial extent of extreme storms at higher temperatures." *Geophys. Res. Lett*. 43(8), 4026–4032. Accessed September 12, 2018. https://doi.org/10.1002/2016GL068509.

Weather Bureau. 1954. "Climatological data: Texas. Supplemental precipitation data." Vol. LIX, No. 6, Kansas City Weather Bureau.

Zaghi, A. E., J. E. Padgett, B. Bruneau, B. Barbato, Y. Li, J. Mitrani-Reiser, et al. 2016. "Forum paper: Establishing common nomenclature, characterizing the problem, and identifying future opportunities in multi-hazard design." *J. Struct. Eng*. 142(12), H2516001.

Zheng, F., S. Westra, and M. Leonard. 2015. "Opposing local precipitation extremes." *Nat. Clim. Change* 5(5), 389–390. Accessed September 12, 2018. https://doi.org/10.1038/nclimate2579.

This page intentionally left blank

CHAPTER 5
FLOOD DESIGN CRITERIA

5.1 COASTAL FLOODING COMPONENTS

Prior to calculating flood loading within coastal locations, the design flood event anticipated depth of floodwater and wave action must be identified. Design Flood Elevation (DFE) is defined as the peak elevation of the design flood, including freeboard. Although this elevation may be relative to various datums (e.g., NGVD 29, MLLW, etc.), NAVD88 is the standard in the United States unless a local or project-specific datum is required. As discussed in further detail later, long-lasting projects should also adjust for SLR when determining the design flood. The DFE is used to obtain flooding depths and calculate certain flood loads based on local topography. Meteorological conditions during tropical (hurricane) and extratropical (nor'Easter) storms (i.e., high winds and low atmospheric pressure) result in increases in sea level, referred to as storm surge. The following definitions for the coastal flooding components making up storm surge are consistent with FEMA. The storm surge combines with the astronomical tide stage and a progressive increase in water level owing to waves breaking in shallower waters (wave setup) to comprise the SWEL. Including wave setup as additive to the SWEL provides a more conservative base and is appropriate for most flood loading calculations. In addition to SWEL, wind-driven waves that ride along the surface can contribute to higher levels of coastal flooding. Figure 5-1 illustrates these components.

The SWEL plus the greater of (1) the maximum wave crest elevation or (2) the maximum vertical extent of wave uprush on a shore or structure (wave runup) are known as the BFE. The SWEL and BFE are determined through coupled hydrodynamic-wave modeling with historical storm validation and are currently provided by the FEMA via FIRMs and associated

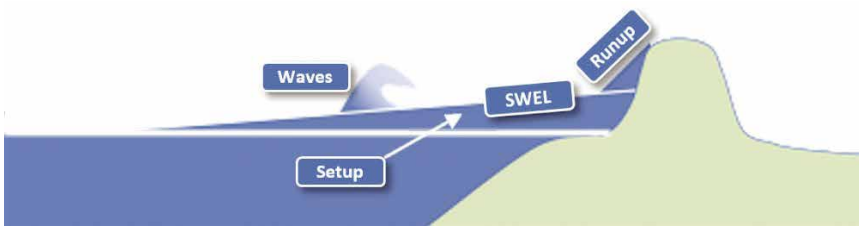

Figure 5-1. Depiction of coastal flooding components. Source: FEMA (2013).

FIS reports. FEMA FIRMs are regulatory documents specified for use in planning and engineering works by various building codes and standards, as will be discussed in later sections. Although FIRMs and FIS reports are considered to be the best available data for many projects, the robustness of the models used in their development can vary by region, and the underlying input data used for the models can be outdated. It is recommended that critical projects validate information contained within the FIRMs and FIS reports with the other sources discussed in the following sections.

FEMA FIRMs depict SFHAs, or *flood zones*, each with expected recurrence intervals (e.g., 1% chance of occurring in a given year). SFHAs subject to a 1% annual chance storm are depicted on FIRMs, with associated BFEs attributed to each zone. These zones are classified as areas subject to wave heights greater than 3 ft (V zones, also referred to as *Coastal* zones), areas subject to wave heights between 3 ft and 1.5 ft (A zones seaward of the LiMWA, also referred to as Coastal A zones), and areas subject to waves of less than 1.5 ft (A zones landward of the LiMWA, also referred to simply as A zones). The LiMWA is depicted on the FIRMs. Post-storm field visits have confirmed that wave heights as small as 1.5 ft can cause significant damage to structures when constructed without consideration of the coastal hazards (FEMA 2013). In addition, flood hazards associated with V and Coastal A waves include increased floating debris impacts, high-velocity flow, erosion, and scour. Therefore, additional design requirements are necessary based on the relative positioning of the LiMWA. An example of FEMA FIRM flood zones for a location in New York City is shown in Figure 5-2.

FIRMs also delineate areas subject to a 0.2% annual chance storm event (e.g., 500-year flood plain) based on SWELs as Zone X but usually not BFEs that incorporate wave action. The 0.2% annual chance zones are not developed using the latest modeling for inland propagation of waves (i.e., wave runup). Therefore, although the 0.2% annual chance SWEL will be higher than the 1% annual chance BFE at most locations, the 0.2% annual chance SWEL may actually be lower than the 1% annual chance BFE at locations

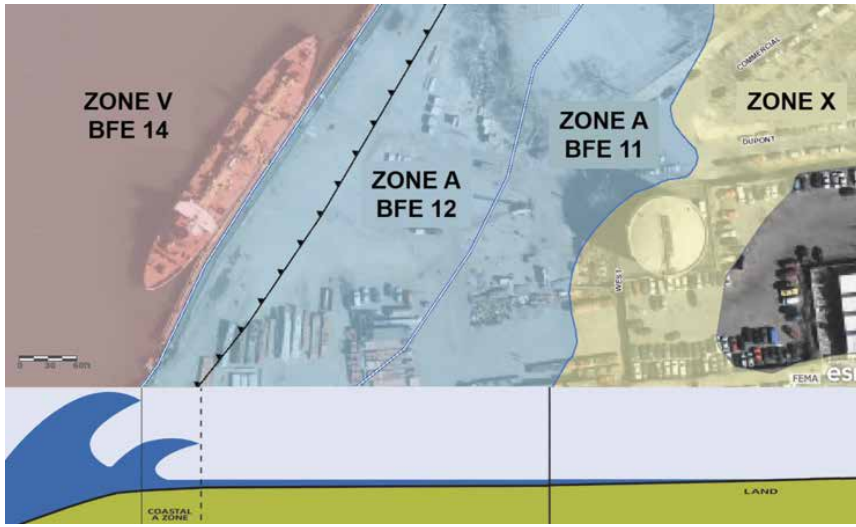

Figure 5-2. FEMA flood insurance rate map zones.
Source: FEMA (2013).

with direct wave exposure. Because the data for the 0.2% annual chance event usually does not include the full effects of wave action, it is recommended that BFEs (which provide the most realistic scenario by coupling wave action with surge) serve as the bases for project DFEs. Freeboard and an accommodation for SLR can then be added to obtain the appropriate level of protection, as discussed in more detail later. The applicable SFHA for a given location will typically fall under one of the classifications shown in Table 5-1.

The Coastal A zone poses a high risk of wave attack, although not as high of a risk as zone V. The exact definition of a Coastal A zone, as excerpted from ASCE 24 (ASCE 2014), is provided in Figure 5-3. Although the FIRM maps will specifically indicate the zone as either V or A, the determination of breaking wave potential requires an evaluation of the potential impacts of SLR (which will expand flood zone boundaries farther inland over time) and the presence of massive structures (which can influence water flows) that may not be accounted for in FEMA's modeling. In addition to the climate, urbanization will contribute to non-stationarity by continuing to change the environment surrounding the infrastructure.

In addition to waves, tides, and coastal storm surge events, other longer-term variations in sea level occur over various timescales and can have an appreciable effect on regional sea level. Such events can range from monthly to decadal and may be repeatable cycles, gradual trends, or intermittent anomalies. Seasonal weather patterns, variations in the Earth's declination,

Table 5-1. Summary of SFHAs.

	Flood zone	Description	Applicable loading categories
SFHAs	V zone (V, VE)	Coastal flood zone with velocity hazard (high-hazard zone) V zone: The coastal area subject to a velocity hazard (wave action) where BFEs are not determined on the FIRM. VE zone: The coastal area subject to a velocity hazard (wave action) where BFEs are provided on the FIRM.	• Hydrostatic • Hydrodynamic • Breaking wave action • Debris impact
	Coastal A zone (A, A1-30, AE, AO, AH, A99, AR)	Coastal flood zone inland of a V zone with possible presence of velocity hazard. The 100-year or base floodplain. There are seven types of A zones: A zone: The base floodplain mapped by approximate methods, i.e., BFEs are not determined. This is often called an unnumbered A zone or an approximate A zone. A1-30 zone: These are known as numbered A zones (e.g., A7 or A14). This is the base floodplain where the FIRM shows a BFE (old format). AE zone: The base floodplain where base flood elevations are provided. AE Zones are now used on new format FIRMs instead of A1-A30 zones. AO zone: The base floodplain with sheet flow, ponding, or shallow flooding. Base flood depths (feet above ground) are provided. AH zone: Shallow flooding base floodplain. BFEs are provided. A99 zone: Area to be protected from base flood by levees or Federal Flood Protection Systems under construction. BFEs are not determined. AR zone: The base floodplain that results from the decertification of a previously accredited flood protection system that is in the process of being restored to provide a 100-year or greater level of flood protection.	• Hydrostatic • Hydrodynamic • Breaking wave action • Debris impact
	A zone (A, A1-30, AE, AO, AH, A99, AR)	Zone with flooding potential (See Coastal A zone for descriptions of zone subcategories).	• Hydrostatic • Hydrodynamic • Debris impact

Source: FEMA (1998).

Coastal A Zone: area landward of a V Zone, or landward of an open coast without mapped V Zones. In a Coastal A Zone, the principal source of flooding will be astronomical tides, storm surges, seiches or tsunamis, not riverine flooding. During base flood conditions, the potential for breaking wave heights between 1.5 feet and 3.0 feet will exist (see Figure 6).

Coastal A Zone design and construction practices described herein are not mandated by the NFIP, but are recommended for communities that wish to adopt higher floodplain management standards. Community Rating System (CRS) credits are available for doing so. Note that some Coastal A Zone practices may be required by the International Building Code, through its reference to ASCE 24-98.

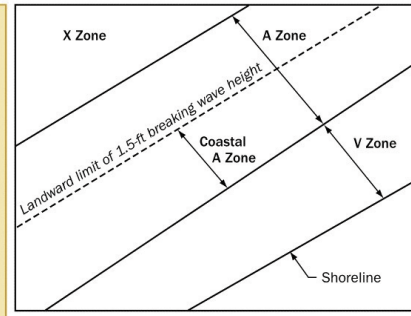

Figure 5-3. Coastal A zone defined. Source: ASCE 24-05.

changes in coastal and ocean circulation, and the ENSO are just a few of the many factors influencing changes in sea level over time. Because of these cycles, a minimum of 30 years of data should be used for estimating sea-level trends to account for longer-term sea-level variations and reduce errors in computing sea-level trends based on monthly mean sea level (NOAA 2009).

Although the exact initiating causes are not fully understood, ENSO, which results in sea surface temperature and atmospheric pressure changes, can cause some of the most significant water-level fluctuations over interannual-to-decadal timescales. Although there is difficulty in separating the observed water-level signals to create a regional model for ENSO, the clearest signals from El Niño on US coastal sea levels have been found along the West Coast, where sea-level variations owing to ENSO have been estimated at close to 8 in. (Hamlington et al. 2015). Although ENSO-related sea-level variability has been observed over the past 60 years, the magnitude of this interannual-to-decadal sea-level change may be amplified owing to climate change (Hamlington et al. 2015). Quantifying the potential increases and decreases resulting from such longer-term non-tidal variations on local sea levels is an area ripe for research, and it can be an important consideration for adaptation efforts, particularly on the US West Coast.

5.2 DESIGN FLOOD ELEVATION STANDARDS

5.2.1 ASCE 24

ASCE 24 is the industry standard for flood-resistant design and construction, and it is adopted by many building codes. Some building codes adopt the IBC, which in turn adopts ASCE 24. The latest version of the

standard is ASCE 24-14 (ASCE 2014). However, depending on the applicable building code refresh period, an earlier publication (e.g., ASCE 24-05) may still be in effect (ASCE 2005). The ASCE standard classifies infrastructure by importance, or an *occupancy/risk category*. The more important the asset, as indicated by the assigned category, the higher the level of protection. ASCE 24-14 will specify the required freeboard (additional depth to account for uncertainties added as a factor of safety) based on the classification of the structure. ASCE 24 DFEs are not explicit in intent to include or not include the effects of SLR.

5.2.2 Federal Executive Order 13690

On January 30, 2015, the US president signed EO 13690, establishing a federal flood risk management standard (FFRMS) (FEMA 2015). Although this EO has since been revoked, EO 13690 was the result of collaboration among various federal agencies and the president's Hurricane Sandy Rebuilding Task Force. The EO set minimum flood protection requirements for federally funded buildings and infrastructure to levels that are similar to the standards specified in ASCE 24. EO 13690 gave flexibility to select one of three approaches for establishing a DFE and, following issuance of EO 13690, the federal Water Resources Council approved revised guidance on implementing the FFRMS. As described in the guidance document, the approaches are as follows:

1. Climate-informed Science Approach (CISA)—use best available, actionable hydrologic and hydraulic data and methods that integrate current and future changes in flooding based on climate science and other factors or changes affecting flood risk to determine the vertical flood elevation and corresponding horizontal floodplain in a manner appropriate to policies, practices, criticality, and consequences.

2. Freeboard Value Approach (FVA)—use the BFE (or 1-percent-annual-chance flood determined using best available data) and an additional height to calculate the freeboard value. The additional height will depend on whether or not the action is a critical action.

3. The 0.2-percent-annual-chance Flood Approach (0.2PFA)—use the 0.2-percent-annual-chance flood elevation (also known as the 500-year flood elevation).

This term *critical action* is defined in the EO as ". . . any activity for which even a slight chance of flooding would be too great . . ." The FFRMS guidance states that the CISA, which provides agency to the designer for DFE criteria development, is preferred:

> The CISA is preferred. Agencies should use this approach when data to support such an analysis are available. . . . [T]he CISA uses existing, sound science and engineering methods (e.g., hydrologic and hydraulic analysis and methods used to establish current flood elevations and floodplain maps), supplemented with best available and actionable climate science and consideration of impacts from projected land cover/land use changes, long-term erosion, and other processes that may alter flood hazards over the lifecycle of the Federal investment. In cases where relevant data are not available, the other two approaches (Freeboard and 0.2-percent-annual-chance) are acceptable methods to determine the FFRMS floodplain, because each of these approaches can improve resilience to current and future flood risk.

Federal EO 13690 was revoked by the president in August 2017.

5.2.3 National Environmental Policy Act

The federal CEQ has released guidance requiring direct coordination between environmental planners and designers with respect to the effects of climate change for new proposed actions (CEQ 2016). The guidance states that agencies should "use the information developed during the National Environmental Policy Act (NEPA) review to consider alternatives that are more resilient to the effects of a changing climate" and that the analysis should also "consider an action in the context of the future state of the environment." Following this guidance, the NEPA analysis should review the build alternative(s) in the context of the impact of climate change and the implications of future climate conditions.

5.3 CLIMATE CHANGE–INFORMED DESIGN FLOOD ELEVATION

DFE criteria are often developed during conceptual or pre-design phases for a project and are subject to cost-benefit and sensitivity testing. The DFE should, at a minimum, conform to stakeholder requirements, industry standards (e.g., ASCE), model codes, and other regulatory requirements. The DFE criteria should be based on the estimated useful life and criticality of the project.

For projects that are anticipated to have a long useful life, it is not always feasible or cost effective to fully account for projected climate risks. As discussed in Chapter 3, adaptable design techniques (e.g., the OM) may be appropriate given the spreads between low- and high-end SLR projections, which increase exponentially over time. In addition, it is customary on many civil works projects to assume an initial economic service life that allows for extension of the service through major rehabilitation. Therefore, an interval

that is less than the asset's anticipated useful life, between substantial completion and a planned intervention point, may be warranted to re-evaluate a project DFE based on the latest CISA at that time.

There are varying definitions of criticality, and methods for determining importance based on the consequence of an undesirable event. Chapter 7 provides several methods for quantifying uncertainty and risk. For the methods described in this chapter, Table 1.5-1 in *Minimum Design Loads for Buildings and Other Structures* (ASCE 2010), titled "Risk Category of Buildings and Other Structures for Flood, Wind, Snow, Earthquake, and Ice Loads" is one tool that can be used to determine criticality (i.e., risk category III and IV buildings and structures can be considered *critical* for the purposes of developing a DFE). Designers should also differentiate between noncritical and critical components within a larger facility or campus (e.g., an airport or maintenance yard). These components include but are not limited to electrical distribution and switch gear areas, motor-control centers, chemical feed equipment, boilers, communications systems, monitoring and safety equipment, HVAC units, fire alarms and suppression systems, furnaces, emergency fuel supplies, emergency generators, and hazardous material storage.

The following sections provide a DFE criteria model that can be used for a wide range of coastal projects. The model consists of a design flood event based on a given AEP, the addition of freeboard as a factor of safety, and an SLR adjustment to obtain the future equivalent flood level. Under all circumstances, designers must meet the minimum of all code- or regulation-mandated requirements.

In addition to flooding that occurs overland, it is important to consider what is happening underground as well. Many structures that are susceptible to storm surge flooding are in close proximity to the waterfront where the soil can be very permeable or consist of heterogeneous fill material with preferential pathways for water. In such cases, it is important to account for a rising groundwater table caused by seepage flows from a rising sea level and/or rainwater infiltration that can result in flood loads extending underground, ponding, and/or uplift on slabs.

5.3.1 1-percent Annual Chance BFE

Designers should evaluate a flood-level condition (e.g., permanent inundation, tidal flooding, or coastal storm surge) most appropriate for the facility in question. The design event specified by policy and engineering judgment (when policy allows design criteria to range over an interval) should be considered as a target point for specific performance parameters (Kilgore et al. 2016). A level of risk tolerance (e.g., 10%, 2%, 1%, 0.2% AEPs) can be obtained from tidal gauge data over the National Tidal Datum Epoch (or modified thereof) and/or analytical flood event data. In addition, the AEP of a known coastal flood elevation can be calculated directly using

historical flood elevation data (e.g., records and reports, high water marks, debris lines, photographs, tidal gauge data, etc.) or indirectly based on modeling output. Engineering judgment should be used for indirect calculations and transformations to evaluate the applicability and statistical significance of the input data to the location of interest.

FEMA publishes flood event data via FIRMs and FISs for most locations. In some cases, designers will be required to perform site-specific hydrologic and hydraulic modeling to simulate design flood events. This may be to assess multiple flood event conditions (e.g., flood return intervals or SLR assumptions) and/or to evaluate proposed conditions (e.g., flooding with and without a new seawall or levee). This is particularly important for locations that may be subject to breaking waves under present or future conditions. Breaking wave heights may increase, and areas subjected to breaking wave forces will likely move farther inland than the areas presently depicted on FIRMs (see Chapter 6 for discussion of breaking wave loads). Site-specific modeling may also be required to evaluate potential *backdoor flooding* under varying design conditions, future conditions, or flooding resulting from combined precipitation and coastal storm events. For example, FEMA NFIP-compliant modeling (e.g., ADCIRC and MIKE 21) is required to meet FEMA's levee certification standards for modification to an effective FIRM or SFHA boundary (via a Letter of Map Revision).

Many FIS reports and FIRMs published in coastal regions are developed using ADCIRC coupled with the SWAN model. ADCIRC is a two-dimensional (2D) coastal circulation and storm surge model developed by a consortium of academia, the USACE, and private companies. SWAN is a spectral model that computes wind-generated waves for the coastal zone that was developed at the Delft University of Technology. The NFIP-compliant ADCIRC+SWAN package can be obtained for free online or for a fee on several graphical platforms. The modeling can be validated by tidal/non-tidal sea-level calibration and by using historical extra-tropical and/or tropical storms to determine SWEL AEPs. FEMA's WHAFIS can be used to simulate inland wave propagation using the calculated SWELs applied to each cross-shore transect in the study area and interpolated using topographic maps, land-use data, and land-cover data (as well as engineering judgment) to determine the extent of coastal flood zones. MIKE 21 is another widely used NFIP-compliant 2D coastal modeling platform developed by DHI. The MIKE 21 platform is broken up into in separate modules for a variety of engineering applications. In addition to storm surge modeling, MIKE 21 modules relevant to climate change impacts include numerical simulation tools respective to coastal erosion, dike/dune breaching, and water quality/ecology.

The SLOSH model, developed by NOAA, is primarily used to establish coastal evacuation zones and for storm surge forecasting. The SLOSH model estimates storm surge heights resulting from historical, hypothetical, or

predicted hurricanes by taking into account the atmospheric pressure, size, forward speed, and track data. The SLOSH model produces a lower-resolution output as compared to the models noted above. SLOSH simulations create two composite products: MEOWs and MOMs. Because the output produced by SLOSH modeling is not representative of a single storm but rather of *worst cases* for all locations within a region from a composite of storms, the storm surge water surface elevations produced by SLOSH are very likely to exceed the actual flooding for a given storm event (Glahn et al. 2009). Because SLOSH projections are not referenced to a specific AEP and do not include wave heights, the model is not recommended for engineering use or as input for load factor calculations. Refer to Figure 5-4 for a comparison of SLOSH output for a Category 2 hurricane at varying forward speeds and FEMA BFEs that are calculated by coupled ADCIRC/SWAN modeling.

Site-specific modeling is not warranted for most noncritical projects because such studies have usually already been performed by FEMA's mapping partners and published in FIS reports and FIRMs for many locations. Published BFEs are required to be used, as a minimum, by most codes, and they are considered to be the best available flood hazard data by FEMA. Therefore, in the absence of more refined site-specific hydrologic and hydraulic modeling, the FEMA BFEs should be utilized as the basis for noncritical project DFEs.

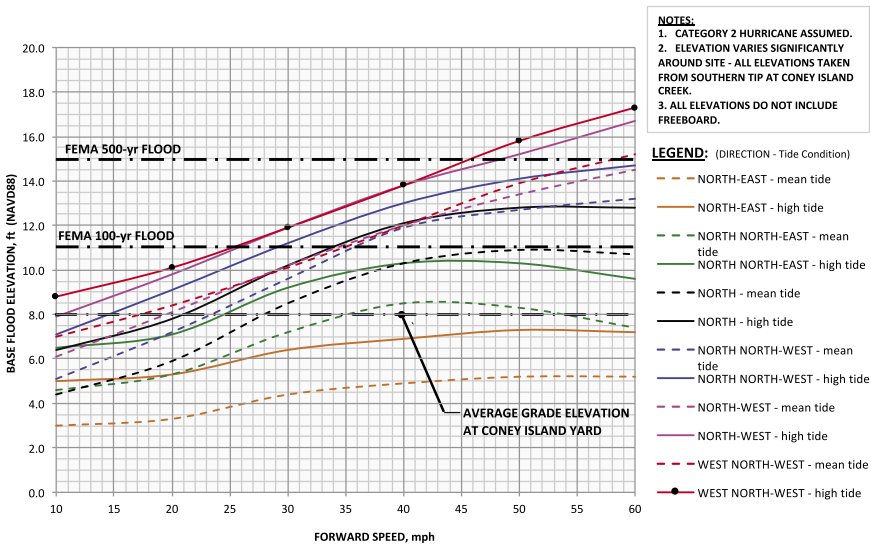

Figure 5-4. SLOSH Category 2 flood elevation versus forward speed with comparison to FEMA BFEs for a location near Coney Island, Brooklyn, NY.

For many locations, the 1% annual chance BFE and the 0.2% annual chance SWEL are provided by FEMA. For coastal locations, the SWEL should not be used as the basis for a project DFE because the full effects of wave action are not included. If the 500-year RP is desired for a project in such a case, a provision for wave action should be added to the SWEL using analytical methods (e.g., USACE's *Coastal Engineering Manual* or FEMA's WHAFIS model) and the data from the applicable FIS transect.

5.3.2 Freeboard as a Factor of Safety

The DFEs are determined by applying freeboard to the BFE. Per FEMA and ASCE, freeboard is a factor of safety, expressed in feet above a flood level. This component is not intended as an estimate for future SLR. Freeboard compensates for potential model and mapping inaccuracies or granularity and the many uncertainties that could contribute to flood heights, such as wave action, constricting or *funneling* obstructions, and other hydrological effects. These uncertainties are likely to be greater in magnitude for urbanized watersheds. In addition, locations in close proximity to the waterfront have additional flood height uncertainty owing to unknowns relating to the generation, propagation, and transformation of incoming waves. Most states and communities have adopted freeboard requirements. The NFIP requires the lowest floor of structures built in flood zones to be at or above the BFE plus 1 ft of freeboard, which should be considered the minimum for all projects within an SFHA. Although 1 to 3 ft of freeboard above a flood level is commonly used for engineering works, Table 5-2 provides proposed recommendations to selecting a freeboard value for projects in coastal floodplains.

5.3.3 SLR Adjustment

Flood elevations published by FEMA do not presently include the effects of SLR. The freeboard specified by ASCE 24 (ASCE 2014) is not explicit about whether it is intended to account for SLR. The EO 13690 criteria is intended to account for uncertainties in future conditions, including "anticipated

Table 5-2. Freeboard as a Factor of Safety Based on Project Type and Location.

	Non-coastal A or V zone	Coastal A or V zone
Noncritical project	1 ft	1–2 ft
Critical project	1–2 ft	2–3 ft

impacts of climate change," but it does not indicate the relative magnitude of SLR versus a safety factor accommodated for in the freeboard. The observed historical SLR at the tidal gauge located in Battery, New York, has been relatively constant at about 1.2 ft per 100 years (NOAA 2017a). As discussed in Chapter 2, observational data and global climate models suggest that, although the upward trend is continuing, more rapid or accelerating future rates of SLR are predicted. These predictions range from approximately 1 ft to over 8 ft by the year 2100, depending primarily upon assumptions made with regard to emissions scenarios, thermal expansion, and rate of ice melting. SLR will also vary locally owing to geologic changes, causing land to subside at varying rates along the seaboard owing to glacial isostatic adjustment, sediment compaction, groundwater and fossil fuel withdrawals, and other nonclimatic factors, oceanographic factors such as circulation patterns, changes in the Earth's gravitational field and rotation, and flexure of the crust and upper mantle owing to melting of land-based ice (NOAA 2017b).

The IPCC has developed five assessment reports since it formed in 1988. It released its fifth assessment report, AR5, between September 2013 and November 2014 (IPCC 2014). Kopp et al. (2016) recommends that practitioners, in conjunction with a similarly constituted set of scientific advisors, review relevant SLR and coastal storm data and projections shortly after future IPCC assessment reports, or every five years at a maximum. Similarly, practitioners and a set of scientific advisors should monitor the publication of federal climate projections and research, such as the projections set forth in the *National Climate Assessment*, for any major changes in assumptions or projections related to SLR and coastal storms. Such reassessment of data can assist engineers in their efforts to apply advances in scientific information into practice.

Climate models producing output on a global scale do not generally provide sufficient detail to be appropriate for the design of engineering works. However, downscaling approaches have been developed to provide regional projections that are sufficiently granular to be relevant for engineering and planning use. In January 2017, NOAA released a transparent and peer-reviewed assessment, titled *Global and Regional Sea Level Rise Scenarios for the United States*. The report was developed using CMIP5 projections, along with additional recent scientific literature, and it provides local SLR projections on 1° grid covering the US mainland coastline, Alaska, Hawaii, the Caribbean, and the Pacific Island territories for six representative scenarios: low, intermediate-low, intermediate, intermediate-high, high, and extreme. At this time, this set of projections are recommended for use for engineering works owing to the credibility of the peer review process afforded in the report, the transparency of the framework used assessing the scientific literature, the granularity of the local projections, and the breadth of coverage.

The New York City Panel on Climate Change report (NPCC 2015) is another example of a transparent and peer-reviewed assessment publication. The assessment utilized observed data, CMIP5 projections, and IPCC AR5 methodologies. The report included local estimates of the effects of climate change that were generally applicable to a 100-mile radius around the New York City metropolitan region, accounting for subsidence, changes in glacial and ice sheet *fingerprinting*, local water mass density, oceanographic processes, and land water storage. The NPCC has estimated the probabilistic rise at the 10th, 25th, 75th, and 90th percentile confidence levels. These projections are provided for the 2020s, 2050s, and 2080s time periods and for 2100. The range of differences in projected SLR between the different models increases as the century progresses. Table 5-3 depicts the latest SLR projections from NPCC, as well as additional *projections* derived by interpolating between the 2050 and 2080 estimates for the year 2070.

As an example, a critical project located in New York City with a useful life of 50 years and an anticipated substantial completion date of construction in the year 2020 should consider including an SLR adjustment up to 43 inches to obtain a future BFE (FBFE). The FBFE would be used for calculating flood loads (i.e., hydrostatic pressure, hydrodynamic pressure, and, depending upon the location of the structure in question, debris impact and/or breaking wave forces). The addition of freeboard as a factor of safety should be added on top of the FBFE to obtain the project DFE.

In addition to increasing the elevation of a flood event, SLR will also widen the boundaries of flood zones. Therefore, consideration of how an anticipated SLR relates to local topography must be given to structures outside of but in the vicinity of higher-level flood zones. For example, if the structure of interest is close to the LiMWA under present conditions, a wave height analysis that simulates inland wave transformation may be warranted to determine whether breaking wave loads should be addressed owing to the projected effects of SLR (refer to Chapter 6 for discussion).

Table 5-3. SLR Projections for New York City.

SLR baseline (2000–2004)	Low estimate (10^{th} percentile)	Middle range (25^{th} to 75^{th} percentile)	High estimate (90^{th} percentile)
2020's	+ 2 in	+ 4 to 8 in	+ 10 in
2050's	+ 8 in	+ 11 to 21 in	+ 30 in
2070	+ 11 in	+ 14 to 29 in	+ 43 in
2080's	+ 13 in	+ 18 to 39 in	+ 58 in
2100	+ 15 in	+ 22 to 50 in	+ 75 in

Source: NPCC (2015).

Engineering designs should consider alternatives that are developed and assessed for the entire range of possible future rates of sea-level change. The alternatives should be evaluated using varying estimates (low, middle, and high, at a minimum) of future SLR for both with and without project conditions (USACE 2013). It is recommended that long-term structures include an accommodation for SLR based on a benefit-cost and/or feasibility assessment considering the sensitivity of project financial costs and externalities (e.g., asset functionality, environmental, community impacts, etc.) to varying SLR projections (e.g., low, middle, and high). Based on these factors, it may be appropriate for critical or noncritical projects to include a middle-range SLR estimate. When project elements can be designed without substantial implications to a higher level (up to a scientifically plausible upper-bound SLR projection), they should be; otherwise, they should be designed so that additional protection can be included at a later date if SLR and storm levels in the future make that appropriate (e.g., designing foundations to support higher flood barriers in the future).

According to the confidence levels prescribed for climate model projections (e.g., CMIP5), there is much greater certainty associated with the near-term (mid-century) scenarios, after which uncertainties associated with the melting of ice sheets and land-based ice caps increasingly dominate. Design criteria should explicitly provide methods to address uncertainty, including future decision milestones for adaptation based on new information as scientific advances unfold. Because engineering works typically have a useful life far beyond the initial period of economic analysis, consideration of project adaptability is an important consideration in project development. These upfront analyses should determine how the SLR scenarios affect risk levels and plan performance and identify the design or operations and maintenance measures that could be implemented to minimize adverse consequences while maximizing beneficial effects (USACE 2013).

For these reasons, a mid-term outlook (e.g., less than the projected useful life of a project) may be appropriate. The project DFE can then be reevaluated following a planned interval based on the latest CISA at that time. Because the degree of uncertainty with regards to SLR increases exponentially with time, designing for, as an example, 100 years of SLR now may prove overly conservative or insufficient, whereas designing to mid-century (e.g., 50 years of SLR now) with the option of providing capital improvements later to adjust the DFE if necessary will provide more flexibility for climate adaptation.

5.4 REFERENCES

ASCE. 2005. *Flood resistant design and construction*. ASCE/SEI 24. Reston, VA: ASCE.

ASCE. 2010. *Minimum design loads for buildings and other structures*. ASCE/SEI 7-10. Reston, VA: ASCE.

ASCE. 2014. *Flood resistant design and construction*. ASCE/SEI 24-14. Reston, VA: ASCE. Accessed February 13, 2016. http://ascelibrary.org/doi/book/10.1061/9780784413791.

ASCE. 2015. *Adapting infrastructure and civil engineering practice to a changing climate*. Accessed February 13, 2016. http://ascelibrary.org/doi/book/10.1061/9780784479193. Reston, VA: ASCE.

CEQ (Council for Environmental Quality). 2016. *Final guidance for federal departments and agencies on consideration of greenhouse gas emissions and the effects of climate change in NEPA reviews*. Washington, DC: CEQ.

FEMA (Federal Emergency Management Agency). 2013. *Flood Insurance Study Number 360497V000B*. Volume 1 of 1 (Preliminary: December 5, 2013). Washington, DC: FEMA.

FEMA. 2015. "Revised guidelines for implementing Executive Order 11988, Floodplain Management, and Executive Order 13690, Establishing a Federal Flood Risk Management Standard, and a process for further soliciting and considering stakeholder input." Washington, DC: FEMA.

Glahn, B., A. Taylor, N. Kurkowski, and W. A. Shaffer. 2009. "The role of the SLOSH model in National Weather Service storm surge forecasting." *Nat. Weather Dig*. 33(1), 3–14.

Hamlington, B. D., R. R. Leben, K.-Y. Kim, R. S. Nerem, L. P. Atkinson, and P. R. Thompson. 2015. "The effect of the El Niño-Southern Oscillation on U.S. regional and coastal sea level." *J. Geophys. Res. Oceans* 120(6), 3970–3986. DOI:10.1002/2014JC010602.

IPCC (Intergovernmental Panel on Climate Change). 2013. "Summary for policymakers." In *Climate change 2013: The physical science basis*, T. F. Stocker et al. (eds.). Cambridge, UK: Cambridge Univ. Press.

IPCC. 2014. *Climate Change 2014: Synthesis report*. Geneva, Switzerland: IPCC.

Kilgore, R. T., G. Herrmann, W. O. Thomas, and D. B. Thompson. 2016. "Highways in the river environment—Floodplains, extreme events, risk, and resilience." *No. FHWA-HIF-16-018*. Washington, DC: Federal Highway Administration.

Kopp, R. E., A. Broccoli, B. Horton, D. Kreeger, R. Leichenko, J. A. Miller, et al. 2016. "Assessing New Jersey's exposure to sea-level rise and coastal storms: Report of the New Jersey Climate Adaptation Alliance Science and Technical Advisory Panel." Prepared for the New Jersey Climate Adaptation Alliance, New Brunswick, NJ.

NPCC (New York City Panel on Climate Change). 2015. "Building the knowledge base for climate resiliency." *Ann. N.Y. Acad. Sci*. 1336(1). ISSN 0077-8923.

NOAA (National Oceanic and Atmospheric Administration). 2009. "Sea level variations of the United States." *NOAA Tech. Rep. NOS CO-OPS 053*. Silver Spring, MD: NOAA.

NOAA. 2017a. *Tides and currents*. The Battery, NY. Station Id: 8518750 (water-level data accessed Mar. 22, 2017).

NOAA. 2017b. "Global and regional sea level rise scenarios for the United States." W. V. Sveet et al. (eds.). *NOAA Tech. Rep. NOS CO-OPS 083*. Silver Spring, MD: NOAA.

USACE (US Army Corps of Engineers). 2013. "Incorporating sea level change in civil works programs." *ER 1100-2-8162*. Washington, DC: USACE.

CHAPTER 6
FLOOD LOADS

6.1 INTRODUCTION

Relative to loads from other extreme events, flood loads have a limited amount of historical data. The current body of research focuses primarily on coastal and riverine areas, and consideration of the effects within developed urban environments is further limited. As such, it is difficult to establish a clear probability-based design approach, which results in inconsistencies in procedures among the various reference standards. This document provides a general overview of flood-resistant design criteria and the differences between the primary standards, as well as a recommended approach to reach a conservative yet reasonable design.

Flood loading is composed of a hydrostatic pressure, a hydrodynamic pressure, and, depending upon the location of the structure in question, a debris impact and/or breaking wave force. The applicability of each load type depends upon the geographic location relative to a coastal area, development of the area, the Design Flood Elevation (DFE), and the type of structure. Primary documents governing flood-resistant design include

- ASCE/SEI 7 (2010) and ASCE 24 (2014);
- *Federal Executive Order 13690* (2015) (noting cancellation of the Executive Order);
- FEMA *Technical Bulletin* 3-93 (1993);
- NYCBC *Appendix G* (2014);
- NYCTA *Design Guide 312* (2014); and
- USACE *Coastal Engineering Manual* (2002).

6.2 DESIGN FLOOD LOADS

It is critical that engineers working in urban regions develop rational approaches for determining flood load forces to augment the guidance currently provided by ASCE/SEI 7 (see Figure 6-1 as an example). In addition, the manner in which SLR is incorporated into the flood depth can have significant effects on the resulting hydrodynamic, debris impact, and breaking wave loads because many of the contributing factors are based on the BFE rather than DFE. For assets that have a remaining design life of 50 years or more, we recommend that the SLR be incorporated into the BFE rather than DFE to adequately approximate the potential dynamic loads.

6.2.1 Hydrostatic Loads

Hydrostatic loads are the most predictable and easily calculated of the flood load categories. The maximum resulting pressure is determined simply by multiplying the DFE at the location of the element to be analyzed by the unit weight of water (62.4 pcf (1000 kg/m^3) for fresh water; 64 pcf (1025 kg/ m^3) for salt water). The calculation of these loads is uniform among the various reference standards.

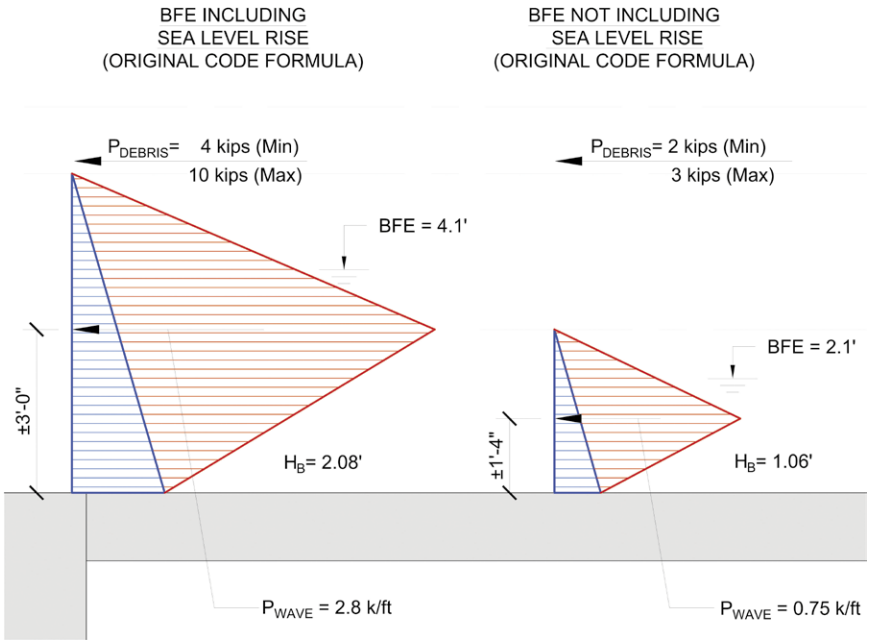

Figure 6-1. Loading with and without SLR.

The hydrostatic loads will be present both above and below grade for exterior walls and first-floor slabs. Although a conservative value of the below-grade pressures can be calculated, assuming the water has fully permeated the soil, the actual pressure will be highly dependent on the hydraulic conductivity of the soil and the associated seepage rate. In many urban areas, the surfaces immediately adjacent to buildings are covered with highly impermeable concrete or asphalt pavement, which will further inhibit the seepage flow. Consideration regarding future improvements to increase permeability on surrounding properties may be appropriate. The assumed rate of water infiltration should be discussed on a project-specific basis to achieve a conservative yet realistic below-grade design pressure. At a minimum, slab uplift pressures should be based on a DFE value that removes any components of freeboard that account for transient *wave action*, which contributes minimally to hydrostatic loading.

6.2.2 Hydrodynamic Loads

Hydrodynamic loads are those pressures associated with moving floodwaters, including the frontal pressure and the drag effect along the sides of a structure. These are essentially nonbreaking wave loads, and they are significantly smaller in magnitude than the breaking wave loads discussed in the next section. Calculation of hydrodynamic pressure is based upon fluid mechanics, utilizing the average flood velocity (V) and drag coefficient (C_D) associated with the structural element in question. Calculation procedures for this type of load are uniform among the noted reference standards.

Topographical features, such land depressions behind bulkheads, levees, or berms that could induce higher velocity sheet flow should be accounted for. For projects that include the design of interior flood-resisting elements, such as dike walls for compartmentalization, hydrodynamic loads are generally neglected; however, this should be clarified on a project-specific basis.

The guidance provided by the commentary to ASCE/SEI 7 (2010) states that "accurate estimates of flow velocities during flood conditions are very difficult to make, both in riverine and coastal flood events." FEMA provides the following two equations in the commentary to ASCE/SEI 7 that offer a range of flood velocities for coastal areas, with the lower limit given in Equation 6-1 and the upper limit in Equation 6-2:

$$V = \frac{d_s}{1\ sec} \tag{6-1}$$

$$V = (g d_s)^{0.5} \tag{6-2}$$

where V = average velocity of water in ft/s, d_s = local stillwater depth in ft, and g = acceleration owing to gravity, 32.2 ft/s^2.

Some public agencies provide prescriptive guidance for design velocity during a design flood event. For example, New York City Transit's *Design Guideline 312* (NYCTA 2014) sets a universal design velocity standard of 5 ft/s. Per the ASCE/FEMA guidelines and using a design stillwater depth of 5 ft, the calculated velocity range would be 5–12.7 ft/s.

Floodwater velocities are highly variable, and there is typically little information available regarding the flow of floodwater within an urban environment. The FEMA *Coastal Construction Manual* states that within the same flood event, velocities can vary from almost zero to very high velocities because the water will be affected by surrounding objects and structures and can flow from different directions during the same event. This behavior makes coastal floodwater particularly difficult to study and quantify. If floodwater behaves like wind in an urban environment, the resulting flow will be highly turbulent, with areas of high-velocity flow near corners of buildings and through streets, whereas other areas will have little or no flow.

6.2.3 Breaking Wave Loads

Breaking wave loads are those that result from water waves propagating over the water surface and striking a building or other structural component. These high-intensity loads are generally applicable in V zones and Coastal A zones, where the proximity to the ocean yields a high probability of breaking wave action. These loads may also be applicable outside of V or Coastal A zones if SLR is considered. The two primary reference standards for calculation of breaking wave forces are ASCE/SEI 7 (Section 5.4) and the US Army Corps of Engineer's *Coastal Engineering Manual* (CEM) (Part 6).

Both the ASCE/SEI 7 and CEM methods for calculating breaking wave height are empirically derived. When waves come into shallower waters, they are transformed by the bathymetric geometry leading into the surf zone, causing refraction and/or diffraction, steepening, and ultimately breaking. Studies show there is a ratio between wave height and wave depth at wave breaking, and waves usually break at the location where their heights equal 0.78h, where h is the water depth. Shoreward of this wave breaking location (the surf zone), wave height is assumed to be governed by water depth and is taken to be 0.78h, where h is the local water depth (McCowan 1894). Although this widely used classic criterion is a useful estimate for obtaining the depth-limited wave, it does not include important shoaling parameters. In addition, if the surf zone is wide, the wave height within the surf zone diverges from the upper limit of 0.78h as waves approach the coast because surf zone turbulence and bottom influence rob the waves of energy. ASCE/SEI 7 uses this depth-limited wave esti-

mation at the structure of interest to define a conservative breaking wave height.

More detailed procedures for site-specific calculations for estimating breaking wave heights can be found in the CEM, which includes using the relative depth as a function wave period and the nearshore slope of the wave approach. This is the slope of approach at the point at which the orbital motion of the wave begins to interact with the bottom surface. The breaking wave height calculation using the breaker depth index (CEM Part 2, Chapter 4) considers slope-induced transformation of the wave, which is conservative in most urban scenarios owing to the presence of piers/bulkheads that abruptly intercept and "cut the bottom" out of the wave, allowing a portion of the "top" to be transmitted with lower energy. Other factors, such as massive shorefront obstructions and inland topography, must also be considered as they may not be accounted for in the underlying wave climate model being used (e.g., FEMA FIS reports) owing to granularity limitations. These factors may warrant special consideration because they can act to decrease or increase the applicable wave impacts based on dominant wave direction and orientation of structures by blocking, funneling, and/or reflecting incoming waves.

Location-specific wave climates are computed by FEMA through a coupled hydrodynamic and wave numerical modeling (via transects presented in the FIS reports). In addition to surge, FIS reports provide significant wave height (H_s) and peak wave period (T_p) parameters for each transect, which are utilized by CEM calculations. Commercial software is also available for simulating wind-generated waves and swells (e.g., the MIKE 21 spectral wave model developed by the Danish Hydraulic Institute). The type of breaking wave anticipated (e.g., spilling, plunging, surging, or collapsing) can be calculated using the surf similarity or Iribarren number as a function of H_s, T_p, and the surf zone bathymetry. Figure 6-2 depicts the types of breaking waves on impermeable slopes related to the Iribarren number. Although ASCE/SEI 7 does not currently provide loading formulas to account for different types of breaking waves, this variable will have a substantial impact on the realistic loading to be anticipated. ASCE/SEI 7 breaking wave force calculations [particularly with higher-order dynamic pressure coefficients (C_p)] may be overly conservative unless plunging waves are present (plunging breaking waves are responsible for the greatest loads and most explosive forces). Therefore, breaker type is an important factor to consider when high-amplitude waves are calculated because the range of slopes conducive to plunging breakers, although characteristic of many beach surf zones, are less common in urbanized areas.

Future SLR will have a significant effect on wave heights resulting from higher extreme water elevations during storms. Table 6-1 depicts breaking wave heights and pressures calculated based on SLR estimates ranging from 0 to 3 ft in 0.5-ft increments under the ASCE guidelines for a risk category IV

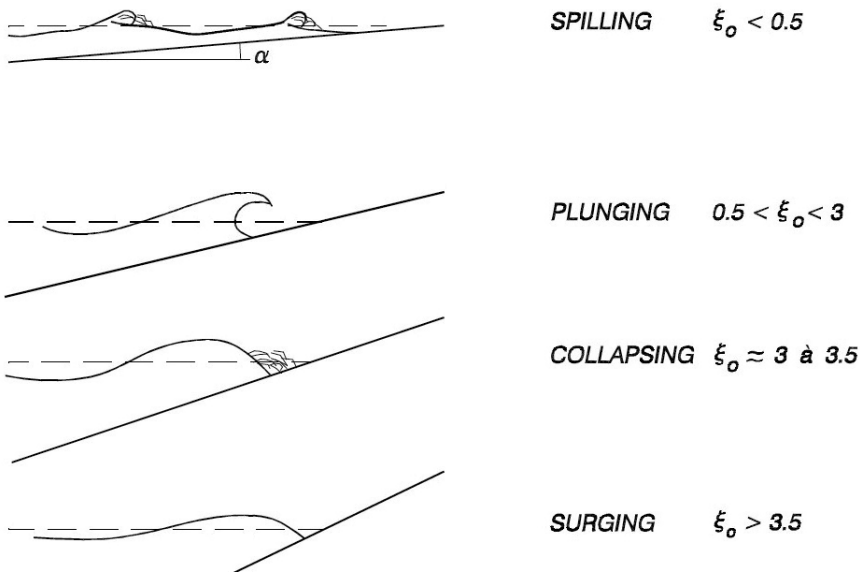

Figure 6-2. Types of wave breaking on impermeable slopes and related Iribarren number values.
Source: USACE (2002), Table VI-5-1.

structure. The resulting breaking wave service pressures (approx. 600 to 2,000 psf) far exceed all other design flood loads (e.g., hydrodynamic, impact, etc.). More refined formulas for the calculation of breaking load forces on different types of structures (e.g., vertical walls, horizontal and inclined surfaces) can be found in CEM Part 6, Chapter 5. When using FEMA FIRMs for guidance on the location of *breaking waves*, it is important to remember that these locations are based on the 1% annual exceedance storm and must be correlated to the project's design return interval. In addition, if future SLR is considered, the breaking wave line depicted on FIRMs will likely move farther inland, depending on obstructions and topography, thus affecting more structures. Because of the highly stochastic nature of wave impacts, there are no reliable formulas for the prediction of impulsive forces caused by breaking waves. For this reason, physical models, which can be used to more realistically analyze breaking waves across surf zones with irregular or otherwise complex bathymetry, should be used as part of the final design for critical structures subject to significant waves. This type of testing can be performed within a wave flume or wave basin with a constructed scale model of the site. Generating design waves in a model minimizes uncertainties with regards to formation and loading; however, it can be quite costly. Without the physical modeling, added conservatism is

Table 6-1. Breaking Wave Magnitude vs. Sea Level Rise Adjustment.

SLR[a]	SLR-adjusted SWEL[b]	SLR-adjusted SWD[c]	Resulting breaking wave height[d]	Top of crest elevation	Maximum pressure[e]	Total wave force[f]	Service level pressure[g]	Equivalent hydrostatic depth[h]
0	11.1	1.3	1.0	2.0	391	0.68	587	9
0.5	11.6	1.8	1.4	2.8	541	1.30	812	13
1	12.1	2.3	1.8	3.6	692	2.12	1,038	16
1.5	12.6	2.8	2.2	4.3	842	3.14	1,263	20
2	13.1	3.3	2.6	5.1	993	4.36	1,489	23
2.5	13.6	3.8	3.0	5.9	1,143	5.78	1,715	27
3	14.1	4.3	3.4	6.7	1,293	7.40	1,940	30

[a]Feet above 1% annual chance still water elevation (SWEL). 1% SWEL not including SLR is equal to 11.1 ft NAVD88 in this example.
[b]1% annual chance SWEL including SLR adjustment relative to NAVD88 (ft).
[c]1% annual chance stillwater depth (SWD) above pier (ft).
[d]Calculated as depth-limited wave pier per *ASCE 7*: 5.4-2 (ft).
[e]Per *ASCE 7*: 5.4-5 (psf).
[f]Per *ASCE 7*: 5.4-6 (kips/ft).
[g]Load factor of 1.5 for Coastal A zone per *ASCE 7*: 2.4 (psf).
[h]$P_{service}$/64 psf (ft).

warranted because many of the inputs relevant to breaking wave forces are neglected in the empirical methods.

6.2.4 Impact Loading

The impact loading to be used in the design of flood barriers varies greatly among the FEMA *Technical Bulletin 3-93*, the *ASCE/SEI 7-05/10 Commentaries*, and the NYCT *Design Guide 312.*

The FEMA 3-93 document utilizes a simplified formula (Equation 6-3) based on the velocity of the impacting object and an assumed duration of impact equal to 1.0 s. For the recommended debris weight of 1,000 lb and a flood velocity of 5.0 ft/s, the resulting impact load is approximately 155 lb.

$$F_i = \frac{WV}{gt} \tag{6-3}$$

where: F_i is the impact force (lb)
W is the weight of the object (lb)
V is the velocity of the object (ft/s)
g is the acceleration owing to gravity (32.2 ft/s^2)
t is the duration of impact (s)

Relative to the procedures presented in NYCT *Design Guide 312* and ASCE/SEI 7, the above calculation may not be representative of the impact forces likely to strike a structure in an urban environment.

The ASCE/SEI 7 commentary utilizes a similar impulse-momentum calculation procedure (Equation 6-4) for design impact loads, but it yields far different results. Although this approach has many variable factors related to building use, flood depth, and local flow interferences, the primary conceptual difference lies in the assumed 0.03-s duration of impact. For a typical essential facility (neglecting the screening effects of nearby elements), the design load of a 1,000 lb object moving at 5.0 ft/s impacting a cantilevered concrete wall will be approximately 8,500 lb.

$$F = \frac{\pi W V_b C_I C_O C_D C_B R_{max}}{2g\Delta t} \tag{6-4}$$

where: F is the impact force (lb)
W is the debris weight (lb)
V_b is the velocity of the object (assume equal to velocity of water) (ft/s)
g is the acceleration owing to gravity (32.2 ft/s^2)
Δt is the duration of impact (time to reduce object velocity to zero) (s)

C_I is the importance coefficient
C_O is the orientation coefficient, = 0.8
C_D is the depth coefficient
C_B is the blockage coefficient
R_{max} is the maximum response ratio for the impulsive load

As an example, the impact force can be computed as follows:

$$F = \frac{\pi(1000)(1.3)(0.80)(1.0)(1.0)(1.37)}{(2)(32.2)(0.03)} = \pm 11{,}600 \text{ lb}$$

The NYCT *Design Guide 312* proposes yet another approach (Equation 6-5) for calculating debris impact loads. Similar to ASCE/SEI 7, the guide specifies a 1,000 lb object and incorporates factors related to the structure's response; however, rather than correlating the flood velocity to the stillwater flood depth, a fixed velocity of 5.0 fps is used and no load reduction related to flood depth or flow blockage is included. Additional differences result from the fact that the design guide procedure bases the response coefficient (C_{str}) only on the overall building type rather than on the mass and stiffness of the individual element being designed, which is loosely described by ASCE/SEI 7. This is unrealistic, because a 1,000 lb object is not large enough to mobilize a response across an entire structure, and the dynamic characteristics will be dominated by the local element response. For the previously discussed design case, the design guide procedure would yield an impact load of 1,000 to 4,000 lb, depending on the construction type.

$$F_i = WVC_DC_BC_{str} \tag{6-5}$$

where: F_i is the impact force (acting at the stillwater elevation) (lb)
W is the debris weight (lb), = 1,000
V is the velocity of the water (ft/s), = 5
C_D is the depth coefficient, = 1.0
C_B is the blockage coefficient, = 1.0
C_{str} is the maximum response ratio for the impulsive load
= 0.2 for timber pile- and masonry column-supported structures three stories or less in height above grade
= 0.40 for concrete pile- or steel moment-resisting frames three stories or less in height above grade
= 0.80 for reinforced concrete foundation walls (including insulated concrete forms)

Of the aforementioned methods, the ASCE/SEI 7 procedure provides the most flexibility and precision in determining project-specific impact loads. Further discussion of the equation components is presented next.

Duration of Impact (Δt). Although the recommended 0.03 s duration of impact in ASCE/SEI 7 is grounded in real-life testing, the base testing involved a range of wooden log sizes with little variation in object or barrier type. As such, the applicability of this value for approximation of impact forces over a wide array of wall types in an urban rather than a riverine environment is questionable.

Testing on a case-by-case basis is simply not practical; however, in-depth dynamic finite element analyses that capture the full collision event could be used to obtain a more refined value. This analysis should include the structural properties of both the impact object and the structural element being designed, with properly calibrated material behavior models to capture the energy dissipated through yielding/damage and damping.

In the absence of a rigorous analysis, using a 0.03 s duration is considered reasonably conservative and can be used within a simplified static or dynamic structural model, especially in cases where the impact load does not have major design repercussions. For projects requiring consideration of special impact loads, such as vessel collisions along waterways, use of a dynamic analysis is advisable in order to avoid unnecessarily conservative or insufficient designs.

Object Velocity (V). The guidance provided by the commentary to ASCE/SEI 7 states that debris impact force is appropriately calculated using an impulse-momentum approach. Simply put, with all other factors being equal, the velocity of debris impacting a structure will be directly proportional to the force imparted on the structure. As a result, the velocity of the object has a significant impact on the resulting load magnitude.

The commentary to ASCE/SEI 7 provides some guidance on calculating debris velocity, but it is not inclusive of all applications. The commentary states that small debris floating near the water surface is likely to travel at or near the velocity of the floodwater; however, this debris is the least likely to cause damage to a structure. Larger debris, which is more likely to cause damage, typically travels at speeds slower than that of the floodwater for riverine flooding outside of the floodway and for coastal flooding, which includes urban flooding during a storm surge event. Conservatively, ASCE/SEI 7 suggests that the debris velocity should be assumed to equal the floodwater velocity because the coefficients included in ASCE/SEI 7 Equation C5-2 (C_D and C_B) account for potential reductions in debris velocity.

Orientation Coefficient (C_o). The orientation coefficient, C_o, is cited to be 0.80 for all cases to reflect the general load reduction owing to oblique impacts (angle of ±53°). Because the primary flow paths in an urban environment—those that achieve the maximum design velocity in the impact equation—will be parallel to building walls, an additional reduc-

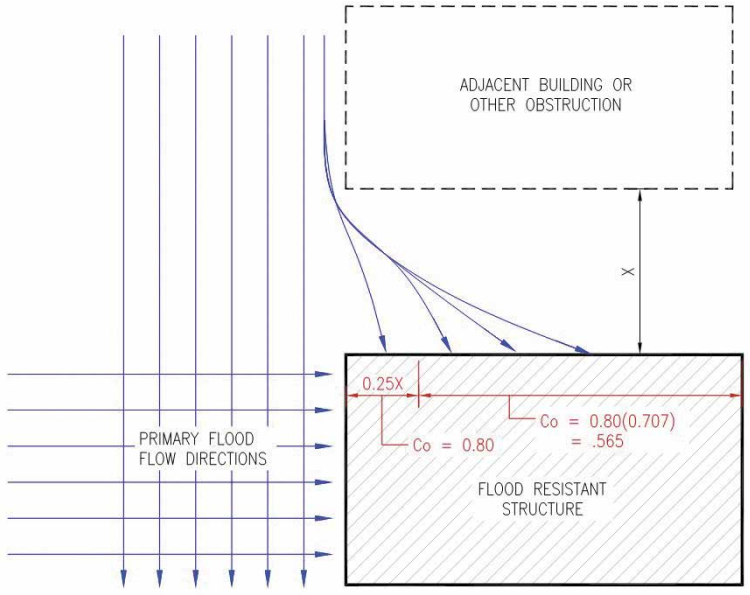

Figure 6-3. Example of modified orientation coefficient for shielded walls.

tion may be warranted in some cases where adjacent structures provide shielding. An illustration, this phenomenon is presented in Figure 6-3, along with a potential strategy for modifying the C_o factor. It should be noted that this modification should be determined on a case-by-case basis at the discretion of the engineer.

Blockage Coefficient (C_B). The blockage coefficient, C_B, is predicated only on the width of the *upstream flow path*, considering 30.0 ft as the threshold for a fully unimpeded flow (C_B = 1.0). Although the streets in urban environments (serving as the flow paths) are typically wider than 30 ft, the presence of buildings, fences, poles, railings, elevated roadways, and other elements influence the flow of water-borne debris.

A more appropriate strategy for determining the degree of screening is to use the qualitative descriptions presented in Table C5-3 to classify the landscape surrounding the structural element being designed. When determining this, objects with inadequate anchorage that are likely to be dislodged during a flood event, should not be considered to provide screening. In most urban cases, "limited upstream screening" can be justified, resulting in a reduction factor of 0.60.

Depth Coefficient (C_D). ASCE/SEI7 notes that the coefficients presented in Table C5-2 are not based on testing data, and if/when better data are available, engineers are advised to use that in lieu of the values provided.

Response Ratio (R_{max}). The response ratio, R_{max}, is used to represent the reduction or amplification of the impact load based on the dynamic characteristics of the element being designed and its natural period relative to the duration of loading. Generally speaking, stiffer structures will experience larger forces, whereas more flexible structure will experience reduced forces (analogous to the behavior of stiff and flexible buildings under seismic loading).

In an effort to validate the ASCE/SEI 7 R_{max} values and investigate the sensitivity of various factors, several dynamic analyses were performed using both the finite element analysis (FEA) program RISA 3D and a simplified Excel-based single degree of freedom program. Each of these analyses utilized a cantilevered concrete wall element with constant material properties, and the thickness of the wall was varied to produce a range of stiffness values and natural frequencies. The applied impact load was represented by a half-sine with a maximum magnitude of 5,000 lb and duration of 0.03 s, as provided in Figure 6-4, with the results provided in Figure 6-5.

As shown in Figure 6-6, the results for an *equivalent* R_{max} for each analysis type emulate the pattern of those values given in ASCE/SEI 7. Discrepancies between the results are likely the result of the damping values assumed—for a complex process such as an impact, calibration of this damping value is difficult because it must account for the effects of energy dissipation through local yielding of the element, deformation of the object itself, and the internal/external friction losses. Additional variations in the RISA results

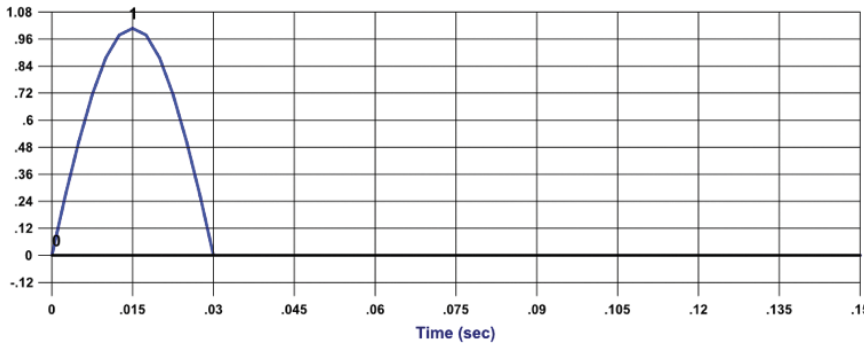

Figure 6-4. Applied impact load time history (before scaling to 5.0 kip maximum).

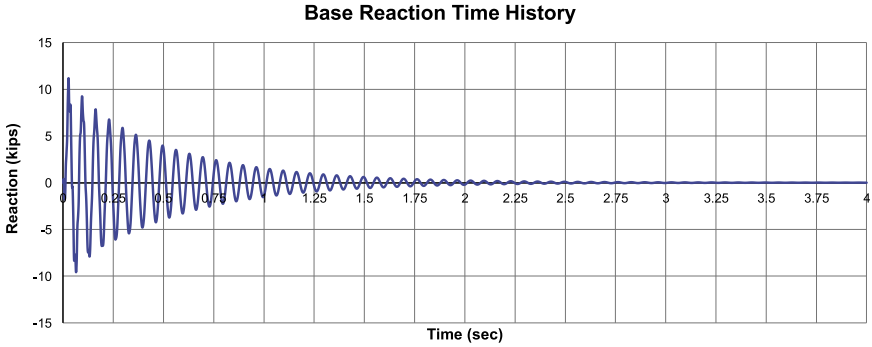

Figure 6-5. FEM analysis—dynamic reaction time history to 5.0-kip impact load.

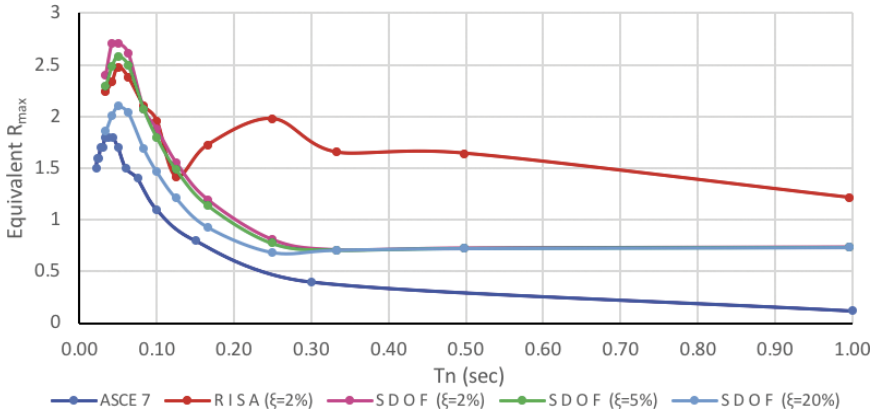

Figure 6-6. Design impact loading from ASCE/SEI 7 commentary.

are owing to the multimodal response engaged as the element flexibility was increased.

This exercise supports the conclusion that the R_{max} values listed in ASCE/SEI 7 Table C5-4 are appropriate for most design cases, with one important clarification. In determining the natural period, the discussion in ASCE/SEI 7 implies that the period of the overall structure should be used in determining this ratio (0.03/TN); however, this strategy is only applicable in the analysis of small one- or two-story buildings that are relatively light. In an urban environment, where buildings are typically much larger, the 1,000 lb debris object will not mobilize the mass of the entire structure, and the governing dynamic modes (and associated load amplification or reduction) will be controlled by the stiffness of the local wall/barrier elements.

General Analysis and Design Application. The assumption of a 0.03-s duration of impact limits the compatibility of the ASCE/SEI 7 equation for use with traditional design equations for steel, concrete, masonry, and aluminum. These equations calculate capacities using static material properties with a typical factor of safety of 1.67 intended for use with sustained (or partially sustained) loads. In addition, ASCE/SEI 7 states that the impact equation is not calibrated for the probability of impact, as is considered in other types of codified loads.

A loading of this duration, which is comparable to that of a blast load, would be more appropriately designed for with a nonlinear dynamic analysis that includes strength increase factors to account for limiting strain rates and removes factors of safety intended for sustained loads. The acceptance criterion for this type of loading also traditionally allows a certain amount of acceptable plastic deformation; however, in the case of flood design, allowing such a plastic deformation may adversely affect watertight seals, and careful consideration must be given to those deformation limits. Additional guidance on SDOF and FEA can be found in various textbooks on structural dynamics, as well as in USACE publications on this topic.

Accounting for all these discussion points, as well as considering the inherent factor of safety associated with the addition of freeboard to the DFE, a reasonably conservative design approach for debris impact load design can utilize the equations in the ASCE/SEI 7 commentary, in combination with a static or dynamic analysis:

- A 1,000-lb debris object as universally cited in each standard. An assumed effective width of 2 ft 0 in. and an effective depth of 2 ft 0 in. is used for the impact object, which correlate more closely to the types of debris that will exist in the city.
- In the absence of detailed hydraulic modeling, a design flood velocity equal to the average of the upper and lower bound velocities specified in the ASCE/SEI 7 commentary.
- A blockage coefficient qualitatively determined based on the surrounding conditions—typically *moderate upstream screening* or *limited upstream screening* is justifiable in urban conditions.
- Wall/member strength ratios evaluated as follows:
  - CASE 1: Concurrent hydrostatic and hydrodynamic loads applied and element capacities calculated using static material properties.
  - CASE 2: Concurrent hydrostatic, hydrodynamic, and impact loads applied and element capacities calculated using dynamic material properties (coefficients for transforming material properties are available in both ASCE 41 and UFC codes).

6.3 LOAD COMBINATIONS

The load combinations for use with the above specified loads are cited in Sections 2.3.3 and 2.4.3 of ASCE/SEI 7 and vary depending on the applicable flood zone. In simple terms, structures in coastal zones will have designs loads equal to two times those landward of the LiMWA.

The combinations include the combined effects of wind loads at their full magnitude acting concurrently with the flood loads. Although it is likely that a hurricane can bring floodwaters and high wind forces, it is not likely that the maximum 3 s wind gust and debris impact load will strike simultaneously on the same surface. As such, considering the wind forces and impact forces separately for the design of walls is justified (note that both should include the applicable hydrostatic and hydrodynamic forces, concurrently).

Similar to the requirements for buildings, it is important that factored loads or strength reduction factors are only used when determining the system's strength capacity. For wall or other deflections, the loads should be at the service level to ensure proper compatibility with the DFE.

Flood protection for buildings typically involves closing a marine door or deploying a barrier at a discreet opening. The combined events of flood and rain exist in this situation, but they do not compound for an individual element as they do when protecting an exterior area. When protecting an area, perimeter walls will keep out the flood, but they will also keep in the rain—solving one problem while creating another. Rainwater is typically collected in an underground drainage network and discharged into city sewers. During a flood event, gravity flow is blocked and water cannot be discharged unless the pumped pressure exceeds the exterior head pressure. Although this condition is trapping fresh water and likely keeping out brackish salt water, internal flooding will occur if not considered properly and discussed with the client.

There are three possibilities for internal water within the protected area in a surge condition: pump against the exterior head pressure, collect internally in detention basins, or accept local ponding. Locations that are susceptible to flooding also generally have a relatively shallow groundwater table, so cost-effective underground detention systems will be limited to shallow-depth products like a Terre Arch. Although exterior projects must contend with a design rain event as well as a design flood event, combining the two will likely yield impossible performance guidelines for the drainage system.

The probability of two independent 100-year events (i.e., 1% annual chance) occurring simultaneously, or even on the same day, is exceedingly low. Of course, flood and rainfall are not independent of one another, and so the mathematic return interval must be adjusted based on available data.

Table 6-2 lists design rain events and the associated rainfall with the 10 highest storm surge events recorded in the New York City region.

In terms of combined rainfall during flood events, Hurricane Donna of 1960 had this greatest concurrent rainfall in the region, considerably more than during Superstorm Sandy. Based on historical data, it appears exceeding unlikely that a 100-year rainfall event would occur at the same time as

Table 6-2. (a) Design Rain Events and (b) Historical Rainfall During Major Storm Events.

(a) Total rainfall in inches by RP and duration

Storm return period	24-h storm duration
1-year	2.9
2-year	3.8
5-year	4.6
10-year	5.3
25-year	6.7
50-year	7.8
100-year	9.0

(b) Top 10 Highest Storm Surge Crests for New York Harbor at the Battery Since 1920.

Date recorded	Storm surge (NAVD88 feet)	Total 24-h rainfall (in.)	Storm event title
10/29/2012	14.06	0.51	Superstorm Sandy
09/12/1960	10.02	3.77	Hurricane Donna
12/11/1992	9.70	2.75	*Unnamed Storm Event*
08/28/2011	9.51	3.13	Hurricane Irene
11/25/1950	9.12	1.83	*Unnamed Storm Event*
03/06/1962	8.92	0.34	*Unnamed Storm Event*
10/31/1991	8.73	0.71	1991 Perfect Storm
03/29/1984	8.53	1.50	*Unnamed Storm Event*
03/14/2010	8.51	0.39	*Unnamed Storm Event*
03/14/1993	8.36	0.01	*Unnamed Storm Event*

a 100-year storm event. In order for a large site to remain *dry* during such a combined event (e.g., 14 ft of surge and 9 in. of rain), tens of thousands of gallons per minute pumping capacity would likely be required. This pumping requirement obviously is not practical, and designing for a storm return interval well over 10,000 years is typically not warranted.

As is the case with other extreme event loads, practical design uses performance-based approaches where capital costs and damage potential is negotiated between the designer and client. In order to facilitate this discussion, Figure 6-7 was developed to show an associated performance for the combined event of storm surge versus rainfall with a site-specific pumping performance curve and adjusted return intervals.

The following notes apply to the example project as presented:

- The horizontal and vertical upper boundaries are defined by the project design rain and surge events, with the intersection falling well above the 2,000-year MRI line and all historic data.
- With a functioning underground drainage system, the 100-year rainfall volume can be drained by gravity until the surge level reaches 7 ft, at which point pumping must be provided.
- Discussions with the client yielded an acceptable pump size for capital cost and maintenance reasons.
- This pumping capacity, which equaled 12,000 gpm, provided for up to approximately 2.5 in. of rainfall volume to be handled, with the total capacity decreasing slightly owing to pumping losses at higher heads.

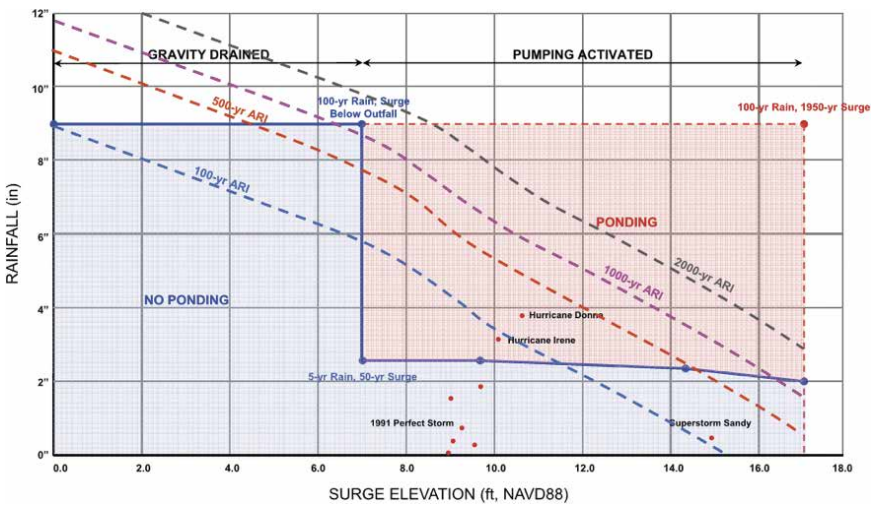

Figure 6-7. Example combined event performance graph.

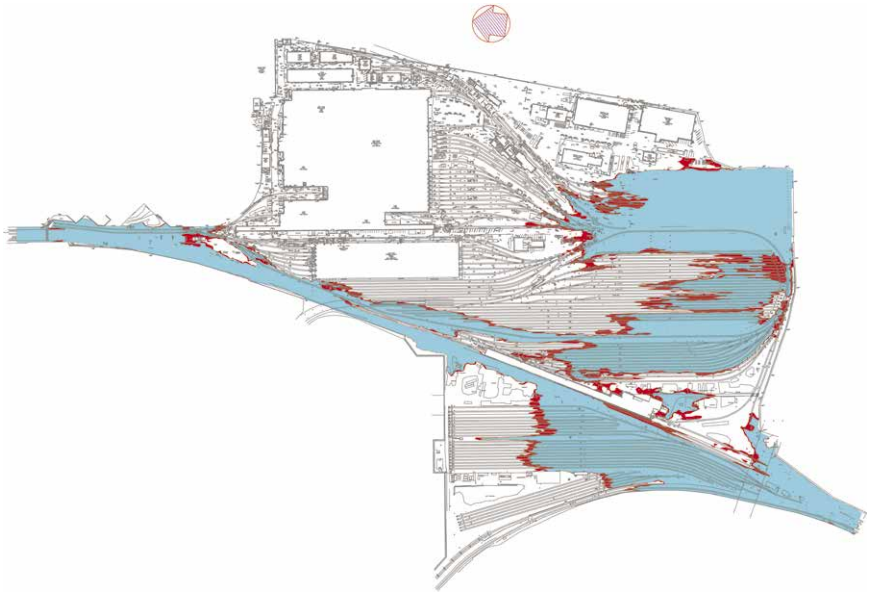

Figure 6-8. Example performance-based hydraulic model to depict site ponding.

With this site-specific performance graph, the yard is *dry* to the left of the pumping curve and will see ponding for events falling to the right. In order to make this more understandable for the client, we also ran a hydraulic model at the full rain and surge condition (upper right point), and it produced the ponding zone shown in Figure 6-8 that was deemed an acceptable risk given the extraordinary return interval.

6.4 DEFLECTION CRITERIA FOR FLOOD LOADS

Although deflection criteria for flood-resisting elements are not codified, lateral drift limits for wind and seismic loads are often a governing design component for buildings/bridges, and a wealth of historical data and documentation are available. The design wind speeds and seismic parameters in the ASCE/SEI 7 code have varying recurrence intervals based on building importance, code version, and analysis application (strength vs. deflection; global vs. local). Serviceability limits for these loads also vary based on application, with global drifts limits intended to ensure occupant comfort and local limits intended to reduce damage to architectural and mechanical, electrical, and plumping components.

Modern codes are trending in the direction of a performance-based approach for wind, whereby the designer (in conjunction with the owner)

may choose a separate return interval for serviceability and strength-related lateral forces. The design of flood-resistant components should follow this same rationale, and the design depth used for calculation of deflections should be chosen based on acceptable effects. In our experience, reasonable deflection limits under hydrostatic load (without freeboard) can be taken as follows:

- 100-year MRI - L/360 (≤0.30 in. for brittle finish)
- 500-year MRI - L/180
- >500-year MRI (e.g., SLOSH Cat 2) - L/90

Note that these limits must be considered with regard to finish type, span, and material, and specific attention should be paid to seams and seals within the watertight envelope that may be adversely affected by large displacements.

For cantilever flood walls, an additional criterion that can control the design is displacement at the grade or soil interface. When the base of the wall deflects under the surge lateral load, it compresses the adjacent grade as the embedment or foundation engages. When this happens, soil, silt, or other debris fills the gap created on the opposite side, resulting in permanent wall rotation even after the load is removed. An acceptable base displacement must be determined based on wall height, type, finishes, location, and acceptable post-event repairs, understanding that this single value can have large first-cost implications. Based on experience, we have seen designers use ½ in. base displacement for sensitive structures and 1 in. or more for more flexible, utilitarian walls. It is important to note that picking a larger value does not increase the potential of a breach because geometric height reduction as a result of base rotation is negligible; it simply means some wall segments may not return to vertical after the event—requiring rebuilding or mechanical straightening. Similar to the wall deflection limits tabulated previously, base displacement limits should increase with higher DFE values.

6.5 LEAKAGE AND SEEPAGE

6.5.1 Leakage

Leakage happens for many reasons—improper closure or deployment; broken, deteriorated, or missing seals; porosity of barrier; subsurface seepage; local washout; bent pieces; and so on. Flood barriers will likely be deployed or closed during a stressful situation with loss of power, driving rain, and high winds, making it nearly impossible to achieve the same precision as a factory or drill test case. For this reason, there must be a complementary drainage system in place and sized to account for the water

leakage that will occur. The appropriate design leakage is heavily dependent on the type of waterproof barrier used and the acceptable level of water retention for a given facility. In the case of a marine door mounted on a reinforced concrete wall, the leakage rate may be almost zero (which may be required for a closed building). In contrast, the leakage for a gate at a tunnel mouth may be 50 gpm, but the net volume will be insignificant relative to the pumps that were sized for the design rainfall on the approach ramp. Each individual system, closure, and leakage path must be considered for a comprehensive mitigation solution.

Whenever barrier products are specified, there should be a project-mandated acceptance criteria in the specifications in order to ensure the system performs as anticipated. Insist that vendors produce test data that meet the criteria for opening and boundary conditions that match those of the site. NYCT's *Design Guide 312* provides guidance on acceptable leakage rates for their system components. Of note, NYCT allows a leakage rate of 0.1 gpm per linear foot of wetted perimeter for hatches, doors, and vertical closures, assuming the existing drainage system on the dry side can handle the storage or discharge of the associated water volume.

6.5.2 Subsurface Seepage

It is critical that subsurface seepage is considered at each location, addressing potential water travel paths through porous soil layers. The flood wall foundations, in addition to resisting the sliding and overturning forces, will need to seal into a relatively impermeable soil layer to ensure no subsurface seepage path during the surge. If no impermeable barrier layer is present, any infiltration flow via subsurface seepage must be added to the rainfall and leakage values to calculate the water management demand design volume. In addition, the flood wall stability must be verified against a potential quick condition and loss of local soil strength, particularly in the case of a retaining wall supported by a shallow foundation on granular soil. A proper seepage analysis will consider the design storm surge duration (e.g., limited 6-hour window), as well as the ground impermeability in paved areas in determining a realistic seepage flow value. As mentioned above, consideration regarding future surface improvements to increase permeability on surrounding properties may also be appropriate. It should be noted that incentives (e.g., LEED credits) for increasing ground permeability to minimize stormwater runoff may continue to influence future projects.

The hydrostatic pressure that interacts with the subsurface structure is based on whether groundwater rises sufficiently to reach the structure during a storm, and the period of time that floodwaters are above the ground elevation in the vicinity of the site with respect to hydraulic conductivity of surface and subsurface strata. For most urban sites (including many in

low-lying areas that have been historically built up on fill), groundwater will not be an issue, and the subsurface seepage duration will be much less than the total storm duration. Seepage analyses that do not properly account for a realistic duration and local ground surface conditions may yield grossly incorrect and impractical pumping, drainage, and cutoff criteria.

To calculate subsurface seepage duration, a model storm should be chosen. The duration of a storm at any specific location will depend on the size, track, and speed of the storm. The other factor is how the storm tide aligns with the astronomical tide. Superstorm Sandy was somewhat close to being in phase with the astronomical tide, and so it had a narrower shape (but higher peak) than it would have had if the storm peaked at low tide. If a large enough storm came in between successive high tides, the peak would be rounded and lower, but the duration of flooding would be longer at the site. Superstorm Sandy, as measured at the Battery, is a conservative storm duration model appropriate for design in the region because it represents a combination of tropical and extratropical storm events (i.e., it equates to an expansive, high-intensity storm) and falls somewhere in between but fairly close to alignment with high tide.

To calculate the period of time that the floodwaters described above will influence seepage, the water-level chart at the Battery during Sandy can be first transformed by the difference between the Sandy storm tide peak (approximately 14 ft) and the project DFE (including SLR but not wave action). Then calculate the duration of time between the points where the resultant storm crest rises above the minimum elevation within the seepage analysis area to the point where it goes below it. The Battery is a widely recognized tidal station with elevations translatable to NAVD 88. Figure 6-9

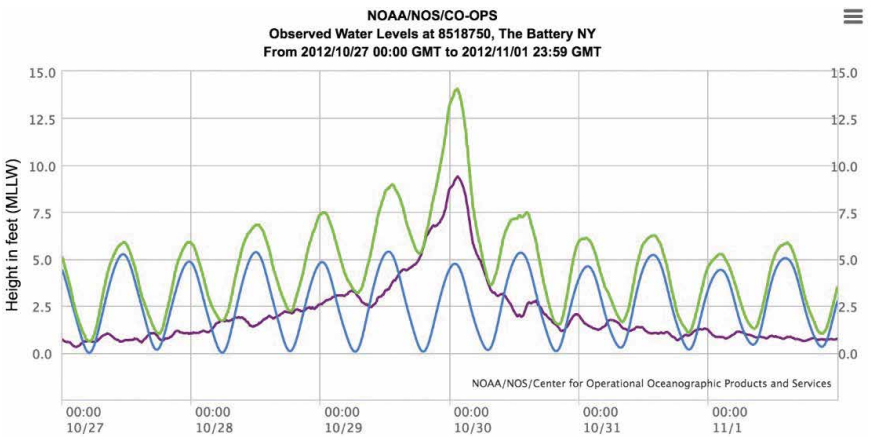

Figure 6-9. Water levels at the Battery, NY, during Superstorm Sandy. Source: NOAA (2017).

shows the historic chart from the Battery tidal station during Superstorm Sandy and depicts the predicted tidal cycle (blue line), storm surge (purple), and resultant storm tide (green) in feet above MLLW and time. The data for this and other storm events can be obtained from NOAA in .csv format.

Geotechnical engineers must work with the client and project team to establish a site-specific, realistic, and reliable design. Soil properties vary greatly in and along the perimeter of a large site, and exploration data are commonly limited to soil borings CPT and field permeability test data. It is therefore important to properly evaluate the variability of the collected data and the associated uncertainties, as well as estimate the reliability of the proposed solution. The geotechnical analyses relating to wall stability and seepage flow should use the mean or "most likely" values of pertinent soil parameters (e.g., strength, unit weight, permeability). Simplified methods of reliability analysis based on evaluating the standard deviation of each pertinent soil parameter are then used to supplement the analyses and to assess the reliability of the results owing to the combined uncertainties in these parameters.

6.6 REFERENCES

ASCE. 2010. *Minimum design loads for buildings and other structures*. ASCE/SEI 7-10. Accessed February 13, 2016. http://www.asce.org/structural-engineering/asce-7-and-sei-standards/. Reston, VA: ASCE.

ASCE. 2014. *Flood resistant design and construction*. ASCE/SEI 24-14. Reston, VA: ASCE.

Executive Order 13690. 2015. *Establishing a federal flood risk management standard and a process for further soliciting and considering stakeholder input*. Accessed August 10, 2018. https://obamawhitehouse.archives.gov/the-press-office/2015/01/30/executive-order-establishing-federal-flood-risk-management-standard-and-.

FEMA (Federal Emergency Management Agency). 1993. *Non-residential floodproofing—Requirements and certification for buildings located in special flood hazard areas in accordance with the National Flood Insurance Program*. Technical Bulletin 3-93. Washington, DC: FEMA.

FEMA. 2005. *Design and construction in coastal A-zones—Hurricane Katrina recovery advisory*. Washington, DC: FEMA.

FEMA. 2011. Coastal Construction Manual (FEMA P-55). Volumes 1 and 2, 4th Ed. Washington, DC: FEMA.

FEMA. 2013. *Flood insurance study number 360497V000B*. Vol. 1 of 1 (Preliminary: December 5, 2013). Washington, DC: FEMA.

FEMA. 2015. *Revised guidelines for implementing Executive Order 11988, "Floodplain management," and Executive Order 13690*, "Establishing a federal

flood risk management standard and a process for further soliciting and considering stakeholder input." Washington, DC: FEMA.
IPCC (Intergovernmental Panel on Climate Change). 2014. *Climate change 2014: Impacts, adaptation, and vulnerability. Part A: Global and sectoral aspects*. C. B. Field et al. (eds.). Cambridge, UK: Cambridge Univ. Press. Accessed February 13, 2016. https://www.ipcc.ch/report/ar5/wg2/.
McCowan, J. 1894. "On the highest wave of permanent type." *Phil. Mag. J. Sci.* 38(233), 351–357.
NOAA (National Oceanic and Atmospheric Administration). 2012. "Global sea level rise scenarios for the US national climate assessment." *Tech. Memo OAR CPO-1*. Silver Spring, MD: NOAA.
NOAA. 2017. *Tides and currents*. The Battery, NY. Station Id: 8518750 (water-level data accessed Mar. 22, 2017).
NYCBC (New York City Building Code). 2014. *Appendix G: Flood resistant construction*. Accessed August 10, 2018. https://www1.nyc.gov/assets/buildings/pdf/2014%20NYCCC%20Flood%20Zones.pdf and https://www1.nyc.gov/site/buildings/codes/nyc-code.page.
NYCTA (New York City Transit Authority). 2014. *Flood resiliency design guideline*. DG 312. New York: New York City Transit Authority.
USACE (United States Army Corps of Engineers). 2002. *Coastal engineering manual*. EM 1110-2-1100. Washington, DC: USACE.

This page intentionally left blank

CHAPTER 7
ADAPTIVE DESIGN AND RISK MANAGEMENT

7.1 UNCERTAINTY AND RISK

Given the uncertainty facing engineers regarding future weather and climate extremes, the development and use of appropriate approaches would seem pragmatic. Risks associated with decision situations are fundamentally attributable to the presence of uncertainty in these decision situations. Without uncertainty, risks are nonexistent.

Engineers cannot predict all the potential conditions for future infrastructure and systems. Although climate scientists have certainty about the signal on a global level, uncertainties about the timing and magnitude of expected change complicates the ability to design for precise specifications. Under such conditions, a design based on standards would not fully capture the range of possible conditions a system will undergo during its lifetime, thus leading to a potential failure.

The uncertainty associated with future climate is not completely quantifiable, and therefore accounting for it in engineering practice would require an appropriate understanding and treatment of uncertainty including engineering judgment. In general, uncertainty sources can be broadly classified for convenience into the following types (Ayyub and Klir 2006):

1. Uncertainty that is recognized and well characterized, such as materials properties;
2. Uncertainty that is recognized but is moderately characterized, such as future precipitation, hurricanes, wind speed, etc.;
3. Uncertainty that is recognized but poorly characterized, such as future energy use by populations worldwide;

4. Uncertainty that is recognized but cannot be characterized, such as global governance and cooperation; and
5. Uncertainty sources of an unknown existence or nature, for example, physical laws or behaviors that are not discovered yet or undiscoverable based on ongoing intellectual pursuits.

It has been a common practice in engineering to group these uncertainties as: (1) aleatory uncertainty and (2) epistemic uncertainty. The former is considered as being inherent to the situation and irreducible with data collection, although the characterization of it can be enhanced, and the latter is reducible with data collection or investigation, although the economics of such pursuit might not justify its reduction. Planning for a changing climate entails not only planning for climatic uncertainty but also for uncertainty about regulatory, environmental, economic, social, and other conditions affecting water utilities, as provided by Means III et al. (2010), to demonstrate using multiple-outcome planning in order to allow water utilities to better integrate their planning across all functions of their agency.

Risk methods provide practical means for dealing and managing uncertainty (Ayyub 2014b). Risk is commonly measured in simple terms as the probability of occurrence of an event or a scenario of events and the outcomes or consequences associated with the occurrence. Risk assessment is primarily concerned with answering three questions (Kaplan and Garrick 1981):

1. What could happen, i.e., what could go wrong?
2. How likely is it to happen?
3. If it does happen, what are the consequences?
4. Risk assessment is a systematic process to identify potential uncertain events including hazards, to determine the consequences of event occurrences, and to estimate its occurrence likelihood.

7.2 DESIGN PHILOSOPHIES

Engineers should develop a new paradigm for engineering practice in a world in which climate change, population growth, and development patterns are altering the risk profiles of individual projects, communities, and even nations. The effects of changes in climate may be difficult to project with a high degree of certainty in many instances; however, clear indications are available of some effects, such as sea-level rise (SLR) and an increase in the number of extreme events occurring in areas where they have rarely been encountered. These events suggest a changing footprint of risk, regardless of the magnitudes of the events on regional or national scales.

Engineers design infrastructure by accounting for uncertainties in order to achieve acceptable safety levels to the public and appropriate physical and economic efficiencies. Out of these underpinnings to design, uncertainty is foundational in developing a design philosophy. Engineering design has changed and sometimes evolved based on an enhanced or a broader understanding of uncertainty.

The five uncertainty sources have been driving engineers toward practice enhancements. For example, the first case, where uncertainty is recognized and well characterized, requires engineers to use the traditional factors of safety, followed by reliability-based design in building codes. For cases 2 and 3, where uncertainty is recognized as moderately or poorly characterized, engineers use reliability-based or risk-informed designs.

Scenario modeling is a strategy used to perform sensitivity analysis and address variability. This modeling is capable of incorporating conditional probabilistic information into the models, such as uncertainties owing to spatial variability of seismic demand, random phasing of ground motion, local soil conditions, and performance of civil infrastructure through fragilities. Another tool is robust decision making (RDM), which can address cases where deep uncertainty is recognized but either poorly characterized or incapable of being characterized. RDM provides an analytic framework that identifies strategies that can perform over a wide range of these poorly characterized uncertainties (Groves and Lempert 2007). Uncertainties where probability distributions are not known or agreed upon can be characterized as deep uncertainties (Lempert et al. 2003). When dealing with climate change, it is important to recognize that it will not be possible to define a system with probability distributions a priori. There will be deep uncertainty around these models, and an RDM strategy could allow a small number of scenarios to be analyzed while incorporating probabilistic information into them (Groves and Lempert 2007). The framework can identify strategies that would be insensitive to vulnerabilities (Groves et al. 2008). These vulnerabilities are the product of deep uncertainty in climate models for both future climate and projections.

When uncertainty is unrecognizable or it is not possible to fully define and estimate the risks and potential costs for a project and reduce the uncertainty in the time frame in which action should be taken, in other words, in cases 4 and 5, engineers should use adaptive design or risk management. Adaptive design or risk management is most effective in cases 4 and 5, although it could be used in other cases. Wilby and Dessai (2010) provide a robust adaptation measures framework called ". . . adaptive management of climate risks . . . ," which ". . . involves careful monitoring of the environment and systematic appraisal of the performance of the measures." This framework consists of inventorying preferred adaptation strategies that are later synthesized into a subset of measures that reduce vulnerability under the present climate regime. These final strategies should be able to perform

well over a wide range of scenarios providing "no regret," regardless of climate change and conditions.

Both RDM and adaptive management have been applied to case studies on water resources. Groves and Lempert (2007) present a case study for water planning in California. Lempert and Groves (2010) built on RDM and provided a methodology for developing sequences of local weather data that are able to reflect current climate trends and climate change. Wilby and Dessai (2010) analyzed a series of robust adaptive measures while carrying out the case study of water management in England and Wales. In addition, the International Upper Great Lakes Study (2012) used robustness as a decision criterion in choosing regulation rules.

The OM, which is a technique of adaptive risk management, as described in Chapter 3, offers the means to produce projects with resiliency to future climate and weather extremes. Engineers should seek alternatives that do well across a range of possible future conditions, including ones that have not been identified yet. In such methods, adaptation is triggered as changes occur. Current design approaches at a particular site are based on probabilities of extreme events. With the growth in population and the dense development of land, risk should be treated more on a regional basis than on a site basis. Such methods would enable the development of cost-effective strategies for making a project more resilient to future climate and weather extremes by including some initial level of enhanced resilience or adaptation rather than retrofitting it later.

Seismic engineering research has embraced the concept of performance-based design, and results are now finding their way into a number of projects. In these cases, both design teams and owners are able to evaluate design options by monetizing the costs and benefits of design options based on a number of different scenarios with different risk profiles. Adaptive risk management would expand this approach for developing and presenting alternatives that do well across a range of possible future conditions. Performance-based design presently covers functionality, durability, and safety at respectively appropriate mean recurrence intervals (MRIs). Adaptive risk management would extend this concept in consistent terms that accounts for the non-stationarity of underlying processes for the purposes of addressing extremes, as described in Chapter 4.

7.3 CLIMATE-RESILIENT INFRASTRUCTURE

Resilience is defined by the Presidential Policy Directive (PPD)-8 (2011) as "the ability to adapt to changing conditions and withstand and rapidly recover from disruption due to emergencies." Measuring resilience is typically based on the performance of an infrastructure system after an external shock, including the time it takes to return to the initial level of performance.

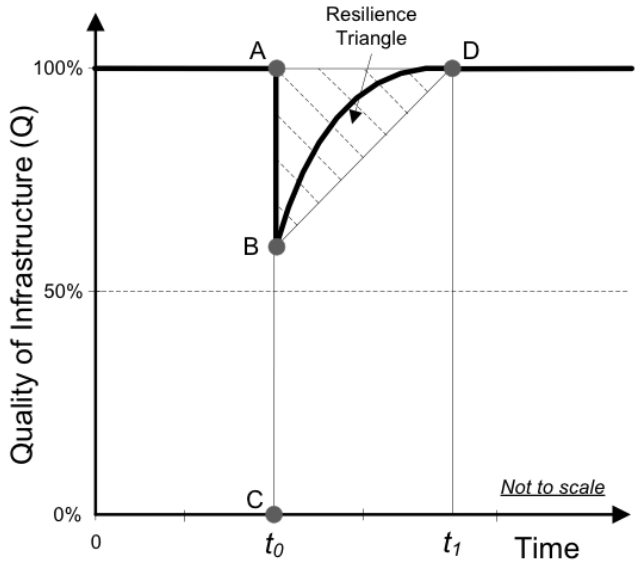

Figure 7-1. The resilience properties and triangle.

This concept is illustrated as shown in Figure 7-1, calling it the resilience triangle, with a resilience index defined as follows:

$$\text{Resilience} = \frac{\int_{t_0}^{t_1} Q(t)dt}{100(t_0 - t_1)} \tag{7-1}$$

where Q is the infrastructure quality or the performance of a system, t_0 is the time of incident or disturbance occurrence, and t_1 is the time to full recovery. According to this model, the units of resilience are performance per unit time, where performance can be measured in percent according to Equation 7-1. The earthquake community uses Equation 7-1 with a suggested framework of resilience called the four "Rs," defined as follows (Bruneau et al. 2003):

- Robustness as the ability of the system and system elements to withstand external shocks without significant loss of performance;
- Redundancy as the extent to which the system and other elements satisfy and sustain functional requirements in the event of disturbance;
- Resourcefulness as the ability to diagnose and prioritize problems and to initiate solutions by identifying and monitoring all resources, including economic, technical, and social information; and

Table 7-1. Definition of Resilience Properties.

Property	Models (Points A, B, C, and D per Figure 7-1)	Units	
Robustness	Robustness = B – C	Percentage	(7-2)
Redundancy	Not defined		
Resourcefulness	Not defined		
Rapidity	$\text{Rapidity} = \frac{A - B}{t_0 - t_1}$	Average recovery rate in percentage per time	(7-3)

- Rapidity as the ability to recover and contain losses and avoid future disruptions.

These properties are defined in Table 7-1 with reference to Figure 7-1.

Another model proposed by Ayyub (2014a) is illustrated in a schematic representation of a system's performance (Q) with aging effects and an incident occurrence with a rate (λ) according to a Poisson process (see Figure 7-2). At time t_i, it might lead to degraded performance, called failure for convenience, of a duration ΔT_f. The failure event concludes at time t_f. The failure event is followed by a recovery event with a duration ΔT_r. The recovery event concludes at time t_r. The total disruption (D) has a duration of $\Delta T_d = \Delta T_f + \Delta T_r$. Figure 7-2 shows for illustration purposes three failure events—brittle (f1), ductile (f2), and graceful (f3) —and six recovery events: expeditious recovery to better-than-new (r1), expeditious recovery to as-good-as-new (r2), expeditious recovery to better-than-old (r3), expeditious recovery to as-good-as-old (r4), recovery to as-good-as-old (r5), and recovery to worse-than-old (r6). These events define various rates of change of performance of the system. The figure also shows the aging performance trajectory and the estimated trajectory after recovery. The proposed model to measure resilience is

$$\text{Resilience}(R_e) = \frac{T_i + F\Delta T_f + R\Delta T_r}{T_i + \Delta T_f + \Delta T_r} \tag{7-4}$$

where for any failure event (f) as illustrated in Figure 7-2, the corresponding *failure profile* F is measured as follows:

$$\text{Failure}(F) = \frac{\int_{t_i}^{t_f} f\,dt}{\int_{t_i}^{t_f} Q\,dt} \tag{7-5}$$

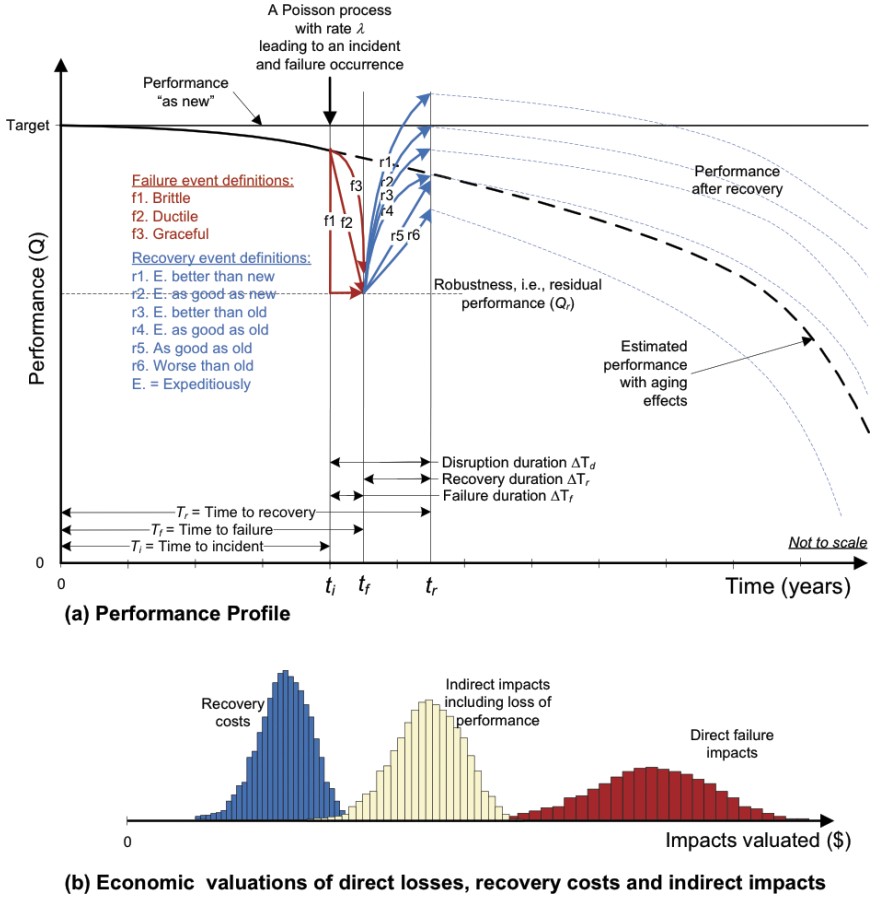

Figure 7-2. Proposed definitions of resilience metrics. Source: Ayyub (2015).

Similarly, for any recovery event (r), as illustrated in Figure 7-3, the corresponding *recovery profile* R is measured as follows:

$$\text{Recovery}\,(R) = \frac{\int_{t_f}^{t_r} r\,dt}{\int_{t_f}^{t_r} Q\,dt} \tag{7-6}$$

The failure-profile value (F) can be considered a measure of robustness and redundancy, and it is proposed to address the notion offered by Equation 7-2, whereas the recovery profile value (R) can be considered a measure

of resourcefulness and rapidity, and it is proposed to address the notion offered by Equation 7-3. Building on the work of Mori and Ellingwood (1993), the time to failure (T_f) can be characterized by its probability density function computed as follows:

$$-\frac{d}{dt}\int_{s=0}^{\infty}\exp\left[-\lambda t\left(1-\frac{1}{t}\int_{\tau=0}^{t}F_L(\alpha(\tau)s)d\tau\right)\right]f_{S_0}(s)ds \tag{7-7}$$

where Q is defined as the system's performance in terms of its strength (S) minus the corresponding load effect (L) in consistent units, in other words, $Q = S - L$. Both L and S are treated as random variables, with F_L = the cumulative probability distribution function of L and f_S = the probability density function of S. The aging effects are considered in this model by the term $\alpha(t)$ representing a degradation mechanism as a function of time t. It should be noted that the term $\alpha(t)$ can also represent improvement to the system. Equation 7-7 is based on a Poisson process with an incident occurrence, such as loading, with a rate of λ. The probability density function of T_f as shown in Equation 7-7 is the negative of the derivative of the reliability function. The times T_i, T_f, and T_r are random variables, as shown in Figure 7-2, and are related to durations as follows:

$$\Delta T_f = T_f - T_i \tag{7-8}$$

$$\Delta T_r = T_r - T_f \tag{7-9}$$

The disruption duration is given by

$$\Delta T_d = \Delta T_f + \Delta T_r \tag{7-10}$$

Figure 7-2 also shows the associated costs, including losses, recovery cost, and indirect costs. These losses and costs should be based on total economic valuations using anthropocentric considerations.

A simplified model (Ayyub 2015) is suggested for a fundamental case having a performance level that would be maintained and sustained over time—in other words, no aging effects, with a brittle failure profile—that is, f1 in Figure 7-2. Also, assume as good as old recovery, in other words, r5 in Figure 7-2. In addition, the following assumptions are made: (1) a planning horizon (t), (2) Poisson process of stressors with a rate (λ), (3) the planning horizon related to the stressor rate as $t = 1/\lambda$, (4) failure probability (p) due to a stressor, and (5) independent failures. It should be noted that the stressors have varied intensities, and not all stressors fail the system and disrupt the system's performance. The failure probability is denoted as p. Fundamental cases are presented in this section: the case of linear recovery and the case of step recovery; however, other cases can be treated in a similar manner.

For the fundamental case of a linear recovery, the resilience metric of Equation 7-4 for one failure-causing event is basically the ratio of two areas according to this figure; in other words, it is the rectangular area tQ_{100} divided by the tQ_{100} without the triangle representing the degraded performance of the system. The triangle has the sides of brittle failure and linear recovery. For a linear recovery path (r), it can be expressed as follows for one failure-inducing event:

$$\text{Linear recovery: Resilience per failure}(R_f) = 1 - \frac{(t_r - t_i)(Q_{100} - Q_r)}{2Q_{100}t} \tag{7-11}$$

For analytical and computational convenience, the concept of non-resilience can be introduced and defined as follows:

$$\text{Linear recovery: Non-resilience per failure}(\overline{R}_f) = \frac{(t_r - t_i)(Q_{100} - Q_r)}{2Q_{100}t} \tag{7-12}$$

The relationship between R_f and

$$\overline{R}_f \text{ is } \overline{R}_f = 1 - R_f \tag{7-13}$$

Equations 7-11 and 7-12 can be generalized to account for the potential of multiple occurrences of failure-inducing events x and their associated probabilities as follows:

$$\text{Resilience } (R_e) = 1 - \sum_{x=1}^{\infty} \left(\exp(-\lambda t) \frac{(\lambda t)^x}{x!} p^x \overline{R}_f^x \right) \tag{7-14}$$

This equation can be reduced to

$$\text{Resilience } (R_e) = 1 - \exp(-\lambda t(1 - p\overline{R}_f)) + \exp(-\lambda t) \tag{7-15}$$

This model offers the simplicity and practicality desired for systems with time-invariant performance and accounts for the rate of events, that is, the rate λ of a Poisson process; the probability of failure (p) given a stressor, that is, the inherent strength of the system; the capacity of the system (Q_{100}); the robustness of the system (Q_r); brittle failure and linear or step recovery to as-good-as-old profiles; non-resilience associated with the occurrence of a failure-inducing event; planning horizon t; and stressor time as a result of a failure-inducing event.

7.4 ADAPTIVE DESIGN IN THE CONTEXT OF HAZARD AND FRAGILITY CURVES

7.4.1 Adaptive Design to Minimize Regret

The durable nature of infrastructure and the even longer-term influence of the associated rights-of-way and footprints suggest that the climate of the future should be taken into account when planning and designing new infrastructure. The impact of climate change in engineering practice is analogous to including forecasts of long-term demands for infrastructure use as a factor in engineering design. However, even though the scientific community agrees that climate is changing, there is significant uncertainty about the location, timing, and magnitude of the changes over the lifetime of infrastructure. These uncertainties are of the latter types described in Section 7.1, that is, uncertainties that are poorly characterized or unrecognizable. As previously discussed, engineers should use for these cases adaptive risk design or adaptive risk management. In these methods, low-regret adaptive strategies could be identified. Engineers should seek alternatives that do well across a range of possible future conditions, including ones that have not been identified yet. In such methods, adaptation is triggered as changes occur, as illustrated in Chapter 3, using the OM.

The mathematical objective here could be to *minimize the maximum regret*, where regret is the difference between a plan payoff in a given scenario and the payoff of the best-performing plan under that same scenario. In common usage, low-regret strategies are policies that would work well under both the current climate and an uncertain future climate. *No regret* is a term that is commonly used; however, most alternatives usually have a cost that is borne by someone who may *regret* having the policy in place.

For instance, there are design implications for a region that experiences a decline in annual average precipitation but increases in short-duration, high-intensity storms. In this case, an average design might result in a misuse of resources and a higher chance of a system failure when service is needed. This is termed *the flaw averages* in the flexible design literature (de Neufville and Scholtes 2011). Flexible design includes the ability to change size and/or functions in the future. Flexible designs would also include redundant systems to protect against failures (de Neufville and Scholtes 2011).

7.4.2 Reliability and Fragility-based Assessment of Adaptive Design

Adaptive design consists of two aspects: updated hazard assessment using the OM and upgrading of the facility's capacity to reflect increases in hazard assessment. Both aspects can be qualitatively and quantitatively represented from the standpoint of hazard curves and increased reliability.

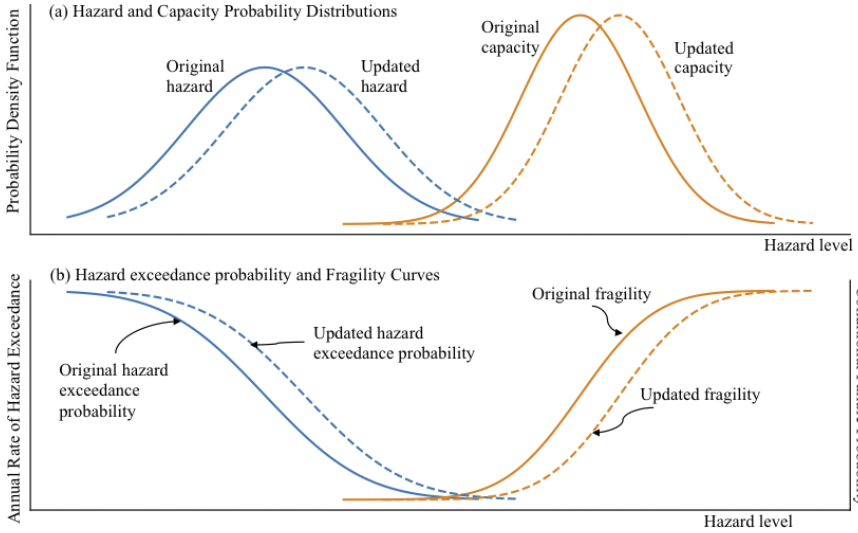

Figure 7-3. Hazard and capacity distributions and curves.

It is customary to represent extreme natural hazards using a hazard curve, which is a plot of the AEP corresponding to various hazard levels (i.e., the hazard curve represents the tail end of the entire hazard distribution because facility safety is best ensured by designing the facility by considering the hazard distribution corresponding to relatively rare events).

Reliability-based design treats hazards with the associated demands and the capacities of components or a system, such as structural members or a building, as random variables. Figures 7-3(a) and (b) illustrate the respective probability distributions and corresponding hazard exceedance curves and fragility curves in the context of adaptive design—in other words, the original and updated curves. Figure 7-4 illustrates the effect of non-stationarity on the hazard exceedance probability curve at the mean and 90th percentile levels. It also shows an initial estimate (say, in the year 2010) of the mean and 90% hazard curves for the year 2050. Note the high standard deviation because of uncertainty. The figure shows another set of curves representing the updated (perhaps in the year 2018) mean and 90% hazard curves for the year 2050 using the OM. Note the assumed illustrative reduction in standard deviation.

A hazard curve can be typically associated with a demand on a component or a system, for example, the wind velocity as a hazard is associated with pressures as demands on components of a building. These associations or relationships entail uncertainties, as illustrated in Figure 7-5. Note that the design demand typically corresponds to an exceedance probability that

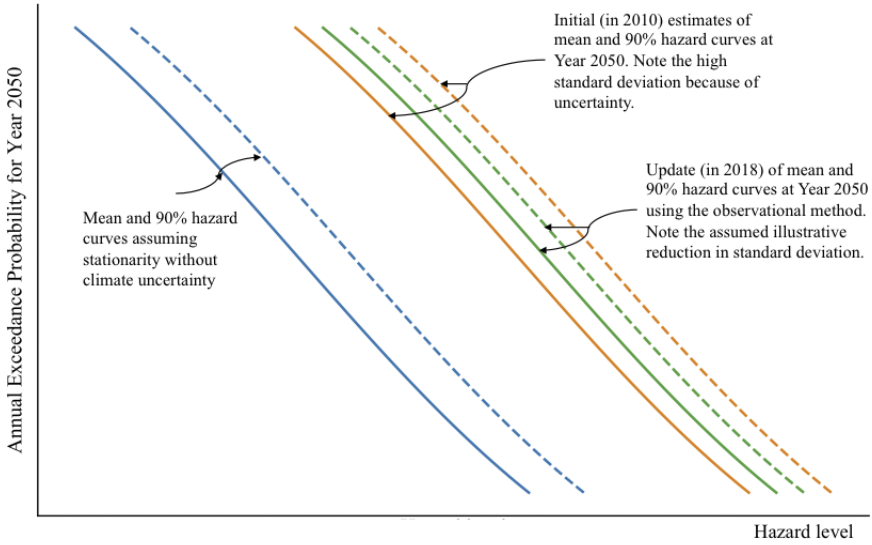

Figure 7-4. Hazard curves based on stationarity, non-stationarity, and subsequent update using the OM.

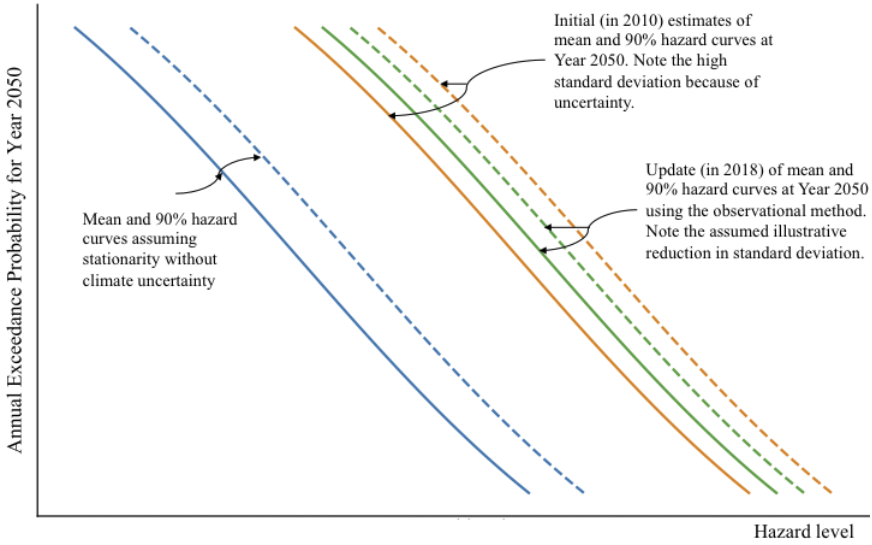

Figure 7-5. Demand distribution and desired performance dependence on hazard level.

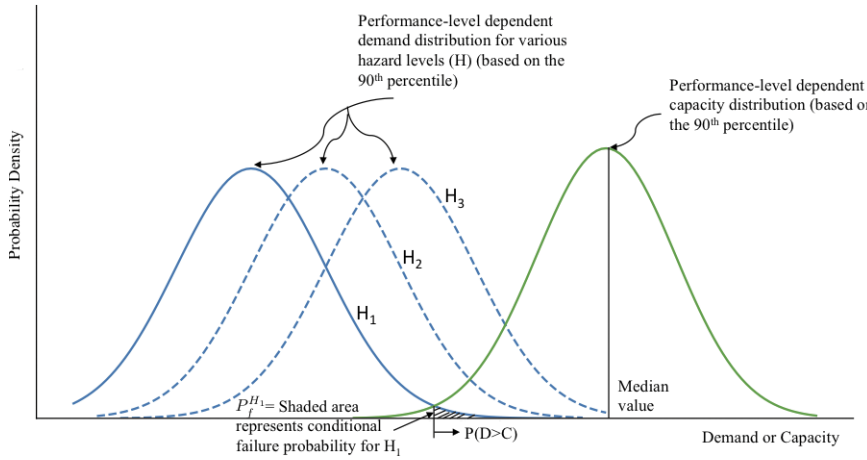

Figure 7-6. Capacity and demand distributions and dependence of probability of failure on hazard level.

is higher than the median demand. Setting the hazard design levels and desired performance levels provides a basis to estimate median or design demands, as shown in the figure. Bringing the demand (D) and capacity (C) probability distributions together on the same figure (see Figure 7-6) illustrates the computation of the conditional failure probability as $P(D > C)$ for the purpose of constructing fragility curves, as provided in Figure 7-7, noting that the uncertainty of capacity (e.g., log-standard deviation) increases with decreasing performance level because of increasing uncertainty in response. The figure also shows that for the same target reliability (expressed in terms of failure probability), several design hazard levels are produced depending on the performance level desired.

The hazard exceedance and fragility curves with the respective uncertainties are shown in Figure 7-8. These curves with a preset hazard probability on the vertical axis can be used to produce hazard design values (H_D) for a robust design that is uncertainty-tolerant. Note that $P_D^{mean} \le P_D^{90\%} \le P_D^{max}$, , where P_D^{max} is a preset value. Figure 7-9 shows the updated curves in the context of adaptive design.

7.5 A METHODOLOGY FOR ADAPTIVE RISK MANAGEMENT

A risk management framework should result in systems that have features to enable updates over time as conditions change. Such a framework would include a monitoring program to evaluate system performance over

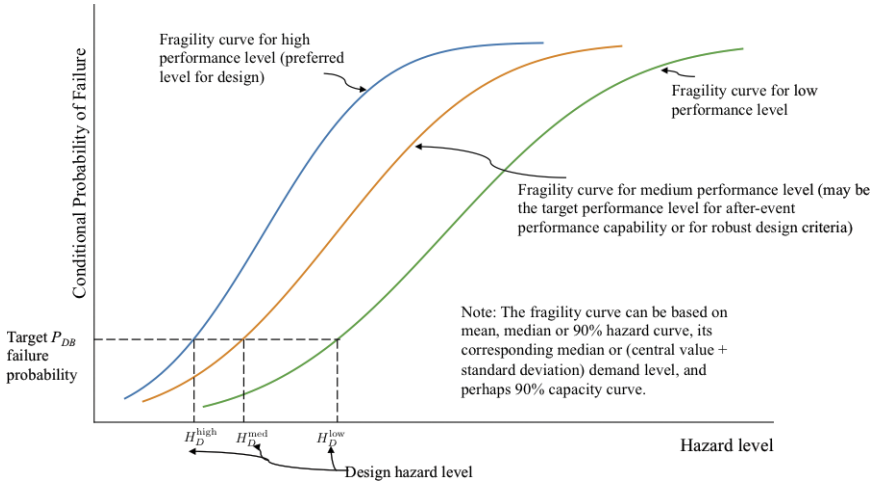

Figure 7-7. Fragility curves for varying performance levels.

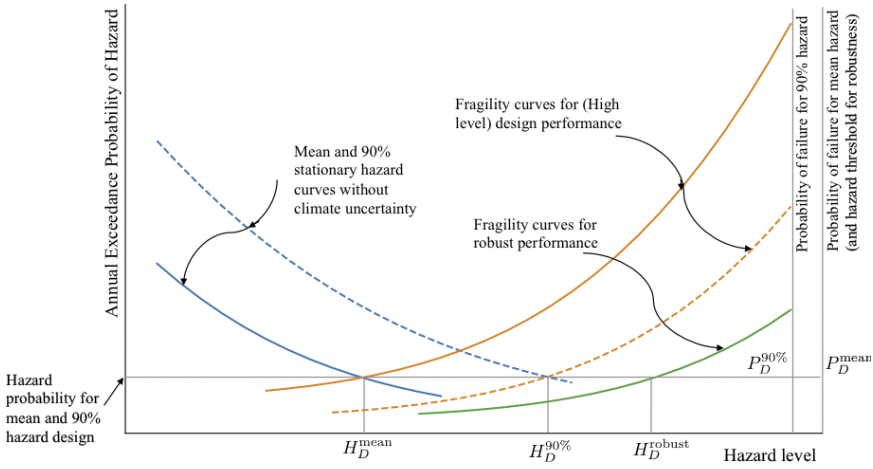

Figure 7-8. Uncertainty-tolerant robust design concepts.

time and flexibility to make needed changes. A climate change risk management program can be incorporated into an organization's asset management program. An asset management system is a "strategic and systematic process of operating, maintaining, upgrading, and expanding physical asset effectively throughout their life cycle" (FHWA 2012). Asset management programs usually collect performance data over the life cycle of a system that can be used to evaluate the system's performance under new and changing conditions.

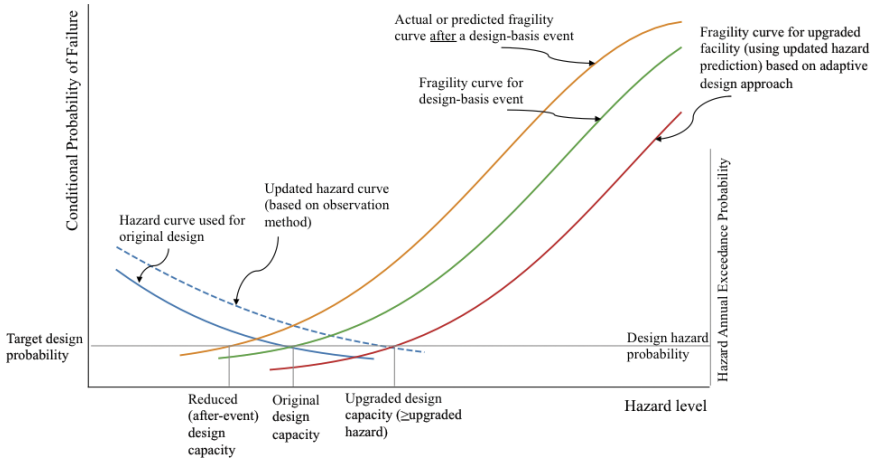

Figure 7-9. Adaptive design updates from a fragility and hazard perspective.

This section offers a high-level methodology for adaptive risk management by building and calling on previous sections. Figure 7-10 shows the following primary steps:

- Context and Objectives
- Hazard Identification and Projection
- Uncertainty Analysis
- Extreme-Value Analysis
- Failure Probability Estimation
- Exposure and Loss Analysis
- Economic Valuation
- Risk Quantification as Loss Exceedance Probabilities
- Development of Feasible Design Adaptations
- Cost and Benefit Estimation and Analysis
- Risk-Informed Decision Analysis
- Hazard and Risk Monitoring
- Risk-Informed Adaptation Analysis for Actions During Life.

Some of the steps of the methodology might require information that is unavailable. In such cases, expert opinion elicitation could be used (Ayyub 2014b).

The methodology is a top-down approach that starts with the climate scenario and projections. The steps are described briefly in subsequent section.

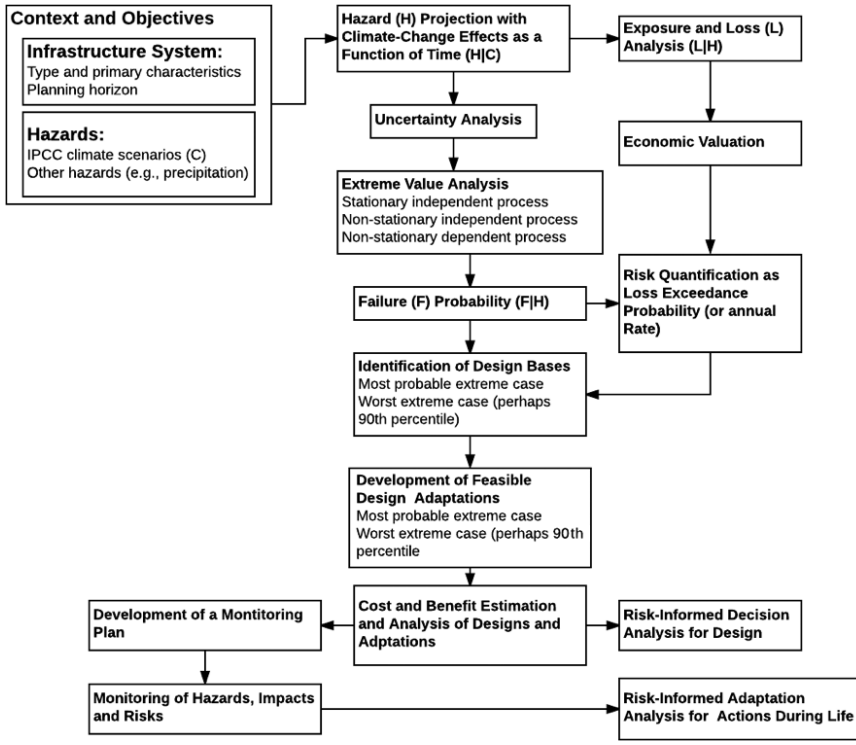

Figure 7-10. Risk-based adaptive design.
Source: Adapted after Stewart and Deng (2015).

7.5.1 Context and Objectives

The context should be defined for the particular system under consideration based on its planning horizon and performance requirements. A suitable climate-specific context could be identified to include selecting appropriate future climate projections corresponding to carbon emission scenarios in relation to changes in population, economy, technology, energy, land use, and agriculture. The uncertainty associated with this context definition falls under the latter types defined in Section 7.1. More than one projection can be identified and used. Adaptive methods are well suited for uncertainty type.

A project-specific context includes selecting project-related key parameters such as an appropriate planning horizon or design life, discount rate, and so on.

Decision- and objective-related contexts include decision criteria, the risk attitude of a decision maker, and any policy- or budgetary-related constraints.

7.5.2 Hazards Identification and Quantification

The list of hazards requiring consideration is context-dependent. Chapter 2 describes climate-related key hazards. Quantifying the probabilities and intensities of such hazards requires the use of uncertainty analysis, a non-stationary stochastic process, prediction methods, extreme-value analysis, and so on. Some of these methods are described in Chapter 4. Uncertainty quantification is necessary to establish bounds on such estimates, such as confidence intervals or interval probabilities. Some of the information needed might be unavailable. In such cases, expert opinion elicitation could be used (Ayyub 2014b).

Available key data sources are listed in Chapter 8.

7.5.3 Prediction of Extremes

Chapter 4 introduces the fundamentals and offers guidance on the prediction of extremes.

7.5.4 Failure Probabilities

Estimating failure probabilities associated with hazards, events, or event scenarios required for a particular decision situation depends on the information available for the investigation. Methods can be classified as analytical approaches, statistical techniques, and Bayesian treatment that brings together subjective and objective information. Methods for computing failure probabilities and developing fragility curves are well established; see, for example, Ayyub (2014b).

7.5.5 Exposure and Consequences

Failures result in consequences and associated severities. Their extent depends on the exposure of populations, property, and the environment. Economic valuation is necessary to accumulate the losses in monetary terms over a planning horizon using an appropriate discount rate. Lee and Ellingwood (2016) provide discussion that could guide analysis for intergenerational life-cycle risk assessment of civil infrastructure exposed to hurricanes under climate change.

7.5.6 Risk Quantification and Associated Economics

Quantifying climate risk for a system brings together the probabilities and consequences in terms of a loss (L) random variable as follows:

$$L = \sum_{t=1}^{T} \left(\sum P(E)P(H|E)P(F|H)(L|F)\mathrm{e}^{-\mathrm{i}t} \right) \tag{7-16}$$

where

L = loss (L) at time t;

$P(E)$ = probability of an event (E) or climate-related scenario at time t;

$P(H \mid \mathrm{E})$ = annual probability of a hazard (H) under the conditions defined by E;

$P(F \mid H)$ = probability of a failure (F) upon the occurrence of H;

$L \mid F$ = loss (L) upon the occurrence of F; and

i = annual discount rate.

Accumulating the loss estimates from Equation 7-16 over all the scenarios, that is, as represented by the inner summation sign, with an appropriate discount rate (i) over a planning horizon (T), that is, as represented by the outer summation sign, produces a total loss random variable (TL) (Gilbert and Ayyub 2016).

Risk management is typically based on the associated economics of improvement options identified for a particular situation—in other words, the cost-effectiveness of a proposed option for reducing the risk associated with the situation. As an example, in the context of SLR and extreme storms, countermeasures aim to reduce vulnerabilities of coastal lines, property and asset exposure, impact on resources and populations, and land use changes. Consequence mitigation strategies aim to reduce the potential consequences given the occurrence of a successful scenario (Ayyub 2014b). The probability of realizing a favorable benefit-to-cost ratio can be represented as follows:

$$P\left(\frac{Benefit}{Cost} \geq 1\right) = 1 - P(Benefit - Cost \leq 0) \tag{7-17}$$

where both benefit and cost in Equation 7-17 are random variables. With the knowledge of their underlying distributions, the probability of realizing a favorable benefit-to-cost ratio can be computed using reliability assessment techniques, including Monte Carlo simulation. It should be noted that the uncertainty associated with the benefit is typically greater than the uncertainty associated with the cost of the strategy.

7.5.7 Monitoring and Adaptation Decisions

Adaptation decisions require the identification of strategies for risk reduction. These strategies might call on technologies. Appendix D provides examples of such technologies. Additional information might also be necessary for the purpose of examining the economics of emerging situation(s) as identified by data collected on the environment or the project or climate information updates. Monitoring using visual examination or through project-based or satellite-based sensors, as examples, could provide this necessary information. The methodology as provided in Figure

7-10 provides a basis for examining the economics of potential actions or solutions, some of which could have been already identified in the design phase of a project using an adaptive design philosophy.

7.5.8 Decision Making under Uncertainty

This MOP covers several methods for decision making under uncertainty, such as RDM in Section 7.2 or minimize–maximum regret in Section 7.4. Other methods include climate-informed decision scaling, safety factors, and so on.

7.6 TARGET RISK LEVELS AND RISK RATING SYSTEM

7.6.1 Target Risk Levels

Several considerations affect how much risk to undertake in designing a system, such as the importance of the system, political and legal constraints, and the economics associated with the costs and benefits for the system. ASCE has dealt with this issue in its standards, such as ASCE/SEI 7 (2010). A similar approach is adopted herein on the extent of analysis to be undertaken for adaptive design and risk management. Table 7-2 provides the risk categories and their definitions as used in ASCE/SEI 7 (2010). Tables 7-3 and 7-4 provide recommended levels of climate analysis as a function of design life and risk category and the characteristics of various levels of climate analysis.

7.6.2 Risk Rating System

The vast majority of urban building stock is constituted of structures that are not designed for flood resistance and are therefore vulnerable to future storm events. In an ideal world, cities would implement global protection systems to simultaneously protect a large number of assets. The cost and political discussions surrounding global strategies make them ultra-long-term endeavors. For that reason, individual entities must be upgraded in the short term to meet potential threats. From a purely qualitative perspective, there are some assets that are more critical than others—damage to a hospital is more problematic than damage to a storage facility—and therefore warrants more attention.

In an effort to provide a standardized criterion to gauge the relative risk to a given asset, a rating system based on a variety of factors related to occupancy, service life, and localized flood probability is warranted. The proposed system outputs a CI value, which is overall qualitative in nature as opposed to a traditional direct monetary value. This system can be utilized

Table 7-2. Risk Categories of Buildings and Other Structures for Flood, Wind, Snow, Earthquake, and Ice Loads (ASCE/SEI 7 2010).

Use or occupancy of buildings and structures	Risk category
Buildings and other structures that represent low risk to human life in the event of failure.	I
All buildings and other structures except those listed in risk categories I, III, and IV.	II
Buildings and other structures, the failure of which could pose a substantial risk to human life.	III
Buildings and other structures not included in risk category IV with potential to have a substantial economic impact and/or mass disruption of day-to-day civilian life in the event of failure.	
Buildings and other structures not included in risk category IV (including but not limited to facilities that manufacture, process, handle, store, use, or dispose of such substances as hazardous fuels, hazardous chemicals, hazardous waste, or explosives) containing toxic or explosive substances where the quantity of the material exceeds a threshold quantity established by the authority having jurisdiction and is sufficient to pose a threat to the public if released.*	
Buildings and other structures designated as essential facilities.	IV
Buildings and other structures, the failure of which could pose a substantial hazard to the community.	
Substances such as hazardous fuels, hazardous chemicals, or hazardous waste that contain sufficient quantities of highly toxic substances where the quantity of the material exceeds a threshold quantity established by the authority having jurisdiction and is sufficient to pose a threat to the public if released.*	
Buildings and other structures required to maintain the functionality of other risk category IV structures.	

*Buildings and other structures containing toxic, highly toxic, or explosive substances shall be eligible for classification to a lower risk category if it can be demonstrated to the satisfaction of the authority having jurisdiction by a hazard assessment as described in Section 1.5.3 that a release of the substances is commensurate with the risk associated with that risk category.

Table 7-3. Recommended Level of Climate Analysis as a Function of Design Life and Risk Category.

	Design life <30 years	Design life 30–75 years	Design life >75 years
Risk category I	Climate analysis level I	Climate analysis level I	Climate analysis level II
Risk category II	Climate analysis level I	Climate analysis level II	Climate analysis level III
Risk category III	Climate analysis level I	Climate analysis level III	Climate analysis level IV
Risk category IV	Climate analysis level II	Climate analysis level IV	Climate analysis level IV

Table 7-4. Characteristics of Various Levels of Climate Analysis.

Level of climate analysis	Characteristics
Climate analysis level I	Use of published values of weather and climate extremes based on historical observations is appropriate
Climate analysis level II	Use of published values of weather and climate extremes based on historical observations and climate projections is appropriate
Climate analysis level III	Use of published values of weather and climate extremes based on historical observations and climate projections is appropriate, assuming independent analysis of sensitivity to uncertainty in projections is acknowledged and accounted for
Climate analysis level IV	Independent, transparent, and rigorous analysis of risk posed by future weather and climate extremes based on historical observations and climate projections is appropriate

to make informed decisions on a larger scale about the allocation of resources and the associated risk reduction to target the most vulnerable areas within a given spectrum of assets. The CI value is used simply to numerically rank an asset *before and after* potential storm mitigation measures are considered to determine a relative *best value* for resource allocation.

The rating for an individual asset aims to capture the relative risk based on the critical factors associated with its use and potential loss. The rating system is consistent with the traditional Equation 7-16 but with specific climatic factors defined to establish the qualitative CI relative to the baseline-defined event (E) resulting in

$$CI = \sum_{i=1}^{N} [P_i V_i (I_i + D_i)] \tag{7-18}$$

where

P = annual probability of a flood event at the asset in question;

V = vulnerability of the asset in question based on existing resiliency measures and their ease of implementation; and

$I_i + D_i$ = loss, consisting of the asset value representing its importance (I) and its expected direct loss (D).

P combines flood zone and recurrence interval data, and it should include a provision for projected SLR as discussed previously in this manual. The CI can be established for a single asset or a summation of assets depending on the user. The formula has the flexibility to establish a single CI for each building within a complex of buildings, allowing prioritization of hardening within a single complex. Alternatively, a single CI can be established for an entire complex of buildings so that it can be ranked against another complex of buildings to establish which is more vulnerable. As a broad example, the formula can prioritize vulnerable assets within a single city or prioritize which city is more vulnerable based on its summation of individual assets.

Tables 7-5 to 7-7 provide example input parameters to generate importance, vulnerability, and loss risk ratings for multiple elements within a given asset class. The parameters selected should be based on the scale of the asset/component class under consideration and should be revisited for project-specific scale. It is important that the attributes of the assets in a given asset class are consistent so that an "apples to apples" comparison can be made for prioritizing resources (e.g., design, funding, etc.).

$$P = 250\, Z\, (RI)^{-1} \tag{7-19}$$

where

P = flood probability for asset or component;

RI = lowest return of flood affecting asset or component; and

Z = factor for flood zone ($Z = 2.0$ for V zone or Coastal A zone, $Z = 1.0$ for other).

$$I = 0.20 i_1 + 0.40 i_2 + 0.40 i_3 \tag{7-20}$$

where

I = importance rating for asset or component;

i_1 = rating for remaining service life;

Table 7-5. Asset Importance Rankings (I).

Category/ value	0	1	2	3	4	5
Remaining service life (i_1)	0 years	10 years	25 years	50 years	75 years	100+ years
Impact on human life (i_2)	None	Minimal (i.e., minor inconvenience)	Disruption of everyday life (e.g., cannot commute)	Disruption of basic needs (e.g., short-term power outage)	Removal of life necessities (e.g., ability to obtain heat, water, food, shelter, etc.)	Imminently hazardous to human life
Number of people affected (i_3)	0–100	101–500	501–1,000	1,001–5,000	5,000–10,000	>10,000

Table 7-6. Asset Vulnerability Rankings (V).

Category/value	3.0	3.5	4.0	4.5	5.0
Existing storm-resilient measures (v_1)	Dry flood-proofed	Wet flood-proofed	Pumping + openings sealed	Openings sealed	None
Implementation of storm-resilient measures (v_2)	Automatic deployment	Automated deployment	Easy manual deployment	Difficult manual deployment	None

Table 7-7. Asset Direct Cost Rankings (D).

Category/value	0	1	2	3	4	5
Cost of repair or replacement (d_1)	<$100,000	< $500,000	< $1,000,000	< $10,000,000	< $50,000,000	> $50,000,000
Downtime if threat occurs (d_2)	None	< 3 days	< 6 days	< 9 days	< 12 days	> 12 days

i_2 = rating for impact to human life; and
i_3 = rating for the number of people affected.

$$V = 0.50v_1 + 0.50v_2 \tag{7-21}$$

where
V = vulnerability rating for asset or component;
v_1 = rating for existing storm-resilient measures; and
v_2 = rating for implementation of resilient measures.

$$D = 0.50d_1 + 0.50d_2 \tag{7-22}$$

where
D = direct cost for asset or component;
d_1 = rating for cost of repair or replacement; and
d_2 = rating for downtime.

7.7 LIFE-CYCLE COST ANALYSIS

The life-cycle cost of an infrastructure asset such as a roadway or bridge is the present-value total costs of building, maintaining, and decommissioning the asset. LCCA is a recognized analytical process to support infrastructure decisions. Infrastructure investments typically involve large initial capital outlays, followed by subsequent smaller rehabilitation costs that may represent sustainment, restoration, or modernization investments. A stylized example of these financial flows over time is presented in Figure 7-11.

Construction and maintenance costs vary according to the type of infrastructure, the materials chosen, environmental factors, and how people use the infrastructure. In roadway design, for example, rigid pavement typically has higher initial costs than flexible pavement. However, flexible pavement might have a shorter service life and require more frequent

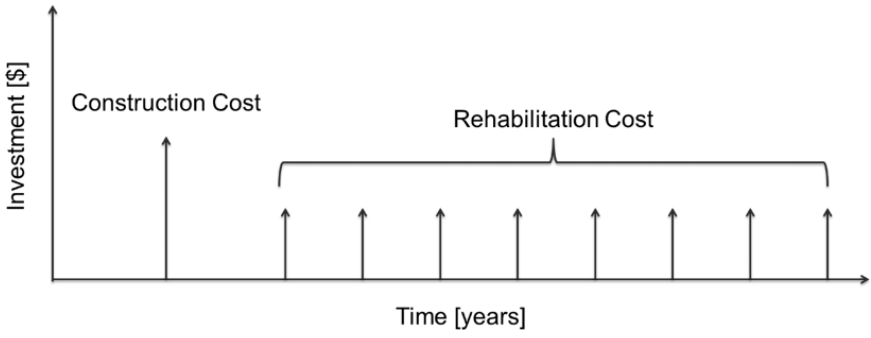

Figure 7-11. Example of infrastructure investments over an asset's life cycle.

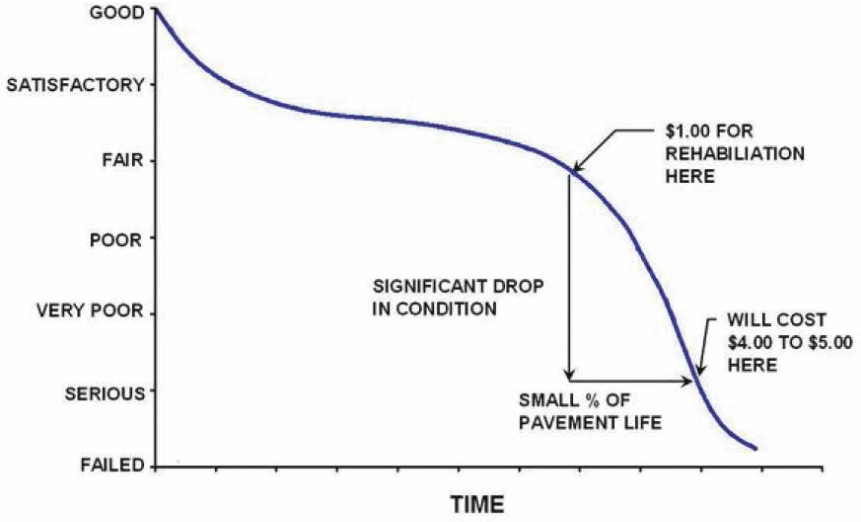

Figure 7-12. Infrastructure deterioration and costs are not linear.

maintenance investments. LCCA methods can inform which option has a lower life-cycle cost over comparable service lives at the design choice phase. LCCA can also inform the timing of rehabilitation options for an infrastructure asset, as shown in Figure 7-12. Minor repairs can be performed sooner to avoid further deterioration that usually results in higher costs. Nevertheless, it is necessary to find a balance to avoid wasting resources by performing unnecessary repairs and also preserve the pavement to prevent more costly rehabilitation practices in the future. Frangopol et al. (1997) suggested a lifetime optimization methodology for planning the inspection and repair of structures that deteriorate over time and illustrated it through numerical examples. The optimization is based on minimizing the expected total life-cycle cost while maintaining an allowable lifetime reliability for the structure.

Methods from infrastructure asset management and LCCA have been adopted by state departments of transportation, airport authorities, military construction agents, and other entities. These methods assist decision makers allocating scarce resources available for infrastructure maintenance and reinvestment. Current infrastructure asset management methods utilize measurement of facility condition and modeling to forecast facility condition by simulating the effects of age, use, prior investments, and other factors. These conditions themselves are subject to inherent uncertainty, and Markov decision processes and other methods can assist in managing uncertainty in infrastructure asset management (see, for example, Madanat 1993).

Durable infrastructure must perform under future climate conditions and climate-influenced usage that deviates from the historical data now populating infrastructure asset management models and assumptions. Climate change impacts, such as SLR, storm surges, unexpected precipitation, hotter temperatures, and others are potential vectors of infrastructure failure and should be taken into consideration in infrastructure asset management models when appropriate. If infrastructure is planned, designed, constructed, and managed based on historical data, some infrastructure will fail as climate change impacts exceed planned risks. Therefore, it might make sense to adjust previously estimated optimal maintenance schedules if climate change impacts alter the infrastructure's potential performance or useful life.

Asset management is defined by the ISO 55000 standard as the "coordinated activity of an organization to realize value from assets" (ISO 2014). The realization of asset value usually balances costs, risks, opportunities, and performance (ISO 2014). Developing a strategic asset management approach for infrastructure where climate change risks and uncertainties are incorporated is essential for agencies and stakeholders. According to the 2017 *ASCE Infrastructure Report Card*, current US infrastructure is rated as a "D+" (ASCE 2017). This grade highlights the deficit of coordinated maintenance and reinvestment, which would be improved through coordinated asset management. The current infrastructure deficit and any reinvestment plans have largely developed without considering the additional stressors from climate change on durable infrastructure. Strategic asset management plans are needed for infrastructure that includes an understanding of the impacts of climate change.

The DOT, in alignment with the Moving Ahead for Progress in the 21st Century Act (MAP-21) legislation, requires state DOTs to produce risk-based transportation asset management plans (TAMPs). States need to assess the criticality of their assets in order to allocate their budgets more efficiently. In developing TAMPs, state DOTs should account for climate risks as presented in the *Climate Change and Vulnerability Framework* (FHWA 2014). The 2014 Transportation Asset Management Peer Exchange concluded that the ". . . overall goal is to ensure systematic consideration of climate change and extreme weather vulnerability and risk in transportation decision making . . ." (FHWA 2014). The DOT framework presented in Figure 7-13 allows state-level DOTs to incorporate vulnerability into their TAMPs.

Although the existing state DOT TAMPs should account for climate change variations, it is unclear how many states have begun this process. As a sample, New York, Colorado, Florida, Pennsylvania, and Wyoming TAMPs were analyzed to see whether they incorporated climate change or mentioned them in their plan. Neither Colorado nor Florida made any mention regarding climate change. New York acknowledged the risk of climate change and presented possible impacts, including more frequent

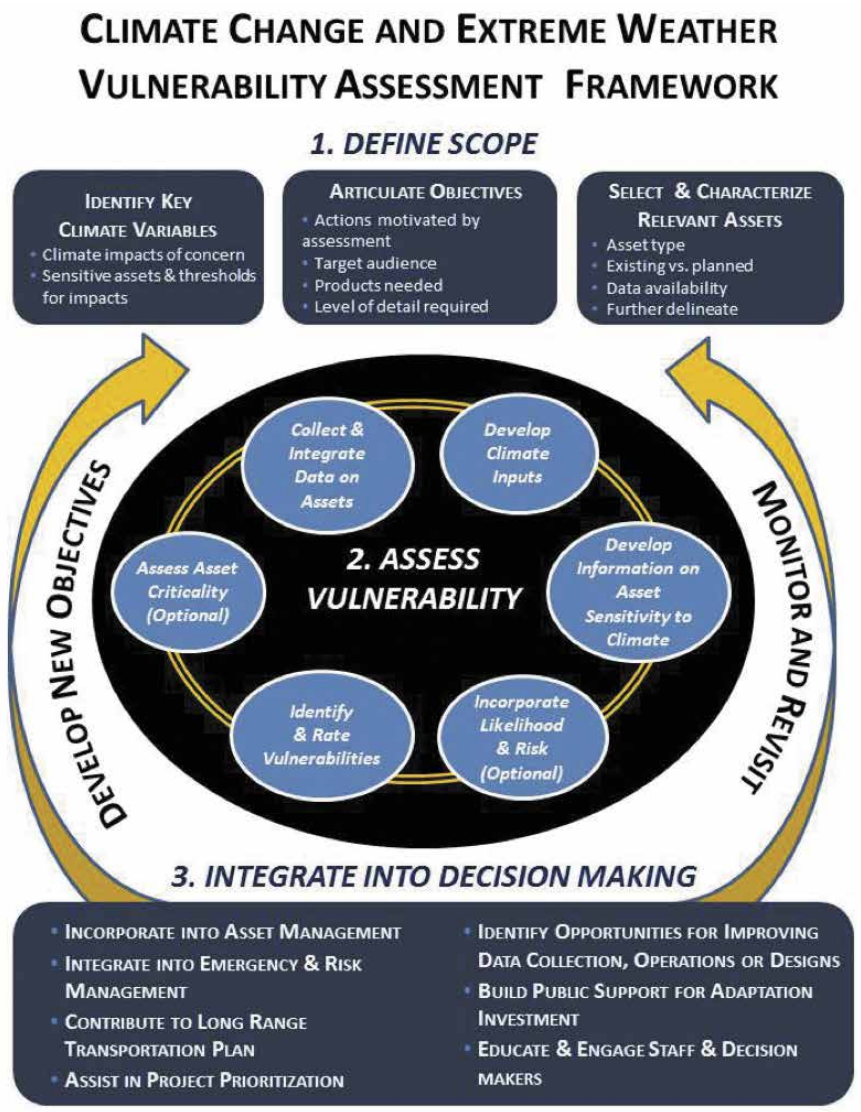

Figure 7-13. Vulnerability assessment framework (FHWA 2012).

severe flooding, storm-damaged assets, and increased costs of damaged assets. They also identified the responsible entity for each of the foreseen impacts. Pennsylvania's TAMP categorized the risk as "medium," thus acknowledging potential impacts of climate change in the state. It did not provide further details on strategies for addressing the impacts. The state

of Wyoming is still considering how to incorporate climate change into planning and design.

Meyer et al. (2010) presented generic asset management system components and explained how to potentially incorporate climate change. A generic asset management system should include (1) goals and policies, (2) asset inventory, (3) condition assessment and performance monitoring, (4) alternatives analysis and program optimization, (5) short- and long-range plans, (6) program implementation, and (7) performance monitoring. Meyer et al. (2010) suggested that an adaptive system management approach will be able to identify which assets are the most vulnerable to changes in the climate.

Climate change considerations would need to be incorporated into the system, initially with goals and policies identifying potential issues and vulnerabilities of the assets. Next, the asset inventory should be able to assess the criticality of the assets and their vulnerability to climate change events. Condition assessment and performance modeling could include risk appraisal into asset modeling and identify high-risk regions. For alternatives evaluation and program optimization, probabilistic approaches should consider uncertainties of climate change. Short- and long-range plans would need to include climate change into design parameters and determine the responsibility of the agency regarding it. Finally, program implementation and performance modeling should monitor how the agency is performing with regards to climate change and if the asset management system is able to cope with variable conditions (Meyer et al. 2010).

Some engineering papers have begun to address asset management and climate change. For example, Orcesi et al. (2016) presented a method to incorporate risk into asset management based on the probability for a component to move from a condition with a score q_1 to a score q_2. The areas of the elements are weighted (A) for the deterioration conditions. The k elements of the infrastructure are weighted with their respective areas over the change in the conditions.

$$P_b(q_1,q_2) = \frac{\sum_{i=a_0}^{a_f-1}\left(\sum_{k=1}^{n_{q_{1,i}\to q_{2,i+1}}} A^k_{q_{1,i}\to q_{2,i+1}}\right)}{\sum_{i=a_0}^{a_f-1}\left(\sum_{k=1}^{n_{q_{1,i}}} A^k_{q_{1,i}}\right)} \tag{7-23}$$

Orcesi et al. established two different types of failure: loss of serviceability and structural failure. Degradation matrixes are built around the probabilities and the degradation of the infrastructure. Climate change is included through the inclusion of extra degradation matrixes.

Alternatively, Huibregtse et al. (2016) presented a different methodology to assess risks through a case study of tunnel flooding in the Netherlands. A test case limit state is determined by the following equation, where V_{capacity} is the volume of the pump cellars of a tunnel, A is the area of the drainage

where the water is collected, Q_{pump} is the pump's capacity, and Δt is the duration of the rain event.

$$Z = V_{\text{capacity}} - (Aq_{\text{shower}} - Q_{\text{pump}})\,\Delta \tag{7-24}$$

The tunnel would fail when the limit state (Z) is lower than 0 and that would represent loss of serviceability for the tunnel. The probability of failure can be calculated through Monte Carlo simulations. Rain intensity is modeled with existing information and a distribution is fitted. For the incorporation of climate change, the paper relies on structured expert judgment. The consequences are modeled with a traffic tool called quick scan. A different threshold is determined for highway roads and regional roads. The consequences associated with highway serviceability loss are 25 times greater than the consequences associated with regional roads. The accepted probability of failure is then adjusted with this multiplier for each of the roads considered.

In addition, LCCA is generally included in state TAMPs. LCCA is an economic "... technique that is used for predicting and assessing the cost performance of constructed assets" (ISO 2008). LCCA should have a probabilistic approach rather than the typical deterministic approach when considering climate change impacts because of uncertainties in their magnitudes and the timing of several types of impacts. Although a deterministic approach could account for variations with a sensitivity analysis, this provides a limited perspective because it only allows for changing one parameter at a time. When accounting for climate change, deep uncertainties need to be considered and managed. Through probabilistic LCCA, a broad range of possible outcomes is assessed and a range of scenarios can be analyzed.

Swei et al. (2016) performed LCCA for pavements with a probabilistic approach using Monte Carlo simulations. Although many analyses have been performed for pavements, few of them incorporated the variability of the costs. Swei et al. (2016) predicted the maintenance schedule of the pavements with a tool called MEPDG. Performance levels were established through existing standards and a Gaussian distribution was fit. Future material costs were modeled with economic probabilistic forecasts. Other inputs that were more difficult to model and with more unknown uncertainties were modeled to account for two different uncertainties: basic uncertainty, which is the variation and stochastic error resulting in the processes changing, and additional uncertainty, which depends on the temporal, geographic, and technological correlations as reliability in the data. The final LCCA cost was determined through Monte Carlo simulations (Swei et al. 2013). Three different metrics were used to compare different project alternatives: the relative mean difference of alternatives ($\Delta\mu$), the difference between the alternatives from a risk-averse perspective (α_{90}), and the prob-

ability that one design has a lower–higher cost than another (β). The equations are presented as follows (Swei et al. 2016).

$$\Delta\mu = \frac{\text{mean cost}_{\text{alt.B}} - \text{mean cost}_{\text{alt. A}}}{\text{mean cost}_{\text{alt.A}}} \tag{7-25}$$

$$\alpha_{90} = \frac{90\%\,\text{cost}_{\text{alt.B}} - 90\%\text{cost}_{\text{alt.A}}}{90\%\text{cost}_{\text{alt.A}}} \tag{7-26}$$

$$\beta = \text{probability}\left(\frac{\text{cost}_{\text{alt. B}} - \text{cost}_{\text{alt. A}}}{\text{cost}_{\text{alt.A}}} > 0\right) \tag{7-27}$$

7.8 REAL OPTIONS FOR RISK MANAGEMENT

Real options include opportunities to expand and cease projects if certain conditions arise, among other options. They are *real* because they usually pertain to tangible assets such as capital equipment or infrastructure rather than to financial instruments. Valuation methods such as NPV should include the benefits that real options may provide.

7.8.1 Core Principle

The core principle is that value is attached to flexibility. Therefore, a real option analysis includes the identification of opportunities for incorporating flexibility into the decision-making process. In addition, changes to an investment decision when new information arises may include (1) delaying the investment, (2) abandoning, (3) switching, (4) expanding, and so on.

7.8.2 Analytical and Computational Methods

Varied analytical and computational methods are available for this purpose, including the following: (1) risk analysis for scenario definition, probabilities and consequences, (2) probability trees for scenarios, (3) engineering economics for valuations, and (4) Bayesian methods for updating probabilities based on additional information.

7.9 COASTAL ADAPTIVE DESIGN AND ADAPTATION

This section showcases adaptation methods widely used in vulnerable coastal regions dealing with climate change, in particular, SLR and storm surge. These engineered adaptation methods include offshore barriers, coastal armoring, elevated development, floating development, floodable development, living shorelines, and managed retreat. Adaptation is issue- and location-specific, and so are potential solutions. These adaptations can be summarized into four actions: accommodate, protect, retreat, and exploit opportunities. Accommodate, or *living with the water*, would include adaptations such as elevating structures, improving flood control/structure design, or enhancing living shorelines. The second type of adaptation action, protection or *keeping the water out*, includes using harder or softer approaches to keep the water away from a community. The third action, retreat or *moving away from the water*, involves an action such as managed retreat. Finally, when a new adaptation method is developed, it is important to exploit opportunities that may exist. For instance, after a flood and relocation effort, a greenway or golf course could be created in the flooded area where a residential or commercial district once existed.

7.9.1 Adaptive Retreat

Managed retreat is a planned abandonment to safely remove a community or structures from encroaching shorelines, allowing the shoreline to advance unimpeded. This includes abandoning efforts to control shoreline erosion, demolishing buildings, and moving existing buildings and infrastructure to higher ground. This can also include buy-back programs to compensate property owners for loss and strict building codes that allow only certain types of relocatable structures. It also includes the banning of new development in areas likely to be inundated. Managed retreat is used when coastal armoring or other shoreline protection methods become too expensive or are unable to adapt to the encroaching shorelines.

There are several advantages to managed retreat. The first is because of new construction setback rules that are usually established. New required distances from the water's edge are usually established to meet the setback standards of FEMA and adapt to the changing climate. The second advantage is that managed retreat has been successfully done with larger structures such as the Cape Hatteras lighthouse, which was moved inland from an eroding beach in the Outer Banks of North Carolina. Also, master plans have been developed for whole villages, such as the 2006 Kivalina Relocation Master Plan for Kivalina, Alaska, which involved looking at seven different sites for relocation. The third advantage is that possible rolling easements can be established that can vary landward from the rising sea level to allow for continued private property ownership and development.

However, there are also several disadvantages to managed retreat. The first is that managed retreat usually involves many hurdles with legal and equity issues, because not all property owners are willing to sell. The second disadvantage, and probably the most common, is that shoreline communities lack the adaptive capacity to relocate. For instance, there may be no room to expand or relocate, such as in San Francisco. Finally, managed retreat comes at a very high cost. An example of this was the estimated $150–250 million to move Kivalina, Alaska, to one of the seven selected sites (see 2006 Kivalina Relocation Master Plan). Not only do considerations such as location, construction costs, and engineering permitting need to be considered, but site cleanup, such as hazmat removal, is also needed following demolition, which significantly increases the cost.

Example 1—Adaptive Design of Relocation for Managed Retreat.

Example 1 showcases the feasibility and design of moving an entire existing village to seven different selected sites (USACE 2006). Figure 7-14 shows the seven proposed relocation sites. For such a project to be successful in the long term, a site must be feasible in terms of adapting to physical processes such as erosion, flooding, and weather; allow for construction and utilities development; and be acceptable to community residents.

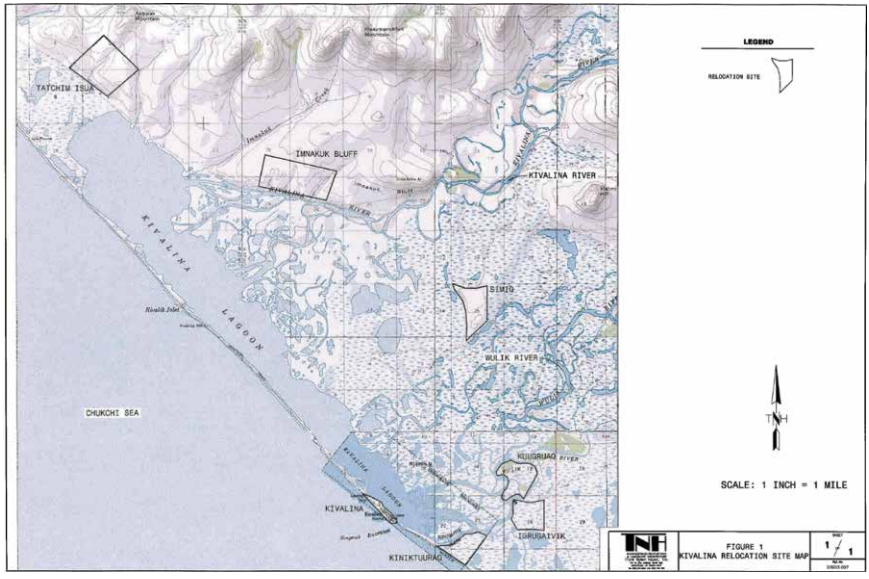

Figure 7-14. Potential seven relocation sites, outlined in black, Kivalina, AK. Source: USACE (2006).

The new town site for Kivalina, Alaska, is proposed to have the same site layout, gravel pad, and basic infrastructures, which include barge and boat landing, a water treatment and distribution system, a sewage collection and treatment system, a power generator system, an airport, landfill, public buildings, and housing. Although each town site contains the same basic infrastructure, there would be differences, such as location of the support facilities in relationship to the village gravel pad, the length of the road to access the landing facilities, the thickness of the village gravel pad, requirements for erosion and flooding control, and the design issues posed.

The phased construction of the infrastructure and relocation of the Kivalina community are proposed to take place over a 10-year period. The first facility to be constructed would be the gravel borrow site. After the borrow site is constructed, a pioneer road to the new runway location can be built. A barge landing should also be constructed early in the project to facilitate the landing of barges and offloading of equipment and materials. A boat landing should also be installed to support the construction camp and contractor staging area. Both the runway construction and new village pad construction should take approximately two to three years each to construct. Once the village gravel pad has been completed, construction of the community infrastructure can begin. The electrical plant should be constructed, followed by the bulk fuel facility. This scheduling of facilities should provide electrical power for the construction process early in the project. Construction following the power plant should begin with the water/wastewater treatment building and the infrastructure to transport raw water to the village and discharge wastewater to the lagoon. Water and sewer infrastructure can be installed concurrently with the construction of housing and public buildings in a phased program over the last three years of the buildout. During construction of the village, the two villages should function simultaneously because schools and office buildings will likely move first, followed by homes. Transportation between the new and old sites must be available for schoolchildren and for moving freight and supplies.

Table 7-8 shows the site ranking for the seven relocation sites. Of the seven alternative sites, Tatchim Isua received the highest overall point value and the highest value in all four categories except for physical environment (primarily because of uncertainty regarding water supply). Imnakuk Bluff took second place, with resolution of land status being the primary outstanding issue. Simiq scored in the middle because there were many unknowns regarding the site and the community had not previously considered it. The four southern sites, and particularly the two coastal sites (Kiniktuuraq and Existing), received lower values primarily because of continued long-term vulnerability to flooding and erosion and construction and utility factors. However, these sites received high scores in terms of social and access factors.

Table 7-8. Site Ranking for the Seven Relocation Sites, Kivalina, AK.

		Site						
	site has generally positive attributes associated with this specific criteria	Tatchim Isua	Imnakuk Bluff	Simiq	Kuuruaq	Igrugaivik	Kiniktuuraq	Existing Site
	site has mixed positive and negative attributes with specific criteria; or criteria is neutral							
	site has generally negative attributes associated with this specific criteria							
PHYSICAL ENVIRONMENT								
Storm surge vulnerability		5	5	5	3	3	1	1
River flooding vulnerability		5	5	5	2	2	3	3
Shoreline erosion vulnerability		5	5	5	2	2	1	1
Site drainage and wetlands		4	3	2	3	1	1	5
Soils—ice content		3	3	2	3	1	1	5
Vulnerability to high winds		1	1	3	3	3	3	3
Water supply—source and quality		4	5	2	2	2	1	1
Subtotal Physical Environment		**27**	**27**	**24**	**18**	**14**	**11**	**19**
CONSTRUCTION & UTILITIES FACTORS								
Sewage disposal availability		5	3	5	3	2	2	1
Ease of water storage and distribution		4	4	2	3	2	1	1
Solid waste disposal availability		5	5	3	1	1	1	1
Gravel requirements to develop site		3	3	2	2	2	1	2
Barge access/distance to site		3	2	1	2	2	5	5
Site for an airport with crosswind runway		4	3	4	3	3	3	2
Community expansion potential		5	5	4	2	2	2	1
Ease of maintaining two sites during construction		1	1	1	3	3	4	3
Permitting obstacles		4	4	3	2	2	2	3
Subtotal Construction and Utilities		**34**	**30**	**25**	**21**	**19**	**21**	**19**
SOCIAL AND ACCESS FACTORS								
Distance from current village site		1	2	3	4	4	5	5
Access to the ocean		3	2	1	4	4	5	5
Access to the Wulik River		1	1	1	5	5	5	4
Access to the Kivalina River		3	5	1	2	2	2	2
Access to the Kivalina Lagoon		4	3	1	4	4	5	5
Access to subsistence camps and traditional use areas		2	2	1	4	4	5	5
Location of boat/gear storage		2	2	1	5	5	5	5
Potential for ice cellar construction		3	3	5	5	5	5	2
General comfort with site		2	3	2	3	3	3	3
Land status		5	2	5	1	5	5	3
Subtotal Social and Access		**26**	**25**	**21**	**37**	**41**	**45**	**39**

Table 7-8. (Continued)

		Site						
	site has generally positive attributes associated with this specific criteria	Tatchim Isua	Imnakuk Bluff	Simiq	Kuuruaq	Igrugaivik	Kiniktuuraq	Existing Site
	site has mixed positive and negative attributes with specific criteria; or criteria is neutral							
	site has generally negative attributes associated with this specific criteria							
COST IMPLICATIONS								
[1] Site preparation costs		5	1	1	1	2	1	3
Access road development costs		4	2	2	3	3	4	5
[2] O&M costs		4	4	3	2	2	1	1
[3] Cost of living (heat, power)		2	2	2	3	3	3	3
Fuel costs for access to subsistence areas, airport, dock		1	2	2	3	3	4	4
Subtotal Cost Implications		**16**	**11**	**10**	**12**	**13**	**13**	**16**
COMPARATIVE TOTAL		**103**	**93**	**80**	**88**	**87**	**90**	**93**
RANK		**1**	**2**	**7**	**5**	**6**	**4**	**3**

[1]Site preparation cost estimates range from $155 to 252 million.
[2]O&M costs reflect differences in costs per village, mostly for maintaining erosion and flood barriers.
[3]Costs for heat and power are assumed to be higher in areas where terrain is subject to higher winds (hillside sites).
Source: USACE (2006).

A conceptual layout of Tatchim Isua is shown in Figure 7-15. It shows the proposed road, pipes, and improvements. It also shows the infrastructure facilities needed, such as water source, airport site, barge landing, sewage treatment, and landfill. The cost estimate to build a new village site at Tatchim Isua was estimated to be $154.9 million (Table 7-9).

Example 2—Adaptive Design of Expanding for Managed Retreat.

Occasionally, when relocating an entire village is cost prohibitive, another alternative is the gradual expansion of an existing community toward safer elevations. This adaptive design example provides a concept to construct an access road across Kivalina Lagoon from the community of Kivalina to

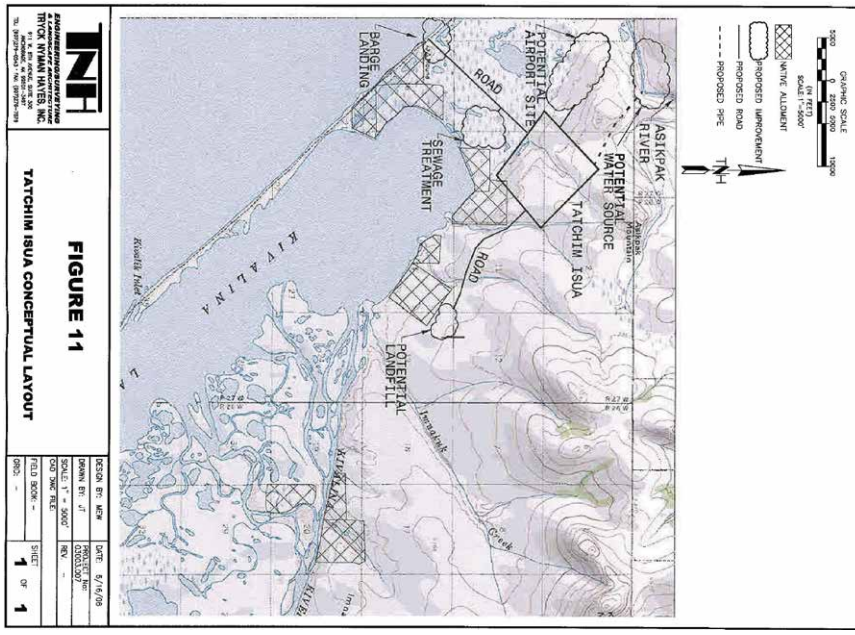

Figure 7-15. Tatchim Isua conceptual layout, Kivalina, AK. Source: USACE (2006).

the opposite shore near the mouth of the Wulik River, where there was no access road before. Figure 7-16 shows the Alaska Department of Transportation's (ADOT) concept of before and after examples of Kivalina, Alaska, under expansion (Smith 2008, Smith and Carter 2011). The proposed road would provide an evacuation route, a haul road for extra gravel as needed for beach nourishment, and a water main from the Wulik River. The proposed road would also include a 12 ft culvert for boat passage, fish migration and water circulation, located between the original village and new gravel pad island. Once the road is put in, upland construction could begin to allow the gradual expansion of the village. New construction would be raised above the 100-year surge elevation and a setback buffer (min. 50 ft) would be established along the shoreline to minimize damage from periodic storms and wave runup. Vegetative cover would also be re-established on coastal berms to help mitigate erosion. The new uplands could be constructed to keep pace with the growing demands of the community. Sand beach material could be initially used, which would transition to coarser gravel beach. The beach face would steepen and stability would increase. Because of the large amount of sediment transported through the area, periodic dredging would be required for maintenance.

Table 7-9. Tatchim Isua Design and Construction Cost, Kivalina, AK.

Site work and airport construction	$164,800,000
Erosion protection	$2,961,750
Construction camp	$606,000
Power and fuel	$5,292,000
Move buildings	$1,125,000
New buildings	$52,690,000
Water/sewer system and landfill	$18,146,638
Transportation system	N/A
Total Cost	**$245,600,000**

Source: USACE (2006).

Figure 7-16. Original concept plan view of Kivalina Lagoon–crossing causeway and bridge design, Kivalina, AK; left panel shows before; right shows after and includes a new gravel pad island with a small boat harbor and an evacuation center and water storage at the end of the causeway.
Source: Smith (2008).

A more recent development of this design was proposed by USACE (2016). The concept project included a road, a concrete bridge, a dredged bridge basin, and a storage pad on the mainland (see Figure 7-17). USACE (2016) defined the road more clearly, which included a 500-ft-long, one-lane concrete bridge consisting of four 125 ft spans of decked bulb tee girders, which would span the channel and adjacent area (see Figure 7-18). The bridge construction was estimated to take a minimum of four years to complete and require multiple mobilization cycles, with a project cost of $79 million because of the harsh environment and remote location.

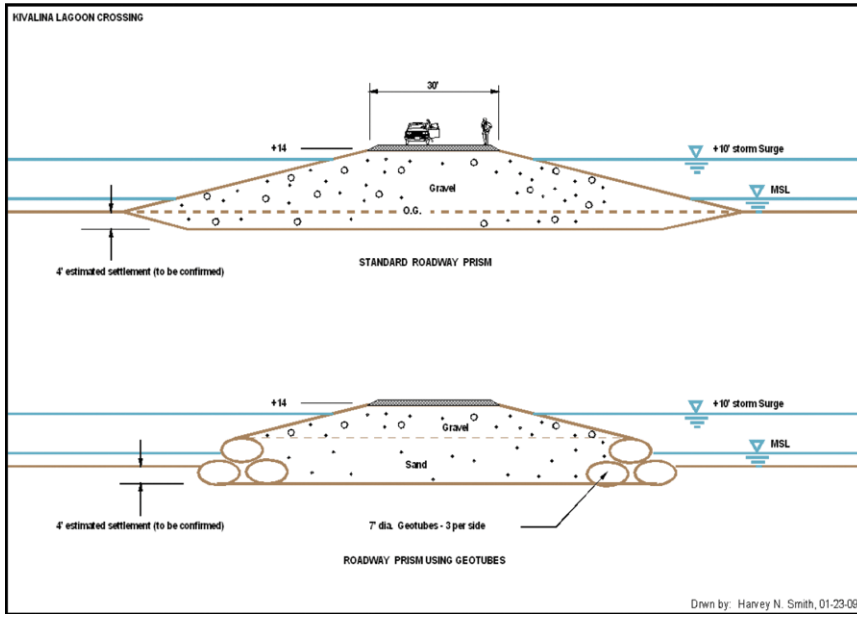

Figure 7-17. Original concept profile view of the Kivalina Lagoon–crossing causeway
Source: Smith (2008).

7.9.2 Accommodate

7.9.2.1 Elevated Developments. Elevated development raises the height of land or an existing structure. Structures can be built upon a shoreline with a low risk of flooding. Buildings can be elevated on fill, constructed with closed foundations (for example, crawlspace foundations, stem wall foundation, or slab-on-grade foundations), or constructed on open foundation (using piers, pilings, or columns). Foundations must be designed and constructed to resist all loads expected to act on the structure and its foundation during an event. This includes preventing flotation, collapse, and lateral movement of the structure. The foundation should also be able to accommodate expected scour and erosion throughout the life of the structure. Elevated development is most cost effective for new buildings, but it may also be good for retrofitting low-lying infrastructure, such as airports. Unfortunately, it is often a short-term strategy unless the structure is high enough to avoid eventual SLR. Also, unless elevated development sits directly over the water, the characteristics of the shoreline can change. Incorporating elevated development into the design of a new house adds $2,000 to $30,000 to the cost of the house, depending on its size and foundation

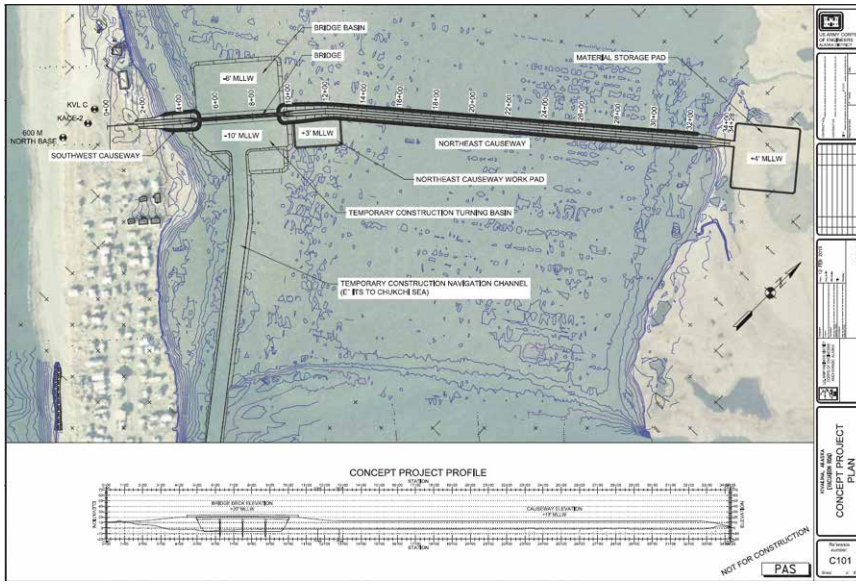

Figure 7-18. Recent concept plan and profile view of Kivalina Lagoon–crossing causeway and bridge design, Kivalina, AK.
Source: USACE (2016).

type, whereas raising an existing building can double this cost (NOAA 2013). So, in general, new construction costs are \$15–\$32/sq ft, whereas retrofitting costs are \$30–\$100/sq ft (Deyle 2012).

Example 3—Adaptive Design of Elevated Developments.

Buildings supported by driven piles or caissons in deep soil strata usually offer the greatest resistance to coastal hazards. An example is an elevated home in Dauphin Island, Alabama, shown in before-and-after photos in Figures 7-19(a) and 7-19(b), respectively (FEMA 2009). The pile foundation consisted of deep vertical piles installed to support the elevated structure. As shown in Figure 7-19(b), when the foundation is deep enough to retain sufficient strength, the vertical piles are inherently less susceptible to scour and erosion, even when exposed to conditions greater than those anticipated during an event. The piles rely primarily on the friction forces that develop between the pile and the surrounding soils (to resist gravity and uplift forces) and on the compressive strength of the soils (to resist lateral movement and maintain the structure stability). The soils at the ends of the piles also help resist gravity loads. Besides minimizing the footprint to avoid dynamically loading, piles also minimize thermal loading, providing an

Figure 7-19(a). Structure near collapse because of insufficient pile embedment before Hurricane Katrina, Dauphin Island, AL.
Source: FEMA (2009).

Figure 7-19(b). The same structure as that shown in Figure 7.19(a) after Hurricane Katrina, Dauphin Island, AL, with a successful pile foundation that supported the elevated home even after scour and erosion removed several feet of soil.
Source: FEMA (2009).

appropriate basis for using piles also in permafrost regions. Figure 7-19(b) illustrates the successful use of deep, open foundations.

7.9.2.2 Floating Developments. Floating development floats on the surface of the water, or they can be floated during a flood, which makes them mostly invulnerable to changing water levels. Floating development lacks propulsion and is moored to shore or anchored to the sea floor. Although small structures such as single-family homes are rather common, the challenge is in floating much larger forms of development such as airports, hotels, and restaurants. Structures can be built to float, whereas they often cannot be retrofitted. Utilities such as electricity, water, and wastewater are supplied to floating development through flexible pipes. The advantages of floating development are that it manages the uncertainty of varying water levels and earthquakes because it is resilient to seismic activity. However, floating development does not work in areas open to wind and wave action from storms, such as the open ocean. Although floating development has not yet been demonstrated in high-density cities, it is now being thought of as an SLR strategy for larger cities or islands. Floating development is expected to cost about the same as elevated development (NOAA 2013).

Example 4—Adaptive Design of Floating Developments.

The world's first floating city is set to appear in the middle of the Pacific Ocean. The floating city, to be located in a lagoon off the coast of Tahiti, would comprise environmentally sound floating platforms or *islands*, with all the necessary infrastructure to support a community at sea, while using adjacent land to accommodate a number of uses to serve the floating city. There are three phases for the construction of the Floating Island Project as proposed by the Seasteading Institute (2017) and Blue Frontiers (2018) in a report entitled "The Floating Island Project" according to EMSI (2017). With the project beginning in 2018, the floating city will be built in the most sheltered waters possible, such as behind a reef break, because the open ocean would make it cost prohibitive (Figure 7-20). The floating islands will feature aquaculture farms, health care, medical research facilities, and sustainable energy production facilities. In addition, nearby sections of land will be developed to support the infrastructure in the sea zone. The first phase would involve constructing 10 large floating platforms 82 ft × 82 ft (25 m × 25 m) and 5 small floating platforms 46 ft × 46 ft (14 m × 14 m) to create the first group of islands. These first islands will include residential units, workspaces, research facilities, communal spaces, a hotel, and a restaurant. In addition, 12.4 acres of land will be developed to include a staging area for platform construction, additional residential units, a communal workspace, and the first of the infrastructure needed to support the sea zone. The cost is

Figure 7-20. Floating Island Project, French Polynesia. Source: Blue Frontiers (2018).

estimated to be $50 million, and it will take two years to complete. For the second phase, 10 large floating platforms (25 m × 25 m) and 5 small floating platforms (14 m × 14 m) will create a second group of islands. These islands will include more residential units, workspaces, research facilities, communal spaces, and an advanced health-care facility. An additional 12.4 acres of land will be developed to include more residential units, expanded support infrastructure, and an advanced agricultural facility. The estimated cost will be $45.8 million, and it will take three years to complete. For the third phase, an additional 10 large floating platforms (25 m × 25 m) and 5 small floating platforms (14 m × 14 m) will create a third group of islands. These islands will include more residential units, workspaces, research facilities, communal spaces, and retail space. An additional 24.7 acres of land will be developed to further expand the land zone to include more residential units, expanded support infrastructure, and a resort hotel. The estimated cost will be $74.8 million, and it will take three years to complete.

7.9.2.3 Floodable Developments. Floodable developments are structures that are designed to withstand flooding or retain stormwater. One example includes infrastructure able to resist damage by occasional flooding. Another example is that it could serve as a backup strategy in case of

shoreline armoring failing. A third example is to create retention areas for storm surges or heavy rainfall. In the retention areas, water would be captured and then later released as an outfall or into the stormwater or wastewater system when floodwaters recede. Floodable development is form of LID in which stormwater is used by infiltrating into the ground, thus creating green space and habitat while reducing demands on wastewater treatment systems. New floodable development could be built to handle SLR, managing salt and/or fresh stormwater. The obvious disadvantage, of course, is that floodable development could be hazardous. Stormwater may be polluted with heavy metals, organic chemicals, and bacteria that could pose a public health hazard during a flood or leave behind contamination. This would be especially true in areas with combined sewer systems, where wastewater and street runoff go into the same system. New treatment methods will be needed for the released water to meet water quality standards if floodable development will be holding and releasing brackish water. It is also unknown if floodable development can be designed or retrofitted to accommodate occasional flooding in a cost-effective way. Armoring or investments in upsizing an existing wastewater system may be more beneficial depending on the site. Floodable development can be integrated into facilities at little to no cost for new construction (NOAA 2013).

Example 5—Adaptive Design of Floodable Developments.

Stormwater wetlands are a prime example of successful floodable development because it provides moderate-to-high pollutant removal, as well as implementing living shorelines, another adaptive design. Design criteria (Ellis et al. 2014) include a contributing drainage area of 35 acres, which is typically needed for wetlands (less when a groundwater connection exists) and requires a large, flat area in a single location. Extended detention above the permanent pool is also required for at least one-half in. of runoff. Furthermore, pretreatment (a sediment forebay) should be provided upstream of all stormwater wetlands. Typically, 70% of the wetland's surface area should be provided in *high marsh* areas of six in. depth or shallower, and approximately 25% should be in deep pools between 18 and 48 in. deep. The construction cost is low, and maintenance is generally medium. An example of this is shown in Figure 7-21 for a shallow wetland with extended detention.

The Jarvis Creek Park Stormwater Pond and Wetland Project (Figure 7-22, Ellis et al. 2014) uses a 13-acre lake that is capable of storing and conveying the necessary stormwater. In this case, a pump station was needed to move the water from the ditch to the lagoon. From the lake, water flows through a vegetated spillway that discharges into the headwaters of Jarvis Creek.

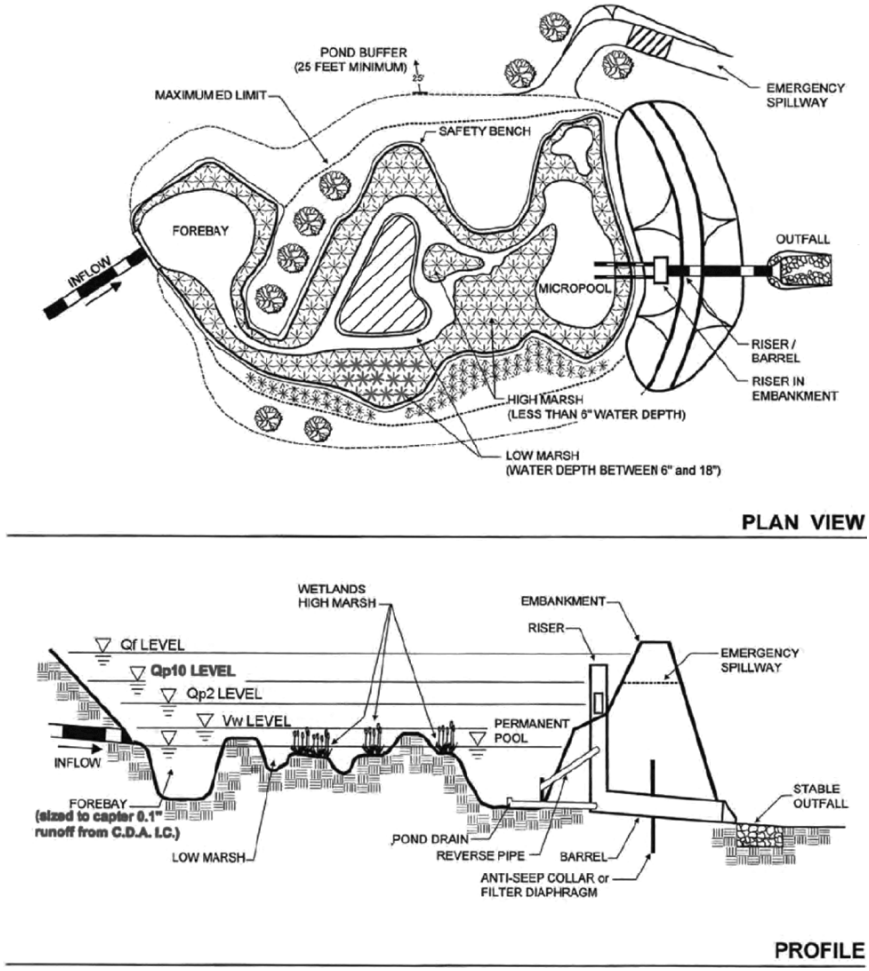

Figure 7-21. A schematic illustration of shallow wetland with extended detention (not to scale).
Source: Ellis et al. (2014).

7.9.3 Protect

7.9.3.1 Offshore Barriers. An offshore barrier is a large structure or a series of structures that manages flows in and out. The barrier may be fixed and allow managed flow through a portal for water exchange, tidal function, and navigation. Alternatively, it could be temporarily deployed just to head off the worst flooding during a storm surge. Barriers are able to protect a large area of land in a single sweep. However, they are expensive

Figure 7-22. Stormwater Pond at Jarvis Creek Park.
Source: Ellis et al. (2014).

to construct and can be ecologically damaging. Also, because it affects sedimentation, it could increase coastal erosion. Temporary barriers are often the most favorable because a barrier that holds back ocean storm surges is not likely to simultaneously function well in the other direction, which can cause upstream flooding.

Example 6—Adaptive Design for Offshore Barriers.

One of the most famous barriers is the Maeslantkering (Figure 7-23), built near the mouth of the sea, about a half-hour drive from downtown Rotterdam, Netherlands. The steel ball joints for each arm are about 30 ft in diameter and weigh 1.5 million pounds, and the storm surge barriers are about 70 ft tall (Sölken 2017). When the gate is closed, the arms float out onto the canal, where they meet and lock. The tubes fill with water and sink onto a concrete bed, forming an impenetrable steel wall against the North Sea. The gate closing takes 2.5 hours. Pressure from the sea is then transferred from the wall to the largest ball joints in the world, embedded in the banks on either side of the river. Computers monitor sea levels hourly and can shut or open the gate automatically.

7.9.3.2 Coastal Armoring. Coastal armoring is onshore linear protection, such as seawalls, that fix the shoreline in its current place. It is the most

Figure 7-23. Maeslantkering, Nieuwe Waterweg, closed.
Source: World66 (2011).

common tool used and can take on different forms depending on the kind of coastline needing protection. The most hardened form, such as engineered seawalls and bulkheads, protects the shoreline from strong wave action. Earthen levees protect low-lying land, usually from river flooding. Emergency armoring usually uses sandbags. The most common softer form, which is used to protect non-hardened shorelines, is beach nourishment. Beach nourishment is the adding of sand to maintain and restore eroding beaches, which also includes building or enlarging sand dunes. Other coastal armoring strategies include offshore breakwaters, which are built parallel to the shore to reduce wave action, and groins, which are built perpendicular to the shore to prevent erosion. Armoring is often used in combination with other strategies to protect infrastructure against both storm surge and baseline SLR. It can be designed to accommodate new development such as bike paths or housing along super levees or sand dunes that may protect threatened habitat. Coastal armoring is engineered only to accommodate up to a certain size of event. It requires costly maintenance and regular monitoring to ensure it stays safe. Structural armoring also gives people a false sense of security and encourages development in areas that are still vulnerable to flooding. Hardened forms such as seawalls and bulkheads have the largest capital costs at $10–$20 million/mi, with ongoing costs of about $1.5 million/mi every 20 to 25 years (Deyle 2012) or capital costs of $150 to $4,000 per linear foot (NOAA 2013). Beach nourishment, however, has lower capital costs of $4.3 million/mi (Deyle 2012) or $300 to $1,000 per linear

foot (NOAA 2013), but it requires re-nourishing every 2 to 6 years. It should be noted that armoring with structures such as seawalls typically protect land and infrastructure but often at the expense of the adjacent beach.

Example 7—Adaptive Design of Levee Improvements.

This example shows an eight-mile levee system in California that spans from the County of San Mateo boundary on the north to the O'Neill Slough Tide Gate at the San Mateo/Belmont boundary to the south (Schaaf and Wheeler 2016). The main function of the levee system is to provide flood protection; however, with the Bay Trail situated on top of or immediately adjacent to the levee, it also serves regional recreation. In adaptive design, in order to select the levee elevation for initial construction, capital costs were weighed against the design life and risk associated with a shortened design life because of higher-than-anticipated SLR. These are the predicted years when the FEMA freeboard would be lost or when physical overtopping in a 1% storm event would occur based on SLR projections through 2100. The economics of providing adaptive resilience to SLR was also assessed. One method to achieve this is to embed sheet pile wall sections for the projected Year 2100 loading with an 80-year design life and add to the wall height in the future. An alternate method is to embed sheet pile wall sections for a 2050 SLR load and with an 80-year design life, add to the wall height in the future, and construct a secondary anchor wall to accommodate transferred loads from the floodwall, as shown in Figure 7-24.

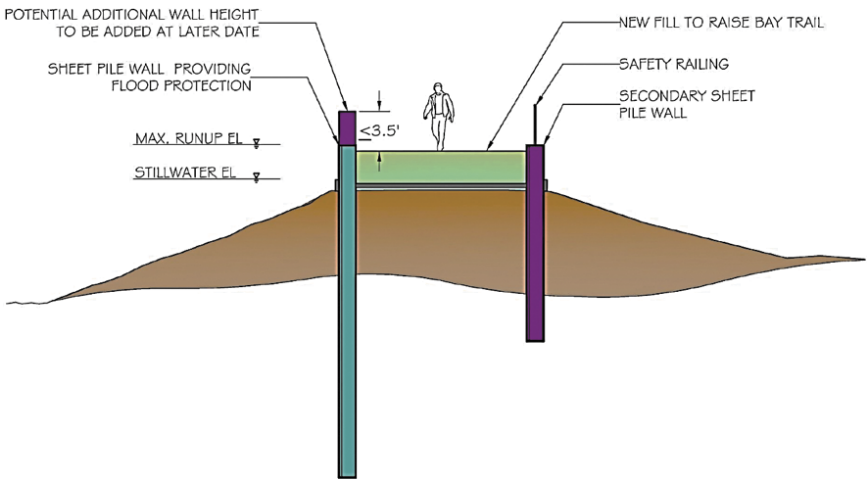

Figure 7-24. Foster City, CA, concept for levee adaptation to SLR. Source: Schaaf and Wheeler (2016).

7.9.3.3 Living Shorelines. Living shorelines are the natural form of shoreline that has the ability to absorb floods, slow erosion, and provide habitat. Living shorelines are essential for healthy estuaries, and they take on various forms, depending on the characteristics of the surrounding waterways. Living shorelines are able to filter pollutants out of water and create critical habitat for fish, wildlife, and millions of organisms, and they are the basis of aquatic food chains. They also provide a recreational open space. Living shorelines require time to develop, which includes management, monitoring, and time to become established. They also require space to grow. Living shorelines are naturally adaptive to SLR if they have space to migrate landward and are supplied with enough sediment to keep pace with SLR. Living

Figure 7-25. Shoreline stabilization projects in North Carolina illustrating the living shoreline approach. (a) Project to replace failing seawall included fill, marsh transplanting, and rock sill; here shown 2 years post-construction. (b) Project to protect the marsh edge, which included rock sill, no fill, and minimal transplants; here shown 4 years post-construction. A drop-down in the sill provides marsh access to nekton. Oysters can be seen colonizing the lower rock surfaces. (c) Project to protect eroding sandy beach includes only natural habitats, achieved with salt marsh transplants and oyster reef restoration; shown here 4 years post-installation.
Source: Currin et al. (2010).

shorelines require modest capital costs at $2.5 million/mi with armoring and $0.25–$1.05 million/mi without armoring (Deyle 2012). Wetlands, for example, include restoration costs between $3,500 and $80,000 per acre, excluding land costs, and construction typically costs between $35,000 and $150,000 per acre, excluding land costs (NOAA 2013). Living shorelines are self-sustaining without armoring, which makes them one of the most attractive means of protection.

Example 8—Adaptive Design for Living Shorelines.

Living shorelines as stand-alone projects or with hardened approaches have been successfully implemented worldwide. Several US states have already implemented regulatory processes designed to encourage or require the use of a living shoreline approach instead of hardened protection. A successful example of this is given in Currin et al. (2010), who reported living shorelines in North Carolina that have been successfully implemented. Their paper reviewed the adverse impacts from bulkheading on those habitats and described alternative approaches to shoreline stabilization, which minimized adverse impacts to the shoreline ecosystem. These efforts ranged from maintaining or transplanting natural shoreline vegetation without additional structural components to incorporating shoreline vegetation with hardened features, such as rock sills or wooden breakwaters, in settings with higher wave energy [Figures 7-25(a), 7-25(b), 7-25(c)]. The combination of hardened structures and natural vegetation is termed a *hybrid* approach to shoreline stabilization. Although the current emphasis on shoreline armoring has been on steeper, higher-energy shorelines, armoring of lower-energy shorelines may become an issue in the future with expanding residential development and projected rates of SLR.

7.10 REFERENCES

ASCE. 2010. *ASCE/SEI 7-16 Minimum design loads for buildings and other structures*. Accessed February 13, 2016. http://www.asce.org/structural-engineering/asce-7-and-sei-standards/. Reston, VA: ASCE.

ASCE Infrastructure Report Card. 2017. Accessed August 10, 2018. https://www.infrastructurereportcard.org.

Ayyub, B. M. 2014a. "Systems resilience for multi-hazard environments: definition, metrics and valuation for decision making." *Risk Anal. J.* 34(2):340–55. DOI: 10.1111/risa.12093.

Ayyub, B. M. 2014b. *Risk analysis in engineering and economics*, 2nd Ed. Boca Raton, FL: Chapman & Hall/CRC.

Ayyub, B. 2015. "Practical resilience metrics for planning, design and decision making." *ASCE-ASME J. Risk Uncertainty Eng. Syst., Part A: Civil*

Eng. 1(3). Accessed September 12, 2018. https://ascelibrary.org/doi/pdf/10.1061/AJRUA6.0000826. DOI: 10.1061/AJRUA6.0000826.

Ayyub, B. M., and G. J. Klir. 2006. *Uncertainty Modeling and Analysis in Engineering and the Sciences*. Boca Raton, FL: Chapman & Hall/CRC.

Blue Frontiers. 2018. Blue Frontiers. Accessed August 8, 2018. https://www.blue-frontiers.com.

Bruneau, M., S. E. Chang, R. T. Eguchi, C. Lee, T. D. O'Rourke, A. M. Reinhorn, et al. 2003. "A framework to quantitatively assess and enhance the seismic resilience of communities." *Earthquake Spectra* 19(4), 733–752. Accessed August 8, 2018. http://courses.washington.edu/cee518/Bruneauetal.pdf.

Currin, C. A., W. S. Chappell, and A. Deaton. 2010. "Developing alternative shoreline armoring strategies: The living shoreline approach in North Carolina." In *Puget Sound Shorelines and the Impacts of Armoring—Proc., State of the Science Workshop,* H. Shipman et al. (eds.). US Geological Survey Scientific Investigations Report 2010-5254, 91–102.

de Neufville, R., and S. Scholtes. 2011. *Flexibility in Engineering Design.* Accessed August 10, 2018. https://mitpress.mit.edu/books/flexibility-engineering-design. Cambridge, MA: MIT Press.

Deyle, R. E. 2012. Sea Level Rise Adaptation Options for Local Governments. Adaptive Planning for Coastal Change–Legal Issues for Local Government Workshop, August 9, 2012, Tallahassee, Florida. Accessed August 12, 2018. http://www.flseagrant.org/wp-content/uploads/2012/03/Deyle_Adaptive_Response_Planning_to_Sea_Level_Rise_FlaSeaGrantWkshop_08-09-12_edited.pdf.

Ellis, K., C. Berg, D. Caraco, S. Drescher, G. Hoffmann, B. Keppler, et al. 2014. *Low Impact Development in Coastal South Carolina: A Planning and Design Guide*. ACE Basin and North Inlet—Winyah Bay National Estuarine Research Reserves, 462 pp. Accessed August 10, 2018. http://www.scseagrant.org/pdf_files/LID-in-Coastal-SC-low-res.pdf.

EMSI (Economic Modeling Specialists International). 2017. "EMSI Impact Analysis: The Floating Island Project." Moscow, Idaho: EMSI.

FEMA (Federal Emergency Management Agency). 2009. "Local officials guide for coastal construction, design considerations, regulatory guidance, and best practices for coastal communities." *FEMA P-762*, Washington, DC: FEMA.

FHWA (Federal Highway Administration). 2012. "Climate change and extreme weather vulnerability assessment." Accessed April 14, 2017. https://www.fhwa.dot.gov/environment/sustainability/resilience/publications/vulnerability_assessment_framework/fhwahep13005.pdf. Washington, DC: FHWA.

FHWA. 2014. "Transportation asset management peer exchange—Preparing for MAP-21 implementation." Accessed April 14, 2017. https://www.fhwa.dot.gov/asset/pubs/hif14013.pdf. Washington, DC: FHWA.

Frangopol, D. M., K.-Y. Lin, and A. C. Estes. 1997. "Life-cycle cost design of deteriorating structures." *J. Struct. Eng.* 123(10), 1390–1401. Accessed September 12, 2018. https://doi.org/10.1061/(ASCE)0733-9445(1997)123:10(1390).

Gilbert, S., and B. Ayyub. 2016. "Models for the economics of resilience." *ASCE-ASME J. Risk Uncertainty Eng. Syst., Part A: Civil Eng.* DOI: 10.1061/AJRUA6.0000867.

Groves, D. G., and R. J. Lempert. 2007. "A new analytic method for finding policy-relevant scenarios." *Global Environmental Change* 17, 73–85.

Groves, D. G., D. Yates, and C. Tebaldi. 2008. Developing and applying uncertain global climate change projections for regional water management planning. *Water Resour. Res*. 44. DOI:10.1029/2008WR006964.

Huibregtse, E., O. W. Napoles, L. Hellebrandt, D. Paprotny, and S. de Wit. 2016. "Climate change in asset management of infrastructure: A risk-based methodology applied to disruption of traffic on road networks due to the flooding of tunnels." *Eur. J. Trans. Infrastruct. Res.* 16(1), 98–113. ISSN: 1567-7141. Accessed August 10, 2018. https://d1rkab7tlqy5f1.cloudfront.net/TBM/Over%20faculteit/Afdelingen/Engineering%20Systems%20and%20Services/EJTIR/Back%20issues/16.1/2016_01a_01%20Climate%20change%20in%20asset%20management%20of%20infrastructure.pdf.

International Upper Great Lakes Study. (IUGLS). 2012. "Lake Superior regulation: Addressing uncertainty in Upper Great Lakes water levels." *Final Report*, 28.

ISO (International Organization for Standardization). 2008. "Buildings and constructed assets—Service-life planning—Part. 5—Life-cycle costing." *ISO 15686-5:2008*. Geneva: ISO.

ISO. 2014. "Asset management—Overview, principles and terminology." *ISO 55000:2014*. Geneva: ISO.

Kaplan, S. and B. J. Garrick. 1981. "On the quantitative definition of risk." *Risk Analysis* 1, 11–27. Accessed September 12, 2018. http://dx.doi.org/10.1111/j.1539-6924.1981.tb01350.x.

Lee, J. Y., and B. R. Ellingwood. 2016. "A decision model for intergenerational life-cycle risk assessment of civil infrastructure exposed to hurricanes under climate change." *Rel. Eng. Syst Saf.* 159:100–107. DOI:0.1016/j.ress.2016.10.022.

Lempert, R. J., and D. G. Groves. 2010. "Identifying and evaluating robust adaptive policy responses to climate change for water management agencies in the American West." *Technological Forecasting and Social Change* 77: 960–974.

Lempert, R. J., S. W. Popper, and S. C. Bankes. 2003. "Shaping the next one hundred years: New methods for quantitative long-term strategy analysis." *MR-1626-RPC.* Santa Monica, CA: RAND.

Madanat, S. M. 1993. "Optimal infrastructure management decision under uncertainty." *Transp. Res., Part C: Emerg. Technol.* 1C(1), 77–88.

Means III, E., M. Laugier, J. Daw, L. Kaatz, and M. Waage. 2010. "Decision support planning methods: Incorporating climate change uncertainties into water planning." Denver, CO: Denver Water/Water Utility Climate Alliance. Accessed December 5, 2017. https://www.wucaonline.org/assets/pdf/pubs-whitepaper-012110.pdf.

Meyer, M., A. A. Amekudzi, and J. O'Har. 2010. Transportation Asset Management Systems and Climate Change: An Adaptive System Management Approach. 89th Annual Meeting of the Transportation Research Board. Washington, DC: National Academies.

Mori, Y., and B. R. Ellingwood. 1993. "Time-dependent system reliability analysis by adaptive importance sampling," *Structural Safety* 12(1), 59–73.

NOAA (National Oceanic and Atmospheric Administration). 2013. "What will adaptation cost? An economic framework for coastal community infrastructure." Accessed August 10, 2018. https://coast.noaa.gov/data/digitalcoast/pdf/adaptation-report.pdf. Charlestown, SC: NOAA Coastal Services Center.

Orcesi, A. D., H. Chemineau, P. H. Lin, P. Van Gelder, and V. Van Erp. 2016. "A risk analysis for asset management considering climate change." *Trans. Res. Proc.* 14, 105–114. DOI: 10.1016/j.Trpro.2016.05.046, 2016.

Presidential Policy Directive (PPD)-8. 2011. Accessed August 9, 2018. https://fas.org/sgp/crs/homesec/R42073.pdf.

Schaaf and Wheeler. 2016. "Levee protection planning and improvements project: Basis of design overview." *CIP 301-657.* Report prepared for the City of Foster City. Accessed August 10, 2018. https://www.fostercity.org/publicworks/project/levee-protection-planning-and-improvements-project-cip-301-657.

Seasteading Institute. 2017. "Floating islands project in Polynesia." Accessed September 12, 2018. https://www.seasteading.org. San Francisco: Seasteading Institute.

Smith, H. N. 2008. Kivalina Retreat and Adaptation, June 2008, Department of Transportation & Public Facilities, State of Alaska. Accessed August 12, 2018. http://www.kivalinaroad.org/engineering.html.

Smith, H. N., and R. A. Carter. 2011. *Over twenty-five years of applied coastal engineering in Alaska, coastal engineering practice*, O. Magoon, R. Noble, and D. Treadwell (eds.). Reston, VA: ASCE.

Sölken, W. 2017. "The Delta Works in the Netherlands." Accessed September 1, 2017. http://www.wermac.org/civil_eng/delta_works_maeslantkering.html.

Stewart, M. G., and X. Deng. 2015. "Climate impact risks and climate adaptation engineering for built infrastructure." *ASCE-ASME J. Risk Uncertainty Eng. Syst., Part A: Civil Eng.* 1(1). Accessed September 12, 2018. https://doi.org/10.1061/AJRUA6.0000809.

Swei, O., J. Gregory, and R. Kirchain. 2013. "Probabilistic characterization of uncertain inputs in the life-cycle cost analysis of pavements." *J. Trans. Res. Board* 2366, 71–77. DOI: 10.3141/2366-09, 2013.

Swei, O., J. Gregory, and R. Kirchain. 2016. "Probabilistic life-cycle cost analysis of pavements." *J. Trans. Res. Board* 2523, 47–55. DOI: 10.3141/2523-06, 2016.

USACE (United States Army Corps of Engineers). 2006. "Relocation planning project master plan, Kivalina, Alaska." Submitted to US Army Corps of Engineers by Tryck Nyman Hayes and URS Corp. Accessed August 10, 2018. http://www.poa.usace.army.mil/Portals/34/docs/civilworks/reports/KivalinaMasterPlanMainReportJune2006.pdf.

USACE. 2016. "Kivalina lagoon crossing planning assistance to states: Causeway & bridge design report, Kivalina, Alaska." Washington, DC: US Army Corps of Engineers, Alaska District.

Wilby, R. L., and S. Dessai. 2010. "Robust adaptation to climate change." *Weather* 65(7), 180–185. DOI: 10.1002/wea.543, 2010.

World66. 2011. New Waterway Storm Surge Barrier. Uploaded to Wikimedia Commons on May 17, 2011. Accessed August 12, 2018. https://commons.wikimedia.org/wiki/File:Maeslantkering_closed.jpg.

CHAPTER 8
DATA AND INFORMATION SOURCES

The application of methods presented in the MOP to relevant ASCE standards as provided in Appendix B requires in many instances access to published tables or derived digital products referenced or specified in the relevant ASCE standard. In all cases, such data, tools, and analytical procedures are based on assumptions made from historic records, as well as on projections of future analyses, including remote sensing missions not yet deployed. Because the observational record is, by necessity, an incomplete sampling of actual events (owing to changes in instrumentation, sampling bias, temporal gaps, instrumentation drift, etc.), some assumptions must be made about the representativeness of the observational record used to generate a statistical description of the past and the characterization of uncertainty of future data discoveries. A variety of statistical tests are performed to determine the goodness of fit of any method used to project the likelihood of future extremes from past events. Data-driven techniques are also used to improve historical data sets, as well as characterize uncertainties in forcings, models, and observations used to understand processes and design future scenarios.

The emerging recognition that climate variability and change affects the stationary assumptions that define infrastructure design has contributed to evidence that records, tools, and procedures developed in the past must be updated regularly. The need of tools to design in a non-stationary environment requires engineers to be aware of emerging data sources, tools, and procedures, as well as of the approaches used in the transition from stationarity. Engineering judgment must be used regarding when and where to use projections of future conditions based on an understanding of ongoing changes in the climate system.

To make such an informed decision, practicing engineers should utilize vetted tools or products that clearly identify sources of input data,

methodologies used to generate any relevant statistical descriptions (e.g., mean, 99 percentiles, annual probability of exceedance), and any recommended application or restriction for their use (Barsugli et al. 2013). Cook et al. (2017) provide thoughtful guidance for engineers considering the use of climate projections:

- Match intended engineering application with the appropriate climate model source;
- Recognize that different climate model sources require various amounts of effort for data extraction and preparation;
- Recognize that climate models have various levels of skill at representing historical mean and extreme statistical metrics, and engineers need to understand the major issues and uncertainties involved;
- Create an ensemble and be transparent about assumptions;
- Test robustness of designs to extremes and alternative scenarios;
- Discuss trade-offs and uncertainties in risk, resiliency, performance, and costs with stakeholders; and
- Design for low regret, adaptability, and robustness, and revisit designs when new information is available.

Conscientious application of these principles drives users to seek out and use tools and products with documented use history for similar application. US federal agencies are an extensive although not a universally recognized source of such tools and products. Thus, the majority of the discussion in the next section focuses on US federal agency tools or products, although the principles of transparency they exhibit should be applied to any source of data.

8.1 US FEDERAL DATA AND INFORMATION SOURCES

Broadly speaking, numerical values used to develop a PDF, APE, or an IDF curve used for engineering design can be derived either from historical observations, output from a climate model, or a combination of both. Observational data, as well as modeled output, can be obtained from a wide variety of federal, state, and local sources, and thus the quality control/quality assurance review it has undergone can vary greatly. Similarly, accessibility may vary significantly across sources. It is beyond the scope of this work to identify and review the quality and appropriateness of these diverse data sets. However, because of the significant demand for such information, US federal agencies have invested considerable time and money into developing clearinghouses for such data, as well as standards for the creation and preservation of associated metadata.

Metadata refers to the *labeling* data collection, quality control, and changes may undergo. The source of data together with the external factors could

modify its representation and may help distinguish between an outlier and an extreme value. Also, its relevance is on the contribution toward an enhanced characterization of the quality of a measurement, as well as the possible sources of uncertainty in its measurement. Metadata can also aid interoperability among agencies, thus procuring a better exchange of standardized data, tools, and procedures.

8.1.1 National Oceanic and Atmospheric Administration

NOAA funds significant federal efforts to obtain, analyze, manage, package, and disseminate data and derived products regarding a wide variety of weather, water, and climate processes. Such observational data and information, derived by NOAA's National Weather Service (NOAA/NWS) and NOAA National Environmental Satellite and Data Information Service (NOAA/NESDIS), can be accessed through many portals. Climate model output is also produced by NOAA programs and laboratories funded by the NOAA Climate Program Office. To facilitate access to large data sets and model output files or for comprehensive coverage, NOAA created the National Centers for Environmental Information (NOAA/NCEI; https://www.ncei.noaa.gov/).

8.1.2 US Geological Survey

The US Geological Survey (USGS) funds significant federal efforts to monitor streamflow, flood, drought, earthquake activity, volcano activity, landslides, and geomagnetism. Data and products derived through its efforts, as well as satellite imagery produced by LandSat, can be accessed online (https://www.usgs.gov/products/data-and-tools/overview). Data sets available through the USGS tend to be of shorter duration and were developed for specific purposes that may or may not align well with a specific engineering need. One notable exception is the USGS Streamflow data, which is considered the standard source for long, high-quality time series of streamflow.

8.1.3 Bureau of Reclamation

The Bureau of Reclamation funds significant federal efforts to support water resources planning and operation, sedimentation and river hydraulics, flood hydrology and meteorology, geographic analysis, and fisheries and wildlife resources, primarily on western federal lands. Data and products of interest (e.g., HydroMet or AgriMet) available from the Bureau of Reclamation are generally not centralized, but they can be obtained from regional programs. Users interested in obtaining these data sets or related products should use the search tool provided online (https://www.usbr.gov/).

Table 8.1. Comparison of Characteristics of Six Publicly Available Sources of Downscaled Climate Model Output for North America.

Source of Input	Model Simulation Choices								
	Global climate model group		Emission scenario		Number of model simulations	Down-scaling method	Spatial Resolution (km)		
	CMIP3	CMIP5	SRES	RCP	(does not include same model runs)	Dynamical	4	6	
						Statistical	12	15	
							25	50	
NARCCAP	CMIP3					Dynamical			
					12				
			A2					50	
NA-CORDEX		CMIP5				Dynamical			
				4.5	12				
				8.5			25	50	
RegCM3	CMIP3				3	Dynamical			
								15	
			A2						
ARRM	CMIP3		B1						
			A1				12		
			A1B			Statistical			
			A2		16				
Reclamation	CMIP3	CMIP5	B1						
							12		
			A1B			Statistical			
			A2		20+				
MACA		CMIP5					4	6	
				4.5					
						Statistical			
				8.5	20+				

Source: Cook et al. (2007).

Note: NARCCAP = North American Regional Climate Change Assessment Program (narccap.ucar.edu); NA-CORDEX = North American Coordinated Regional Climate Downscaling Experiment (nacordex.org); RegCM3 = USGS Regional Climate Model Version 3 (regclim.coas.oregonstate.edu); ARRM = Asynchronous Regional Regression Model (cida.usgs.gov); Reclamation = US Department of the Interior Bureau of Reclamation; MACA = Multivariate Adaptive Constructed Analogs (maca.northwestknowledge.net); csv = Comma separated values (file format); netCDF = Network Common Data Form; dpy = days per year; RCP = Representative Concentration Pathway; and SRES = Special Report on Emissions Scenarios.

Model Output Attributes						Extraction and Access Features			
	Historical Period		Future Period		Time Step	Units	Data format	File format	Data access
	1950	1958	2000	2015	3 h	Flux ($kg/m^2/s$)	calendar	csv	user interface
	1965	1973	2030	2045	daily				
	1980	1988	2060	2075	monthly	Depth (mm/day)	fixed	netCDF	Server download
	1995	2000	2090	2100	decadal				
					3 h	flux			
	1970		2040						
			2070				360 dpy	netCDF	server download
		2000							
	1950		2000		3 h	flux			
					daily				
					monthly		360 dpy	netCDF	server download
		2000		2099					
				2020	daily	flux			user interface
	1960				monthly				
					decadal		365 dpy	netCDF	
		2000		2099					
			2000		daily	flux	calendar	csv	
	1960								
						depth		netCDF	server download
		2000		2099					
	1950		2000			flux	calendar	csv	user interface
					daily				
					monthly	depth		netCDF	
		2000		2099					
	1950		2000			flux	calendar	csv	user interface
					daily				
						depth		netCDF	
		2000		2099					

8.1.4 National Aeronautics and Space Demonstration

NASA funds significant federal efforts to observe and model Earth systems relevant to geoscience research and engineering practice. Data on various weather, water, and climate systems can be accessed either through the NASA Earth Observing System (https://eospso.nasa.gov/) or the NASA Center for Climate Simulation (https://www.nccs.nasa.gov/).

8.1.5 US Army Corps of Engineers

The USACE funds significant data collection and dissemination activities in support of its core mission objective, i.e., the development and management of the nation's water resources. Relevant data on a broad spectrum of interest to engineering practice (e.g., dam capacity, sedimentation, levees, flow), although centralized, can be accessed through the online search engine (http://www.usace.army.mil/).

8.1.6 Department of Energy

The DOE funds significant efforts to understand climate change and its impacts, including rising temperatures, wildfires, drought, increased levels of electricity demand, on the nation's energy infrastructure. Data and derived products of these DOE efforts with relevance to engineering practice may be identified through the agency's Public Data Listing available online (https://energy.gov/data/downloads/open-data-catalogue).

8.2 UNDERSTANDING CLIMATE MODEL OUTPUT AND ITS UTILITY

As discussed in *Adapting Infrastructure and Civil Engineering Practice to a Changing Climate* (ASCE 2015), global climate models (GCMs) are the primary tools that climate scientists use to make quantitative projections of future global and regional climate. Climate models project systematic changes in climate and weather conditions. Climate projections introduce additional climatic uncertainties beyond those that can be estimated from observations of the past. For example, there is significant uncertainty regarding the magnitude and rate of climate change over the design life of the systems and elements of our built environment. Engineering design is primarily concerned with climate and weather extremes, but the projection of future extreme events and their frequency of occurrence have even greater uncertainty than changes in mean conditions. GCMs tend to underestimate the variance and serial persistence in observed climate, which implies that

they may underestimate climate extremes. Engineering design and planning are generally conducted at regional and local scales, but GCMs perform better at lower spatial resolution and over longer timescales. Regional modeling currently performed with downscaling techniques is used to obtain higher-resolution regional and local projections. However, the uncertainty is much larger on regional and local scales. Generally, uncertainty increases as the planning horizon increases with scenario-related uncertainties dominating other types of uncertainty such as model and parameter uncertainties.

Barsugli et al. (2013) pointed out that "To characterize climatic uncertainty, current scientific practice recommends using ensembles of climate projections that account for various sources of uncertainty: different emissions scenarios, global models, or downscaling methods." Although various funders and producers of climate data have undertaken no comprehensive effort, some narrower efforts have been completed. Cook et al. (2017) proposed a framework for incorporating climate trends into design standards and applications, including selecting the appropriate climate model source (Table 8-1) based on the intended application, understanding model performance and uncertainties, addressing differences in temporal and spatial scales, and interpreting results for engineering design. Additional perspectives on the use of climate model projections, especially in water utility planning, have been developed by the Water Utility Climate Alliance (WUCA 2009, 2015).

8.3 REFERENCES

ASCE. 2015. *Adapting infrastructure and civil engineering practice to a changing climate*. Accessed February 13, 2016. http://ascelibrary.org/doi/book/10.1061/9780784479193. Reston, VA: ASCE.

Barsugli, J. J., G. Guentchev, R. M. Horton, A. Wood, L. O. Mearns, X. Liang, et al. 2013. "The practitioner's dilemma: How to assess the credibility of downscaled climate projections." Eos Trans. *Amer. Geophys. U.* 96, 424–425. DOI: 10.1002/2013EO460005.

Cook L., C. Anderson, and C. Samaras. 2017. "A framework for incorporating downscaled climate output into existing engineering methods: Application to precipitation frequency curves." *J. Infrastruct. Syst.* 23(4), 17–27. DOI: 10.1061/(ASCE)IS.1943-555X.0000382.

WUCA (Water Utility Climate Alliance). 2009. "Options for improving climate modeling to assist water utility planning for climate change." Accessed August 10, 2018. https://www.wucaonline.org/assets/pdf/pubs-whitepaper-120909.pdf. San Francisco, CA: WUCA.

WUCA. 2015. "Actionable science in practice: Co-producing climate change information for water utility vulnerability assessments: Final report of the piloting utility modeling applications (PUMA) project." Accessed August 10, 2018. https://www.wucaonline.org/assets/pdf/pubs-puma-white-paper-20150427.pdf. San Francisco, CA: WUCA.

APPENDIX A
TERMINOLOGY

This appendix defines terminology most relevant to this MOP, drawn primarily from Ayyub (2014).

Adaptation is the action or process of adapting or being adapted.

Adaptive risk management is defined as the coordinated and adaptive activities with regard to risk. See also *risk management*.

Climate is the weather conditions prevailing in an area in general or over a long time period.

Climate change refers to a change in global or regional climate patterns, in particular a change apparent from the mid- to late-twentieth century onward and attributed largely to the increased levels of atmospheric greenhouse gases.

Consequence is the immediate, short-term and long-term effect of an event affecting objectives, for example, SLR. These effects may include human and property losses, environmental damages, and loss of lifelines.

Countermeasure is an action taken or a physical capability provided with the principal purpose of reducing or eliminating vulnerabilities or reducing the occurrence of attacks.

Critical infrastructure consists of systems and assets, whether physical or virtual, that are vital to a nation such that the incapacity or destruction of such systems and assets would have a debilitating impact on security, national economic security, national public health or safety, or any combination of those matters.

Design basis value is the accepted level for design that might include a factor of safety.

Exposure is the extent to which an organization or stakeholder concerns are subject to an event and defined by things at risk that might include population at risk, property at risk, and ecological and environmental concerns at risk.

Hazard is a source of potential harm or a condition that may result from an external cause (e.g., earthquake, flood, or human agency) or an internal vulnerability, with the potential to initiate a failure mode.

Fragility is the conditional probability of failure at a particular hazard level.

Ignorance is a deficiency in knowledge. Within the realm of conscious ignorance, incompleteness and inconsistency are the primary categories defining it.

Likelihood is the chance of something happening, whether defined, measured, or determined objectively or subjectively, qualitatively, or quantitatively, and described using general terms or mathematically, such as a probability or a frequency over a given time period.

Maximum credible level is an estimate associated with a confidence level or percentile level such as 90%.

Probable maximum value is the central tendency of the maximum value.

Probability is a measure of chance of occurrence, likelihood, odds, or degree of belief that a particular outcome or event will occur, expressed as a number between 0 and 1, where 0 is impossibility and 1 is absolute certainty. This measure meets the axioms of probability theory. Probability has at least two primary interpretations: (1) a frequency representing the occurrence fraction of an outcome in repeated trials or an experiment as sometimes termed an objective probability and (2) subjective probability that is based on the state of knowledge.

Residual risk is the amount of risk remaining after realizing the net effect of risk-reducing actions.

Resilience is defined by several sources as (1) the ability to adapt to changing conditions and withstand and rapidly recover from disruption due to emergencies. (2) the ability to prepare for and adapt to changing conditions and to withstand and recover rapidly from disruptions. Resilience includes the ability to withstand and recover from deliberate attacks, accidents, or naturally occurring threats or incidents. (3) the persistence of a corresponding functional performance under uncertainty in the face of disturbances. The third definition is consistent with the risk definition of the "effect of uncertainty on objectives."

Risk should be associated with a system and is commonly defined as the potential loss resulting from an uncertain exposure to a hazard or resulting from an uncertain event that exploits the system's vulnerability. Risk should be based on identified risk events or event scenarios. A broadly applicable definition of risk is defined as the effect of uncertainty on objectives in order to cover the following considerations: (1) An effect is a deviation from the expected that can be positive and/or negative effect. (2) Objectives can have different aspects, such as financial, health and safety, and environmental goals, and can apply at different levels, such as strategic, organization-wide, project, product, and process. (3) Risk is often expressed in terms of a combination of the consequences of an event, including changes in circumstances, and the associated likelihood of occurrence as provided in the commonly used definition.

Risk acceptance is the degree of risk associated with a system or endeavor that a decision maker perceives and accepts the associated actions under a given

set of circumstances and with the associated costs. A decision maker's risk tolerance and resources are the foundation of risk acceptance.

Risk analysis is the technical and scientific process to comprehend the nature of risk and to determine the level of risk by examining the underlying components or elements of risk.

Risk assessment is an overall process of (1) risk identification, (2) risk analysis, and (3) risk evaluation.

Risk attitude is an organization's approach to assess and eventually pursue, retain, take, or turn away from risk.

Risk aversion is the attitude to turn away from risk.

Risk communication involves perceptions of risk and depends on the audience targeted; hence, it is classified into risk communication to the media, the public, and the engineering community.

Risk context is the external and internal parameters or considerations to be taken into account when managing risk and setting the scope and risk criteria for the risk management policy.

Risk criteria are the terms of reference against which the significance of a risk is evaluated reflecting the organizational objectives expressed in external and internal contexts and in keeping with standards, laws, policies, and other requirements.

Risk identification is the process of finding, recognizing, and describing risks including sources, events, scenarios, and their causes and potential consequences involving historical data, theoretical analysis, informed and expert opinions, and stakeholders' needs.

Risk management is defined as the coordinated activities to direct and control an organization with regard to risk following a framework consisting of designing, implementing, monitoring, reviewing, and continually improving risk management throughout the organization. Risk management should be founded in strategic and operational policy, objectives, mandate, practices, and commitment through organizational arrangements including plans, relationships, accountabilities, resources, processes, and activities.

Risk neutrality is having the same attitude regardless of the potential loss.

Risk owner is a person or entity with the accountability and authority to manage a risk.

Risk seeking is the attitude to pursue, retain, or undertake the risk for potential return.

Risk tolerance is the degree of risk associated with normal daily activities that people tolerate, usually without making a conscious decision. As for organization or stakeholders, it is the readiness to bear the risk after risk treatment in order to achieve its objectives. Risk tolerance can be influenced by legal or regulatory requirements.

Safety is the judgment of risk tolerance, or acceptability in the case of decision making, for the system.

Scenario is defined as joint events and system's state that lead to an outcome of interest. A scenario defines a suite of circumstances of interest in a risk assessment. Thus, there may be loading scenarios, failure scenarios, or downstream

flooding scenarios. A scenario can also be defined as the joint occurrence of events following a particular order or sequence in occurrence.

Stakeholder is a person, such as a decision maker and owner, or organization, that can affect, be affected by, or perceive themselves to be affected by a decision or activity.

Sustainability, according to ASCE in its Policy Statement 418 (2016), is a set of economic, environmental and social conditions in which everyone has the capacity and opportunity to maintain and improve its quality of life indefinitely, without degrading the quantity, quality, or availability of natural, economic, and social resources. Sustainable development is the application of these resources to enhance the safety, welfare, and quality of life for everyone. Several other definitions are available: (1) Creating and maintaining conditions under which humans and nature can exist in productive harmony and that permit fulfilling social, economic, and other requirements of present and future generations. (2) Ability to maintain or improve standards of living without damaging or depleting natural resources for present and future generations. (3) The creation of manufactured products that use processes that minimize negative environmental impacts, conserve energy and natural resources, are safe for employees, communities, and consumers and are economically sound. (4) The practice of increasing the efficiency with which buildings and their sites use and harvest energy, water, and materials; and protecting and restoring human health and the environment, throughout the building life cycle: siting, design, construction, operation, maintenance, renovation, and deconstruction.

System is a group of interacting, interrelated, or interdependent elements, such as people, property, materials, environment, and processes.

Uncertainty is the state of deficiency in information with two uncertainty types identified as follows: (1) Aleatory uncertainty is the inherent, random, or nonreducible uncertainty, such as material strength randomness. (2) Epistemic uncertainty is the knowledge-based subjective uncertainty that can be reduced with the collection of data or attainment of additional knowledge.

Vulnerability is defined as the intrinsic properties of a system making it susceptible to a hazard or a threat or a risk source that can lead to an event with a consequence; or it is an inherent state of the system, for example, physical, technical, organizational, or cultural, that can be exploited by an adversary to cause harm or damage.

Weather is the state of the atmosphere at a place and time, such as heat, dryness, sunshine, wind, rain, and so on.

REFERENCE

Ayyub, B. M. 2014. *Risk analysis in engineering and economics,* 2nd Ed. Boca Raton, FL: Chapman & Hall/CRC.

APPENDIX B
ASCE STANDARDS AND CLIMATE CHANGE

B.1 OVERVIEW

This MOP is designed to provide ASCE standards committees and practicing engineers with an understanding of and the means to address the challenge posed by changes in weather and climate extremes through time. This manual is not intended to be a substitute for existing standards but rather a resource for enhancing professional judgment with regard to their development and application. Consequently, the authors spent significant time characterizing the sensitivity of various ASCE standards to changes in weather and climate extremes.

At the time of the preparation of this manual, ASCE had 60 standards in effect. Of those 60, 36 were determined to be sensitive in some manner to changes in weather and climate extremes (Table B-1). Many of the remaining 24 were simply insensitive to environmental conditions or covered engineering activities of such a short duration that changes in weather and climate extremes were not relevant. For example, ASCE/SEI Standard 49, *Wind Tunnel Testing for Buildings and Other Structures,* last updated in 2012, provides the minimum requirements for conducting and interpreting wind tunnel tests to determine wind loads on buildings and other structures. Because these are purely controlled tests, they are not affected by changes in environmental conditions outside the facility. ASCE/SEI 39, *Design Loads on Structures During Construction,* last updated in 2014, describes the minimum design requirements for construction loads, load combinations, and load factors affecting buildings and other structures that are under construction. It addresses partially completed structures as well as temporary support and access structures used during construction. Although these structures must be designed and constructed to withstand various weather extremes,

Table B-1. ASCE Standards and Sensitivity to Changes in Weather and Climate Extremes.

Complete reference number	Title of standard	Sensitivity grouping*
ANSI/ASCE 1-82	N-725 Guideline for Design and Analysis of Nuclear Safety-Related Earth Structures	II
ANSI/ASCE 3-91	Standard for the Structural Design of Composite Slabs	I
ASCE 4-98	Seismic Analysis of Safety-Related Nuclear Structures and Commentary	III
ASCE/SEI 5-13 and 6-13	Building Code Requirements and Specification for Masonry Structures	III
ASCE/SEI 7-10	Minimum Design Loads for Buildings and Other Structures	I
SEI/ASCE 8-02	Specification for the Design of Cold-Formed Stainless Steel Structural Members	I
ANSI/ASCE 9-91	Standard Practice for Construction and Inspection of Composite Slabs	I
ASCE/SEI 10-15	Design of Latticed Steel Transmission Structures	I
SEI/ASCE 11-99	Guideline for Structural Condition Assessment of Existing Buildings	III, IV
ANSI/ASCE/EWRI 12-13	Standard Guidelines for the Design of Urban Subsurface Drainage	III, IV
ANSI/ASCE/EWRI 13-13	Standard Guidelines for the Installation of Urban Subsurface Drainage	III, IV
ANSI/ASCE/EWRI 14-13	Standard Guidelines for the Operation and Maintenance of Urban Subsurface Drainage	III, IV
ASCE 15-98	Standard Practice for Direct Design of Buried Precast Concrete Pipe Using Standard Installations (SIDD)	IV
AF&PA/ASCE 16-95	Standard for Load and Resistance Factor Design (LRFD) for Engineered Wood Construction	I
ASCE 17-96	Air-Supported Structures	I
ASCE/SEI 19-10	Structural Applications of Steel Cables for Buildings	I
ASCE 20-96	Standard Guidelines for the Design and Installation of Pile Foundations	IV
ANSI/ASCE/T&DI 21-13	Automated People Mover Standards	I, IV
ASCE/SEI 24-14	Flood Resistant Design and Construction	II

Table B-1. (Continued)

Complete reference number	Title of standard	Sensitivity grouping*
ASCE 26-97	Standard Practice for Direct Design of Buried Precast Concrete Box Sections	III
ASCE 27-00	Standard Practice for Direct Design of Precast Concrete Pipe for Jacking in Trenchless Construction	III
ASCE 28-00	Standard Practice for Direct Design of Precast Concrete Box Sections for Jacking in Trenchless Construction	III
ASCE/SEI 31-03	Seismic Evaluation of Existing Buildings	III
SEI/ASCE 32-01	Design and Construction of Frost-Protected Shallow Foundations	IV
EWRI/ASCE 33-01	Comprehensive Transboundary International Water Quality Management Agreement	II, III
EWRI/ASCE 34-01	Standard Guidelines for Artificial Recharge of Ground Water	III
ASCE/EWRI 40-03	Regulated Riparian Model Water Code	III
ASCE/SEI 41-13	Seismic Evaluation and Retrofit of Existing Buildings	III
ASCE/SEI 43-05	Seismic Design Criteria for Structures, Systems, and Components in Nuclear Facilities	III
ASCE/EWRI 45-05	Standard Guidelines for the Design of Urban Stormwater Systems	II, III, IV
ASCE/EWRI 47-05	Standard Guidelines for the Operation and Maintenance of Urban Stormwater Systems	II, III, IV
ASCE/SEI 48-11	Design of Steel Transmission Pole Structures	I
ASCE/SEI 52-10	Design of Fiberglass-Reinforced Plastic (FRP) Stacks	I
ANSI/ASCE/EWRI 56-10	Guidelines for the Physical Security of Water Utilities	II
ANSI/ASCE/EWRI 57-10	Guidelines for the Physical Security of Wastewater/Stormwater Utilities	II
ASCE/EWRI 60-12	Guideline for Development of Effective Water Sharing Agreements	II, III

*Groups are as follows: I—change in loading, II—change in surface hydrology (including flood extent or frequency, or inundation owing to SLR), III—change in groundwater table height (including that owing to SLR), and IV changes in temperature.

their service life is sufficiently short that changes in weather and climate extremes are likely not relevant.

This appendix is designed to allow the reader to better understand the breadth of ASCE standards that are sensitive to changes in weather and climate extremes and how that sensitivity helped shape the MOP.

B.2 SENSITIVITY OF ASCE STANDARDS TO CHANGES IN EXTREMES

A review of the 41 active ASCE standards that are sensitive to changes in weather and climate extremes helps illustrate how complex interactions between engineering practice and environmental conditions can be. Designing for anticipated loads is critical in many engineering design efforts and is likely the most expected way changes in extremes should be accounted for. Conversely, understanding how soil properties may change through time owing to drought, increased precipitation, or SLR may be of equal importance.

An examination of the 41 standards mentioned previously led to the recognition of four broad areas of sensitivity to change in weather and climate extreme: (1) changes in loading, (2) changes in surface hydrology (including flood extent or frequency, or inundation owing to SLR), (3) changes in groundwater height or chemistry (including that owing to SLR), and (4) changes in temperature.

B.2.1 Changes in Design Loads

ASCE/SEI 7-10, published in 2010 and updated in 2016, provides requirements for general structural design and includes means for determining dead, live, soil, flood, snow, rain, atmospheric ice, earthquake, and wind loads, as well as their combinations, which are suitable for inclusion in building codes and other documents. One of the most widely used ASCE standards, ASCE/SEI 7, is also referenced in many other ASCE standards when those standards discuss aspects of design or construction that may be affected by loads it covers. For example, Section 2.1 of ASCE/ANSI 3 specifies that "Loads not covered by the building code shall be in accordance with ASCE/SEI 7."

Changes in weather and climate extremes are directly relevant to the calculation of flood, snow, rain, atmospheric ice, and wind loads. Earthquake loads may also be affected as soil properties, and thus the transmission of seismic energy to foundations, change owing to changes in soil properties such as soil moisture content changes through time (e.g., when the groundwater table rises or falls owing to long-term changes in regional precipitation).

ASCE/SEI 7-10 is also important as the source of the concept of an *importance factor*, which accounts for the degree of risk to human life, health, and

welfare associated with damage to property or loss of use or functionality (see Table 7-2).

B.2.2 Changes in Surface Hydrology and Flood Frequency

ASCE/SEI 24 provides minimum requirements for design and construction of structures located in flood hazard areas and subject to building code requirements. Identification of flood-prone structures is based on flood hazard maps, studies, and other public information. This standard applies to new structures, including subsequent work, and to work classified as substantial improvement of existing structures that are not historic. Standard ASCE/SEI 24-14 introduces a new concept, Flood Design Class, that bases requirements for a structure on the risk associated with unacceptable performance.

The standard includes requirements for the following: basic siting and design and construction requirements for structures in flood hazard areas; minimum elevations for the lowest floor, flood damage-resistant materials, and floodproofing measures, each tied to a structure's Flood Design Class; structures in high-risk flood hazard areas subject to flooding associated with alluvial fans, flash floods, mudslides, erosion, high-velocity flow, coastal wave action, or ice jams and debris; structures in coastal high-hazard areas (V zones) and Coastal A zones; flood damage-resistant materials; dry floodproofing and wet floodproofing; attendant utilities and equipment, including electrical service, plumbing systems, mechanical/HVAC systems, and elevators; building access; and miscellaneous construction, including decks and porches, concrete slabs, garages and carports, accessory storage structures, chimneys and fireplaces, pools, and tanks. A detailed commentary containing explanatory and supplementary information to assist users of the standard is included for each chapter.

Changes in surface hydrology also affect rates of erosion and sedimentation and can have significant implications for stormwater management. Three standards, ASCE/EWRI 45-05, 46-05, and 47-05, are bundled together and are intended to supplement ASCE Manual 77.

ASCE/EWRI 45-05 provides guidelines for the design of urban stormwater systems, covering topics such as site analysis, system configuration, hydrology, hydraulic design, nonstructural considerations, structural design, and materials. ASCE/EWRI 47-05 provides guidelines for the operation and maintenance of urban stormwater systems, including operation and maintenance plans, water quality, periodic inspection, and maintenance. Section 3.0 states that the Operation and Maintenance Plan should cite the need to update operation and maintenance plans when significant climate change effects have occurred.

B.2.3 Changes in Groundwater

Changes in precipitation can change groundwater recharge rates, and thus effect water table height on a variety of spatial scales. These effects, which can be exacerbated by increased groundwater withdrawal, can lead to changes in soil moisture and the physical properties of soil, especially in areas dominated by hydrophilic clays. Such changes can have significant implications for how soils interact with buried structures or the foundations of various surface structures.

ASCE 26-97, published in 1997, provides a good example. Specifically, Section 8.1.7 states that "Any live load, surcharge, groundwater, internal hydrostatic pressure, or other loadings" should consider effects of drought, extreme precipitation, and Section 8.1.8 states that "Location of ground water table with respect to bottom of box section" should consider drought, extreme precipitation or flooding effects.

B.2.4 Changes in Temperature

Changes in temperature extremes, their duration, or daily range can influence materials properties and durability and the performance of joints, hinges, or other connectors. Changes in freeze–thaw cycle can change soil properties or the depth of permafrost. Such changes can have implications for foundation design or complex mechanical systems.

SEI/ASCE 32-01, published in 2001, addresses the design and construction of frost-protected shallow foundations in areas subject to seasonal ground freezing. Foundation insulation requirements to protect heated and unheated buildings from frost heave are presented in easy-to-follow steps with reference to design tables, climate maps, and other necessary data to furnish a complete frost-protection design. The advantages of this technology include improved construction efficiency over conventional practices, increased energy efficiency, minimized site disturbance, and enhanced frost protection. A commentary is included to provided background information and important technical insights.

ANSI/ASCE/T&DI 21-13, establishes the minimum requirements for the design, construction, operation, and maintenance of automated people mover (APM) systems. Collectively, the standards present the requirements to assure the safety and performance of APM systems. Section 2.1 "Ambient Conditions" discusses operating conditions that should be considered during design and specifies sources of historical climatic data that shall be considered when specifying design climatic values. Source number 1 is a basic compilation of low, high, and mean values of temperature, humidity, steady and gusting winds, rainfall rates, and other climatic characteristics, as compiled by NOAA. Source number 2 summarizes the NOAA data in convenient form. Source number 3 provides temperature data and methods for calculating 50-year return temperatures specified in Section 2.1.1.1.

APPENDIX C

METHODOLOGY FOR L-MOMENT AND OTHER STATISTICAL COMPUTATIONS

The mathematical basis for the statistical computations in Section 4.3.3. *Extreme Historical Storm Events and Floods* is presented in this appendix.

The GEV probability distribution is given by

$$F(x;\kappa,\alpha,\xi) = \exp\left[-\left\{1-\kappa\left(\frac{x-\xi}{\alpha}\right)\right\}^{1/\kappa}\right]$$
$$x(F) = \xi + \alpha\frac{\{1-(-\log F)^{\kappa}\}}{\kappa} \tag{C-1}$$

where ξ = location parameter, α = scale parameter (> 0), and κ = shape parameter.

L-moments are linear functions of probability-weighted moments (PWMs).

$$\beta_r = E\{X[F_X(x)]^r\} \tag{C-2}$$

where β_r is the r^{th} order PWM and $F_X(x)$ is the cumulative distribution function of X. Unbiased sample estimators of the first four PMWs are given by

$$\beta_0 = \frac{1}{n}\sum_{j=1}^{n} X_j = mean \qquad \beta_1 = \sum_{j=1}^{n-1}\left[\frac{n-j}{n(n-1)}\right]X_{(j)}$$
$$\beta_2 = \sum_{j=1}^{n-2}\left[\frac{(n-j)(n-j-2)}{n(n-1)(n-2)}\right]X_{(j)} \qquad \beta_3 = \sum_{j=1}^{n-3}\left[\frac{(n-j)(n-j-1)(n-j-2)}{n(n-1)(n-2)(n-3)}\right]X_{(j)} \tag{C-3}$$

where $X_{(j)}$ represents the ranked AMS, with $X_{(1)}$ the highest value and $X_{(n)}$ the lowest value. The first four L-moments are computed as follows:

$$\lambda_1 = \beta_0 \qquad \lambda_2 = 2\beta_1 - \beta_0 \qquad \lambda_3 = 6\beta_2 - 6\beta_1 + \beta_0$$
$$\lambda_4 = 20\beta_3 - 30\beta_2 + 12\beta_1 - \beta_0 \tag{C-4}$$

The L-moment ratios are calculated as follows:

$$\tau_2 = \frac{\lambda_2}{\lambda_1} \qquad \tau_3 = \frac{\lambda_3}{\lambda_2} \equiv L - skew$$
$$\tau_4 = \frac{\lambda_4}{\lambda_2} \equiv L - kurtosis \tag{C-5}$$

Computation of the precipitation depth d for a given point nonexceedance probability F is as follows (Asquith 1998).

$$X_d(F) = \xi + \frac{\alpha}{\kappa}\{\, 1 - [-\ln(F)]^{\kappa}\} \tag{C-6}$$

If a storm depth for a given duration is known, the storm's *point* annual nonexceedance probability can be estimated by

$$F = \exp - \left\{ 1 - \frac{\kappa}{\alpha}\left[X_d(F) - \xi \right] \right\}^{1/\kappa} \tag{C-7}$$

The parameters of the GEV distribution are estimated from L-moments by

$$Z = \frac{2}{\tau_3} - \frac{ln(2)}{ln(3)} \qquad \kappa \approx 7.8590\,Z + 2.9554\,Z^2$$
$$\alpha = \frac{\lambda_2 \kappa}{(1 - 2^{-\kappa})\Gamma(1 + \kappa)} \qquad \xi = \lambda_1 + \frac{\alpha}{\kappa}\{\Gamma(1 + \kappa) - 1\} \tag{C-8}$$

Implementation of the L-moment method for the Log-Pearson Type III distribution follows Hosking (1990).

$$F(x;\mu,\sigma,\gamma) = G\left(\frac{\left(x-\mu+\frac{2\sigma}{\gamma}\right)}{\left|\frac{1}{2}\sigma\gamma\right|}, \frac{4}{\gamma^2}\right), \quad \gamma > 0$$

$$F(x;\mu,\sigma,\gamma) = 1 - G\left(-\frac{\left(x-\mu+\frac{2\sigma}{\gamma}\right)}{\left|\frac{1}{2}\sigma\gamma\right|}, \frac{4}{\gamma^2}\right), \quad \gamma < 0 \qquad \text{(C-9)}$$

$x(F)$ not explicitly defined

$$\mathrm{G(x,}\alpha) = \frac{1}{\Gamma(\alpha)}\int_0^x t^{\alpha-1}e^{-t}dt \qquad \text{the incomplete gamma integral.}$$

The EV1 is defined by

$$f(x) = \frac{1}{\beta}\exp\left(-\frac{x-\mu}{\beta}\right)\exp\left[-\exp\left(-\frac{x-\mu}{\beta}\right)\right] \qquad \text{(C-10)}$$

where

μ = location parameter $\quad \beta$ = scale parameter

x = extreme (large) value

The L-moment implementation of the EV1 is as follows:

$$F = \exp\left[-\exp\left\{-\frac{x-\xi}{\alpha}\right\}\right] \qquad x(F) = \xi - \alpha\log(-\log F)$$

$$\xi = \beta_0 - \alpha\gamma \qquad \gamma = 0.5772 \qquad \alpha = \frac{2\beta_1 - \beta_0}{\log 2} \qquad \text{(C-11)}$$

$$y = \frac{x-\xi}{\alpha} \quad \text{(reduced variate)} \qquad \mathrm{y}_T = -\ln\left[-\ln\left(1-\frac{1}{T}\right)\right]$$

The T-year event precipitation Q_T (or flow) is then

$$Q_T = \xi + \alpha\left[-\ln\left[-\ln\left(1-\frac{1}{T}\right)\right]\right] \qquad \text{(C-12)}$$

where T is the RP in years.

This page intentionally left blank

APPENDIX D
ADAPTATION TECHNOLOGIES

As discussed in Chapter 6, flood loads resulting from extreme events (typically consisting of hydrostatic and hydrodynamic pressures, debris impact and/or breaking waves) will need to be addressed for many locations as part of planning and design for infrastructure resiliency to address climate change. This section provides an overview of flood protection techniques used for adaptation and presents specific flood protection products and technologies available on the market as of this date.

D.1 COMPOSITE WALL STRENGTHENING TECHNIQUES

Many existing structures utilize exterior masonry bearing or non-bearing walls as the façade wall (or backup wall). Typically, the best-case scenario is that the walls were correctly designed for a component and cladding wind pressure on the order of 30 psf, resulting in a construction that lacks the capacity for flood load resistance. The simplest design solution is replacing of the structural backup wall or adding new members to provide intermediate support; however, for cases where this is not feasible, composite strengthening techniques may be utilized. Some of these techniques include

- Steel plate reinforcing attached with post-installed anchors;
- Fiber-reinforced polymers (FRP); and
- Fabric-reinforced cementitious matrixes (FRCM).

Each technique requires different materials and calculations. Because existing masonry walls typically have a relatively low lateral force-resisting strength, it is unlikely that any reinforcing measure applied will satisfy the

maximum reinforcing ratio (ρ_{max}) limits required for a ductile failure. The design calculations should utilize an allowable stress design (ASD) approach that verifies the compressive stress in the masonry against an acceptable limit.

D.2 SLAB STRENGTHENING FOR UPLIFT PRESSURES

As previously discussed, seepage dependent uplift pressures will develop below a ground-floor slab. The simplest design remedy for a slab that does not possess adequate strength to resist these pressures is the addition of a topping slab of sufficient thickness and weight to oppose the uplift; however, many times a sufficiently sized topping slab is not feasible, either for architectural reasons or because of insufficient foundation capacity. In these cases, enhancing the slab capacity via composite strengthening is usually the best approach. This can be achieved by providing a thin reinforced topping slab layer with a bonding agent, adhering the new slab to the old, or via one of the techniques discussed for wall strengthening. This will allow the slab to span between existing columns and walls, provided they support enough dead load to oppose the net uplift.

For cases where the span between existing building columns and/or walls is too large or those where a structure does not possess adequate overall dead load, the installation of intermediate tie-down anchors may be the preferred option for uplift resistance. These tie downs are typically drilled anchors or micropiles installed within the footprint of the building at locally demolished portions of the slab. The piles are installed with compact rigs that are able to operate within confined interior spaces, and a cast-in-place concrete pile cap is poured over the pile and doweled into the remaining portion of the ground floor slab. Although this option is feasible for soil-supported buildings, it is better suited for sites with rock at or near the surface. When rock is close to the surface, a simple tie-down anchor drilled into the rock may be possible depending on the resistance required. Generally, soil anchors do not have enough capacity, but they can be considered for small net uplift pressures. A subsurface seepage analysis may be warranted to determine uplift loads anticipated to result from the design storm event.

D.3 DELEGATING FLOOD BARRIER DESIGN

Projects that specify proprietary flood barriers will include a portion of delegated design to be performed by the vendor upon purchase. For these situations, there are several responsibilities that must be undertaken by engineers:

- Clearly specify required loading conditions and acceptable deflection criteria on the drawings and/or the specifications.

- Verify that vendor's products can support the loading conditions and spans. In some cases, new foundation elements within the sidewalk or building footprint may be required and should be accounted for on the design drawings.
- Design the structural head and jambs at the openings under consideration for the required forces.
- Clarify what connection is required at the interface of the flood barrier and existing structure, and provide details as needed.
- For deployable (assembled) flood barriers, ensure that storage, maintenance, and logistical requirements are addressed in consultation with the owner.

Additional guidance is provided below for currently available building and opening hardening products, exploring operation, maintenance, and applicability for different project types.

D.4 TEMPORARY PROTECTION MEASURES

Some sites designated for flood hardening, such as train storage and maintenance yards, possess an expansive perimeter and therefore require an extended design and construction period. Because full perimeter protection must be in place for flooding to be effectively resisted, the site and assets within are at greater risk until construction is completed. As such, promptly installed, impermanent flood hardening measures may be advisable to mitigate the exposure of the site until permanent protection elements are finalized. It is appropriate for these temporary measures to be designed for a reduced flood-level event (e.g., BFE + 1 ft) as they are intended to be in place for a relatively short period of time, during which the likelihood of a particular design storm is reduced. In addition, although subgrade seepage may be a concern for a permanent solution, it may be appropriate to ignore these criteria for temporary protection, greatly eliminating construction time and cost.

Oftentimes, for large sites that have been in operation a significant amount of time, high-impact, low-cost measures can be cleaning existing drainage systems and providing backflow prevention. Site drainage systems in place for a long period of time (i.e., more than half a century) have higher likelihood of containing zones of partial collapse and/or partial or full blockage from silt deposits. Effective perimeter protection will exacerbate any internal drainage problems and restoring an existing system to full functionality is not a large cost. In addition, a significant source of water infiltration to many sites during Superstorm Sandy was backflow of surcharged water from the city combined stormwater–sewer system. All potential entry paths should be sealed or fitted with a backflow prevention device or a perimeter measure

may trap backflow water within the area protected by a wall. Some low-cost options for temporary perimeter protection include

- Sandbags: Sandbags resist flood loads via their own inherent mass and corresponding friction with the ground surface. To be effective, the bags must be stacked in an interlocking fashion to achieve a watertight (or nearly watertight) seal and must be proportioned to have sufficient weight to resist the design hydrostatic pressures. On sites where sufficient space and access are available, these tend to be the cheapest and easiest to install relative to other temporary protection measures, but they may be less reliable. Sandbags may be subject to vandalism, so protection (e.g., enclosing fencing) should be considered. A positive is that a *mass* protection has a small amount of inherent seepage protection. If soil is washed out below the bags the heavy weight above will partially sink and readjust to help reseal the breach.
- Conversion of existing fences: Many sites are surrounded by perimeter fences (of various materials and configurations) for security purposes. Although these fences typically do not have adequate resisting capacity for use under design flood loads, they can often adequately handle lower floods (i.e., that would be appropriate for a temporary design) with some modifications. As shown in Figure D-1, the typical retrofit for an existing chain link fence includes a galvanized metal deck spanning horizontally between vertical posts, with a continuous concrete curb at the base partially embedded in the soil. The curb provides a watertight seal, upper-level seepage control, and increased bearing area for the footing (e.g., Sonotube). It should be noted that footings with a *restrained* condition at grade (usually present in the form of a concrete sidewalk or paved area) have significantly larger load-resisting capacities than those that are *unrestrained*. Refer to Figure D-1 for elevation and section views of a temporary flood shield design utilizing metal decking secured to existing fencing and existing post footings for support.

D.5 URBAN FLOOD PROTECTION PRODUCTS

The following section provides a broad review of urban flood protection products used today, listing the manufacturers, operational characteristics, and pros and cons of each system. When considering different flood products, it is important to note that there are presently very few *or equals* in terms of products. Alternate products are sometimes available, but most products are fairly unique in their design and functionality. There is not a one-size-fits-all solution with urban flood resiliency and each product has very definite pros and cons based on the application. Therefore, fair and

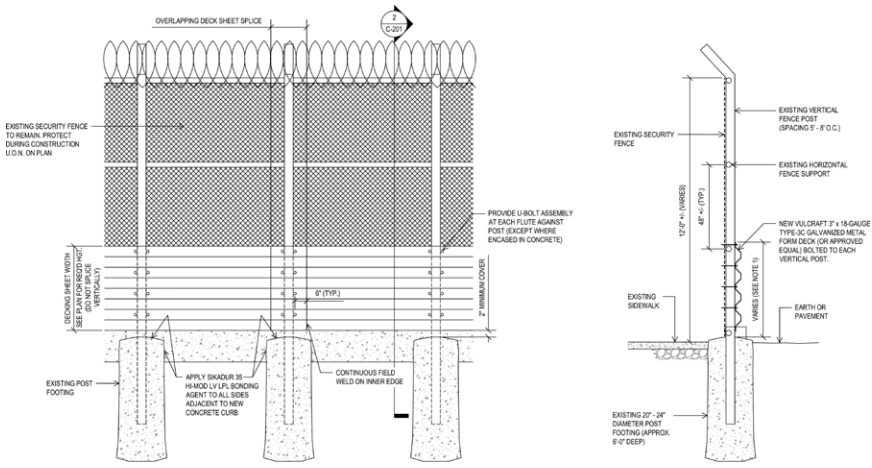

Figure D-1. Temporary fence retaining wall.

accurate dialogue with stakeholders, including the owner and end user, is critical to the design process.

To establish a minimum acceptable standard for a product, flood protection systems are should meet the following criteria:

- Based on the area of protection, the system shall not exceed a predetermined leakage rate. In lieu of owner or project-defined standards, the following parameters can be used:
  - Gratings:
    - Inserts—0.3 gpm/1 linear ft of crack
    - Covers on angle iron frame—0.5 gpm/1 linear ft of crack
    - Covers on concrete—1.0 gpm/1 linear ft of crack
  - Water tight hatches and doors—0.1 gpm/1 linear ft of perimeter
  - Vertical closures—0.1 gpm/1 linear ft of perimeter
  - Rollup flexible covers and barriers—0.5 gpm/1 linear ft of perimeter
  - For closure devices and methods not listed here, the leakage rate shall be determined based on the end-users needs and the capabilities of the technology.
- The system shall be able to hold back floodwaters at or below the required leakage rate for up to 72 hours (flash flooding, not tidal surge, being the controlling condition).
- The system shall withstand the impacts based on the current ASCE/SEI 7 standard.
- The system shall be capable of being deployed within 24 hours of an anticipated storm event.

- The system shall seal around all utility connections without interrupting the required signals.
- Components shall be resistant to saltwater corrosion.
- Cables and cable splices shall be submersible and resistant to contaminated floodwater.
- All cable and conduit penetrations shall have a watertight seal.
- All control and power panels shall be contained in watertight enclosures.
- The system shall be reusable for multiple events.
- Any system installed near or on a roadway shall be resistant to rock salt corrosion. It shall also require minimal effort to clear any debris from gaps prior to an event to prevent jamming when deployed.
- The system shall not float, overturn, or experience catastrophic failure if the water level of a flood exceeds the height of any system component.
- The system shall minimize the amount of storage space required.
- The system shall have its components protected in-place against theft or vandalism.
- The system's primary deployment (if applicable) shall not require electrical power, unless by an uninterrupted source of backup power installed within the system.
- The system shall preserve all emergency exit routes or code-compliant alternate means of egress must be provided.
- All system elements that have a limited life (e.g., gaskets or sealants) shall be readily replaceable.

Preferred but not required system characteristics include the following:

- Easy to assemble, deploy, use, remove, and store;
- Minimal impact to existing architecture or appearance;
- Minimal need to modify the existing infrastructure; and
- Whenever possible, the system shall be stored at the area of protection to minimize the need to transport components.

System automation has the significant benefit of minimizing the need for personnel and the time to deploy the protection. However, there are safety concerns that must be addressed when proposing an automated system. An automated system needs layers of safety precautions to prevent individuals from becoming trapped or isolated without proper ventilation. Also, automated systems that generally sit dormant are relied upon in an instant for critical protection. An automated system should be regularly tested, safeguarded, and have a reliable source of power to ensure it will properly deploy when needed meet these needs.

It is important to note that although many of the following products have undergone a rigorous testing protocol, most, if not all, are relatively new on the market, so *usable lifespan* is an estimation at this point. In addition, it is important to work with the end user on how and when a product

will be deployed. Ease of installation and associated performance (leakage) of a factory test may not accurately reflect the actual speed for successful storage retrieval and erection in the hours prior to a storm event considering a potential context of moderate wind and rain conditions, as well as overall situational duress.

Example D.1 Dam-It Dam (Category: Water-Filled Barrier)

Figure D-2. Installed water-filled cofferdam.
Source: Courtesy of Dam-it Dams (reproduced with permission).

Figure D-3. Installed water-filled cofferdam.
Source: Courtesy of Dam-it Dams (reproduced with permission).

Overview

- Water-filled cofferdam dam replacement for sandbags ideal for large area protection;
- 15-year product history;
- Two side-by-side water-filled fabric tubes inside an outer-casing made of heavy-duty geotextile woven polypropylene;
- Inflated lengths from 1 to 16 ft; standard supplied lengths are 50 and 100 ft (custom available as needed);
- Longest currently installed length: 1,000 ft (individual cofferdams are joined together coupling collar connections);
- Made in America; and
- Aqua Dam and Tiger Dam are other similar US-based water-filled flood barrier systems.

Commentary

The most obvious problem is the requirement for a water source and the length of time required to fill the tubes. For traditional flood protection along a river or other body of water, the water source is obvious and there is typically plenty of time to set up and fill the tubes. However, in an urban setting, a suitable water source may not be available, and the filling time may prove to be a significant deployment challenge. Water-filled protection devices typically have two global problems—a tendency to roll and only functioning well to a depth of about two-thirds their height. The proprietary internal fabric design overcomes the issue of rolling; however, the second issue remains. As the depth of water in front of the tube approaches the height of the tube, the water pressure outside at the base of the tube approaches the water pressure inside the tube and water starts flowing beneath the tubes. If the tubes are overtopped they become essentially weightless (except for the submerged weight of the fabric) and can catastrophically fail. Vandalism and general damage can also be an issue as a large amount of flexible material must be stored safely and handled by machinery. Because this product is deployed on the surface, subsurface seepage and washout are not addressed by this product.

This product is relatively easy to store and reasonably lightweight compared to other systems—no heavy equipment is required to deploy. Another advantage is its ability to perform very well on uneven ground, around bends or corners, and at any desired, changeable length without major modification.

If the design flood depth does not exceed 12 ft and if there is a convenient water source and pumps capable of filling the tubes quickly, water-filled tubes can offer good surface protection and are cost effective. The upper limit of effective design flood depths for these systems is approximately 12 ft.

Example D.2 FloodBreak (Category: Multiple Passive Barrier Products)

I. Passive Flood Barriers

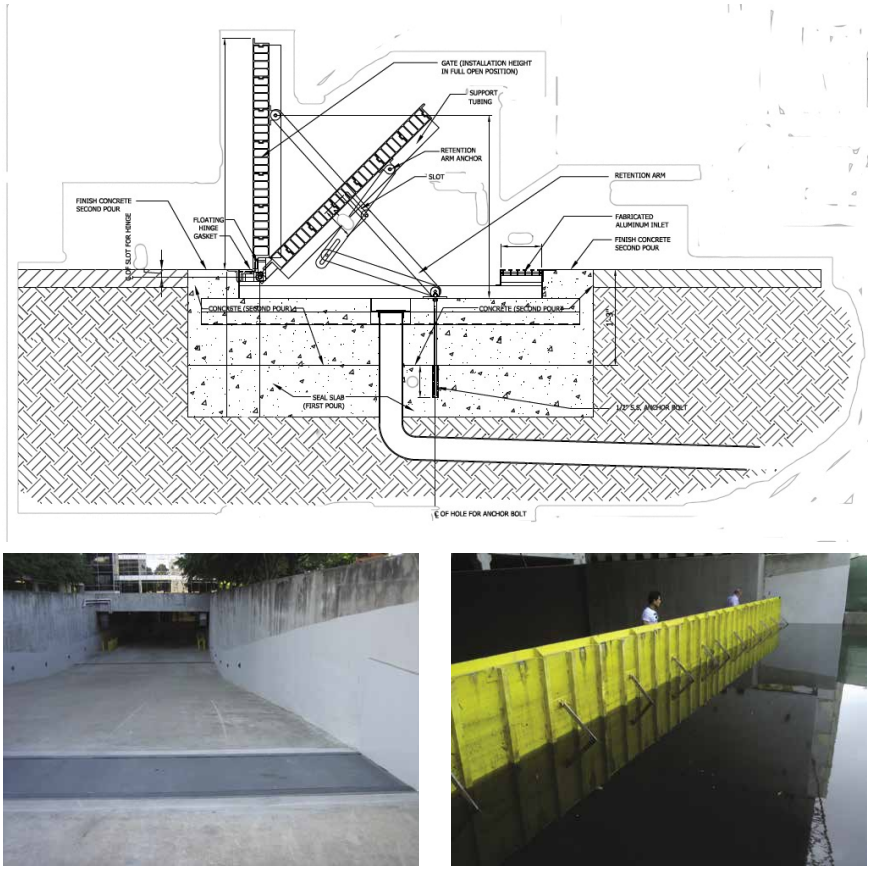

Figure D-4. Section view of passive flood barrier (top) and passive flood barrier installed in stored (bottom left) and deployed (bottom right) positions. Source: Courtesy of FloodBreak (reproduced with permission).

Overview

- Automatic floodgates that are passively deployed by the rising floodwater without power or human intervention;
- Barrier is a buoyant aluminum beam that is stored in an in-ground channel and self-deploys during a flood;

- Custom designed to meet load requirements, including live loads (pedestrian or HS-25 trucks) and hydrostatic pressure. Comply with performance requirements and design criteria in accordance with ASCE 24, *Flood Resistant Design and Construction*. Comes in three vertical load capacity grades—pedestrian, vehicle, roadway;
- No practical height or length limitation owing to the modular, self-supporting design;
- Barrier works with relatively shallow excavation depths and foundations compared to protection heights;
- Barriers seal on each side to *wiper walls* that are part of the barrier system and designed to anchor to structural support walls;
- Made in America;
- Spring Dam is a similar product headquartered in the UK; and
- Aquafragma is a similar patented product headquartered in Cyprus that may be manufactured in America. The seals are all hidden below the top surface, fully protected from the environment and human activities. When the barrier is upright, the seals are planar with hydrostatic action pressing the seals on flat plates, achieving maximum water tightness. It does not need any side or *wiper walls* because the flood gate is upright before floodwater reaches grade level.

See examples D.9 and D.10 for similar US-manufactured bottom-hinged flood gates.

Commentary

Self-deploying systems, particularly ones that do not require human intervention or electrical power, have obvious advantages because the barrier is permanently installed in the location of protection, and therefore they need no off-site storage, no transportation, and no dependence on people. This particular barrier is ideal for flash flooding, where adequate advance warning is not common. In addition, its limited foundation depth is attractive for ease of construction and avoiding conflicts with existing utilities that could limit other off-the-shelf solutions or locations of use. Components are aluminum and stainless steel (with EPDM gaskets), so they are rust and corrosion resistant and will provide long service life with minimal maintenance. A reliable inspection and maintenance program is recommended to ensure that the system is not damaged and will operate as designed. In addition, it is important the system does not become obstructed from above in the future.

The barrier is able to be manually deployed quickly via lifting lugs or with an optional lift. A smooth sealing surface and a straight and flat rigid surface are required for installation. The barrier can be blended into architectural walls and floors to make it less noticeable. Add-on gasket cover protection plates can be provided for particularly abusive environments.

Subsurface seepage and washout is not addressed by this product. For Aquafragma, the stability of the product is provided by gravity, from dead-weights added at the front and rear side after installation, and hence no preparatory works are required other than a shallow recess in the ground. In addition, no seals are exposed to the environment and hence, there is no risk of vandalism or tire or shoe damage.

II. Vent Shaft Protection

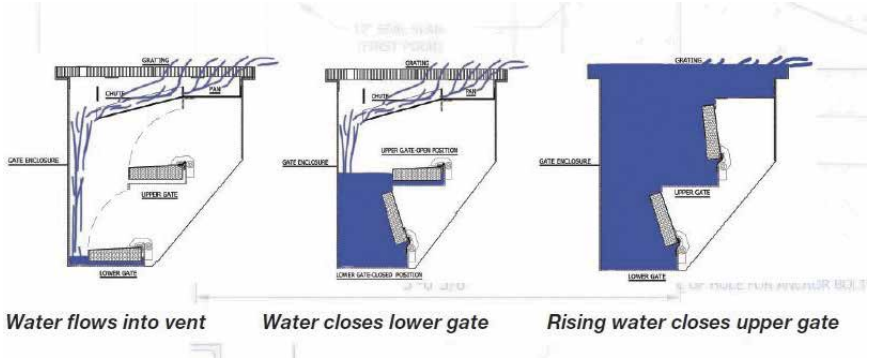

Figure D-5. Section view schematic of automatic closure device design.
Source: Courtesy of FloodBreak (reproduced with permission).

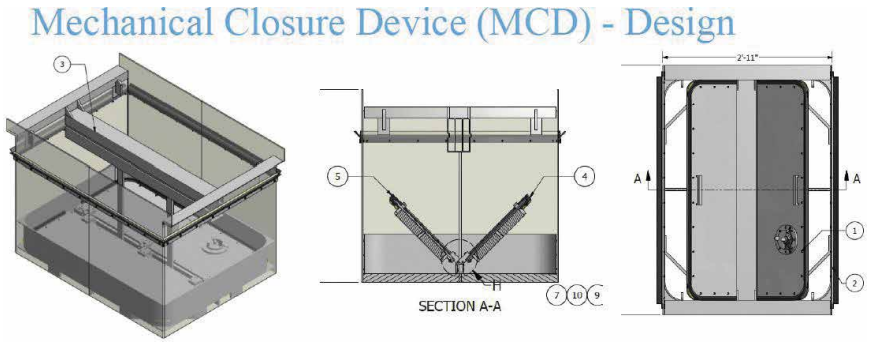

Figure D-6. Schematic views of mechanical closure device design, manually operated.
Source: Courtesy of FloodBreak (reproduced with permission).

Commentary

Mechanical closure devices are installed at existing vent shafts by removing existing frames and grating and installing new frames and grating to

Figure D-7. Installation of mechanical closure device.
Source: Courtesy of FloodBreak (reproduced with permission).

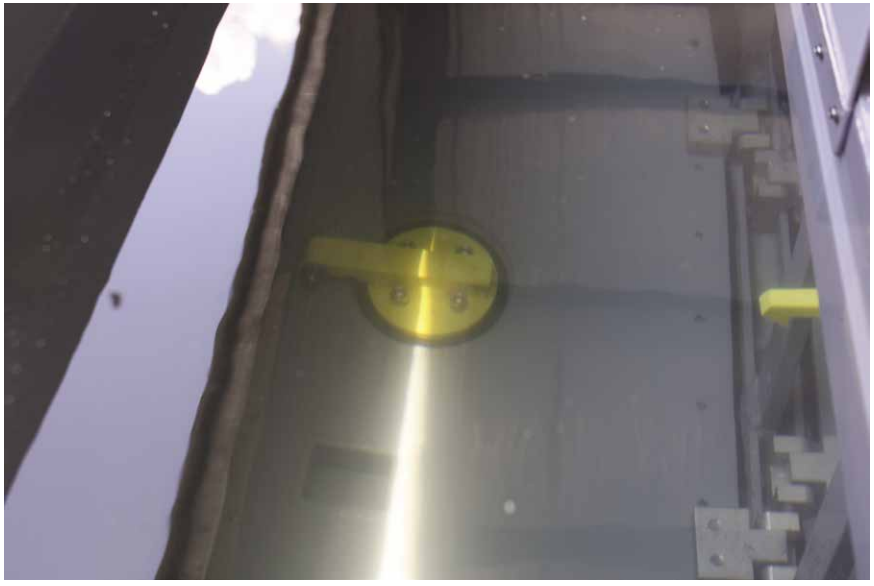

Figure D-8. Typical mechanical closure device under hydrostatic testing.

match sidewalk grade (it has to be shimmed). Each unit is inserted level to assure proper operation of the door mechanism and sized based on 3D laser imaging.

Overview

- Self-closing and self-opening vent shaft insert to protect subterranean points of entry (e.g., to subway system);
- Insert has weep holes to allow the chamber to naturally drain into the existing drainage system after an event;
- Panels automatically reopen after flood recedes; and
- Fits beneath existing structural sidewalk grating.

Commentary

This is the only product we have seen for this application, and it is being installed in many New York City locations. Similar to previously described systems, self-deploying systems, particularly ones that do not require electrical power, have obvious advantages as the barrier is permanently installed in the location of protection, and thus it needs no off-site storage, no transportation, and no human intervention. This particular barrier is ideal for flash flooding, where adequate advance warning is not common. Units were installed for NYCT in 2010 and recently field tested, where they operated as designed. With reliable inspection and maintenance, the system seems good for the application.

III. Louvered Vent Panel

Figure D-9. Typical louvered vent panel.
Source: Courtesy of FloodBreak (reproduced with permission).

Overview

- Self-closing vent panel system or window add-on aluminum box that allows air to circulate freely and close segmentally as floodwaters rise;
- Internal side wiper seals make the panels watertight on the edges;

- Only water-activated panels close, keeping the air circulation above the flooding unrestricted;
- Custom made to any opening size and can be installed on the interior or exterior of the opening; and
- Panels automatically reopen after flood recedes.

Commentary

This is a relatively new offering from FloodBreak, and it is the only product we have seen for this application. (System is installed in NYC and London and is scheduled for the World Trade Center and the MTA Fan Plant.) Similar to previously described systems, self-deploying systems, particularly ones that do not require electrical power, have obvious advantages as the barrier is permanently installed in the location of protection and it needs no off-site storage or transportation. This particular barrier is ideal for flash flooding, where adequate advance warning is not common. Because it is a new product, no actual incident data is available, only vendor testing. With reliable inspection and maintenance the system seems good for the application.

Example D.3 TrapBag (Category: Sand-Filled Barrier)

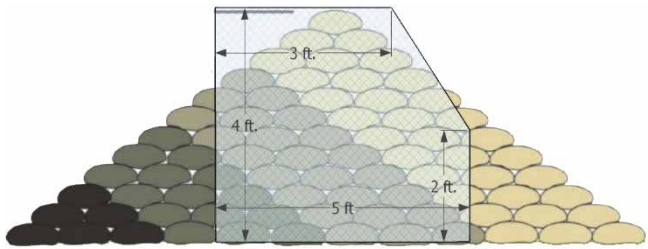

(a) Trapbag uses 40% less fill material than a stacked sandbag wall. A 100 ft section of a 4 ft high TrapBag wall replaces approximately 8,000 sandbags.

(b) Multi-stacked bags (c) Finished system

Figure D-10. Installation of TrapBag system.
Source: Courtesy of TrapBag (reproduced with permission).

Figure D-11. Installation of TrapBag system.
Source: Courtesy of TrapBag (reproduced with permission).

Overview

- A consecutive system of high industrial strength, trapezoid-shaped, fillable bags (cells);
- Each self-contained cell is designed and fabricated of woven, UV-protected textile;
- The unique accordion-like cells are quickly deployed, self-supporting, and rapidly filled;
- Self-erecting;
- 2 ft/4 ft/6 ft stackable systems provide multiple height protection;
- Cells can be filled with sand, gravel, rock or concrete;
- Proven durability with a 10-year life expectancy;
- USA-based headquarters but manufactured in Guatemala (TAA Qualified Product);
- Bags can remain filled in place with only openings deployed or entire length can be deployed; and
- An optional UV cover can be provided for extended use.

Hesco is a similar US-based sand-filled flood barrier system.

Commentary

Each TrapBag system consists of a 50 ft segment of cells in a tightly compacted, accordion-like style for easy shipping and storage. Segments are made to be consecutively spliced together; they are also stackable and require no special fill material. Systems conform to uneven terrain as well as curved formations, creating a safe and secure barrier for all environmental needs.

With simple training available and minimal labor requirements, many cities, counties, states, and even countries have successfully implemented TrapBag Barrier systems to their emergency preparedness planning.

TrapBag systems are non-reusable; dismantling requires cutting to release contents, but they are easily cleaned up with the same filling method. The bags are a faster and more reliable version of a basic sandbag.

The bags come in 50 ft segments broken by internal baffles into 1-m widths. Each cell is trapezoidal, but it can be custom shaped upon request. Multiple lengths can be spliced together and the bags can conform to uneven ground terrain and go around corners. Sealant is applied to the filled bags at building interfaces. With the materials on site, long, straight segments can be erected very quickly, but crowed sites are challenging. Because a mass wall, minor scouring at the base of the bag is sealed by its own weight.

Drawbacks come when figuring out where to store or obtain large volumes of sand when needed. Filled bags are easy targets for vandalism, where puncturing is the method for dismantling. Cleanup after the storm is extensive and the bags are not reusable. Because this product is deployed on the surface, subsurface seepage and washout is not addressed by this product. The bags are a faster and more reliable version of a basic sandbag.

Example D.4 ILC Dover (Category: Multiple Soft Barrier Products)

I. Vertical Flex Gate

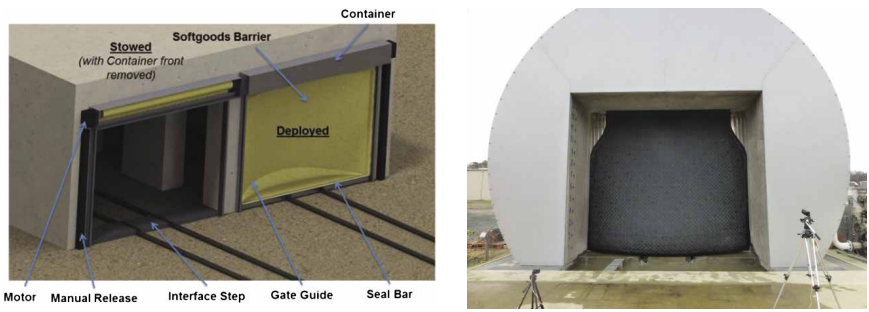

Figure D-12. Vertical flex gate schematic (left) and installed gate (right). Source: Courtesy of ILC Dover (reproduced with permission).

Overview

- All products made in America;
- Woven Kevlar-reinforced fabric gate with a waterproof membrane;
- Tested up to 16 ft wide and 14 ft tall (full water static head);
- None installed yet but one out to bid;
- Stores overhead in a container and is *rolled down* by either hand crank or motor;

- Tension from the water pressure produces a seal in slotted side track; and
- The fabric folds horizontally on the water side and is bolted down through a seal bar—the water weight helps with the seal.

Commentary

The fabric barrier is a strong puncture-resistant material that rolls down from a minimal in-place storage container. With minimal training, the gate can be manually or automatically deployed in a matter of minutes by a single person. Because it is made of a flexible fabric, the material needs room to bulge in order to engage. The base connection does leak more than most products, but the barrier meets the guidelines stated previously. In open areas, the leakage is much less than a design rain event and should be easily accommodated by the storm water system as long as local provisions are made. This is not a product for completely dry floodproofing. It can be used in interior public spaces where drains are present to capture the expected leakage.

II. Stairwell Flex Gate

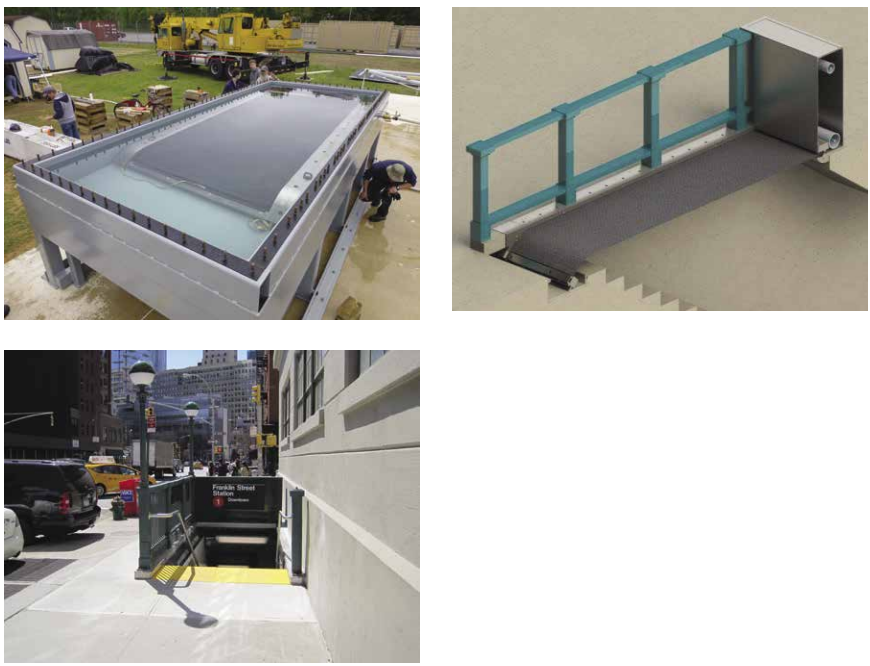

Figure D-13. Hydrostatic testing of stairwell flex gate (left) and schematic of flex gate (right).
Source: Courtesy of ILC Dover (reproduced with permission).

Overview

- Woven Kevlar-reinforced fabric gate with a waterproof membrane;
- Tested in up to 16 ft of water;
- Many installed in lower Manhattan for NYCT;
- Stores vertically in a container at the head of the stair and is *rolled across* the opening by either hand crank or motor;
- Tension from the water pressure produces a seal in slotted side track; and
- The fabric connects to an insert on the stair side for the end seal.

Commentary

Similar discussion to the vertical flex gate but in a horizontal application. The frame and container come preassembled and are easily retrofitted into existing public stairs.

III. Flex Wall

Figure D-14. Testing flex wall system.
Source: Courtesy of ILC Dover (reproduced with permission).

Overview

- Woven Kevlar-reinforced fabric gate with a waterproof membrane;
- Stores in a side or base container and is pulled to cover the opening;
- If base mounted, the fabric connects to manually deployed aluminum posts (in pre-installed mounts) on the end and in the center; and
- If side mounted, the fabric slides along a top tension cable and folds on the water side and is bolted down with a seal bar.

Commentary

Similar discussion to the vertical flex gate but intended for shorter openings. Quick to install but may practically require two people.

IV. Resilient Tunnel Plug

Figure D-15. Resilient tunnel plug.
Source: Courtesy of ILC Dover (reproduced with permission).

Overview

- Woven Vectran-reinforced fabric air-inflatable tube with a waterproof membrane designed for rapid tunnel inflation;
- Stores in an on-site container as a folded fabric bundle;
- Can be configured to any opening shape;
- Held by friction against the tunnel perimeter surfaces;
- 16 ft diameter, 32 ft long plug tested to hold 30 ft of water; and
- One known installation.

Commentary

Depending on the use of the tunnel, the obvious problems with this system is other systems in the tunnel such as rail lines, conduit, ducts, plenums, lighting, and so on that would prevent the plug from achieving a good seal. Although accessory pads can be placed over the rails to allow a better seal, in general the tunnel will need to be retrofitted (or designed) with a protrusion-free zone where the plug can be deployed. In addition, any parallel ducts or conduits will need to be sealed to ensure water does not bypass the plug altogether. Finally, the tunnel structure must be able to resist the outward pressure of the plug. Surfaces that are counter-balanced by water volume should not be a problem. However, surfaces adjacent to sealed cavities (e.g., formed by a roadway on top of an air plenum) must resist this large inflation pressure. The inflation pressure can be reduced by making the plug longer (with more friction area), but this is an iterative problem that must be evaluated.

Example D.5 Muscle Wall (Category: Water-Filled Barrier)

Overview

- Hollow polyethylene segmental water-filled container that comes in 1 ft, 2 ft, 4 ft, and 8 ft heights;
- Segments slide together with a male-female connector—connection has a 22° range of motion (a corner unit is available);
- Adjacent segments are ratchet-strapped together and then the wall is covered with a waterproofed-strapped liner that is held in place with sandbags;
- Leading edge of the waterproofed liner covers foam applied to the surface—if concrete or asphalt. If soil a trench or staking is required on the leading edge; and
- Relatively low deployment time estimates:
  - 2 ft system - 6 people × 3 h = 600 linear ft
  - 4 ft system - 8 people × 4 h = 600 linear ft
  - 8 ft system - 10 people × 7 h = 600 linear ft

Commentary

This type of barrier does not contract or fold or reduce in size when empty, so a large off-site storage space and transportation are required—including the sandbags as well. The barrier has all the problems associated with water-filled barriers, including the requirement for a water source and lack of stability if water depth exceeds about two-thirds of the structure height. The instability may be somewhat countered by anchoring, but no anchoring is described—and may not realistically be possible on concrete or asphalt where sliding is a concern with the narrow footprint. An issue with any solid-form structure is the seal between the barrier and any end-walls, that is, how to fit 6 ft wide units into a 29 ft wide opening. After use the units must be drained. The waterproofing liner is sliced during installation for strap holes—and presumably able to be reused only if the future holes align perfectly.

EXAMPLE D.6 SAVANNAH TRIMS (CATEGORY: GLASS FLOOD BARRIERS)

Overview

Glass railings, curtainwall, and doors that can withstand ASCE impact forces as and up to 8 ft of hydrostatic pressure (no breaking waves)

Figure D-16. Flood-resistant store-front glass system.
Source: Courtesy of Savannah Trims (reproduced with permission).

Commentary

Savannah Trims is the only manufacturer we have found that makes building (non-aquarium) flood barriers from glass. The curtainwall systems pass the proper thermal and shading tests, as well as the required flood loads. Mullions are watertight and they seal to a base concrete curb.

The Savannah Trims Flood Glass is a store-front glass system composed of structurally glazed laminated glass that is hurricane rated and face mounted relative to the mullion position. It is engineered to job-specific flood loads for the appropriate mullion spacing, reinforcing, and glass area, based on supplied flood heights. The systems have been both flood chamber and impact tested.

There are several mullion options and aesthetic treatments such mullion color and beauty caps. Glass color and energy requirements can in most cases be accommodated.

The Savannah Trims Flood Glass is best suited for the following requirements or conditions:

1. Long expanses of store-front glass: Traditional flood barriers would require time and manpower for installation of posts and barriers. These traditional components would also require storage space;
2. Passive deployment: The Savannah Trims Flood Glass is a ready to go at all times and requires no deployment. If combined with Savannah Trims Flood Resistant Doors it can be as simple as lock and go;

3. Savannah Trims also produces a version of the flood glass as a Flood Railing;
4. Tight property and sidewalk conditions: Close property lines and limited space adjacent to the building often created problems with the design and installation of traditional barriers; and
5. Sloped site or nonstructural ground conditions.

EXAMPLE D.7 UK FLOOD BARRIERS (CATEGORY: PASSIVE FLOOD BARRIER)

Self-Activating Flood Barrier (SAFB)

Overview

- Water-activated self-rising flood barrier—no storage, electricity or human intervention required;
- Water-side collection trench buoyantly lifts the barrier as the water level rises;
- Barrier has the ability to be manually closed;
- The basin where the barrier rises from provides base restraint for the cantilevered wall;
- British patented product that is being manufactured in New York State—Made in America; and
- Presray has a similar self-closing flood barrier product.

See examples D.9 and D.10 for similar self-closing flood barrier products

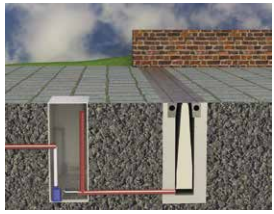

Resting Position

In non-flood conditions, all operational parts of the barrier are concealed in the underground basin

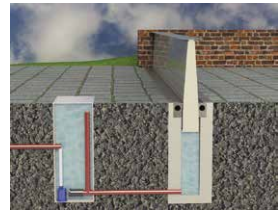

Deploying

When floodwater rises to within a predetermined level below flood level, the basin housing the floating wall starts to fill up through an inlet pipe from the adjacent service pit

Fully Deployed

The floodwall floats and rises. When the basin is totally filled, the angled support block will lock the barrier into position making it watertight

Figure D-17. SAFB operation.
Source: Courtesy of UK Flood Barriers/US Flood Barriers (reproduced with permission).

Figure D-18. Current SAFB installations.
Source: Courtesy of UK Flood Barriers/US Flood Barriers (reproduced with permission).

Commentary

The SAFB uses advancing floodwaters to automatically raise the barrier. It can be used in many applications, including along a waterway, river, or coastal terrain, within flood walls, to surround a building, to protect underground car parks, in a roadway, and to surround critical infrastructure.

A totally passive flood barrier is very attractive, but although the barrier will close slowly, closing *on its own* may raise safety concerns. These have been overcome with telemetry systems and pre-development warnings that can be built in to address these concerns. The barrier is stored vertically below ground and therefore has no impact on the aesthetics of the building or its surroundings. Foundations can be designed to accommodate this system in new build designs, proving cost saving, and with no operational cost for its lifetime in excess of 50 years, this system proves hard to beat on many fronts. The SAFB can also be built into a bund wall above ground level. Stored in a covered sub-ground container, if dirt/silt gets in, it would sit below the barrier and have no impact on deployment or the closing operation. In addition, the SAFB is designed to flush away

any silt as a drainage system would. As with passive flood barriers, it is important the system does not become obstructed from above in the future. This can be overcome by the use of signage and hatching to prevent vehicles parking over the system. There are multiple inlet holes for the floodwaters to enter, and these can be fitted with a screening device to keep out debris and/or animals.

There is even an option for a rail barrier, where a rail segment is mounted to the top of the barrier, travels up during a flood, and rejoins the adjacent track as the flood recedes in order to close off tunnels, and so on.

EXAMPLE D.8 WALZ & KRENZER (CATEGORY: CUSTOM WATERTIGHT CLOSURES)

I. Sliding and Hinged Watertight Marine Gates

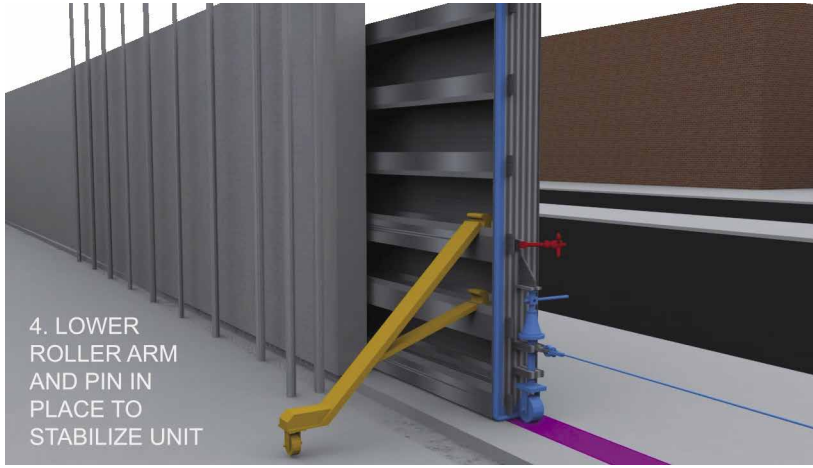

Figure D-19. Schematic of sliding watertight marine gate.

Overview

- Walz & Krenzer engineers structural steel large hinged or sliding gates that are designed to operate manually—automation can certainly be added;
- Gate generally span horizontally and travel by ground support so a large overhead frame is not required; and
- Gates have a two-part hinge designed to close the gate without the base seal dragging along the ground—then it drops into place vertically creating a compression seal on a flat base—no base lip, trench, or inserts are required.

Figure D-20. Hinged watertight flood gate installations.
Source: Courtesy of Walz & Krenzer (reproduced with permission).

Commentary

Walz & Krenzer design large (50+ feet wide) structural gates that can be closed by a single person with a hand drill-controlled winch in just minutes. These gates have wide flange members on their side with fitted stiffeners to span the horizontal opening. The gates can be sliding or swinging depending on the application. A base wheel and a rear stabilizer arm provide the stability while the winch closes the gate. The gate opens in the same manner with an opposite side winch. The gates can be designed on the inside or outside of the flood wall, but the unseating connection design is bulkier and needs larger hardware to seal. Not having a base track to clean or maintain in a traffic wear condition is a big benefit to this product.

Gates can have a *flush sill mechanism*, which lifts the bottom gasket when the gate is swinging and lowers it when the gate is closed. This prevents the bottom seal from dragging along the ground. The gasket drops into place vertically creating a compression seal on a flat base- no base lip, trench, or inserts are required.

II. Hinged Watertight Marine Doors

Figure D-21. Hinged watertight marine doors installed.
Source: Courtesy of Walz & Krenzer (reproduced with permission).

Overview

- Walz & Krenzer has a long history of providing watertight doors for marine vessels and used this expertise to develop commercial products;
- Additional labeled sets of gaskets precut for each installation should be kept on site as *attic stock*;
- Available for most door sizes for pressure requirements ranging from weathertight to 1,000 ft pressure head;
- Remote control and power operated hinged doors available; and
- Doors can be operated from both sides or from one side only. Options include view ports, remote indication and operation, cylinder assist, and insulation.

III. Watertight Emergency Egress Hatches

Overview

- Hatch covers reinforced to support HS20 loading;
- Force required to open hatch does not exceed 30 lb; and
- Hold-open arm automatically locks in the open position.

Figure D-22. Watertight emergency egress hatch.
Source: Courtesy of Walz & Krenzer (reproduced with permission).

EXAMPLE D.9 PRESRAY (CATEGORY: MULTIPLE DEPLOYED BARRIERS)

General Overview

- Large suite of flood products.
- Self-closing flood barrier (SCFB)—See Example D.7 for system discussion.
- Bottom-hinged flood gate—See Example D.2 for system discussion.

I. Stackable Flood Barriers

Figure D.23. Stackable Flood Barrier installed.
Source: Courtesy of Presray (reproduced with permission).

Overview

- Two types—FastLogs (general-duty) and CGSL Stop Logs (heavy-duty);
- One of the most used and most known barriers; and
- Lightweight 6 in. tall aluminum planks that stack together, tightened with edge *dogs*, and bolt clamped at the top.

Commentary

The aluminum log systems are fast and easy to install. Planks can span up to a maximum of around 12 ft, jamb-to-jamb, before needing a deployed center post and kicker for long opening coverage. The only real negative is the logistics of storage and retrieval. For individual openings, especially with no intermediate posts, this is a very practical solution. As a perimeter solution the storage and sheer number of pieces becomes problematic.

II. Removable Flood Barrier

Figure D-24. Removable flood barrier.
Source: Courtesy of Presray (reproduced with permission).

Overview

- Custom-built drop-in aluminum panel up to 40 ft^2 in size; and
- Dual pneumatic seals.

Commentary

This is a simple lightweight panel that drops into a jamb frame to seal a specific opening. It is very reliable and easy to use. Although inflatable gasket seals can have calibration and lifespan issues, the fact that two are used helps to minimize risk. If storage and retrieval are easily accommodated, this is a simple system to use.

III. Hinged Floodgate

Overview

- Custom-built aluminum gate with a steel perimeter frame; and
- Dual pneumatic seals.

Commentary

This discussion is similar to that of Example D.8 except that the seals and base insert varies. Presray has a three-sided steel frame as part of the gate, whereas other suppliers have three separate pieces. Both do not

Figure D-25. Hinged floodgate.
Source: Courtesy of Presray (reproduced with permission).

require removal of a base cover plate for operation, which is an advantage. Presray uses inflatable seals, whereas other suppliers use a compressed rubber p-gasket. Again, although inflatable gasket seals can have calibration and lifespan issues, the fact that two are used minimizes the risk.

IV. Sliding Floodgate

Overview

- Custom-built aluminum gate with a steel perimeter frame; and
- Seals are molded neoprene.

Commentary

This is similar to the hinged gate except that the seals are molded and not inflatable.

Figure D-26. Sliding floodgate.
Source: Courtesy of Presray (reproduced with permission).

Example D.10 PS Flood Barriers (Category: Multiple Deployed Barriers)

General Overview

- Large suite of flood products—all products made in America;
- SCFB—See Example D.7 for system discussion;
- Bottom-hinged flood gate—See Example D.2 for system discussion; and
- Flood plank—See Example D.9 for system discussion.

I. Fire-Rated Doors

Overview

- 90-minute fire-rated door equipped with panic bar closure;
- Single or paired doors available;
- Tested for flooding and impact up to 8 ft;

Figure D-27. Fire-rated watertight doors installed.
Source: Courtesy of PS Flood Barriers (reproduced with permission).

- Available in mild or stainless steel; and
- Compression gasket.

Commentary Many building projects consider flood doors as a means of protection, and PS Flood Barriers is one of the few, maybe only, door that is fire rated with code-required panic hardware.

II. Hinged Floodgate

Overview

- Available in mild steel, stainless steel, or aluminum; and
- Compressed rubber seals.

Commentary

This discussion is similar to that of Example D.8; both do not require removal of a base cover plate for operation and use compression rather than inflatable gaskets, which is an advantage.

Figure D-28. Hinged floodgate.
Source: Courtesy of PS Flood Barriers (reproduced with permission).

III. Sliding Floodgate

Figure D-29. Sliding floodgate.
Source: Courtesy of PS Flood Barriers (reproduced with permission).

Overview

- Available in mild steel, stainless steel, or aluminum; and
- Compressed rubber seals.

Commentary

This discussion is similar to that for Example D.8 except that PS Flood Barriers handle extra-large openings with an overhead frame. Both do not require removal of a base cover plate for operation and use compression rather than inflatable gaskets, which is an advantage. The base track required for PS Flood Barriers is much more substantial than that of some other products because the base seal varies in configuration.

D.6 PRODUCT WEBSITES

Dam-it Dams Portable Water Filled Dams. Grand Blanc, MI. https://www.damitdams.com.
FloodBreak Automatic Floodgates. Houston, TX. http://floodbreak.com/products.
ILC Dover. Frederica, DE. http://www.ilcdover.com/flood-protection.
Muscle Wall Holdings LLC. Logan, UT. http://www.musclewall.com/.
Presray Corporation. Wassaic, NY. http://www.presray.com/.
PS Doors. Grand Forks, ND. https://www.psfloodbarriers.com.
Savannah Trims, Inc. West Palm Beach, FL. http://floodbreak.com.
TrapBag. Fort Meyers, FL. http://www.trapbag.com.
UK Flood Barriers / US Flood Barriers. Worcestershire, UK. http://www.ukfloodbarriers.co.uk/.
Walz & Krenzer, Inc. Oxford, CT. http://wkdoors.com.

INDEX

Tables are indicated by *t*; Figures are indicated by *f*; Equations are indicated by *e*